THE UNIVERSITY OF TEXAS AT AUSTIN
CENTER FOR TRANSPORTATION RESEARCH

TECHNICAL REPORT 0-6636-1
TxDOT PROJECT NUMBER 0-6636

Laboratory and Field Studies of Photocatalytic NOx and O3 Removal by Coatings on Concrete

Neil Crain
Maria Juenger
Clement Cros
Alexandra Terpeluk
Lisa Burris
Elena McDonald-Buller
David Sullivan
Yosuke Kimura
Jarett Spinhirne
Michael Rung

December 2016; Published March 2017

http://library.ctr.utexas.edu/ctr-publications/0-6636-1.pdf

Technical Report Documentation Page

1. Report No. FHWA/TX-17/0-6636-1	2. Government Accession No.	3. Recipient's Catalog No.
4. Title and Subtitle Laboratory and Field Studies of Photocatalytic NO_x and O_3 Removal by Coatings on Concrete		5. Report Date December 2016; Published March 2017 6. Performing Organization Code
7. Author(s) Neil Crain, Maria Juenger, Clement Cros, Alexandra Terpeluk, Lisa Burris, Elena McDonald-Buller, David Sullivan, Yosuke Kimura, Jarett Spinhirne		8. Performing Organization Report No. 0-6636-1
9. Performing Organization Name and Address Center for Transportation Research The University of Texas at Austin 1616 Guadalupe Street, Suite 4.202 Austin, TX 78701		10. Work Unit No. (TRAIS) 11. Contract or Grant No. 0-6636
12. Sponsoring Agency Name and Address Texas Department of Transportation Research and Technology Implementation Office P.O. Box 5080 Austin, TX 78763-5080		13. Type of Report and Period Covered Technical Report, 09/01/2010–12/31/2016 14. Sponsoring Agency Code
15. Supplementary Notes Project performed in cooperation with the Texas Department of Transportation and the Federal Highway Administration.		

16. Abstract

This project involved thorough testing of titanium dioxide (TiO_2)-containing commercial photocatalytic coatings applied to portland cement concrete for highway applications, focusing on the use of these coatings as an abatement method for atmospheric nitrogen oxide (NO_x) and ozone (O_3). The study consisted of four parts: laboratory chamber testing; outdoor exposure studies; modeling; and field application. Full-factorial experiments in laboratory chambers designed to examine the impact of variables such as temperature, relative humidity, time, and pollutant concentrations on NOx and O_3 removal by the coatings demonstrated that a commercial stucco was the best performer of the four original materials tested. After one and two years of outdoor, roadside exposure, the NOx removal capacity of the stucco decreased significantly, but could be improved by soap and water washing. A Comprehensive Air Quality Model with extensions (CAMx) for the Houston-Galveston-Brazoria and Dallas-Fort Worth areas showed the potential of the stucco to reduce average ozone concentrations if large areas of highway structures are coated. Testing at a field site in north Austin, however, showed no conclusive difference between air quality in areas with coated and uncoated highway barriers. Therefore, while photocatalytic concrete coatings have promise for improving air quality, the data from this project suggest that such improvements may not be significant enough to be measured experimentally in common roadway configurations such as the site tested for this study.

17. Key Words	18. Distribution Statement
Nitrogen Oxides, Nitric Oxide, Ozone, Photocatalytic Materials, Titanium Dioxide, Anatase	No restrictions. This document is available to the public through the National Technical Information Service, Springfield, Virginia 22161; www.ntis.gov.

19. Security Classif. (of report)	20. Security Classif. (of this page)	21. No. of pages	22. Price
Unclassified	Unclassified	344	

Form DOT F 1700.7 (8-72) Reproduction of completed page authorized

THE UNIVERSITY OF TEXAS AT AUSTIN
CENTER FOR TRANSPORTATION RESEARCH

Laboratory and Field Studies of Photocatalytic NO_x and O_3 Removal by Coatings on Concrete

Neil Crain
Maria Juenger
Clement Cros
Alexandra Terpeluk
Lisa Burris
Elena McDonald-Buller
David Sullivan
Yosuke Kimura
Jarett Spinhirne
Michael Rung

CTR Technical Report:	0-6636-1
Report Date:	December 2016; Published March 2017
Project:	0-6636
Project Title:	Photocatalytic NOx/HRVOC/O3 Removal in Transportation Applications
Sponsoring Agency:	Texas Department of Transportation
Performing Agency:	Center for Transportation Research at The University of Texas at Austin

Project performed in cooperation with the Texas Department of Transportation and the Federal Highway Administration.

Center for Transportation Research
The University of Texas at Austin
1616 Guadalupe, Suite 4.202
Austin, TX 78701

http://ctr.utexas.edu/

Disclaimers

Author's Disclaimer: The contents of this report reflect the views of the authors, who are responsible for the facts and the accuracy of the data presented herein. The contents do not necessarily reflect the official view or policies of the Federal Highway Administration or the Texas Department of Transportation (TxDOT). This report does not constitute a standard, specification, or regulation.

Patent Disclaimer: There was no invention or discovery conceived or first actually reduced to practice in the course of or under this contract, including any art, method, process, machine manufacture, design or composition of matter, or any new useful improvement thereof, or any variety of plant, which is or may be patentable under the patent laws of the United States of America or any foreign country.

Notice: The United States Government and the State of Texas do not endorse products or manufacturers. If trade or manufacturers' names appear herein, it is solely because they are considered essential to the object of this report.

Engineering Disclaimer

NOT INTENDED FOR CONSTRUCTION, BIDDING, OR PERMIT PURPOSES.

Research Supervisor: Dr. Maria Juenger

Acknowledgments

The researchers would like to thank the Texas Department of Transportation for supporting this work, particularly the efforts of project managers Duncan Stewart and Wade Odell. The project advisors on the project management committee provided very useful guidance: Pat Henry, Jackie Ploch, Clifton Coward, Lisa Lukefahr, and Andy Naranjo. We also appreciate the advice of technical contacts Mark Sather and Ruben Casso from the Environmental Protection Agency, Doug Boyer from the Texas Commission on Environmental Quality, and Christopher Klaus from the North Central Texas Council of Governments.

The field site and outdoor exposure sites would not have been successful without the help of the TxDOT North Austin District office, especially Jamie Witten, Joseph Carrizales and Lowell Choate, Terry McCoy, Erica Ramirez, Wayne Rehborg, and James Wilhem.

Cyril Durrenberger was the senior technical advisor for this project and a good friend. Cyril spent much of his adult life working for the state of Texas trying to improve environmental quality and the life of everyday Texans. Unfortunately, Cyril passed away in April of this year. Cyril will be missed not only at UT but also throughout the state he loved.

Table of Contents

Chapter 1. Executive Summary **1**

Chapter 2. Literature Review **4**

2.1 Introduction 4

2.2 Titanium dioxide photocatalysts 4

2.3 Photocatalysis on titanium dioxide 5

2.4 TiO_2 application methods 5

2.5 Laboratory scale photocatalytic oxidation research 7

2.5.1 Nitrogen oxides removal 7

2.5.2 VOC removal 11

2.6 Substrate/TiO_2 interactions and durability of photocatalytic specimens 13

2.6.1 Effect of substrate properties on photocatalysis 13

2.6.2 Effect of concrete properties on photocatalysis 14

2.6.3 Effect of TiO_2 on substrate properties 15

2.6.4 Durability of photocatalytic specimens 15

2.7 Self-cleaning properties of photocatalytic specimens 16

2.8 Pilot scale and field tests of photocatalytic pollution reduction 17

Chapter 3. Materials and Testing for Laboratory and Outdoor Exposure Studies **20**

3.1 Concrete samples and coatings preparation 20

3.1.1 Description of concrete samples 20

3.1.2 Concrete slab preparation 22

3.1.3 Coatings 23

3.2 Methods for characterization of concrete and coatings 27

3.2.1 X-ray diffraction 27

3.2.2 Scanning electron microscopy 27

3.3 Outdoor exposure tests setup 28

3.3.1 Houston 28

3.3.2 Austin 29

3.3.3 Laboratory 30

3.4 Pollutant removal experimental setup 31

3.4.1 Description 31

3.4.2 Characterization 32

Chapter 4. Coating Screening Tests for Pollutant Removal **35**

4.1 Preliminary tests 35

4.2 Full factorial tests and replicates 36

4.3 Chamber testing quality assurance 40

Chapter 5. Photochemical Modeling **42**

5.1 Description of CAMx model and dry deposition 42

5.1.1 Modeling episodes 42

5.1.2 CAMx dry deposition algorithm 45
5.2 Surface resistances determination for the stucco 47
5.2.1 Description of experiments 47
5.2.2 Deposition of pollutant species to the reactor surfaces 48
5.2.3 Determination of reactor transport resistance 49
5.2.4 Determination of pollutant deposition velocity 50
5.2.5 Calculation of coating surface resistances 50
5.3 Photochemical modeling in CAMx 50
5.3.1 Determination of solar insolation 52
5.3.2 Spatial representation of highways and barriers 52
5.3.3 Results 55
5.3.4 Summary and key findings 59
Chapter 6. Long-Term Outdoor Exposure Results 61
6.1 Periodic field testing 61
6.1.1 Monitoring of field sites 61
6.1.2 Exposure site monitoring results 63
6.2 Materials characterization before and after 1 and 2 years of exposure 64
6.2.1 X-ray diffraction analysis of field specimens 64
6.2.2 XRD analysis of environmental chamber specimens 65
6.2.3 Scanning electron microscopy analysis of field samples 65
6.2.4 SEM results for environmental chamber specimens 73
6.3 Pollutant removal testing after 1 and 2 years of exposure 75
6.3.1 Samples coated and exposed for 1 year 75
6.3.2 Samples coated and exposed for 2 years 76
Chapter 7. Roadside Field Study 79
7.1 Roadside field site selection 79
7.1.1 Roadway safety 79
7.1.2 Site orientation 79
7.1.3 Existing highway barriers 80
7.1.4 Sampling points 80
7.1.5 Electrical power 80
7.1.6 Site security 81
7.2 Selected roadside field site location and configuration 81
7.3 Preparation and installation of roadside field site photocatalytic stucco 85
7.4 Roadside test site equipment and analytical instruments 85
7.5 Data collection results 86
7.5.1 Data availability year 1 86
7.5.2 Data availability year 2 87
7.6 Analysis of field site data 88
7.6.1 Analysis of roadway field test site data for year 1 88
7.6.2 Analysis of roadway field test site data for year 2 94

7.7 Quality assurance for roadway field test site 101
Chapter 8. Conclusions and Recommendations 102
8.1 Summary and conclusions 102
8.2 Recommendations 103
References 105
Appendix A 111
Appendix B 113
Appendix C 116
Appendix D 122
Appendix E 125
Appendix F 126
Appendix G 131
Appendix H 262
Appendix I 300

List of Figures

Figure 2.1 Photocatalytic oxidation of butyraldehyde (from Ye et al., 2006) 11
Figure 3.1 Dimensions of slab specimens: (a) full size; (b) half size 21
Figure 3.2 Completed slab formwork 21
Figure 3.3 Concrete barrier specimen: (a) side elevation; (b) front elevation 22
Figure 3.4 Application of the photocatalytic stucco 24
Figure 3.5 Application of the white paint 25
Figure 3.6 Clear paint 1 application by sprayer 26
Figure 3.7 Application of the clear paint 2 spray 26
Figure 3.8 Houston site: (a) map; (b) digital image of field site facing I-10 29
Figure 3.9 Austin site: (a) map; (b) digital image of field site facing I-35 30
Figure 3.10 Lab site: (a) map; (b) digital image of north facing site 31
Figure 3.11 Photocatalytic testing setup 32
Figure 3.12 CO_2 decay test to evaluate uniformity of mixing 33
Figure 4.1 Preliminary results for photocatalytic coatings 36
Figure 4.2 Comparison of NOx removal by the photocatalytic coatings 38
Figure 4.3 ANOVA results for the clear paint 1 and the stucco (blue vertical lines indicate critical values of Lenth t-ratio above which a parameter is deemed significant) 39
Figure 5.1 June 1–30, 2006 CAMx episode: (a) horizontal modeling domain showing the outer 36km x 36km Eastern U.S., nested 12km x 12km East Texas, and 4km x 4km DFW grids; (b) vertical layer structure 43
Figure 5.2 August 13–September 15, 2006 CAMx episode: (a) horizontal modeling domain showing the outer 36km x 36km Eastern U.S., nested 12km x 12km East Texas, 4km x 4km HGB/Beaumont/Port Arthur, and 2km x 2km Houston/Galveston grids; (b) vertical layer structure 44
Figure 5.3 Resistance pathways to dry deposition from Wesely (1989) 46
Figure 5.4 The locations of highways in the DFW area (red) assumed to have barriers. 54
Figure 5.5 The locations of highways in the HGB area (red) assumed to have barriers. 55
Figure 5.6 Daily maximum ozone concentrations averaged over 8 hours for the base case and photocatalytic stucco study within the (a) DFW nine-county and (b) HGB eight-county areas 56
Figure 5.7 Difference in daily maximum ozone concentrations averaged over 8 hours and maximum differences in ozone concentrations averaged over 8 hours in the DFW area between the base case and photocatalytic stucco study (base case—stucco) 57
Figure 5.8 Difference in daily maximum ozone concentrations averaged over 8 hours and maximum differences in ozone concentrations averaged over 8 hours in the Houston/Galveston area between the base case and photocatalytic stucco study (base case—stucco) 57

Figure 5.9 Difference in daily maximum ozone concentrations averaged over 8 hours in the DFW area between each of photocatalytic stucco-coated cases and the base case 58
Figure 5.10 Maximum differences in ozone concentrations averaged over 8 hours in the DFW area between each of photocatalytic stucco-coated cases and the base case 59
Figure 6.1 Concrete washing procedure 61
Figure 6.2 Water collection procedure for concrete specimens 62
Figure 6.3 SEM images of control surface: (a) before exposure; (b) after exposure in Houston; (c) after exposure in Austin; (d) after exposure at the lab site 66
Figure 6.4 SEM images of control cross section: (a) before exposure; (b) after exposure in Houston; (c) after exposure in Austin; (d) after exposure at the lab site 67
Figure 6.5 SEM images of the stucco surface: (a) before exposure; (b) after exposure in Houston for 1 year; (c) after exposure in Austin for 1 year; (d) after exposure at the lab site for 1 year; (e) after exposure in Houston for 2 years; (f) after exposure in Austin for 2 years; (g) after exposure at the lab site for 2 years 68
Figure 6.6 SEM images of the stucco cross sections: (a) before exposure; (b) after exposure in Houston for 1 year; (c) after exposure in Austin for 1 year; (d) after exposure at the lab site for 1 year; (e) after exposure in Houston for 2 years; (f) after exposure in Austin for 2 years; (g) after exposure at the lab site for 2 years 69
Figure 6.7 SEM images of the white paint surface: (a) before exposure; (b) after exposure in Houston; (c) after exposure in Austin; (d) after exposure at the lab site 70
Figure 6.8 SEM images of the white paint cross section: (a) before exposure; (b) after exposure in Houston; (c) after exposure in Austin; (d) after exposure at the lab site 71
Figure 6.9 SEM images of the clear paint 1 surface: (a) before exposure; (b) after exposure in Houston; (c) after exposure in Austin; (d) after exposure at the lab site 72
Figure 6.10 SEM images of the clear paint 1 cross section: (a) before exposure; (b) after exposure in Houston; (c) after exposure in Austin; (d) after exposure at the lab site 73
Figure 6.11 SEM images of uncoated environmental chamber specimen after testing: (a) surface; (b) cross section 74
Figure 6.12 SEM images of the stucco environmental chamber specimen after testing: (a) surface; (b) cross section 74
Figure 6.13 SEM images of the white paint environmental chamber specimen after testing: (a) surface; (b) cross section 74
Figure 6.14 SEM images of the clear paint 1 environmental chamber specimen after testing: (a) surface; (b) cross section 75
Figure 6.15 NOx removal by the stucco in all three field sites for both morning and afternoon inorganic levels conditions. 76
Figure 6.16 NOx removal by the stucco in all three field sites for both morning and afternoon inorganic levels conditions after 2 years of outdoor exposure 77
Figure 7.1 Historic wind rose for ozone season in Austin 80
Figure 7.2 Google satellite image of roadway field test site 81
Figure 7.3 Google satellite image of roadside field test site (with callouts) 82

Figure 7.4 Additional highway barriers and road hazard barrels 82
Figure 7.5 Schematic of roadside field test site 83
Figure 7.6 Sampling goosenecks 83
Figure 7.7 Schematic drawing of sample line configuration 84
Figure 7.8 Photocatalytic sampling port (gooseneck) and proximity to roadway (goosenecks were placed on the northernmost barrier facing south) 84
Figure 7.9 Uncoated barrier sampling port (gooseneck) and proximity to roadway (goosenecks were placed on the northernmost barrier facing south) 85
Figure 7.10 Cumulative distributions of the daily maximum one-hour NO_2. 89
Figure 7.11 Cumulative distributions of the daily maximum one-hour O_3 values. 90
Figure 7.12 Linear regression for NO 90
Figure 7.13 Linear regression for NO_2 91
Figure 7.14 Linear regression for NO_x 91
Figure 7.15 Linear regression for O_3 92
Figure 7.16 Diurnal pattern for mean hourly concentration for NO_2 for Aug. 22–28 93
Figure 7.17 Diurnal pattern for mean O_3 concentration for August 2015 93
Figure 7.18 Plots of the difference between the outputs for the NO_x and O_3 analyzers used for this study sampling the same air parcels 96
Figure 7.19 NO_2 diurnal pattern for March 30 through April 5 98
Figure 7.20 O_3 diurnal pattern for May 25 through May 31 98
Figure 7.21 O_3 diurnal pattern for April 27 to May 3 100
Figure 7.22 O_3 diurnal pattern for July 6 to July 12 100

Figure F.1: XRD analysis of uncoated control barrier core before exposure and after exposure in Houston, Austin, and the lab sites 126
Figure F.2: XRD analysis of the stucco barrier core before exposure and after exposure in Houston, Austin, and the lab sites 126
Figure F.3: XRD analysis of the stucco barrier core before exposure and after 2 years of exposure in Houston, Austin, and the lab sites 127
Figure F.4: XRD analysis of the white paint barrier core before exposure and after exposure in Houston, Austin, and the lab sites 127
Figure F.5: XRD Analysis of the clear paint 1 barrier core before exposure and after exposure in Houston, Austin, and the lab sites 128
Figure F.6: XRD analysis of uncoated control environmental chamber specimen core 128
Figure F.7: XRD Analysis of the stucco environmental chamber specimen core 129
Figure F.8: XRD Analysis of the white paint environmental chamber specimen core 129
Figure F.9: XRD Analysis of clear paint 1 environmental chamber specimen core 130

List of Tables

Table 3.1 TiO2 content of commercial coatings 24
Table 4.1 Full factorial parameters and their levels 36
Table 4.2 Comparison between the calculated relative uncertainty and relative difference observed between initial and replicated experiments 41
Table 5.1 Experiments run to determine kinetic parameters for inclusion in CAMx model 48
Table 5.2 Highway and barrier surface area (km^2) within the nine-county DFW and eight-county HGB regions. 53
Table 7.1 Roadside field test site support equipment and analytical instruments 86
Table 7.2 Percent data availability for photocatalytic stucco site – year 1 87
Table 7.3 Data availability for control site – year 1 87
Table 7.4 Percent data availability for photocatalytic stucco site – year 2 88
Table 7.5 Percent data availability for control site – year 2 88
Table 7.6 Mean difference in NO_2 concentrations Site 2 (photocatalytic) minus Site 1 (control)[1,2] 97
Table 7.7 Mean difference in O_3 concentrations Site 2 (photocatalytic) minus Site 1 (control)[12] 99

Table A.1: Absorption and Specific Gravity of Aggregates 111
Table A.2: Tricon Precast Concrete Barrier Mixture Design Sheet 111
Table A.3: Tricon Precast Concrete Barrier Mixture Cylinder Strength Results & Admixture Information 112
Table A.4: Mixture Design Used in The Laboratory-Mixed Slab Specimens 112
Table C.1: Nitrate and Nitrite Concentrations of Wash Water from the Houston Field Site 116
Table C.2: Nitrate and Nitrite Concentrations of Wash Water from the Austin Field Site 118
Table C.3: Nitrate and Nitrite Concentrations of Wash Water from the Lab Field Site 120
Table D.1: Average L* Values of Specimen Surfaces for the Houston Field Site 122
Table D.2: Average L* Values of Specimen Surfaces for the Austin Field Site 123
Table D.3: Average L* Values of Specimen Surfaces for the Lab Field Site 124
Table E.1: Temperature Data for Houston Site 125
Table E.2: Temperature Data for Austin Site 125
Table E.3: Temperature Data for Lab Site 125

Glossary

ANOVA	analysis of variance
AQRP	Texas Air Quality Research Program
ASTM	American Society for Testing and Materials
CAMS	continuous ambient monitoring station
CAMx	Comprehensive Air Quality Model with extensions
CEI	International Commission on Illumination
CMRG	Construction Materials Research Group
DFW	Dallas/Fort Worth
EDS	energy dispersive spectroscopy
EPA	United States Environmental Protection Agency
HGB	Houston/Galveston/Brazoria
LEADS	Leading Environmental Analysis & Display System
NAAQS	National Ambient Air Quality Standards
NO	nitric oxide
NO_2	nitrogen dioxide
NO_x	oxides of nitrogen
O_3	ozone
PMIS	Pavement Management Information System
ppb	parts per billion (by volume)
ppbv	parts per billion by volume
ppm	parts per million (by volume)
PSE	Lenth pseudo standard error
PTFE	polytetrafluoroethylene
RH	relative humidity
SEM	scanning electron microscopy
TiO_2	titanium dioxide
TCEQ	Texas Commission on Environmental Quality
TUV	Tropospheric Ultraviolet and Visible
TxDOT	Texas Department of Transportation
UT	The University of Texas at Austin

VOC	volatile organic compound
XRD	x-ray diffraction
XRF	x-ray fluorescence
ZnO	zinc oxide

Chapter 1. Executive Summary

Air pollution is a topic of concern in numerous urban areas in developed and developing countries. It is responsible for damage to vegetation, animals, materials, and, most importantly, to human health. Nitrogen oxides (NOx) are considered to be one of the key ambient air pollutants (Maynard, 2004). NOx are important not only because of their direct health effects on people but also because they take part in the formation of ground-level ozone (O_3). Hence, finding ways to remove NOx from ambient air would have beneficial health effects as well as reducing ground-level O_3 concentrations. Titanium dioxide (TiO_2) is a naturally occurring semiconductor material that has been used in laboratories studies to remove NOx from air using sustainable, solar energy when in close proximity to NOx sources (Husken et al., 2009; Agrios and Pichat, 2005; Chen and Poon, 2009a).

This study investigated the use of TiO_2-containing coatings for concrete as an abatement method for atmospheric NOx and O_3. The study consisted of four parts: laboratory chamber studies evaluating four different commercially available TiO_2-containing coatings; outdoor exposure studies to evaluate the environmental stability of the coatings; modeling to determine the potential effect of a photocatalytic coating on non-attainment areas in Houston and Dallas; and a field study to evaluate the "real world" effectiveness and durability of the coating found most effective in the first two parts of the study.

The laboratory chamber studies consisted of screening tests, a full factorial experiment to determine the factors influencing the photocatalytic activity of TiO_2, and kinetic studies to measure input parameters for modeling of the photocatalytic affect in the Houston and Dallas metropolitan areas. Four commercial TiO_2-containing coatings were examined in the screening tests, which examined NOx, O_3, and non-methane hydrocarbon removal: a stucco containing TiO_2, two clear commercial paints (clear paints 1 and 2) containing TiO_2, and a white paint containing TiO_2. In these tests, clear paint 1 and the stucco removed the most NOx and non-methane hydrocarbons and were selected for the full factorial experiments. The results from the full factorial experiments were analyzed using analysis of variance (ANOVA), and temperature, relative humidity, light intensity, and contact time were determined to significantly affect NOx removal. This analysis showed that the stucco photocatalytic coating consistently removed more NOx compared to the clear paint, especially after repeated testing of the same sample.

Three of the commercial coatings were tested in outdoor exposure studies in three locations, adjacent to highways in Austin and Houston and at the J. J. Pickle Research Campus in Austin. Exposed samples included "coupons" for laboratory chamber testing and concrete highway barriers. Surface temperature and color change of the photocatalytic coatings and concrete controls were monitored as well as the composition of "wash" water. Small cores were removed and analyzed for composition using x-ray diffraction and scanning electron microscopy. Undamaged coupons were returned to the laboratory for chamber testing. The control and stucco-coated samples were returned to the field and tested for an additional year. Test results suggested that the white paint was ineffective at NOx removal and that the clear paint was washed off following rain or water washing. Therefore, the stucco is the only effective and environmentally stable coating of those examined.

The exposed coupons were chamber-tested to determine the effect of outdoor exposure on NOx removal. Chamber tests conducted after 1 year of outdoor exposure indicated that the Houston area stucco-coated coupon had retained only 50 to 75% of its original NOx removal

capacity. Tests conducted after 2 years of outdoor exposure in Houston found that the stucco coating had retained approximately 30 to 50% of its original NOx removal capacity. After 2 years, the test coupons exposed to Austin weather and traffic had retained approximately 55% to 80% of its original NOx removal capacity. The removal efficiencies for all of the test coupons increased after rinsing the coupons with a soap solution. These results suggest that non-polar materials such as grease or high molecular weight alkanes may be blocking the active sites reducing removal efficiencies. The Houston test coupon showed the lowest removal rates for all conditions, indicating that higher traffic areas may result in faster degradation of photocatalytic performance.

Kinetic data derived from the chamber experiments were integrated into the Comprehensive Air Quality Model with extensions (CAMx; ENVIRON, 2010). Modeled simulations were conducted using two test episodes (i.e., historical time periods) that are utilized by the Texas Commission on Environmental Quality (TCEQ) for attainment demonstrations. Differences between the base case (no photocatalytic coating) and the test case (photocatalytic coating applied to highway barriers in the designated metropolitan area) showed a reduction of the daily 8-hour maximum averaged ozone concentrations in the Dallas-Fort Worth (DFW) area ranging from -0.0001 to 0.09 ppb. Differences in daily maximum 8-hour averaged ozone concentrations in the Houston/Galveston/Brazoria (HGB) area ranged from 0.0006 to 0.04 ppb.

A roadside field test site (test site) was established at the Parmer Lane toll plaza on SH 45 (also known as the Lake Creek Toll Plaza). The site was operated from March 2015 to October 2015 and again from March 2016 to September 2016. The test site consisted of a series of concrete highway barriers coated with the photocatalytic stucco (1100 linear feet [7700 ft^2]) and a similar set of uncoated barriers. The cost of coating the barriers was approximately $20,000 including materials and labor. Sampling stations were placed on the northern side of the roadway in the direction of the prevailing summer winds in Austin. The sampling stations were outfitted with matching O_3 and NOx analyzers. The data from the analyzers and the quality assurance procedures were maintained by Sutron's Leading Environmental Analysis & Display System (LEADS) software, the same software used by the TCEQ to maintain their continuous ambient monitoring stations (CAMs). To determine if there was an effect of the photocatalytic coating on ambient NOx or O_3 concentrations, the data were submitted to an independent statistician. The data were presented to the statistician blind, in that the identity of the sites was not revealed. The statistical analysis was to determine if there were any significant differences between the NOx or O_3 concentrations at the two test sites and if any observed differences persisted or changed with time. Data considered in the analysis were composed of days with at least 18 hours of validated ambient air measurements. Because the ambient air data from the two tests sites were compared as part of the analysis, only those data for which both test sites had complete data could be considered. Using these criteria there were more than 230 days across the two sample seasons that were available for analysis. Overall, after monitoring over parts of 2 calendar years, the statistician reported, "there does not appear to be any consistent evidence of the effectiveness of the photo-catalyst treatment." Differences in the concentrations between the two sites were small, most frequently within the uncertainty of the measurements. Additionally, the maximum observed concentration frequently changed between the sites. For example, for year two the site with the highest O_3 concentration was almost equally divided between the two sites (54% to 46%).

Utilization of photocatalytic materials to reduce ground levels of O_3 depends on a reliable, durable catalytic material. Further, the material must be relatively inexpensive given that the interstate highway system that the Texas Department of Transportation (TxDOT) supports covers thousands of miles alone, without consideration for the other roadways TxDOT maintains such as

the U.S. highways, state highways, farm-to-market roads, tollways, etc. Without a statistically significant reduction in ground level NOx or O_3, use of the selected photocatalytic stucco, at the current cost, cannot be considered an option for air pollution abatement.

Chapter 2. Literature Review

2.1 Introduction

Air pollution is a topic of concern in numerous urban areas in developed and developing countries. It is responsible for damage to vegetation, animals, materials, and most importantly to human health. Nitrogen oxides are considered to be one of the key ambient air pollutants (Maynard, 2004). Nitric oxide (NO) and nitrogen dioxide (NO_2) are the two major components of oxides of nitrogen (NO_x). NO_x is mainly emitted during combustion processes in power plants, vehicles and industrial applications (Chaloulakou et al., 2008). NO_2 is also formed in the atmosphere by oxidation of NO.

Exposure to NO_2 has been associated with cardiovascular and pulmonary diseases (Brunekreef and Holgate, 2002). Nitrogen oxides in the atmosphere are also responsible for acid rain and are precursors of another major and even more harmful air pollutant: ozone (Lippmann, 1989; Marsili-Libelli, 1996). Hence, finding novel ways to remove NO_x from ambient air could have beneficial effects. Photocatalytic materials may have the ability to remove such pollutants from air using sustainable, solar energy when applied in close proximity to one of the major NO_x sources, roadways (Agrios and Pichat, 2005; Chen and Poon, 2009a).

2.2 Titanium dioxide photocatalysts

Titanium dioxide (titania, TiO_2) is a naturally occurring compound that is used in a variety of applications, from consumer products to architectural coatings. It is also the preferred semiconducting material for photocatalytic applications (Husken et al., 2009). There exist in nature three main TiO_2 structures, or phases: rutile, anatase, and brookite. Rutile is the most common and thermodynamically stable form and is used mostly as a paint pigment. Brookite is rare and has few general commercial applications (Beeldens and Van Gemert, 2004; Maynard, 2004). Anatase is chemically stable at room temperature, nontoxic, and economically favorable for use as a photocatalyst when compared to other semiconducting materials like zinc oxide (ZnO) (Chaloulakou et al., 2008; Husken et al., 2009). The most common, commercially available form of TiO_2 for photocatalysis is Degussa P-25, with an average primary particle size of 21 nm and an 80/20 anatase-to-rutile ratio (Brunekreef and Holgate, 2002; Strini et al., 2005). Many researchers investigating photocatalytic materials have utilized this commercial product for direct testing or for comparison to other semiconducting materials.

While anatase is generally considered the most practical and best-suited TiO_2 phase for photocatalytic applications, substantial research has gone into mixed-phase preparations. Toma et al. (2004) studied the removal of NO_x by varying parameters of TiO_2 material including mass of catalyst, surface area containing the photocatalyst, and the anatase-to-rutile ratio, which was varied by changing the cooling temperature of heated P-25 powder. They found that better photocatalytic removal occurred with higher ratios of anatase to rutile at temperatures below 600°C (Lippmann, 1989; Marsili-Libelli, 1996; Toma et al., 2004a). Ozawa et al. (2005) claimed that mixed-phase titania preparations can have higher photocatalytic performances than pure anatase or pure rutile in terms of reduction of acetaldehyde (CH_3CHO). They also stated that an anatase-brookite combination is more effective at reducing this same pollutant than pure anatase, probably due to the "anatase-brookite coupling, resulting in an increase in charge separation efficiency" Ozawa et al., 2005).

Some researchers have explored creating photocatalytic materials through new processes or doping existing photocatalysts with metals to try to achieve improved photocatalytic efficiency. Znaidi et al. (2001) used a sol-gel method, in which hydrolysis and polymerization of a metal alkoxide are controlled at room temperature to produce an amorphous powder; the process is followed by a thermal treatment that crystallizes the powder. They compared the photochemical activity of several sol-gel synthesized TiO_2 powders with commercial powders including Degussa P-25. Results of this research showed that the commercial Degussa P-25 achieved higher photocatalytic degradation of phenol than the TiO_2 synthesized in the study (Znaidi et al., 2001; Husken et al., 2009).

Pepe et al. (2004) tested photocatalytic efficiency of TiO_2 materials doped with low amounts of metal ions. Both sol-gel prepared TiO_2 and commercial products were tested. The TiO_2 was applied to cementitious and marble substrates for testing. It was found that metal doping can result in enhanced photocatalytic degradation of pollutants, and that the magnitude of enhancement is a function of the nature of the doping elements and the amount and structure of TiO_2. In particular, magnesium enhanced the photocatalytic activity of rutile; however, the magnesium-doped rutile material still had lower photocatalytic activity than the pure anatase form (Pepe et al., 2004).

2.3 Photocatalysis on titanium dioxide

Photocatalysis is a process that occurs at the surface of a semi-conductor exposed to light. When a photon with energy equal to or larger than the band gap of the semiconductor is absorbed, an electron (e^-) from the valence band is promoted to the conduction band. The result is the presence of a "hole" in the valence band (h^+). The h^+ and e^- are strong oxidizing and reducing agents, respectively. The electron-hole pair may react with electron donors or acceptors adsorbed on the semi-conductor surface. If reaction does not occur, the electron-hole pair recombines and the energy is dissipated as heat (Fujishima and Honda, 1972; Hoffmann et al., 1995; Chen and Poon, 2009a). Oxygen and water, adsorbed at the semi-conductor surface, are catalyzed to form reactive species, superoxide anion (O_2^-) and hydroxyl radical (OH•):

$$h^+ + H_2O \rightarrow OH^{\bullet} + H^-$$

$$e^- + O_2 \rightarrow O_2^-$$

Hydroxyl radicals and superoxide anions are strong oxidizing and reducing agents, respectively. They can react with pollutant molecules adsorbed to the photocatalytic surface, such as NO_x or hydrocarbons, to form nitric acid, carboxylic acids, or carbon dioxide (Dalton et al., 2002; Allen et al., 2005; Ballari et al., 2010a; Laufs et al., 2010; Ohko et al., 2010).

2.4 TiO_2 application methods

Many researchers have tested the efficiency of TiO_2 when added to cement during mixing of concrete, cement paste, or other cementitious materials. Dylla et al. (2010) tested the relative photocatalytic efficiency of four TiO_2-containing concrete mixtures by varying two material parameters, fines content and percentage of TiO_2. Concrete slabs were prepared with 3 and 5% by mass of commercially available TiO_2 nanomaterial (Cristal Millennium PC105). The higher concentration of TiO_2 showed a slightly higher photocatalytic activity in this experiment; however,

according to the authors, it was not certain whether this increase justified the higher cost associated with increased TiO_2 concentration (Dylla et al., 2010).

Kawakami et al. (2007) studied NO_x removal capabilities of cement mortars, varying TiO_2 particle size and TiO_2 concentration. The preparations with the smallest particle sizes of TiO_2 were found to be the best at removing NO_x. The mortar specimens containing the finest particle size TiO_2 also exhibited considerably higher flow and lower air content compared to other preparations (Kawakami et al., 2007).

Several researchers studied the photocatalytic efficiency of TiO_2 applied as a surface covering. Hassan et al. (2010) conducted a study of several application methods of TiO_2 to the exterior of concrete pavement. The methods tested included a thin coating consisting of sand, cement, TiO_2, and water; a water-based hardened concrete surface treatment commercially known as PURETi; and sprinkling nano-sized TiO_2 onto a fresh concrete surface directly after casting. Each method was evaluated in terms of photocatalytic efficiency. They found that the thin coating with 5% TiO_2 and the PURETi product were the most efficient at removing nitrogen oxide (Hassan et al., 2010). Murata et al. (2000) found concrete paving blocks with a 5–7 mm layer of TiO_2 in cement mortar to be an effective method for NO_x removal (Murata et al., 2000).

Rachel et al. (2002) examined different application techniques of TiO_2-containing surface coatings, including the sol-gel method, sputtering, and a patented method for coating inorganic fibers with TiO_2. Several sol-gel methods were used to produce the TiO_2 and then the material was applied by dip-coating. Sputtering refers to thin film deposition by ejecting atoms from a substrate through bombardment with energetic particles. An additional method in which TiO_2 was mixed with white cement and water to form a thin layer was also studied (Rachel et al., 2002). Each of these methods was compared in terms of photocatalytic efficiency. It was found that for certain substrates, the sol-gel method was less efficient than a TiO_2 slurry due to the comparatively smaller active surface produced by the sol-gel technique.

Agrios and Pichat (2005) compared various preparations of TiO_2 on fixed supports, including the sol-gel method and synthesis of mixed-phase TiO_2. Regarding films, they discussed several significant challenges to placing TiO_2 as a thin coating on organic materials, including thermal issues and photocatalytic degradation of the substrate. To counter this problem, they suggested that low temperature sol-gel techniques can be performed, or "cold sintering," which applies high pressure to fuse crystals of TiO_2 into a film. The use of an intermediate layer between the substrate and TiO_2 film can also reduce photocatalytic degradation issues (Agrios and Pichat, 2005).

Two studies compared TiO_2 as an additive to cement versus applied as a surface covering for mortar. Strini et al. (2005) found that a pure TiO_2 film achieves a much greater photocatalytic activity than samples with varying amounts of photocatalytic material added to the cement matrix (Strini et al., 2005). Diamanti et al. (2008) also compared TiO_2-containing mortars in which photocatalytic materials were added to the cement either in powder form, as an aqueous suspension, or as a surface covering. This test found that the specimens containing TiO_2 as a surface covering were the most efficient (Diamanti et al., 2008).

Several studies examined commercial photocatalytic paints. Auvinen and Wirtanen (2008) tested six different interior photocatalytic paints with varying binder systems for their effects on indoor air quality in terms of elimination of VOCs. They found that aged, water-borne lime paint achieved the lowest VOC removal, indicating that the chemical nature of the paints may change with aging. Varying the substrate, including glass, gypsum, or plaster, did not affect photocatalytic efficiency of the paints (Auvinen and Wirtanen, 2008). Laufs et al. (2010) investigated the impact

of pigmentation on reduction of NO_x from commercial TiO_2-containing paints. They found that the non-catalytic TiO_2 contained in the white paint might have reduced the amount of active sites, thereby contributing to its decreased photocatalytic activity compared to a blue paint (Laufs et al., 2010).

2.5 Laboratory scale photocatalytic oxidation research

Numerous studies of photocatalytic removal of air pollutants have been carried out at the laboratory scale. Most of these studies have focused on the capacity of TiO_2 containing materials to remove a single pollutant. As a result, the materials studied were usually exposed to air containing only the one pollutant of interest instead of a mixture of pollutants similar to what can be found in urban outdoor air. Moreover, realistic environmental conditions or air mixtures were rarely used in previous laboratory studies, making it difficult to evaluate expected removals in outdoor air. However, the results from previous laboratory studies can be used to better understand the mechanisms leading to the oxidation of NO_x and other pollutants and what parameters affect the photocatalytic process.

2.5.1 Nitrogen oxides removal

Nitrogen oxides (NO_x) are pollutants of concern because of their role in the photochemical processes occurring in urban atmospheres (Marsili-Libelli, 1996). Numerous researchers have focused on NO_x removal through photocatalysis as a possible pathway to reduce NO_x concentrations in outdoor air.

Proposed reaction mechanisms

There is disagreement in the literature about the mechanisms that take place during the heterogeneous photocatalysis of NO_x. Understanding the mechanisms involved in these reactions is necessary in order to properly describe and evaluate the kinetic parameters controlling the reaction process.

It is commonly accepted in the literature that the reactive species created at the surface of the photocatalytic material are OH• and O_2^- (Hoffmann et al., 1995; Fujishima et al., 2008). Two mechanisms for the destruction of NO have been proposed, each involving one of these reactive species as the initiator of the removal process.

Several researchers (Devahasdin et al., 2003; Hunger et al., 2010; Ballari et al., 2010a) proposed a mechanism involving hydroxyl radicals and it is the most commonly used mechanism in the literature. The proposed mechanism is as follows:

$$NO_{ads} + OH^{\bullet} \rightarrow HNO_2$$
$$HNO_2 + OH^{\bullet} \rightarrow NO_{2,ads} + H_2O$$
$$NO_{2,ads} + OH^{\bullet} \rightarrow HNO_3$$

This mechanism requires the presence of water since the oxidant OH• is created by photolysis of water on the photocatalytic surface. However, the presence of oxygen is not required since the superoxide anion O_2^- is not involved in the reaction mechanism.

In contrast, a different mechanism has been hypothesized by Hashimoto et al. (Hashimoto et al., 2000) and recent experimental data tend to confirm its validity (Laufs et al., 2010). The proposed mechanism is as follows:

$$O_2^- + H_2O \rightarrow HO_2 + OH^-$$
$$HO_2 + NO \rightarrow NO_2 + OH^{\bullet}$$
$$NO_2 + OH^{\bullet} \rightarrow HNO_3$$

This mechanism was proposed because during experiments conducted in pure nitrogen instead of air, photocatalytic destruction of NO was nonexistent (Laufs et al., 2010). Hence, it was asserted that oxygen played a role in the photocatalytic destruction of NO, through the superoxide anion.

Dependencies

Irradiance

Several researchers have studied the effect of irradiance on the photocatalytic activity of TiO_2 (Lim et al., 2000; Lin et al., 2006; Bengtsson and Castellote, 2010; Monge et al., 2010; Ballari et al., 2010a; 2011). Both the light intensity and the nature of the light have been shown to have an effect on the photocatalytic activity of TiO_2. Given the large variations in experimental conditions used to test photocatalytic materials, and the variation in materials tested themselves, it is difficult to quantitatively compare results from different studies. However, some qualitative results have been found across different studies (Ollis et al., 1991; Lim et al., 2000; Ballari et al., 2010b; Bengtsson and Castellote, 2010). The photocatalytic activity of TiO_2-containing materials increases linearly with light intensity for low light intensity, until light intensity reaches about one sun equivalent (1 mW cm^{-2}). Above that cut off, the photocatalytic activity increases proportionally to the square root of the light intensity (Bengtsson et al., 2010, Ollis et al., 1991).

Temperature

There is little published literature concerning the effect of temperature on NO_x conversion on photocatalytic surfaces. Two studies were conducted to evaluate the effect of temperature on photocatalytic decomposition of NO by TiO_2 for two different temperature ranges. In a realistic outdoor temperature range (21–30°C), Bengtsson and Castellote (2010) found that NO conversion decreased very slightly with increased temperature (Bengtsson and Castellote, 2010). However, for much higher temperatures (37–227°C), Lim et al. (2000) found increased NO conversion with increasing temperature (Lim et al., 2000). Summertime surface temperatures can exceed the lower-bound temperature studied by Lim et al. (2000).

Humidity

Numerous studies have looked at the effect of variations in relative humidity (RH) on the photocatalytic activity of materials containing TiO_2 for removal of NO_x. Researchers agree on the fact that high RH reduces photocatalytic activity, and it is assumed that competitive adsorption is responsible for this effect. When the RH of the air surrounding the photocatalytic surface is

increased, water molecules adsorb to the surface in higher quantity, leaving fewer empty surface sites for NO and NO_2 molecules to be adsorbed and oxidized. However, researchers have found varying levels of RH from which the activity starts to decrease. In a study of commercially available photocatalytic paints (Maggos et al., 2007a), it was found that photocatalytic activity decreased between 20 and 50% RH. Murata et al. (2000) tested NOxer concrete blocks and found 30% to be the threshold after which activity decreased (Murata et al., 2000). Ballari et al. (2011) found that the conversion of NO and NO_2, separately or in a mixture in the ppb range, decreased almost linearly with increasing RH, in the range of 10–70% RH (Ballari et al., 2011). Dylla et al. (2010) and Hüsken et al. (2009) found similar results for NO in the range of 30–80% RH (contact times between 2.4 and 7.1 minutes) and 10–80% RH (contact time of 1.2 seconds), respectively, with conversion decreasing from about 35–40% at low RH down to 15% at high RH (Husken et al., 2009; Dylla et al., 2010). Laufs et al. (2010) also found similar results for NO and NO_2 in the 10–80% RH range. However, they also looked at changes between 0 and 10% RH. In that narrow range, they found a strong increase in NO_2 conversion while NO conversion decreased faster for RH values greater than 10% (Laufs et al., 2010).

Bengtsson et al. (2010) noted a different behavior where NO conversion was constant in the 0–40% RH range and decreased for higher values of RH. The inlet NO concentration was higher than for previous experiments, around 1 ppm. They concluded that water was not necessary for NO conversion since it was higher in dry conditions, and the opposite conclusion was made for NO_2 (Bengtsson and Castellote, 2010).

Devahasdin et al. (2003) worked with source levels of NO, in the ppm range, and found a different effect of RH on conversion of NO. The NO conversion actually increased with increasing RH up to 50%, after which the NO conversion remained constant up to 75% RH (Devahasdin et al., 2003).

Concentration

Bengtsson et al. (2010) found that in the concentration range between 100 and 1000 ppb, the conversion rate of NO is not dependent on the initial concentration injected into the test chamber, confirming that the reaction is this concentration range is first order (Bengtsson and Castellote, 2010). Laufs et al. (2010) confirmed this result in the 25 to 1000 ppb concentration range and showed that it was true for NO_2 decomposition as well. Also, when introducing both NO and NO_2 to the chamber inlet, the individual reaction rates of each species were not affected, suggesting that there is no inhibition of the decomposition of one compound by the other (Laufs et al., 2010).

Lim et al. (2000) found a different result where NO conversion decreased with increased inlet concentration. They were, however, working with source concentrations of 50 ppm and above, which are not observed in ambient air and hence less relevant for this project (Lim et al., 2000).

Contact time

The length of time that the pollutant of concern is in the vicinity of the photocatalytic surface is an important factor in determining the removal efficiency achieved by the material. Most researchers have found that a longer contact time increased conversion of NO_x (Devahasdin et al., 2003; Husken et al., 2009; Bengtsson and Castellote, 2010; Dylla et al., 2010; Ballari et al., 2011). Devahasdin et al. (2003) also noticed that, as contact time increased, NO_x conversion eventually reached a plateau where increasing contact time did not improve conversion (Devahasdin et al.,

2003). Fluid mechanics around the surface of the photocatalytic material also influences NO_x removal. In order to reduce contact time, researchers increase gas flow rate through their test reactor. In some cases, as noted by Laufs et al. (2010), this changes the fluid conditions around the material surface. If the air flow becomes turbulent over a larger section of the material, transport of the pollutant to the surface is increased, making NO_x removal more efficient (Laufs et al., 2010). In that case, the contact time is not the defining factor as much as air movement over the surface.

Catalyst load

Several researchers have found that NO_x conversion increased with the catalyst load present in the photocatalytic material, until reaching a plateau (Devahasdin et al., 2003; Toma et al., 2004b; Husken et al., 2009; Ohko et al., 2009; Puzenat, 2009; Chen and Poon, 2009a; Bengtsson and Castellote, 2010). Puzenat (2009) explained that a plateau is reached because, when a certain load is present, not all the TiO_2 can be completely illuminated. This limit depends on the type of matrix that the TiO_2 is mixed into for the fabrication of the final material, since this will influence light penetration. Influence of catalyst load on various photocatalytic materials such as cement pastes (Chen and Poon, 2009a), mortars (Husken et al., 2009; Bengtsson and Castellote, 2010) and TiO_2 slurry (Devahasdin et al., 2003; Ohko et al., 2009) were studied in the literature. The effect of catalyst loading on paints has not been reported.

During experiments focused on removal of NO by TiO_2 particles supported on silica gel, Lim et al. (2000) found that 1.8 milligrams of NO were decomposed for each gram of TiO_2. After this NO conversion had been reached, no further oxidation occurred, even when varying contact time in the reactor. However, the NO concentration used for the experiment was in the hundreds of ppm, three orders of magnitude higher than concentrations found in ambient air (Lim et al., 2000). Further research is necessary to elucidate when the active sites of paints and other types of coatings are saturated.

By-product formation

Photocatalytic oxidation of NO_x is accompanied by the formation of by-products both in air and on the photocatalytic material surface. If complete oxidation occurs, the final product is nitric acid (HNO_3), adsorbed on the material surface (Dalton et al., 2002; Ohko et al., 2009; Laufs et al., 2010). The HNO_3 can be removed by water to regenerate the photocatalytic surface. There is not agreement in the literature about other by-products that can be created during photocatalytic oxidation of NO_x. For various types of photocatalytic surfaces, researchers have found that, in case of incomplete oxidation, intermediates of the oxidation process can be detected at the surface or in the air above the surface (Gustafsson et al., 2006; Bowering et al., 2007; Langridge et al., 2009; Ohko et al., 2010); reported intermediate products include nitrate (NO_3), NO_2, dinitrogen pentoxide (N_2O_5), nitrous oxide (N_2O) and nitrous acid (HNO_2). However, on photocatalytic paints, Laufs et al. (2010) did not find significant formation of HNO_2, N_2O and H_2O_2, and other by-products were not reported.

Monge et al. (2010) also found ozone to be a by-product of photocatalytic oxidation of NO_x during batch experiments under natural and artificial sunlight. This is the only study that reported formation of ozone.

2.5.2 VOC removal

Photocatalytic oxidation can also be applied for the mineralization of volatile organic compounds (VOCs). If complete mineralization is obtained, products of the VOC destruction are CO_2 and H_2O only. However, there is concern about the potential formation of other by-products from these reactions, as well as the competition that could occur between VOCs and NO_x for adsorption to reaction sites.

Pollutants studied and effectiveness

VOC removal through photocatalytic oxidation has been tested in the past; however, many of the studies do not necessarily have direct applicability to pollutant removal in ambient air. Most researchers have studied removal of one or a few specific VOCs and avoided mixtures (Alberici and Jardim, 1997; Lichtin and Sadeghi, 1998; Muggli et al., 1998; Obuchi et al., 1999; Einaga et al., 2002; Ao et al., 2003; Wang and Ku, 2003; Imoberdorf et al., 2005; Liu et al., 2006; Ye et al., 2007; Bouazza et al., 2008). Moreover, the concentrations usually studied correspond to levels greater than common ambient levels in urban areas, which are typically in the sub-ppm to low ppm range (Jia et al., 2008; Lu et al., 2010). Various types of VOCs have been studied and mineralization mechanisms have been postulated for some of them.

Alcohols, aldehydes, alkanes, and carboxylic acids are usually involved in chain reactions during photocatalytic oxidation (Obee and Brown, 1995; Muggli et al., 1998; Obuchi et al., 1999; Huang et al., 2003; Liu et al., 2006; Ye et al., 2006). Hydroxyl radicals can attack adsorbed molecules at the photocatalytic surface. Alcohols are photocatalytically oxidized to the corresponding aldehyde. Subsequently, aldehyde photocatalytic oxidation forms a corresponding carboxylic acid or a shorter carbon chain aldehyde. This process shortens aldehyde chains until formaldehyde is formed, which then produces formic acid and finally CO_2 and H_2O (Figure 2.1). Depending on the amount of reactive species present on the photocatalytic surface and the time available for the reactions to occur, almost complete mineralization can be obtained. Conversion rates of about 20 to 50%, depending on experimental conditions, were usually obtained for these families of VOCs (Obuchi et al., 1999; Ye et al., 2006) (contact times were not reported).

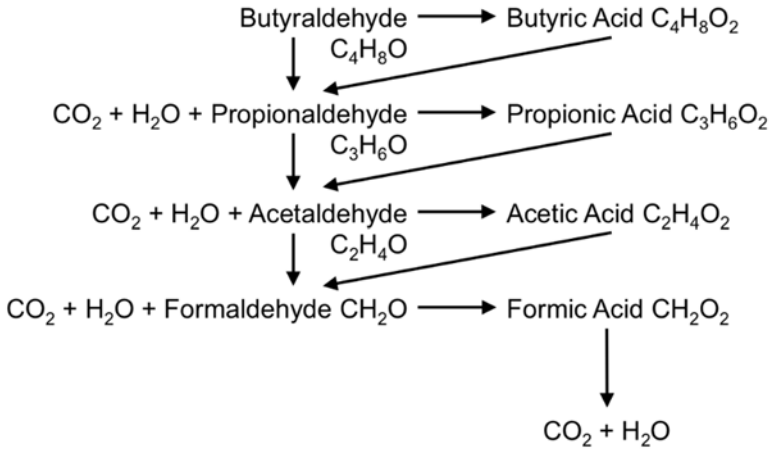

Figure 2.1 Photocatalytic oxidation of butyraldehyde (from Ye et al., 2006)

Photocatalytic oxidation of aromatic hydrocarbons such as benzene and toluene have also been extensively studied (Obee and Brown, 1995; Alberici and Jardim, 1997; Lichtin and Sadeghi,

1998; Einaga et al., 2002; Ao et al., 2003; Wang and Ku, 2003; Bouazza et al., 2008). The mechanisms leading to the mineralization of those compounds are not as well understood and there is disagreement in the literature about the extent of mineralization that occurs for these compounds. Some researchers have found that the mineralization was complete and only CO_2 and H_2O were produced (Obee and Brown, 1995; Wang and Ku, 2003), while others reported formation of carbon deposits that caused deactivation of the catalyst since the intermediates were strongly adsorbed to the surface. The carbon deposits also changed the color of the photocatalytic material (Alberici and Jardim, 1997; Lichtin and Sadeghi, 1998; Einaga et al., 2002; Ao et al., 2003; Bouazza et al., 2008). Obee and Brown (Obee and Brown, 1995) worked with significantly lower concentrations (sub-ppm levels) than other researchers, which might explain the difference in observations for deactivation by carbon deposits. Phenol has been found to be a by-product of benzene in the early stages of photocatalytic oxidation (Einaga et al., 2002; Wang and Ku, 2003). If contact time permits further oxidation, the aromatic ring can be broken producing carboxylic acids, ketones and alkynes (Wang and Ku, 2003).

Alkenes and alkanes and other hydrocarbons have also been studied by a few researchers (Obee and Brown, 1995; Brigden et al., 2001; Bouazza et al., 2008; Poulston et al., 2009). They found that these chemicals were usually efficiently converted by photocatalytic surfaces with removal rates between 60 and 100%, depending on experimental conditions (contact time of 2 minutes for Poulston et al., 2009 and Brigden et al., 2001; others were not reported). The only by-products reported were CO_2 and H_2O. Spectrophotometry (Brigden et al., 2001; Bouazza et al., 2008; Poulston et al., 2009) and gas chromatography (Obee and Brown, 1995; Brigden et al., 2001; Poulston et al., 2009) were used to measure species concentrations.

Dependencies

Contact time influences the amount of VOC conversion that occurs at the surface of the photocatalytic material. Ye et al. (2007) found that increasing contact time increased conversion for various aldehydes and tetrachloroethylene (PCE). Increasing the contact time by a factor of eight (contact times between 1 and 16 seconds) roughly increased the conversion from 20 to 80% (Ye et al., 2007). Ao et al. (2003) found similar trends for aromatic hydrocarbons.

The presence of humidity also affects how VOCs are removed by photocatalytic surfaces. Humidity seems to affect VOC removal differently, depending on the specific properties of the VOC. Some researchers found that increased humidity led to increased conversion for benzene, toluene, and cyclohexene (Lichtin and Sadeghi, 1998; Einaga et al., 2002; Bouazza et al., 2008), but others found the opposite effect, including for some of the same VOCs (Einaga et al., 2002; Ao et al., 2003; Imoberdorf et al., 2005; Bouazza et al., 2008). Bouazza et al. (2008) noted that the adsorption affinity of the VOC of interest to the photocatalytic surface compared to the adsorption affinity of water was an important factor. If the VOC has a higher adsorption affinity than water, increased RH will not significantly affect the amount of VOC adsorbed on the surface but will lead to increased formation of hydroxyl radicals that oxidize VOCs. On the other hand, a VOC that has an adsorption affinity lower than that of water will lose adsorption sites to water, hence reducing the amount of VOC that is oxidized (Bouazza et al., 2008). Obee et al. (1995) also found that bi-molecular Langmuir adsorption accurately described the effect of water vapor on the removal of VOCs by photocatalytic surfaces. They found that there was an RH value for which the conversion reached a maximum, and that RH value depended on the gas phase concentration of the VOC of interest. Lower gas phase VOC concentrations were converted best at low humidity, while higher gas phase concentrations were more effectively oxidized at higher humidity levels. This behavior

was observed for various types of VOCs, including an aldehyde, an aromatic hydrocarbon, and an alkene (Obee and Brown, 1995).

Light intensity also affects VOC conversion by photocatalytic surfaces. Several researchers have found that increasing light intensity also increased VOC conversion (Ollis et al., 1991; Obee and Brown, 1995; Wang and Ku, 2003; Ching et al., 2004; Imoberdorf et al., 2005; Shiraishi et al., 2005). Ching et al. (2004) and Ollis et al. (1991) reported an empirical relationship between light intensity and reaction rate for formaldehyde photocatalytic oxidation: the oxidation rate is proportional to the light intensity for low intensities, proportional to the square root of the intensity for medium intensities and constant for high intensities. However, quantitative bounds for low, medium, and high intensities were not given. Moreover, the type of UV light source (and associated wavelengths emitted) was not found to affect VOC removals.

A few researchers (Ao et al., 2003; Chen and Zhang, 2008; Poulston et al., 2009) have studied the photocatalytic oxidation of mixtures of VOCs. Chen et al. (2008) found that for mixtures containing up to three VOCs, there was no interference and each VOC was removed as if it were alone. However, when testing a mixture containing 16 VOCs, interferences appeared. In that case, the VOCs that had the strongest adsorption affinity with the photocatalytic surface were more likely to be oxidized.

Ao et al. (2003) and Poulston et al. (2009) studied mixtures that included both VOCs and NO_x. Ao et al. (2003) found that the presence of VOCs in the mixture decreased the amount of NO converted but, on the other hand, the presence of NO increased the conversion of the VOC, probably because of NO_2 (product of the oxidization of NO) reacting with the VOC. Poulston et al. (2009) did not find such consistent results when testing alkanes and alkenes in the presence of NO. Propene and ethane had similar or better conversions in the presence of NO but ethane conversion was lower. On the other hand, increasing VOC concentrations were accompanied by increasing NO conversion, except for propene, which had the opposite effect.

2.6 Substrate/TiO_2 interactions and durability of photocatalytic specimens

2.6.1 Effect of substrate properties on photocatalysis

Many researchers have explored the effects of the properties of the substrate on photocatalytic efficiency. Fernandez et al. (1995) characterized TiO_2 applied to different rigid substrates, including glass, quartz, and steel. Deposition on glass and quartz was conducted using a dip-coating procedure and on stainless steel by an electrophoretic deposition process. Samples were evaluated for photocatalytic activity and also for surface properties using x-ray photoelectron spectroscopy, scanning electron microscopy with energy dispersive spectroscopy (SEM/EDS), x-ray diffraction (XRD), and UV-VIS absorption spectroscopy. The quartz substrate specimen was found to show the greatest photocatalytic activity and also showed better crystallization of the anatase structure than the glass substrate. The TiO_2 deposited on steel had a greater percentage of rutile due to the high temperature associated with the deposition process. The migration of cationic impurities including Si^{4+}, Na^{+}, Cr^{3+}, and Fe^{3+} to the TiO_2 layers in glass and steel contributed to decreased photocatalytic activity of these prepared materials (Fernandez et al., 1995).

Rachel et al. (2002) studied the photocatalytic efficiency of Degussa P-25 TiO_2 applied to glass, cement, red brick, and inorganic fibers. These efficiencies were compared to that of Degussa P-25 in aqueous suspension. For the sputtering application, photocatalytic efficiency was negligible. For the sol-gel technique, it appeared that glass achieved higher photocatalytic efficiency than red brick or cement. The inorganic fibers achieved the highest photocatalytic

activity of the materials tested, although the authors stated that method of application might have been more influential on photocatalytic efficiency than substrate composition (Rachel et al., 2002). Auvinen & Wirtanen (2008), in their study of photocatalytic interior paints on indoor air quality, found that substrates had no noteworthy influence on photocatalytic behavior. The substrates tested included glass, gypsum plaster, and polymer-modified plaster (Auvinen and Wirtanen, 2008).

Surface roughness of the substrate was found to be an important parameter governing photocatalytic efficiency. Husken et al. (2009) examined the application of two commercial TiO_2 products incorporated into concrete paving blocks. High surface roughness was found to contribute to higher photocatalytic activity due to the increased availability of the active surface area. Ramirez et al. (2010) found that higher surface roughness contributed to good adhesion of the photocatalytic material during the dip-coating process. For example, a plaster substrate retained most of the TiO_2 after dip-coating, which presumably is an indication of an ability to maintain photocatalytic activity. Weathering behaviors were also evaluated in this study, and it was determined that concrete substrates were less abraded than plasters. Surface roughness was shown to play a role in durability and adhesion of photocatalytic material in this case (Ramirez et al., 2010). Dehn et al. (2004) were in agreement with these results, recognizing the advantage of roughening the concrete surface so as to increase stability of a coating and thus, its reactivity (Dehn et al., 2004).

2.6.2 Effect of concrete properties on photocatalysis

Many studies addressed concrete substrates specifically, with photocatalytic material used as an admixture to cement or applied as a surface covering. Several researchers looked into designing a specific concrete mixture that would enhance pollutant removal. Poon & Cheung (2007) discussed the influence of recycled materials incorporated into the concrete mix on photocatalytic efficiency. They found that recycled aggregate achieved a much higher removal than sand, and that this removal was enhanced slightly when furnace bottom ash was also incorporated. Higher porosity of the material was found to have a direct influence on photocatalytic activity. Incorporation of glass led to greater light transmittance of the concrete, allowing UV irradiation to penetrate the substrate more fully. Poon & Cheung (2007) also found that the recycled concrete with larger aggregate sizes achieved a higher porosity and therefore a higher photocatalytic activity.

Ramirez et al. (2010) confirmed the relationship of porosity and photocatalytic efficiency in their study, finding that TiO_2 adhered more successfully to porous substrates and thus achieved higher reaction rates. Ruot et al. (2009) measured pore size distribution directly and were able to show that higher porosity influenced photocatalytic efficiency (Ruot et al., 2009). Dylla et al. (2010) studied the effect of varying both fines content and percentage of TiO_2 on photocatalytic efficiency. There was a significantly higher photodegradation rate achieved when fines were eliminated from the mix. Laufs et al. (2010), in their study on indoor paint, found that the addition of non-photocatalytic material into a photocatalytic paint reduced the photocatalytic activity by reducing number of pores and therefore active sites. Higher porosity mixes achieved higher photocatalytic activity, confirming the results found in the other studies.

Lackhoff et al. (2003) found that photocatalytic activity of several cementitious specimens with both TiO_2 and ZnO used as semiconductors was reduced due to cement ageing, most rapidly during the first 4 weeks. After 8 weeks, it was found that photocatalytic efficiency stabilized. The authors suggested that this result could be explained by a reduction of active sites due to carbonation. Carbonation decreases sorptivity, increases weight of cement, and can lead to calcite formation, which blocks the cement surface pores (Lackhoff et al., 2003). Chen & Poon (2009)

found that the number of active photocatalytic sites was the most important factor in determining photocatalytic efficiency. These authors found that NO_x removal decreased with increasing curing age due to filling of capillary pores and carbonation (Chen and Poon, 2009b).

2.6.3 Effect of TiO_2 on substrate properties

Several researchers looked at the effects of adding a photocatalyst admixture to concrete on the concrete property development. Both Jayapalan et al. (2010) and Lee et al. (2010) suggested that the addition of TiO_2 nanoparticles accelerates early hydration of cement as additional nucleation sites are provided (Jayapalan et al., 2010; Lee et al., 2010). Jayapalan et al. (2010) also suggested that nanoparticles increase the rate of concrete shrinkage. Lackhoff et al. (2003) found than concrete specimens containing TiO_2 photocatalysts had higher compressive strengths than those containing ZnO additions. Kawakami et al. (2007) found that compressive strength, modulus of elasticity and flexural strength decreased proportionally with increasing amount of TiO_2 between 5% and 15%. These researchers also evaluated flow and air content of the mortars and found these properties to be related to type of TiO_2 rather than its amount.

Zhang (2011) studied the impact of TiO_2 additions on the compressive strength of pavement concrete mixtures. Additions of 0.5, 1, 2, and 3% of TiO_2 by mass of cement were tested. Strength was enhanced with addition of nanoparticles most significantly for addition of 1% of TiO_2 (Zhang, 2011). Comparing the Zhang (2011) and Kawakami et al. (2007) studies, there appears to be an optimum amount of TiO_2, beyond which enhancement of strength properties is reduced. This is because of optimization of the filler effect, as described by Lothenbach et al. (2011). Murata et al. (2000) found that concrete paving blocks containing a layer of TiO_2 had comparable compressive strength and skid resistance to concrete blocks without a TiO_2 layer (Murata et al., 2000).

Zhang & Li (2011) looked at chloride permeability of two types of pavement concrete containing nanoparticles. Both SiO_2 and TiO_2 were tested. They found that TiO_2 was the more effective at reducing chloride penetration. This is because the TiO_2 created finer concrete pore structures with higher resistance to chloride penetration (Zhang and Li, 2011).

2.6.4 Durability of photocatalytic specimens

Several studies examined the durability of photocatalytic specimens. Hassan et al. (2010) studied abrasion resistance and load wheel testing (LWT) for concrete specimens prepared with several types of photocatalytic coatings including PURETi, a thin coating similar to stucco, and sprinkling TiO_2 on fresh concrete. Two concentrations of TiO_2 were used in the thin coating and sprinkling method, 3 and 5%. The highest NO removal efficiency after the LWT was found for the PURETi product. The highest removal after the rotary abrasion test was for the 5% thin coating. The results of the LWT indicate that NO removal efficiency of the weathered samples improved over the original state for all samples except the 5% TiO_2, which decreased only slightly in efficiency. The authors attributed this to the exposure of active sites below the surface caused by this type of weathering. Rotary abrasion appeared to decrease the NO removal efficiency for the 5% coating as well as the PURETi product, and improved it for the other specimens. All samples were evaluated using scanning electron microscopy (SEM) and it was found that PURETi had a much more uniform distribution of TiO_2 compared to the sprinkling method (Hassan et al., 2010).

Ramirez et al. (2010) also studied weathering resistance of photocatalytic materials on cementitious substrates. Cementitious specimens were prepared using the sol-gel method and then were exposed to varying abrasion conditions. Specimens were analyzed for retention of TiO_2 using

SEM with EDS. The more porous and rough specimens were found to retain more TiO_2 particles after abrasion. For example, plasters were more affected by abrasion than concrete substrates (Ramirez et al., 2010).

Several researchers looked at durability of concrete using long-term outdoor exposure tests. Yu (2003) found that photocatalytic paving blocks became deactivated significantly after 4 months of exposure in areas with high human intrusion levels. This was attributed to the accumulation of non-polar species such as grease, since the blocks were placed close to restaurants and other areas of high human traffic. The conclusion of this study was that photocatalytic paving blocks should be placed in areas that do not experience high human intrusion (Yu, 2003). Motohashi & Inukai (2007) found that significant variation in soiling and durability between specimens occurred before and after 5 years of outdoor exposure. By measuring wet methylene blue decomposition, it was determined that many coatings possessed significantly lower photocatalytic activity after the exposure. The authors recommend that future research address the specific causes for this reduction in efficiency so that the effect can be prevented if possible (Motohashi and Inukai, 2007).

2.7 Self-cleaning properties of photocatalytic specimens

In many studies, self-cleaning properties of photocatalytic materials were considered. TiO_2 surfaces have the ability to maintain their cleanliness under ultraviolet light and can decompose organic matter that soils the surface (Fujishima et al., 2008). This self-cleaning behavior can be explained by the hydrophilic nature of TiO_2 surfaces, which results from the presence of OH^- groups at the surface of the material. These OH^- groups are increased with exposure to ultraviolet light. Water combines with these groups, causing sheeting instead of formation of water droplets at the surface of a TiO_2-coated material (Agrios and Pichat, 2005).

The hydrophilicity of photocatalytic materials can be measured through the contact angle of water applied to the sample surfaces. Diamenti et al. (2008) reported a decrease in contact angle for several samples after 4 days of exposure to UV irradiation. They also found that the magnitude of decrease in contact angle was related to photocatalytic performance; the highest decreases were found with the most photoactive samples. Motohashi and Inukai (2007) evaluated the self-cleaning performance of several commercial photocatalytic coatings over a 5-year period of outdoor exposure. Even specimens that did not maintain significant photocatalytic activity after outdoor exposure did maintain low contact angles. Significant differences in both photocatalytic activity and contact angle were recorded for the range of commercial materials, which consisted of varying enamel paints both containing TiO_2 and with TiO_2 painted as a top clear coat (Motohashi et al., 2004).

Self-cleaning properties were evaluated in a number of tests by measuring changes in color of the photocatalytic specimen. The CIE L*a*b* colorimetric system was used in many of these tests for evaluating changes in color. The CIE system is three-dimensional and is suitable for measurement of small variations in color over time. The a* value describes value between red and green, b* between blue and yellow, and L* between white and black. Motohashi and Inukai (2007), in the same study mentioned earlier, evaluated changes in L* values, which indicate brightness, using a color meter. All specimens evaluated in this study were white. Delta L* value results ranged from near zero to as low as -12, depending on the photocatalytic product that was used. These values were compared to degree of weathering for each of the coatings. Variations in these results occurred depending on the coating tested. The coatings that contained a polyurethane enamel paint, barrier primer, and TiO_2 clear coat had the best overall performance when considering both weathering and color changes.

Guerrini et al. (2007) conducted a colorimetric monitoring program for the "Dives in Misericordia" church in Rome, Italy, and the Music and Art City Hall in Chambery, France over 6 years of observation. The church in Rome, Italy saw little color changes with the exception of slight differences between internal and external sides of the large sails that make up the church's structure. Slight variations in the b* parameter may have been a result of the presence of inorganic substances that collected on the surface. The Music and Art City Hall saw constant values of color, regardless of the directional position of the façade measured (Guerrini and Peccati, 2007).

Chen et al. (2011) evaluated color changes of rhodamine B dye on various mortar mixtures with TiO_2 added to the cement matrix using the CIE L*a*b* system with a spectrometer. The dye faded at a rate that was independent of the content of TiO_2, indicating that the photocatalytic material was effective in discoloring the dye under UV irradiation through its self-cleaning ability. Diamanti et al. (2008) measured color changes of fiber-reinforced mortars with varying amounts of anatase in both powder and suspension forms. The samples, which were white at the beginning of the test, were monitored using a spectrophotometer for color changes. A change in color occurred for almost all samples that were exposed outside. A yellowing effect was exhibited by samples with higher photocatalytic activity (Chen et al., 2011).

Pepe et al. (2004) evaluated the self-cleaning properties of metal-doped TiO_2 specimens by recording time for photodegradation of an alcoholic extract of cigarette smoke on various photocatalytic specimens. In this study, nano-sized TiO_2 contained in cement doped with magnesium or cerium achieved photodegradation of the substance in the least amount of time. Diffuse reflectance spectra were also recorded for the different materials (Pepe et al., 2004).

Yu (2003) conducted a study of NO_x removal efficiency of paving blocks in order to evaluate the possibility of deactivation of photocatalytic activity of blocks exposed to daily human intrusion. Water washing was an ineffective means to regenerate photocatalytic activity, possibly due to the presence of non-polar species such as grease (Yu, 2003).

2.8 Pilot scale and field tests of photocatalytic pollution reduction

Photocatalytic materials have been applied in many construction projects in recent years. Notable projects include the Basketball Facility at Louisiana State University, which architect Richard Meiers designed using photocatalytic stucco cement to reduce effects of mildew in the wet environment of Louisiana. The I-35W Bridge reconstruction project in Minneapolis, Minnesota included the construction of three wavy 30 ft (9 m) towers with photocatalytic stucco cement incorporated into the mix. At Dalton State University, photocatalytic stucco Aria was incorporated into the cement matrix in the construction of a tower to provide an iconic image for the school (Simms, 2010). The photocatalytic materials in these projects were selected for their self-cleaning capacities and air quality was not monitored. In each case, self-cleaning goals have been successful based on visual inspections.

Only a few real scale applications of photocatalytic materials for pollution removal have been carried out and reported in the literature. The results are often difficult to analyze because there is uncertainty about the pollution in the absence of the photocatalytic surface. In some cases, a non-photocatalytic section was kept next to the newly photocatalytically treated section for comparison. Both sections had to be close so that conditions (weather, traffic, surrounding buildings and shade) would be similar, but the proximity made it difficult to evaluate how air mixing between both sections influenced the results. Two studies have been conducted at pilot scale, one in a parking garage (Maggos et al., 2007b) with ceiling painted with photocatalytic paint and illuminated by artificial UV light, and another in an artificial outdoor street canyon (Maggos

et al., 2008) using transportation containers to build walls coated with photocatalytic mortar. Both studies used a combustion engine as a source of pollution. In the parking garage, the photocatalytic paint was responsible for about a 20% reduction in NO_x concentration. The authors noted that the field efficiency of the paint was not as good as what had been measured in the laboratory and postulated that the presence of organic materials was responsible for the difference. In the artificial street canyon, reductions of up to 80% in NO_x concentrations were observed. Wind direction was an important factor in determining the final removal obtained. However, Laufs et al. (2010) noted that the artificial street canyon had an unrealistically high surface-to-volume ratio, which might explain the observed removal efficiency.

NOxer® concrete blocks have been tested on both roadways and sound barriers and proved to be efficient at removing NO_x. Concentrations of NO_x were measured in close proximity to NOxer® covered sound barriers and compared to results were the barriers were covered with a non-reactive material. Removals of about 20% were measured (Toulan, 2006; Rousseau, 2010). Weeklong tests using passive samplers were conducted on roadways paved with NOxer® blocks. The details of the field study are unclear. However removals of 20 to 50% were reported (Rousseau, 2010).

A field study was conducted in Vanves, France, where a section of a high traffic road was modified so that half its pavement was photocatalytic while the other half was not (Petit, 2009). Air quality measurements were made continuously on site for a year. The results showed that for the first 3 months, the treated half of the road section was efficient at removing pollutants, especially during pollution peaks where NO_2 concentrations were up to 40% lower over the photocatalytic section of the road. However, after about 3 months, the NO_2 concentrations in the two test sections were the same. The authors assumed that fouling of the road surface (dirt deposited on the road) was responsible for this phenomenon. Various cleaning procedures were conducted on the road but no significant improvement was observed. Pressure washing was attempted at the end of the study as a last resort but the results were not reported. This suggests that treating surfaces near roadways, which are not as likely to foul might be a better approach for pollution removal.

A similar test was conducted in Bergamo, Italy (Guerrini and Peccati, 2007). Two data collection campaigns were carried out in November 2006 and January 2007. During the first campaign, it was found that NO_x concentration, during daytime, were about 40 to 50% lower above the photocatalytic surface than above the regular asphalt. During the second campaign, the difference was 20 to 30%. No other measurements were reported after these periods so it is difficult to evaluate the longevity of the solution. A recent study in Denmark with paving blocks containing TiO_2 showed similar results, with a 22% reduction in NO_x under ideal conditions (high insolation and low humidity) compared to a reference section (Folli et al., 2015). However, the validity of the analysis has been questioned, and the removals may be overstated (Kleffman, 2016).

The Missouri Department of Transportation underwent improvements to Route 141 in 2012. A portion of the highway was constructed using a two-lift system in which the top lift utilized photocatalytic cement concrete. Pollutants in storm water runoff were to be evaluated as part of the project to understand photocatalytic performance of the pavement. Temperatures of the section were also to be monitored. This project aimed to minimize costs associated with inclusion of photocatalytic material while maintaining mechanical properties of the pavement (Stone, 2010). No data from this project have been reported in the literature to date. Another study by Rheade and Panesar (2012) with roadway application of the technology is on the McDonald-Cartier highway in North York, Ontario. Five bays of noise barriers made with photocatalytic concrete

were placed on the side of the highway and air quality monitoring has been conducted in 3-week campaigns. So far, NO, NO_2, and NO_x air concentrations have been measured in close proximity to the wall (0.1 m) and further away from the wall (1 m, 2 m) on the road-side of the barrier. No air quality improvement was recorded in close proximity to the barrier versus further away from the barrier: the air monitoring methods and parallel wind created by traffic were hypothesized to have negatively affected the results. Monitoring on the non-road side of the barrier was to be used for further investigation. Rheade and Panesar (2012) also tested the physical properties of photocatalytic concrete and found that they were comparable to conventional concrete, aside from a potential sensitivity to scaling that is being investigated further.

Chapter 3. Materials and Testing for Laboratory and Outdoor Exposure Studies

The first stage of this research involved preparing concrete specimens coated with commercial photocatalytic coatings to verify the effectiveness of the coatings in laboratory chamber testing and to determine the effects of prolonged outdoor exposure. This chapter describes the fabrication of concrete specimens (i.e., the substrates for the photocatalytic coatings), the coatings that were evaluated and their method of application, material characterization testing, outdoor field exposure study sites, and the laboratory chamber test setups for measurement of NO_x and ozone removal.

3.1 Concrete samples and coatings preparation

3.1.1 Description of concrete samples

Two types of concrete specimens were selected for testing: slabs and barriers. The slab specimens were created for both tests in the environmental chamber as well as for placement at the outdoor field exposure sites.

Concrete slabs were produced in two sizes: "full" and "half." The dimensions of the full-size slabs were determined based on the size of the chamber used for testing pollutant removal, described in section 3.4. In addition to the full-size slabs, half-size slabs were also created for chamber tests. These half-size slabs were not placed at any field sites and were only used in chamber tests. Figure 3.1 shows the dimensions (in inches) of the full and half-size slabs.

Formwork for producing the concrete slabs was prepared using wooden boards, plywood, screws, and L-shaped brackets for securing. Adhesive-ready Teflon® polytetrafluoroethylene sheets were obtained, cut to size, and placed on the bottom face of the formwork. The purpose of the Teflon was to create a smooth surface for coating without applying any greases or oils that could interfere with the chamber testing. An example of completed formwork is shown in Figure 3.2.

In order to accurately understand the performance of concrete transportation structures with photocatalytic coatings, actual sections of highway barrier were obtained from Tricon Precast Ltd., located in New Braunfels, Texas. Three 5-ft (1.5 m) sections of barrier were purchased, one for each of the three field sites (described in section 3.3). Each barrier was divided into four sections of equal width. To divide the sections, strips of aluminum flashing were installed using both mechanical anchors and flashing sealant. Sections were prepared and coated according to the manufacturers' recommendations—one each for the stucco, the white paint, and clear paint 1—which are described in section 3.1.3. The fourth section of each barrier was left uncoated for monitoring as a control section. A drawing with details of the dimensions and sectioning for the highway barrier specimens is shown in Figure 3.3.

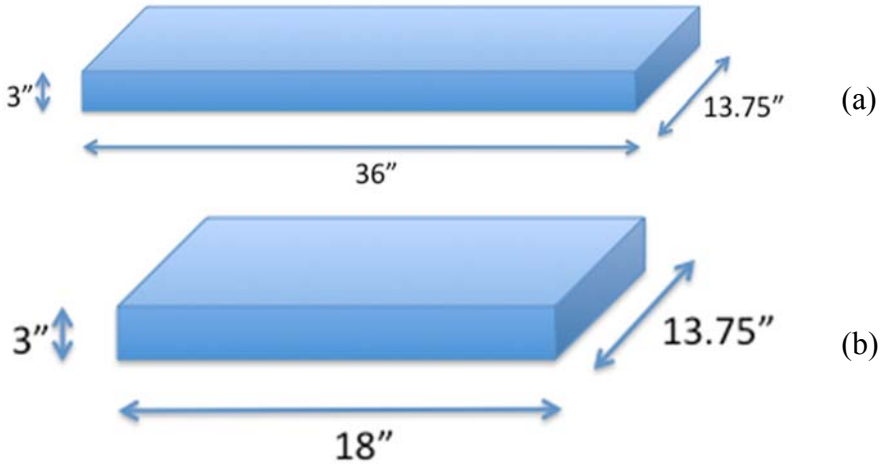

Figure 3.1 Dimensions of slab specimens: (a) full size; (b) half size

Figure 3.2 Completed slab formwork

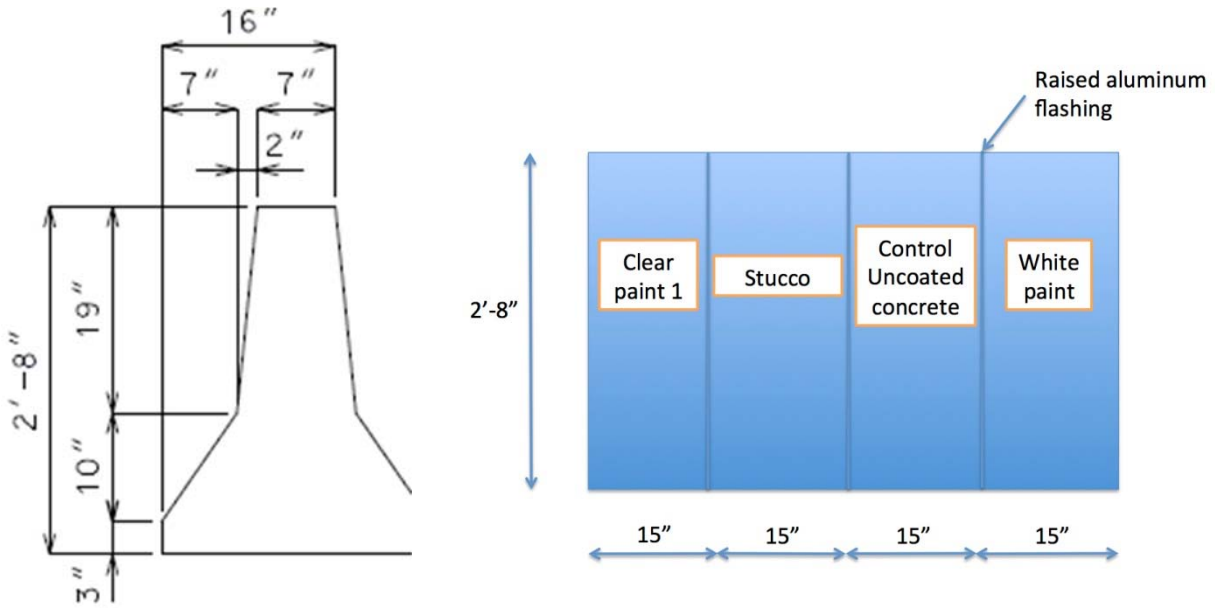

(a) (b)

Figure 3.3 Concrete barrier specimen: (a) side elevation; (b) front elevation

3.1.2 Concrete slab preparation

Materials

The materials used for mixing the concrete slab specimens were selected based on typical materials and materials suppliers used by Tricon Precast in their mixture design for highway barriers. The cement selected was an ASTM C150 Type III cement from Capitol Aggregates in San Antonio, Texas. The supplementary cementitious material was a Headwaters Limestone Class F Fly Ash from Jewett, Texas, complying with ASTM C618.

The coarse and fine aggregates were obtained from the Hanson Servtex plant in New Braunfels, Texas. Both aggregates were composed of limestone. No additional sieving or re-proportioning was done after receiving the aggregates. The coarse aggregate had a maximum aggregate size of 1 in. (2.5 cm), which was chosen both for its practicality in terms of the proposed slab thickness and because it is the actual size used by Tricon Precast in the production of highway barriers. The absorption and specific gravity of the coarse and fine aggregates were calculated according to ASTM C127 and ASTM C128, respectively, and are included in Appendix A.

Mixture Design

The mixture design for the slab specimens was determined based on the typical mixture design used by Tricon Precast in the preparation of highway barriers. Therefore, the concrete mixture design was kept consistent between the two types of specimens that were used in this project. The concrete mixture was a 25% fly ash replacement of Type III cement by weight with a nearly 1:1 ratio of coarse to fine aggregate by weight. The mixture design obtained from Tricon Precast is shown in Appendix A. Also provided in Appendix A is the mixture design used for the slab specimens, which was taken from the Tricon Precast design and adapted for the volume of concrete necessary for the slabs, cylinders, and fresh property testing.

Slab Specimen Batching, Mixing, and Testing Procedures

The procedures followed for batching and mixing of concrete were in accordance with ASTM C192: Standard Practice for Making and Curing Concrete in the Laboratory, with specific guidelines from Pesek (2011). More details about batching and mixing for this specific project can be found in Terpeluk (2012).

Concrete Quality Control Testing

Fresh concrete was tested in terms of slump, unit weight, and air content for each mixture. These tests were performed in accordance with the following ASTM standards:

- Slump: ASTM C143 (2010)
- Unit Weight: ASTM C138 (2010)
- Air content: ASTM C231 (2010)

In addition, three 4-in. x 8-in. cylinders (10 cm x 20 cm) were cast per mixture for 28-day compressive strength testing of hardened concrete. For mixtures 1 through 9 (Appendix A), hardened cylinders were cured in the same way as the concrete slab specimens. This allowed actual strength of the slab specimens to be measured under the specific curing conditions. For mixtures 10 through 14, the cylinders were cured according to ASTM C 39 (2010), and six cylinders were cast for each of these mixtures.

Slab Specimen Curing and Coating Procedures

All concrete slab specimens were cast in wood forms (Figure 3.2) and demolded after 24 hours. They were then kept in a 73°F (23°C), 100% RH chamber for 6 days to represent ideal curing times. After 6 days, the specimens were moved to a laboratory room with a 73°F (23°C), 50% RH environment for 14 days to equilibrate to a lower moisture rate. By keeping the curing times and conditions consistent, these factors could be eliminated as variables in the testing. All specimens were coated after 21 days ± 24 hours. The formwork-finished side of each specimen was used for coating to most accurately represent surfaces of actual highway structures. The manufacturers' recommended procedures were followed for coating the specimens, as described in Section 3.1.3. In order to isolate the flat surface of each sample as a variable in the chamber testing, the sides and bottom of each slab were coated with sodium silicate. This sodium silicate coating prevented the sides and bottom of each slab from having any photocatalytic effect in the chamber tests.

3.1.3 Coatings

Several commercially available photocatalytic coatings were selected based on their commercial availability, performance in published testing, and relevance in terms of application procedure. Four products were selected for initial testing, with the intention that some would be eliminated from the project based on preliminary performance in the chamber tests or difficulty in application. The four products selected for initial testing included a photocatalytic stucco, two photocatalytic clear paints, and one photocatalytic white paint. The products were each applied to trial samples of concrete to determine ease of application. All products were applied to concrete substrates based on the manufacturer's recommendations.

The stucco is composed of portland cement, proprietary admixtures, and photocatalysts. The manufacturer recommends that when applying the stucco to concrete, surfaces be prepared in accordance with ASTM C926. For the final coat, the stucco is mixed with clean sand meeting ASTM C897 in a ratio of approximately one part stucco cement to two to three parts sand by volume. According to the manufacturer's directions, two-thirds of the mixing water and one-half of the total sand volume are mixed and the stucco cement is then added to create the stucco. The remaining portion of the sand and sufficient water to achieve the desired workability are then added. The stucco mortar is then mixed for at least 5 minutes until uniformity is achieved. Retempering (i.e., the addition of water) can be done once up until 1.5 h from initial mixing, at which time the stucco should be discarded. The stucco was applied to concrete using a hand trowel in a 1/8-in. layer. To achieve a 1/8-in. layer, approximately 500 g of stucco were used per full-size slab, or 145 g/ft^2 (1.56 kg/m^2). Figure 3.4 shows an example of the application method.

Figure 3.4 Application of the photocatalytic stucco

The stucco was analyzed using x-ray fluorescence (XRF)[1] and was found to contain approximately 5% TiO_2 by total mass. The stucco was also analyzed using x-ray diffraction (XRD) and found to contain anatase. The amount and type of TiO_2 for all coatings are shown in Table 3.1. A comparable stucco without TiO_2 was also tested in this study, but only in one laboratory chamber test, to isolate the role of the photocatalyst on the stucco's performance. Those results are presented in section 6.3.1. The stucco was from the same manufacturer and was applied in the same way as the photocatalytic stucco.

Table 3.1 TiO2 content of commercial coatings

Product Name	TiO_2 (% total weight)	Type of TiO_2
Stucco	5.0	Anatase
White paint	9.7	Rutile
Clear paint 1	1.0	Anatase
Clear paint 2	2.35	Anatase

[1] Clifton Coward at the TxDOT Laboratory in Cedar Park, Texas, performed all XRF testing reported in this study.

The white paint is a silica sol and water glass-based exterior paint that is appropriate for mineral substrates. According to the manufacturer's recommendations, the substrate must be dry, sound, non-chalking, clean, and dust-free prior to application of the paint. The white paint can be applied by paintbrush, roller, or airless sprayer. A minimum drying time of 12 hours is required between coats. The paint is applied in a two-coat process. The base coat is diluted with up to 5% of the primer or up to 10% for strongly absorbent surfaces. The top-coat consists of the white paint in its undiluted form. The two-coat system should be applied at a rate of about 0.45 kg/m^2 for a smooth substrate, although exact values can only be determined during the application process. Figure 3.5 shows the paint application process.

Figure 3.5 Application of the white paint

The undiluted white paint was analyzed by XRF and determined to contain 9.70% TiO_2 by total mass, as shown in Table 3.1. The dried paint was also analyzed using XRD and it was found that TiO_2 is present most prominently in the form of rutile.

The clear paint 1 is a water-based photocatalytic spray that can be applied to virtually any surface, including both interior and exterior surfaces. Clear paint 1 contains anatase TiO_2, titanium hydroxide, and de-ionized water. The product is applied by spraying to a clean surface only. A layer of protective basecoat is first applied at a concentration of 0.2 kg/m^2. A layer of the clear paint 1 is then applied in a concentration of 0.2 kg/m^2. The product can be applied using a sprayer or electrostatic spray system, although a sprayer was used for this application. Professionals from a local distributor of the product applied the clear paint to the concrete specimens at the Construction Materials Research Group (CMRG) building located at the J. J. Pickle Research Campus. Figure 3.6 shows the application process at CMRG in April 2011.

Figure 3.6 Clear paint 1 application by sprayer

According to the manufacturer, the clear paint 1 contains 1% anatase by total weight, shown in Table 3.1. This product was not analyzed by XRF or XRD because it had an insufficient amount of solids for testing using these methods.

The clear paint 2 is a water-based photocatalytic spray. According to the manufacturer, it should be applied 5 in. (12.7 cm) from a surface using a fine sprayer. It is at a rate of 8 fluid ounces (236 ml) per 250 to 500 ft^2 (23–46 m^2) of surface. Figure 3.7 shows the application of clear paint 2.

Figure 3.7 Application of the clear paint 2 spray

According to the manufacturer, clear paint 2 contains 2.35% anatase by total weight, as shown in Table 3.1. Clear paint 2 was eliminated from testing prior to the installation of the field sites due to poor results in preliminary chamber testing.

3.2 Methods for characterization of concrete and coatings

All specimens to be placed in the field sites were characterized before and after 1 year of exposure. The stucco-coated specimens were tested for a second year of exposure. The field site specimens were characterized using XRD and SEM.

3.2.1 X-ray diffraction

Small cores (3 in. [7.6 cm] diameter, 0.5 in. [1.3 cm] depth) of concrete were removed from the coated sections of one barrier prior to 1 year of outdoor exposure. Two cores were removed from each of the coated subsections of the barrier, one for SEM and one for XRD. The sections were removed at the surface of the barrier using either a Hilti TE-C-BK-TW percussion core bit or a Hilti DD 120 coring rig. Samples were assumed to be approximately similar between the barriers and slabs with a given coating before exposure, and therefore sections were only taken from one barrier in the initial state. Cores were then taken from all of the barriers and slabs after 1 year of exposure. Additional cores were taken from the stucco specimens after 2 years.

The samples to be used for XRD were crushed using a Scienceware Micromill grinder until they passed through a #325 sieve (45 μm). The samples were then placed in vials and stored under vacuum until they were tested. When ready for testing, the samples were loaded into the holders and placed in the Siemens D500 diffractometer. Samples were scanned from 10° to 70° 2θ. Samples were analyzed for the presence of different forms of TiO_2 as well as for concrete reaction products. The presence of TiO_2 and reaction products were compared for specimens before and after exposure to better understand the effect of outdoor exposure on composition of a concrete specimen coated with photocatalytic material.

3.2.2 Scanning electron microscopy

The second core of concrete that was obtained from the specimens was used for SEM. It was first broken in half using a hammer and chisel to create two sections. The first section was reserved for viewing the fractured surface using SEM. The second section of concrete was sliced to approximately 0.24 in. (6 mm) thickness with a Buehler Isomet 1000 precision saw using ethanol as the lubricant. This piece was used to view a cross section of the concrete and coating. The sawed sample was placed under vacuum for at least 24 hours prior to epoxy impregnation. The procedure followed for epoxy impregnation was from Williams (2006). The grinding and polishing times followed the procedures described by Drimalas (2007). The cross-section samples were placed in a two-part epoxy resin from Epoxy Technology using an epoxy impregnation device so that a vacuum could be held on the samples during placement. The samples were allowed to cure for 24 hours at 73°F (23°C) prior to removal from the holder.

After fully curing, the samples were removed from the holders and ground with #180, 400, 800, and 1200 grit sandpaper by hand. The samples were moved to finer grit sandpaper when scratches on the specimen and the stabilization of the width of cracks within the sample revealed that grinding at a particular level was complete. Typically, this took approximately 10–15 minutes per grit size. After grinding, the samples were polished with 3, 1, and 0.25 μm diamond paste using an automated Buehler Automet 2000 powerhead. The samples were polished with the 3 and 1 μm diamond paste for 1 hour each, followed by the 0.25 μm diamond paste for 1.5 hours. The samples were polished in increments of 15 minutes and the direction of the revolving head was changed after each increment. The samples were then cleaned with ethanol and placed under vacuum until ready to be analyzed with SEM.

All samples were coated and placed into a Quanta 650 FEG variable pressure SEM with an automated backscattered electron detector. The accelerating voltage was 30 kV. Bruker XFlash® Detector 5010 energy dispersive spectroscopy (EDS) was used to identify phases with the sample. All images were run at a 5.0 µm spot size with a 3 microseconds dwell time. Samples that were obtained before and after the field exposure period were compared in terms of presence and distribution of TiO_2.

3.3 Outdoor exposure tests setup

Three field sites were created to understand how the specimens would perform after exposure to outdoor conditions near major highways with significant air pollution from traffic. Two of the field sites were located near major highways in Houston and Austin, Texas, while the third was kept near the laboratory at the J. J. Pickle Research Campus in Austin.

3.3.1 Houston

The Houston site selected was at the TxDOT district office located at 7600 Washington Avenue, close to I-10 in Houston, Texas. Figure 3.8 shows the location of the concrete specimens and weather station in relation to the highway. This field site is referred to throughout this report as the *Houston field site*.

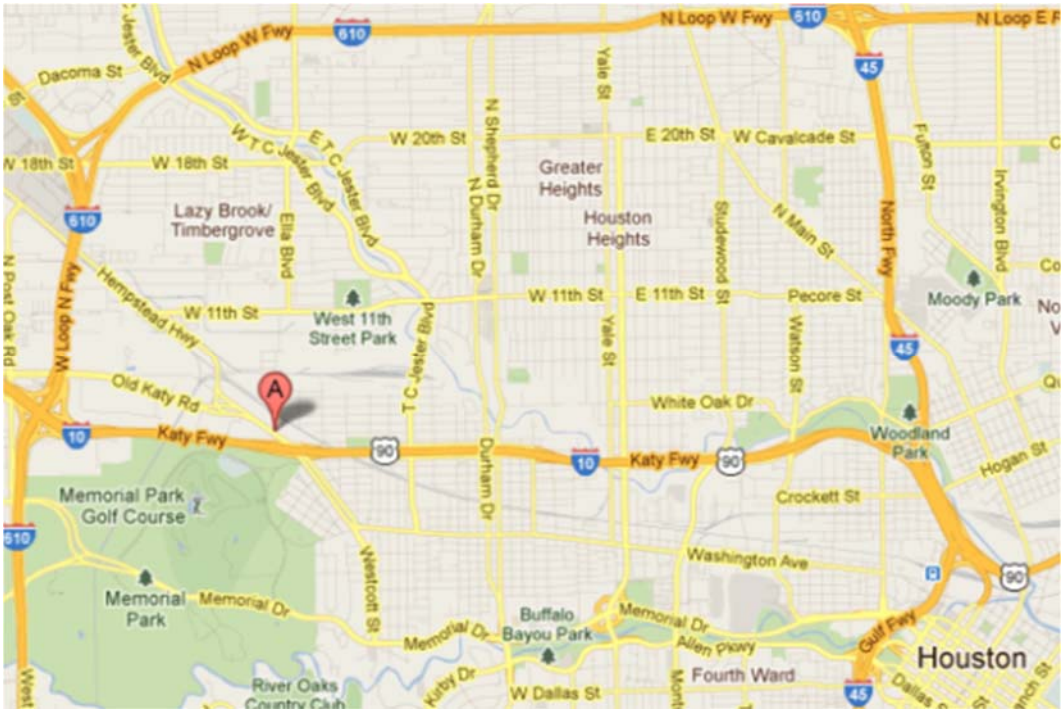

(a)

(b)

Figure 3.8 Houston site: (a) map; (b) digital image of field site facing I-10

3.3.2 Austin

The second field site selected was at the TxDOT district office at 7901 North I-35 in Austin, Texas near the intersection of I-35 with Route 183. Figure 3.9 shows its location and proximity to I-35. This field site is referred to throughout this report as the *Austin field site*.

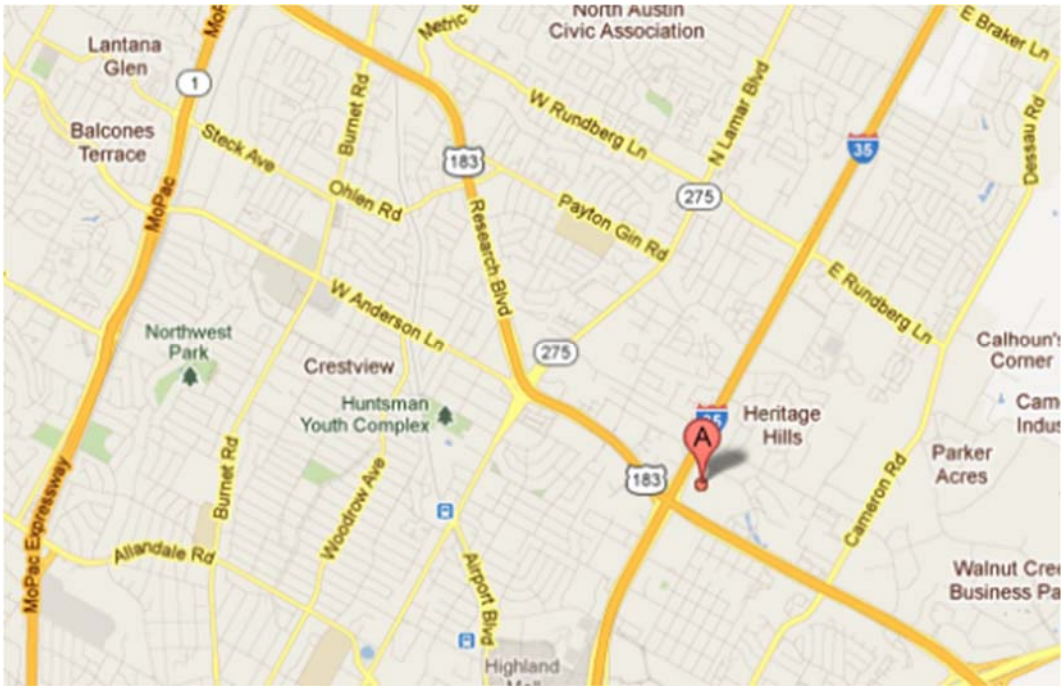

(a)

(b)

Figure 3.9 Austin site: (a) map; (b) digital image of field site facing I-35

3.3.3 Laboratory

The third location was at J. J. Pickle Research Campus at 10100 Burnet Road in Austin, Texas. This site was not directly adjacent to any major highway; however, its proximity to the laboratory allowed for more frequent monitoring and evaluation. Figure 3.10 shows its location. This field site is referred to throughout this report as the *lab field site*.

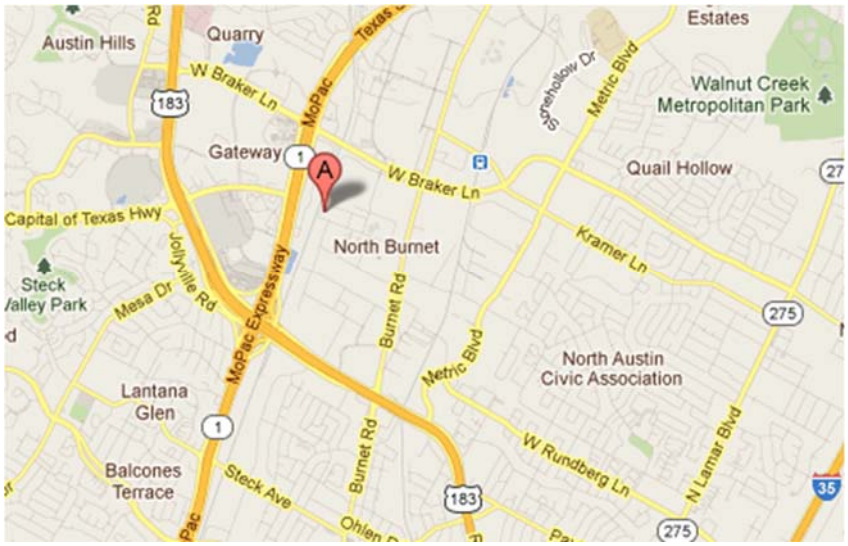

(a)

(b)

Figure 3.10 Lab site: (a) map; (b) digital image of north facing site

3.4 Pollutant removal experimental setup

3.4.1 Description

An experimental system was designed and constructed to test the three photocatalytic coatings and uncoated concrete. A schematic of the experimental system is presented in Figure 3.11.

A 150-L stainless steel electro-polished chamber was used to test coated concrete samples. Eight UV lamps (40 W, 280-400 nm, λ_{max} = 310 nm, model QFS-40; Q-Lab Corp., Cleveland, OH, USA) were installed in the chamber. The inlet and outlet of the chamber were equipped with RH probes (model HD2XVSX; Veries Industries, Portland, OR, USA) and thermistors (model 44203; YSI, Yellow Springs, OH, USA). A third thermistor was also placed in the middle of the reactor, above the concrete sample. Stainless steel blocks were made to fit at each end of the concrete samples in order to create a flat surface extending the entire length of the chamber. This allowed the development of a uniform flow field over the sample surface. Once a sample and the stainless steel blocks were placed in the chamber, the air volume was reduced to 115 L. Concrete samples were centered under the UV lights. Half-size samples (see section 3.1.1 for details) were used conduct tests at short contact times because of instrument limitations and to conserve similar fluid dynamics conditions over the sample surface.

Process air was provided by two zero air generators (model 701; Teledyne, San Diego, CA, USA). The process air was split and a portion of the air was passed through an impinger filled with distilled water to adjust the RH. Pollutant species mixed with nitrogen were obtained in gas cylinders (Praxair, Danbury, CT, USA). Experimental ozone was produced by passing pure oxygen through a UV-based ozone generator (Model 97-0067-01; UVP, LLC, Upland, CA, USA). Pollutant species were introduced at a known rate through mass flow controllers (Series FMA 5500; Omega Engineering, Inc., Stamford, CT, USA; Series GFC 1700; Aalborg, Orangeburg, NY, USA). The process air, the pollutants, and the ozone were then passed through a mixing zone before being introduced in the chamber. The mixing zone consisted of a succession of sections of tubing of two different diameters.

Sampling of chamber air occurred both in the inlet and outlet of the chamber. A system of solenoid valves (models SV123/133; Omega Engineering Inc.) was used to automatically switch sampling between the inlet and outlet of the chamber. When sampling occurred at the outlet, an exhaust pump was used to remove a flow rate of gas equal to the flow rate going to the instrument

in order to keep a constant gas flow rate through the chamber. Measurements for NO, NO_2, and NO_x concentrations were made by a chemiluminescence analyzer (model 200E; Teledyne). Ozone concentrations were measured using a UV absorbance ozone analyzer (model 1008-AH; Dasibi, Glendale, CA, USA). The non-methane VOC concentration was measured using a methane/non-methane hydrocarbon analyzer (model 55i; Thermo Fisher Scientific, Waltham, MA, USA). The analytical instruments were calibrated daily using a dynamic dilution calibrator (model 700E; Teledyne) and EPA protocol gas standards (Praxair).

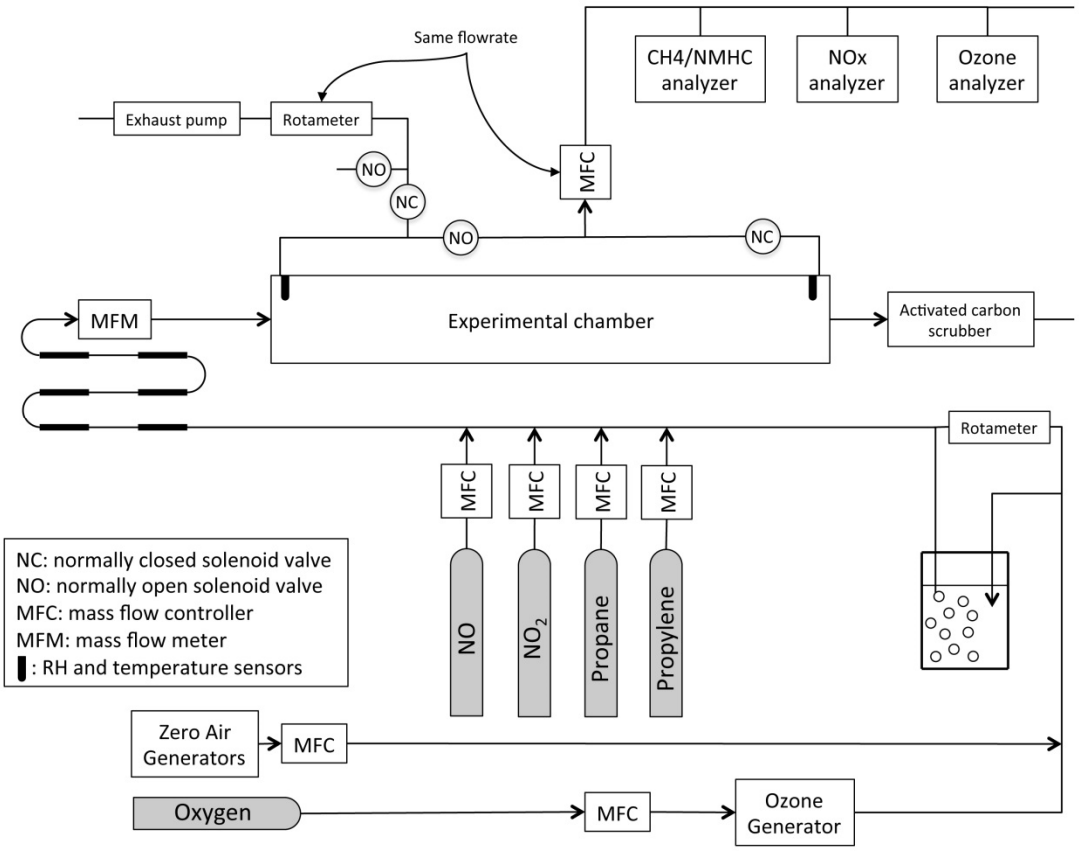

Figure 3.11 Photocatalytic testing setup

3.4.2 Characterization

Mixing

A test was conducted to evaluate the uniformity of mixing in the experimental chamber. The test procedure followed the methods outlined in ASTM D5116-10. CO_2 was used as a tracer gas and injected into the chamber inlet for two hours to ensure that steady-state conditions were reached. The CO_2 injection was then stopped and the CO_2 concentration decay was monitored using a Q-Trak (TSI, Inc.) CO_2 monitor as shown in Figure 3.12. The flow rate in the chamber was set to 5 L/min, the lowest flow rate used for these experiments.

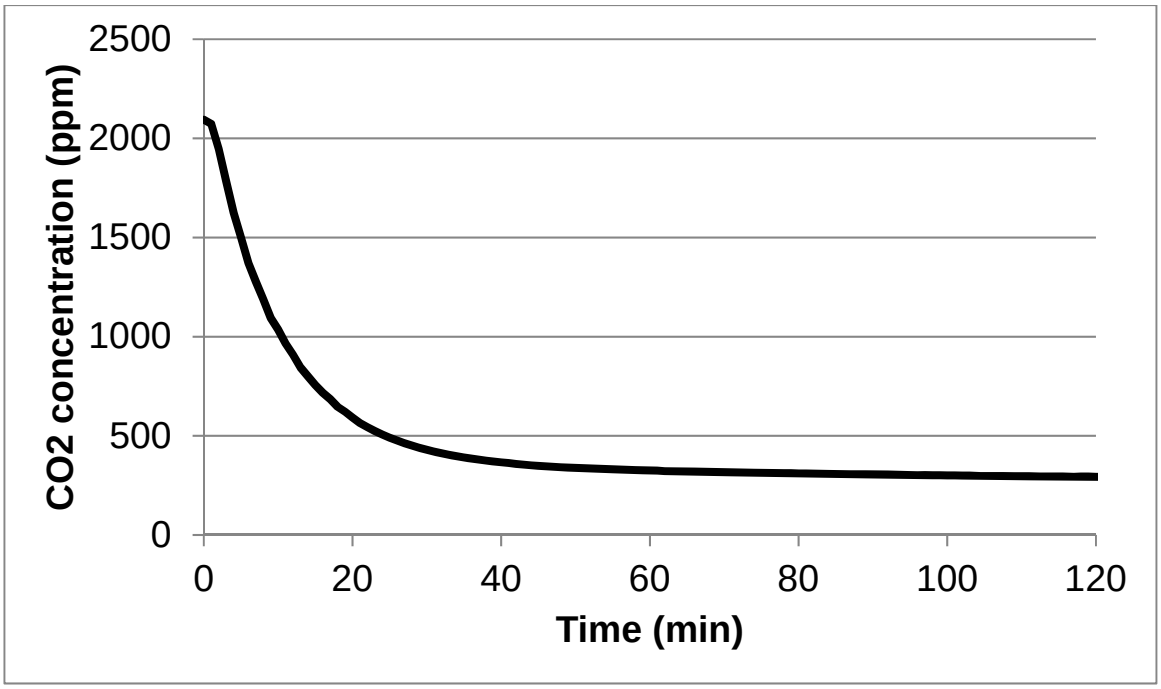

Figure 3.12 CO_2 decay test to evaluate uniformity of mixing

The mixing level was calculated using the following equation from the ASTM D5116-10:

$$\eta = \left\{ 1 - \frac{\left[\sum_{i=1}^{n} \left| c_{exhaust}(t_i) - c_{theoritical}(t_i) \right| \right] \times (t_i - t_{i-1})}{\left[\sum_{i=1}^{n} c_{theoritical}(t_i) \right] \times (t_i - t_{i-1})} \right\} \times 100\% \qquad (3.1)$$

η	mixing level (%)
t_i	time of the ith concentration measurement taken (min)
$c_{exhaust}$	measured CO_2 concentration in the chamber exhaust (ppm)
$c_{theoretical}$	concentration that would be measured in the exhaust if the reactor was a perfect well-mixed reactor (ppm)

The variable $c_{theoretical}$ is calculated from a mass balance on an ideal well-mixed reactor and is:

$$c_{therotical}(t_i) = (c_{t=0} - c_0)e^{-\lambda t_i} + c_0 \qquad (3.2)$$

$c_{t=0}$	CO_2 concentration measured at the beginning of decay test (ppm)
c_0	CO_2 concentration in inlet air after injection was switched off (ppm)
λ	chamber air exchange rate (min^{-1}).

For the chamber used in this study, the test yielded a mixing level of 90%, which is above the 80% limit for a well-mixed chamber (ASTM D5116-10).

Environmental parameters

Temperature in the environmental chamber could be varied from 27°C to 42°C. RH, in this temperature range, could be varied from 10% to 65%. Ultraviolet light intensity could be varied from 1 to 2 mW/cm^2 in increments of 0.5 mW/cm^2. For all residence times, maximum pollutant concentrations were 200 ppb NO, 100 ppb NO_2, 200 ppb ozone, 0.5 ppm propylene, and 2.5 ppm propane. Residence time in the reactor containing a concrete sample could be varied from 4.5 to 23 minutes. Contact time with the material (defined as residence time multiplied by the fraction of the bottom of the reactor covered with a concrete coupon) could be varied from 15 to 3 minutes for full-size samples and from 7.5 to 1.5 minutes for half-size samples. Full-size and half-size samples are described in section 3.1.1.

Chapter 4. Coating Screening Tests for Pollutant Removal

4.1 Preliminary tests

Preliminary tests were conducted on four commercially available photocatalytic coatings. The tests were conducted to eliminate coatings that were inefficient and identify effective coatings for further testing. The two coatings with the highest removal efficiencies were subjected to more detailed testing described in the section 4.2.

The preliminary tests were run at a contact time of 7.5 minutes and pollutant concentrations of 135 ppb NO_x, 85 ppb ozone, and 3 ppm non-methane hydrocarbons (2.5 ppm propane, 0.5 ppm propylene). NO_x removals were calculated using steady-state concentration data obtained during the tests.

First, percent removal by the uncoated concrete was calculated using equation 4.1.

$$R_b = 100 \times \left(1 - \frac{c_{out,b}}{c_{in,b}} \right) \tag{4.1}$$

$c_{in,b}$ pollutant concentration measured in the chamber inlet for the test run with uncoated concrete (ppb)
$c_{out,b}$ pollutant concentration measured in the chamber outlet for the test run with uncoated concrete (ppb)
R_b pollutant removal by the uncoated concrete (%)

The removals for the photocatalytic coatings were calculated in a similar fashion. For each test, the removal by the uncoated concrete was subtracted to determine the removal fraction for the photocatalytic coating over the uncoated concrete as described by:

$$R = 100 \times \left(1 - \frac{c_{out}}{c_{in}} \right) - R_b \tag{4.2}$$

c_{in} pollutant concentration measured in the inlet of the chamber (ppb)
c_{out} pollutant concentration measured in the outlet of the chamber (ppb)
R pollutant removal by the coated concrete (%)

Results (Figure 4.1) show that the stucco exhibited the highest NO_x removal while the white paint showed almost no NO_x removal. Clear paints 1 and 2 exhibited very similar performance for NO_x removal. Ozone removal by the clear paint 1 was slightly lower than ozone removal by the clear paint 2. However, clear paint 1 not only removed ozone but also some of the hydrocarbons, while clear paint 2 did not remove any hydrocarbons. For that reason, clear paint 1 was chosen for further testing.

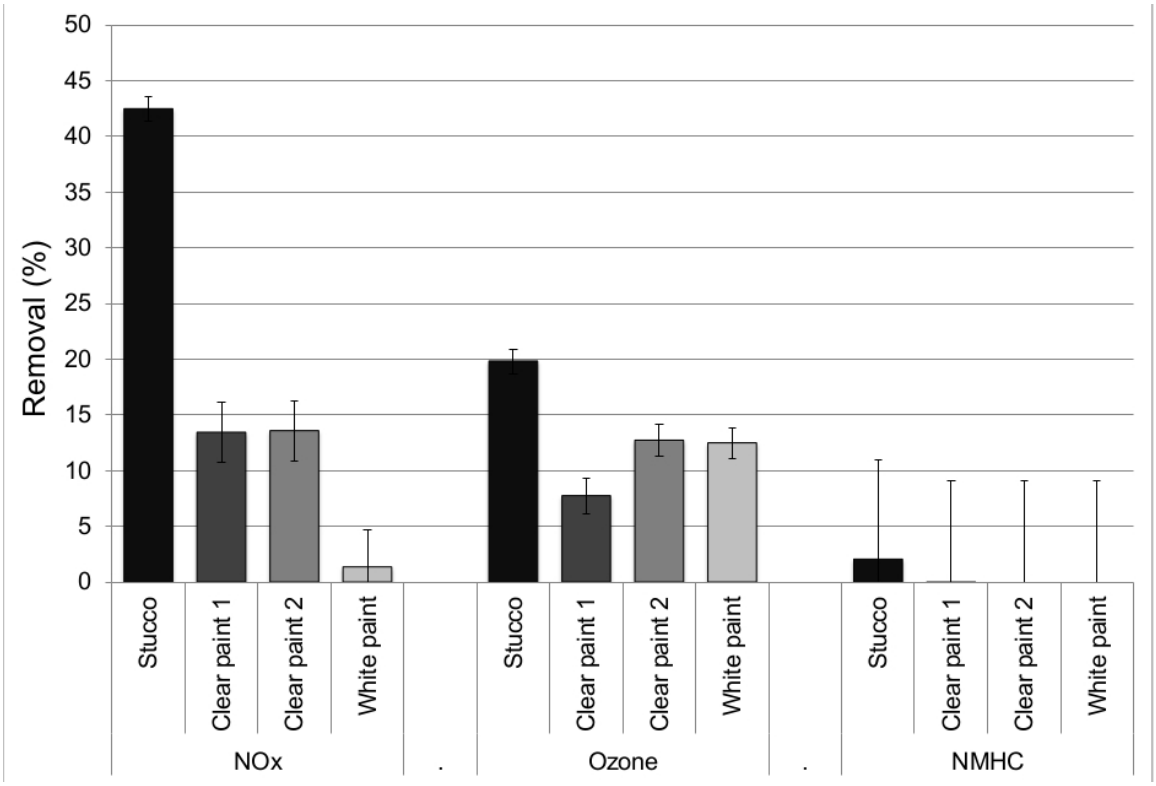

Figure 4.1 Preliminary results for photocatalytic coatings

4.2 Full factorial tests and replicates

Full factorial experiments were run on the stucco and the clear paint 1. Six parameters were varied between two levels, as indicated in Table 4.1, for a total of 64 tests per coating. In addition to the two coatings selected, an uncoated concrete sample was also tested for comparison.

Table 4.1 Full factorial parameters and their levels

	Level 1	**Level 2**
Contact time	15 minutes	1.5 minutes
Relative humidity	65% RH	20% RH
Temperature	~ 40°C	~ 30°C
Organic pollutants propane (VOC) propylene (HRVOC)*	 2.5 ppm 0.5 ppm	 0.25 ppm 0.05 ppm
Light intensity	2 mW cm^{-2}	1 mW cm^{-2}
Inorganic pollutants NO NO_2 Ozone	"Afternoon" condition 50 ppb 150 ppb	"Morning" condition 150 ppb 20 ppb

*Highly reactive volatile organic compounds

Eight consecutive experiments were conducted on a single sample before it was removed from the chamber and the next sample was tested. Each sample was rinsed with distilled water before the first experiment and between each round of eight experiments. The water rinsing was designed to mimic rain events in the field that can remove oxidized species. For rinsing, full-size samples were placed horizontally and one gallon of distilled water was poured on the sample in increments of 0.25 gallon (0.95 L). Between each incremental rinse the sample was left to drip for about a minute. Finally, the sample was tilted to an angle of approximately 30° and one gallon (3.8 L) of distilled water was poured on the sample, running off quickly. The sample was then set to dry in the laboratory for a day. Half-size samples were rinsed following the same methodology, but using half the amount of water.

NO_x removals were determined as described in Section 4.1. The results from the full factorial experiments were analyzed using JMP software (JMP 9; SAS, Cary, NC, USA) to establish the most important parameters affecting NO_x removal. Analysis of variance (ANOVA) was used. The contrast for each environmental parameter was calculated as the difference of the average of the responses at level 1 and level 2 (see Table 4.1). Ten percent of the experiments were repeated. The Lenth method was used to provide approximate tests of significance (Tamhane, 2009). The Lenth method provides an estimate of the standard error, called the Lenth pseudo standard error (PSE), where:

$$PSE = 1.5 \times \text{Median}(|\theta_i|: \theta_i < 2.5 \times \tau_0) \tag{4.3}$$

and

$$\tau_0 = 1.5 \times \text{Median}(|\theta_i|) \tag{4.4}$$

θ_i ith contrast

Long contact time experiments were conducted to simulate similar experiments run by previous researchers. By comparing our results to previous research, it was possible to evaluate whether the addition of environmental parameters (additional pollutant species in particular) affected NO_x removal by the coatings. As shown in Figure 4.2, removal efficiency for stucco ranged from 23 to 85%. Dylla et al. (2010) observed similar removal efficiencies for concrete containing TiO_2 at contact times up to 7.1 minutes. Dylla et al. (2010) did not include other air pollutants such as ozone and VOCs in their study. These results suggest that for coatings similar to the photocatalytic stucco, the presence of other pollutants in the air mixture does not significantly influence NO_x removal. Removals observed for clear paint 1 ranged from 0 to 32%. The removal exhibited by the clear paint 1 decreased over time. The first eight experiments presented on the top left of Figure 4.2 (long contact time, low RH, morning inorganics) were the initial experiments run during the experimental program. It is during these experiments that the best performance of the clear paint 1 was recorded, with all removals between 12 and 32%. It appears that the performance of the clear paint 1 degraded after the first sample wash: all subsequent removals observed were below 15% with only one experiment yielding a removal over 12%. Such changes were not observed with the stucco.

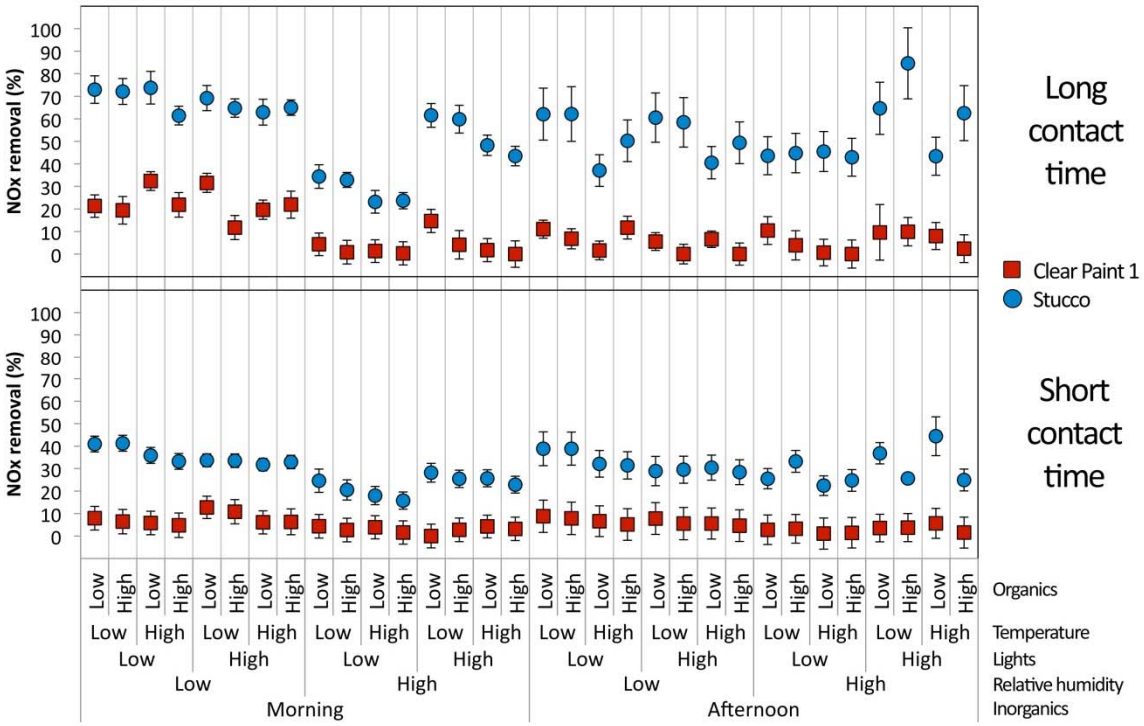

Figure 4.2 Comparison of NOx removal by the photocatalytic coatings

The same set of experiments was conducted with a shorter contact time of 1.5 minutes. This contact time was obtained using half-size samples as described in section 3.4.2. Again, the stucco was superior to clear paint 1 with removal efficiencies ranging from 16 to 44% compared to 0 to 13% for the clear paint. Similar levels of NO_x degradation were observed by Ballari et al. (2011) and Husken et al. (2009), who tested photocatalytic paving stones and found removals in the range of 3 to 63% for similar contact times, light intensities, RH, and inorganic pollutant concentrations (Husken et al., 2009; Ballari et al., 2011).

Results from ANOVA using NO_x removal data for the clear paint 1 and the stucco, respectively, are shown in Figure 4.3. NO_x removal by clear paint 1 and the stucco were significantly affected by four environmental parameters: RH, temperature, lights, and contact time.

Clear Paint 1

Term	Contrast	Lenth t-Ratio
Relative humidity	-3.40733	-8.02
Contact time	2.14001	5.04
Inorganics	-1.99021	-4.69
Organics	-1.26356	-2.98
Temperature	-0.91601	-2.16
Lights	0.14898	0.35

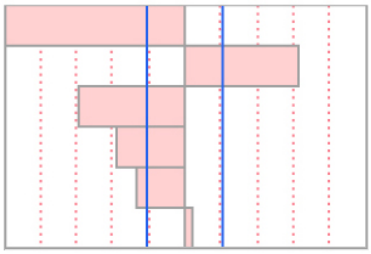

Stucco

Term	Contrast	Lenth t-Ratio
Contact time	11.9010	17.03
Relative humidity	-5.1022	-7.30
Temperature	-3.5288	-5.05
Lights	2.5321	3.62
Inorganics	0.2316	0.33
Organics	-0.0180	-0.03

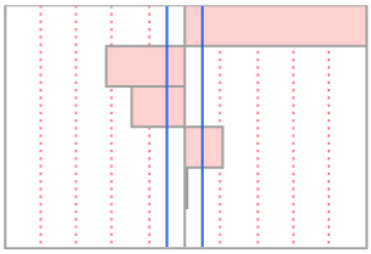

Figure 4.3 ANOVA results for the clear paint 1 and the stucco (blue vertical lines indicate critical values of Lenth t-ratio above which a parameter is deemed significant)

Increasing the contact time increases the probability of pollutants coming in contact with the material surface and being adsorbed or reacted, hence the positive contrast for that effect. The negative contrast observed for increasing RH has been observed by other researchers (Maggos et al., 2007a; Ballari et al., 2011). It is generally accepted that higher RH leads to more water molecules adsorbing to the material surface hence competing with pollutant species for adsorption sites, reducing the removal efficiency. An increase in temperature also negatively affects NO_x removal by both the clear paint 1 and the stucco. Bengtsson et al. (2010) studied the effect of temperature on photocatalytic coatings in the 21–30°C range and also found decreased removal with increasing temperature. It was hypothesized that the increase in temperature affected adsorption and desorption rates of the pollutants to the photocatalytic material.

It is interesting to note that light intensity appears to affect the stucco only. A major difference between the two coatings is that the stucco is applied in a thicker and more porous coat. It is possible that certain active sites in pores did not receive enough light to be activated at the low light level but that the higher light level allowed them to become active and remove pollutants, hence explaining the increase in removal with enhanced light intensity.

For clear paint 1, levels of both organics and inorganics affect NO_x removal. The higher concentrations of organics may lead to competitive adsorption at the catalyst surface, which could negatively impact NO_x removal by clear paint 1. The literature on the subject is sparse and results vary: Ao et al. (2003) found that the presence of VOCs in the air mixture led to reduced NO removals while Poulston et al. (2009) found inconsistent results: the presence of certain VOCs

increased NO removal while others decreased it. For inorganics, if reaction sites or adsorption sites at the sample surface are limited in number, the higher NO_x concentration in the morning condition ($[NO_x]$=170 ppb) compared to afternoon ($[NO_x]$=50 ppb) could account for the decrease in NO_x removal. Husken et al. (2009) also found lower NO concentrations to be more efficiently removed when NO concentration was varied from 0.1 to 1 ppm. However, other researchers found no change in removal with higher inlet concentrations (Bengtsson and Castellote, 2010; Laufs et al., 2010) as observed in this study for the stucco.

Ozone removals by the coatings were calculated for the afternoon tests (only tests where ozone was present). Ozone removals averaged 14% and 27% for the clear paint 1 and the stucco, respectively. Analysis of variance of the data showed that ozone removal by the stucco was not significantly affected by any of the parameters.

Considering the superior performance of the stucco for NO_x and ozone removal, it was chosen for inclusion in the large-scale photochemical modeling described in Chapter 5. More detailed discussion of the full-factorial results on the stucco can be found in Cros et al. (2015).

4.3 Chamber testing quality assurance

Ten percent of the experiments involving the selected coating (stucco), as well as experiments conducted on the uncoated concrete, were repeated to evaluate repeatability of the chamber testing methodology. The experiments to be repeated were chosen randomly and run after the completion of the full factorial tests. For each replicate experiment, the relative difference with the initial experiment was calculated and compared to the calculated uncertainty obtained using error propagation calculations for the experimental system. Uncertainty was calculated using:

$$\Delta R = \sqrt{\left(\frac{1}{c_{in}}\right)^2 \Delta c_{out}{}^2 + \left(\frac{c_{out}}{c_{in}{}^2}\right)^2 \Delta c_{in}{}^2 + \left(\frac{1}{c_{in,u}}\right)^2 \Delta c_{out,u}{}^2 + \left(\frac{c_{out,u}}{c_{in,u}{}^2}\right)^2 \Delta c_{in,u}{}^2} \qquad (4.5)$$

ΔR	calculated uncertainty due to instrument measurements using error propagation
c_{in}	inlet pollutant concentration for experiment run on stucco-coated concrete (ppb)
c_{out}	outlet pollutant concentration for experiment run on stucco-coated concrete (ppb)
$c_{in,u}$	inlet pollutant concentration for experiment run on uncoated concrete (ppb)
$c_{out,u}$	outlet pollutant concentration for experiment run on uncoated concrete (ppb)

The uncertainty for measured concentrations was calculated using calibration data collected prior to each day experiments were conducted. The instrument error was taken as the relative difference between measured concentration and expected calibration concentration. A paired t-test was run on the calibration data for each instrument and p-values obtained were 0.80, 0.99, and 0.91 for NO, NO_2, and ozone calibration data, respectively.

The results of the replicate experiments are presented in Table 4.2. For the stucco-coated concrete, the relative difference between NO and NO_2 removals in the initial and replicated experiments is less than the calculated uncertainty for the measured NO_x concentration, indicating that the removals obtained in the replicated experiments are within the range of precision of the instruments. For ozone removal, the difference between the initial and replicated experiments is larger than the calculated uncertainty. These results suggest possible aging effects of the coating or chamber effects on ozone removal. For the uncoated concrete, the difference between NO_2

removals in the initial and replicated experiments is lower than the calculated uncertainty. However, for NO and ozone that is not the case, removals were higher in replicate experiments. Again, aging of the sample or chamber might explain this observation.

Table 4.2 Comparison between the calculated relative uncertainty and relative difference observed between initial and replicated experiments

	NO	NO_2	Ozone
Stucco-coated concrete			
Relative uncertainty due to instruments measurements	7.8%	14.6%	10.9%
Relative difference between initial and replicated experiment	2.9%	12.9%	15.7%
Uncoated concrete			
Relative uncertainty due to instruments measurements	5.4%	32.6%	15.7%
Relative difference between initial and replicated experiment	10.6%	26.4%	37.1%

In this report, uncertainties presented in figures showing pollutant removals by the coatings were calculated as follows:

- For the stucco, the relative uncertainty is calculated as the square root of the squared sum of the relative uncertainty due to instruments and the relative difference between initial and replicated experiments.
- For other coatings, the relative uncertainties due to instrument measurements were used.

Chapter 5. Photochemical Modeling

5.1 Description of CAMx model and dry deposition

Ground-level ozone, formed by the photochemical reactions of oxides of nitrogen (NO_x) and volatile organic compounds (VOC), is a pervasive air quality concern in the U.S. In March 2008, the U.S. Environmental Protection Agency (EPA) established primary and secondary National Ambient Air Quality Standards (NAAQS) of 0.075 ppm for ozone concentrations averaged over 8 hours. Future rulemaking based on the EPA's new periodic review of the air quality criteria and standards for ozone is expected in 2013. Texas has historically faced significant air quality challenges associated with urban areas located in its eastern half. Houston and Dallas are both classified as nonattainment under the NAAQS for ozone concentrations averaged over 8 hours; Austin and San Antonio, among other moderately sized cities in eastern Texas, have measured ozone concentrations near the level of the NAAQS and have been proactive participants in the Texas near-nonattainment-area program aimed at understanding and predicting factors that influence ozone formation in their areas and the effectiveness of measures to improve air quality.

Reductions in emissions of ozone precursors and improvement and long-term maintenance of air quality are mandated in State Implementation Plans (SIPs) for achieving attainment with NAAQS. Models such as the Comprehensive Air Quality Model with extensions (CAMx; ENVIRON, 2010), which is used by the State of Texas for attainment demonstrations and air quality planning, play a central role in the design of strategies for achieving reductions of ozone and its precursors. The purpose of this study was to evaluate the predicted ozone reductions that could be achieved by the application of photocatalytic coatings to portland cement concrete highway barriers in the Houston and DFW areas. Laboratory studies designed to emulate roadway conditions were used to establish the removal rates of ozone and NO_x by a TiO_2-containing stucco material. These data were applied in CAMx episodes developed to support air quality planning in the Houston and DFW areas, respectively, and used to predict the relative changes in ozone concentrations averaged over 8 hours. The modeling methodology used for this study leveraged recent work sponsored by the Texas Air Quality Research Program (AQRP) (Kimura et al., 2011), that examined ozone deposition to built environment surfaces.

5.1.1 Modeling episodes

CAMx is a an open-source Eulerian photochemical grid model that allows for integrated assessments of gaseous and particulate air pollution over spatial scales ranging from sub-urban to continental[2]. This work assessed the effects of photocatalytic coating application to highway barriers during two CAMx episodes (i.e., historical time periods) that are being utilized by the Texas Commission on Environmental Quality (TCEQ) for attainment demonstrations and SIP development: (1) May 31–July 2, 2006[3], which was developed for the DFW area, and (2) August 13–September 15, 2006[4], which was developed for the HGB/Beaumont/Port Arthur area. The horizontal grid structures for the two episodes consisted of a 36-km x 36-km outer Eastern U.S. grid, a nested 12-km x 12-km East Texas grid, and a nested 4-km x 4-km grid over the respective urban areas (with an additional nested 2-km x 2-km grid for Houston/Galveston). Horizontal grid

[2] http://www.camx.com/home.aspx

[3] http://www.tceq.texas.gov/airquality/airmod/data/dfw8h2

[4] http://www.tceq.texas.gov/airquality/airmod/data/hgb8h2

domains and vertical layer structures for the DFW episode are shown in Figure 5.1 and for the HGB area in Figure 5.2.

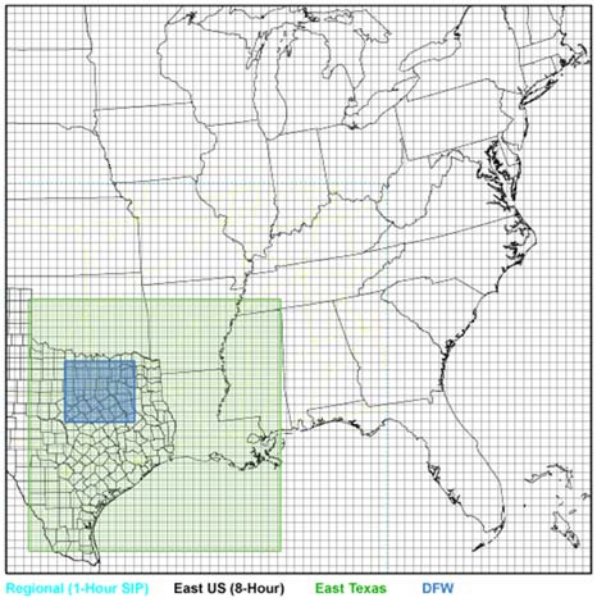

(a)

MMS Layer	Layer Top (m AGL)	CAMx Layer	Layer Center (m AGL)	Thickness (m)
38	15179.1	28	13637.9	3082.5
36	12096.6	27	10631.6	2930.0
32	9166.6	26	8063.8	2205.7
29	6960.9	25	6398.4	1125.0
27	5835.9	24	5367.0	937.9
25	4898.0	23	4502.2	791.6
23	4106.4	22	3739.9	733.0
21	3373.5	21	3199.9	347.2
20	3026.3	20	2858.3	335.9
19	2690.4	19	2528.3	324.3
18	2366.1	18	2234.7	262.8
17	2103.3	17	1975.2	256.2
16	1847.2	16	1722.2	249.9
15	1597.3	15	1475.3	243.9
14	1353.4	14	1281.6	143.6
13	1209.8	13	1139.0	141.6
12	1068.2	12	998.3	139.7
11	928.5	11	859.5	137.8
10	790.6	10	745.2	90.9
9	699.7	9	654.7	90.1
8	609.7	8	565.0	89.3
7	520.3	7	476.1	88.5
6	431.8	6	387.9	87.8
5	344.0	5	300.5	87.1
4	256.9	4	213.8	86.3
3	170.6	3	127.8	85.6
2	85.0	2	59.4	51.0
1	33.9	1	17.0	33.9

AGL - Above ground level.

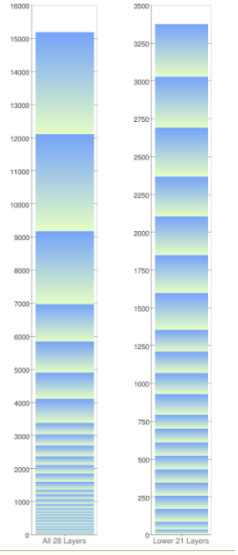

(b)

Figure 5.1 June 1–30, 2006 CAMx episode: (a) horizontal modeling domain showing the outer 36km x 36km Eastern U.S., nested 12km x 12km East Texas, and 4km x 4km DFW grids; (b) vertical layer structure
From: http://www.tceq.texas.gov/airquality/airmod/data/dfw8h2/dfw8idsh2_camx_domain.html.

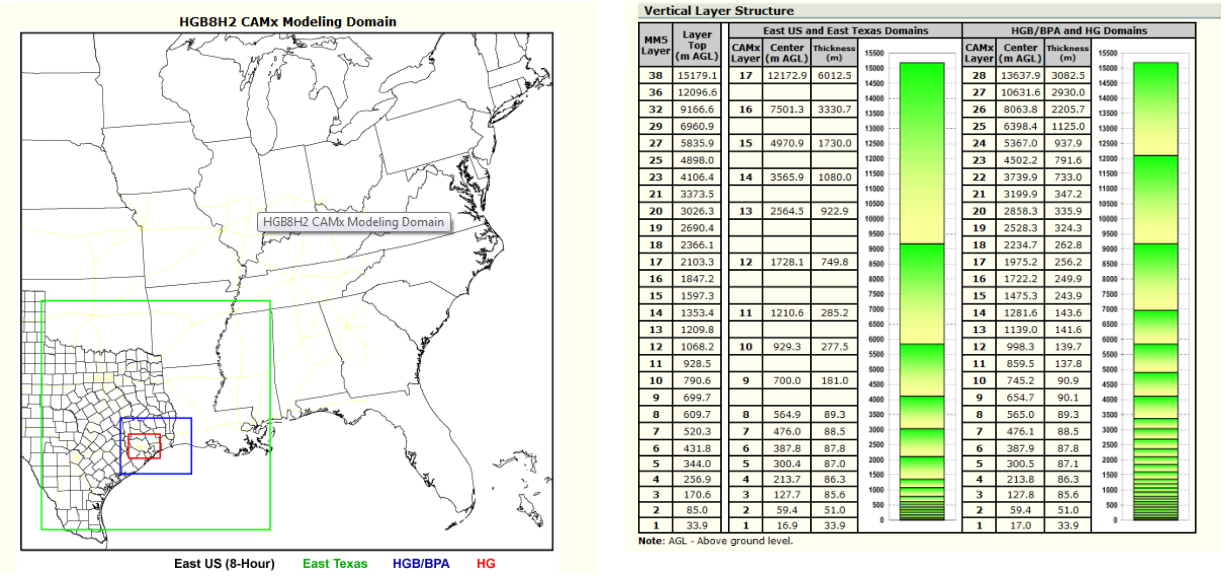

(a)

Vertical Layer Structure

MM5 Layer	Layer Top (m AGL)	East US and East Texas Domains: CAMx Layer	Center (m AGL)	Thickness (m)	HGB/BPA and HG Domains: CAMx Layer	Center (m AGL)	Thickness (m)
38	15179.1	17	12172.9	6012.5	28	13637.9	3082.5
36	12096.6				27	10631.6	2930.0
32	9166.6	16	7501.3	3330.7	26	8063.8	2205.7
29	6960.9				25	6398.4	1125.0
27	5835.9	15	4970.9	1730.0	24	5367.0	937.9
25	4898.0				23	4502.2	791.6
23	4106.4	14	3565.9	1080.0	22	3739.9	733.0
21	3373.5				21	3199.9	347.2
20	3026.3	13	2564.5	922.9	20	2858.3	335.9
19	2690.4				19	2528.3	324.3
18	2366.1				18	2234.7	262.8
17	2103.3	12	1728.1	749.8	17	1975.2	256.2
16	1847.2				16	1722.2	249.9
15	1597.3				15	1475.3	243.9
14	1353.4	11	1210.6	285.2	14	1281.6	143.6
13	1209.8				13	1139.0	141.6
12	1068.2	10	929.3	277.5	12	998.3	139.7
11	928.5				11	859.5	137.8
10	790.6	9	700.0	181.0	10	745.2	90.9
9	699.7				9	654.7	90.1
8	609.7	8	564.9	89.3	8	565.0	89.3
7	520.3	7	476.0	88.5	7	476.1	88.5
6	431.8	6	387.8	87.8	6	387.9	87.8
5	344.0	5	300.4	87.0	5	300.5	87.1
4	256.9	4	213.7	86.3	4	213.8	86.3
3	170.6	3	127.7	85.6	3	127.8	85.6
2	85.0	2	59.4	51.0	2	59.4	51.0
1	33.9	1	16.9	33.9	1	17.0	33.9

Note: AGL - Above ground level.

(b)

Figure 5.2 August 13–September 15, 2006 CAMx episode: (a) horizontal modeling domain showing the outer 36km x 36km Eastern U.S., nested 12km x 12km East Texas, 4km x 4km HGB/Beaumont/Port Arthur, and 2km x 2km Houston/Galveston grids; (b) vertical layer structure
From: http://www.tceq.texas.gov/airquality/airmod/data/hgb8h2

In order to maintain consistency between the two episodes for the purposes of this work, the CAMx version utilized for the Houston episode was changed from v.4.53 to v.5.20.1pr to match the more recent version used for the Dallas episode. In addition, the asymmetric convective model (ACM2) parameterization, which is a recently implemented alternative to K-theory for the representation of vertical diffusion in CAMx, had been used by the TCEQ in the Dallas episode, but not in the Houston episode. The ACM2 parameterization was used for the Dallas episode, but not used for the Houston episode to be consistent with the original modeling episode developed by TCEQ.

For the purposes of this work, three additional changes were required for each of the CAMx modeling episodes:

1. Modification of the dry deposition algorithm to account for removal of ozone and NO_x by highway surfaces and by uncoated or photocatalytic stucco-coated concrete barriers;
2. Modification of the land use/land cover data to spatially represent highways and traffic barriers; and
3. Modification of the Tropospheric Ultraviolet and Visible (TUV) radiative transfer model, a pre-processor for CAMx to calculate photolysis rates, to output UV solar irradiance (W/m^2), which was needed because the activity of photocatalytic coatings is light dependent.

These modifications are described in detail below. For each episode, a base case CAMx simulation was conducted that included explicit consideration of the dry deposition of ozone and NO_x to highways and uncoated barriers. A sensitivity study was conducted for each episode that

was the same as the base case, but evaluated the removal of pollutants by photocatalytic stucco-coated (instead of uncoated) barriers during sunlit hours.

5.1.2 CAMx dry deposition algorithm

In the CAMx episodes considered in this work, the dry deposition process for gases is modeled using algorithms developed for the Regional Acid Deposition Model (Wesely and Hicks, 1977; Wesely, 1989; Walmsley and Wesely, 1996; Wesely and Hicks, 2000). The dry deposition mass flux density is modeled as shown in Eq. 5.1.

$$F^{i}{}_{c} = v^{i}{}_{d} \cdot C^{i}{}_{z} \tag{5.1}$$

where

F^{i}_{c} dry deposition flux of the gas (ppbv m sec^{-1}), *i*, of interest

v_{d} dry deposition velocity of *i* (m sec^{-1})

C^{i}_{z} concentration or mixing ratio of *i* at a reference height *z* (ppbv), which is at the mid-point of first vertical layer height in CAMx

In these algorithms, the dry deposition velocity is modeled using an approach analogous to Ohm's law in electrical circuits shown in Figure 5.3 and the following equation:

$$v_{d}{}^{i} = \left(r_{a} + r_{b}{}^{i} + r_{c}{}^{i}\right)^{-1} \tag{5.2}$$

where

r_{a}^{i} aerodynamic resistance above the surface (sec m^{-1})

r_{b}^{i} quasi-laminar sub-layer resistance to the transport of *i* (sec m^{-1})

r_{c}^{i} surface resistance (sec m^{-1}) to the uptake of *i*

The resistances are described in detail elsewhere (Wesely and Hicks, 1977; Wesely, 1989; Walmsley and Wesely, 1996; Wesely and Hicks, 2000). This work necessitated only modifications to the components of the bulk surface resistance in the dry deposition algorithm for urban land use.

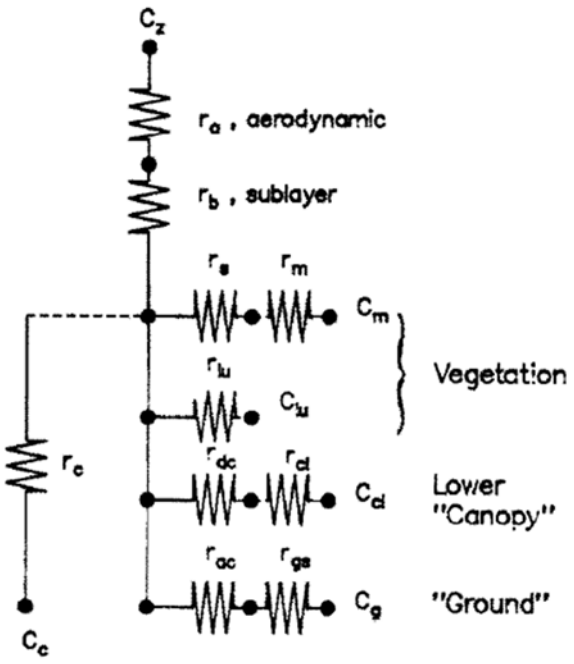

Figure 5.3 Resistance pathways to dry deposition from Wesely (1989)

Note that all resistances and concentrations are expressed in units of sec m-1 and ppbv, respectively, in this work. Cz is the ambient concentration of the pollutant and Cs is the bulk substrate concentration that is assumed to be zero (i.e., no surface emissions). r_a is the aerodynamic resistance above the surface, r_b is the quasi-laminar sub-layer resistance to the transport, and r_c is the surface resistance (sec m-1). r_s is the surface bulk resistance for leaf stomata (sec m-1); r_m is the bulk mesophyllic resistance (sec m-1); r_{lu} is the leaf cuticular resistance, or otherwise the outer surfaces, in the upper canopy; r_{dc} is the resistance due to buoyant convection in the lower canopy; r_{cl} includes resistances associated with leaves, twig, bark, or other exposed surfaces in the lower canopy; and r_{ac} and r_{gs} are resistances associated with canopy height and density and soil and leaf litter at the ground surface (sec m-1), respectively.

The components of the bulk surface resistance, shown in Figure 5.3, are inferred from measurements of net vertical fluxes above the bulk surface for eleven broad land use categories (urban, agricultural land, range land, deciduous forest, coniferous forest, mixed forest including wetland, salt and fresh water, barren land that is mostly desert, non-forested wetland, mixed agriculture and range land, and rocky open areas with low-growing shrubs) and five seasons (mid-summer with lush vegetation, autumn with unharvested cropland, late autumn after frost but no snow, winter with snow on the ground and subfreezing, transitional spring with partially green short annuals). Wesely (1989) notes that these may not be representative of surface resistances for a particular land cover, geographic location, or time of day. In CAMx, a land use input file is required that assigns the areal fractional distribution (0 to 1) of the eleven land use categories in each individual grid cell. Surface resistances are calculated for each land use category, for each time step within the numerical integration, in a grid cell, and dry deposition velocities for land use categories are weighted by their spatial extent to obtain an average dry deposition velocity at the mid-point of the lowest vertical layer of the model. In general, for ozone, for example, the hierarchy of resistances (high to low) associated with Wesely's land cover categories yields

deposition velocities that are highest for agricultural land, followed by forested areas and rangeland, and lowest for water, barren, and urban areas.

5.2 Surface resistances determination for the stucco

In order to determine surface resistances for the coating selected through laboratory experiments, it was necessary to separate the transport resistance from the surface resistance that control the deposition of pollutants onto materials. We will here describe the process used to determine the surface resistances necessary for inclusion of photocatalytic materials into the CAMx model.

First, deposition to the reactor walls and the transport limited deposition velocity of the reactor was calculated. They are independent of the material tested. Then, the deposition velocities of the various pollutants on the uncoated and stucco-coated concrete surfaces were measured. Finally, the transport-limited deposition velocity for the reactor was used to back calculate the surface resistances to the deposition of the pollutants to the uncoated and stucco-coated concrete surfaces.

5.2.1 Description of experiments

Experiments were run in the same reactor used for full factorial testing. Parameters found to influence removal by the uncoated concrete and the stucco-coated concrete were varied to obtain relationships between the tested parameters and the deposition rate of pollutants to the material surface. The effect of contact time was not tested because it influences the rate of deposition through the transport resistance, which is calculated by CAMx and does not need to be empirically added to the current model.

Temperature, humidity, and light intensities were varied for the stucco-coated concrete while only humidity was varied for the uncoated concrete. Table 5.1 lists the various tests conducted.

Table 5.1 Experiments run to determine kinetic parameters for inclusion in CAMx model

Material	Temperature (°C)	Water vapor (ppm) (corresponding RH)	Light intensity (mW/cm^2)
Uncoated concrete	35	11100 (20%)	2
		27750 (50%)	
		36100 (66%)	
Stucco-coated concrete	30	27750 (66%)	2
	35	27750 (50%)	
	35	27750 (50%)	1
			1.5
	35	11100 (20%)	2
		36100 (66%)	

5.2.2 Deposition of pollutant species to the reactor surfaces

Deposition of pollutants in the test chambers occurs both on the chamber surfaces and the sample surface. An empty chamber experiment allows determination of deposition to chamber surfaces. Doing so, once a sample is introduced in the chamber, it is possible to determine how much removal actually occurs on the sample surface versus the chamber surfaces. The deposition to the chamber walls is expected to be small given that they are made of stainless steel, which is not a reactive material. Other surfaces inside the chamber might be more reactive (UV lamps, lamp holders) but their surfaces are small.

The deposition velocity of O_3, NO, and NO_2 to the reactor walls were measured by injecting air containing the gases into the reactor, keeping other experimental conditions identical to the ones used for other experiments. The deposition velocity of the gases was measured using a steady-state mass balance on the well-mixed reactor:

$$v_{d,k,w} = \frac{\lambda V_{empty}}{A_{w,empty}}\left(\frac{c_{k,inlet}}{c_k} - 1\right) \tag{5.3}$$

$v_{d,k,w}$ deposition velocity of gas k to the chamber walls (m/h)
λ reactor air exchange rate (h)
V_{empty} air volume of the reactor, when empty (m^3)
$A_{w,empty}$ area of exposed reactor walls, when empty (m^2)
$c_{k,inlet}$ gas k concentration in the chamber inlet (ppb)
c_k gas k concentration in the chamber outlet (ppb)

5.2.3 Determination of reactor transport resistance

For each pollutant, the transport resistance is a function of the fluid mechanics inside the reactor, which were held constant for these experiments. The transport resistance in the reactor was calculated using ozone deposition to a highly reactive surface: concrete coated with a potassium iodide solution (125 mg KI / 100 mL distilled water). In this specific case, the surface resistance to the deposition of ozone on the material is negligible so the transport resistance is the only resistance to deposition. Thus, the deposition velocity on the potassium iodide-coated concrete in this case is:

$$\frac{1}{v_{d,O_3,KI}} = \frac{1}{v_{t,O_3}} + \frac{1}{v_{s,O_3,KI} \approx \infty} = r_{t,O_3} + \left(r_{s,O_3,KI} \approx 0\right) \tag{5.4}$$

$v_{d,O3,KI}$ deposition velocity of ozone on the potassium iodide-coated concrete (m/h)
$v_{t,O3}$ transport-limited deposition velocity of ozone in the reactor (m/h)
$v_{s,O3,KI}$ reaction-limited deposition velocity of ozone in the potassium iodide-coated concrete (m/h)
$r_{t,O3}$ transport resistance to the deposition of ozone to tested materials in the test reactor (h/m)
$r_{s,O3,KI}$ surface resistance to the deposition of ozone to potassium iodide-coated concrete (h/m)

The deposition velocity of ozone on the potassium iodide-coated concrete is determined using a mass balance on the well-mixed reactor:

$$v_{t,O_3} = v_{d,O_3,KI} = \frac{\lambda V_{sample}}{A_{sample}}\left(\frac{c_{O_3,inlet}}{c_{O_3}} - 1\right) - v_{d,O_3,w}\frac{A_{w,sample}}{A_{sample}} \tag{5.5}$$

V_{sample} air volume of the reactor in the presence of a concrete sample (m^3)
A_{sample} projected area of the concrete sample tested (m^2)
$A_{w,sample}$ area of exposed reactor walls in the presence of a concrete sample (m^2)

The measured value for the transport-limited deposition velocity of ozone in the reactor was used to estimate the transport-limited deposition velocities in the reactor for NO and NO_2, $v_{t,NO}$ and $v_{t,NO2}$, respectively. Mass transfer correlations for gas flow above a flat plate were used to determine the relationship between $v_{t,O3}$ and $v_{t,NO}$ and $v_{t,NO2}$ (Asano, 2007):

$$v_{t,NO} = \left(\frac{D_{NO}}{D_{O_3}}\right)^{2/3} \times v_{t,O_3} \text{ and } v_{t,NO_2} = \left(\frac{D_{NO_2}}{D_{O_3}}\right)^{2/3} \times v_{t,O_3} \tag{5.6}$$

D_{NO} NO diffusion coefficient (m^2/h)
D_{NO2} NO_2 diffusion coefficient (m^2/h)
D_{O3} O_3 diffusion coefficient (m^2/h)

5.2.4 Determination of pollutant deposition velocity

The deposition velocity for each pollutant, in each condition tested, was calculated using a steady-state mass balance on the well-mixed test reactor:

$$v_{d,k} = \frac{\lambda V_{sample}}{A_{sample}}\left(\frac{c_{k,inlet}}{c_k} - 1\right) - v_{d,k,w}\frac{A_{w,sample}}{A_{sample}} \tag{5.7}$$

$v_{d,k}$ deposition velocity of pollutant k on the material surface (m/h)

5.2.5 Calculation of coating surface resistances

Using the values obtained from the previous paragraphs, it was possible to calculate the surface resistance for the uncoated concrete and the stucco-coated concrete surfaces for all experimental conditions. A linear correlation between an environmental parameter and deposition velocity was obtained, except between light intensity and deposition velocity for the stucco where a power law was used. This expression was then used to calculate the surface resistance as:

$$r_s = \frac{1}{v_d} - \frac{1}{v_t} \tag{5.8}$$

r_s surface resistance (h/m)
v_d deposition velocity (m/h)
v_t transport-limited deposition velocity (m/h)

The resulting expressions for the surface resistances of the coated and uncoated concrete, empirically determined through laboratory experiments, are presented in section 5.3.

5.3 Photochemical modeling in CAMx

The heterogeneity of urban environments has typically not been recognized in the urban land use type category in the dry deposition algorithms of Wesely (1989) and Walmsley and Wesely (1996), and within CAMx. In a recent project sponsored by the Texas AQRP, Poppendieck et al. (2012) and Kimura et al. (2012) examined whether refinements in land use/land cover classifications and dry deposition rates in urban settings could appreciably affect predicted ozone concentrations. The research included two major phases: (1) extensive experiments to determine the reactivity, or inversely the surface resistance, of eighteen large built environment surface materials with ozone, and (2) applications of CAMx with refined urban deposition calculations to account for variations in built environment surfaces, urban vegetation, and updated surface resistances. Travis County, which includes the city of Austin, served as the case study area. Geospatial data were collected for three broad types of built environment surfaces in areas classified as urban in Travis County, including the transportation network, residential properties, and commercial and tax-exempt properties. Among the primary data sources utilized for the project were TxDOT's Pavement Management Information System (PMIS), the City of Austin's 2003 ArcGIS transportation and building footprint files, the Travis County Appraisal District database, Google Earth, and field surveys conducted by the team. New land use/land cover categories based on pavement, siding, or roofing material type were developed and replaced areas previously classified broadly as urban in Travis County. These data were matched with surface

resistances for fresh and weathered materials, respectively, determined from the experiments to obtain new estimates of dry deposition velocities and ozone concentrations using CAMx. Refined characterization of the urban built environment on the dry deposition of ozone in Austin, Texas, resulted in decreases in predicted daily maximum 8-hour average ozone concentrations of 0.2 to 1.3 ppb. The results were primarily attributed to deposition to urban vegetation and highlighted the importance of characterizing Texas urban landscapes undergoing rapid development (Kimura et al., 2011; Poppendieck et al., 2011).

This project leveraged the previous experience gained by the AQRP project, but only focused on characterizing highways and highway barriers in the DFW and HGB areas, respectively. For the purposes of this work, surface resistances for illuminated coated and uncoated concrete barriers were obtained in the course of this project and implemented in CAMx, according to the equations presented in Appendix B.

Temperature and water vapor concentrations needed for the surface resistance formulations were obtained from the CAMx meteorological algorithms. Land use/land cover data characterizing highways and surrounding barriers and modifications to the TUV radiative transfer model are described in detail in sections below. Since photocatalytic activity of the coating occurs in the presence of UV light, it was necessary for modeling purposes to establish a light intensity threshold below which the photocatalytic activity of the coating is considered negligible and the photocatalytic coating behaves like any urban surface. The minimum light intensity used for chamber experiments was 1 mW/cm^2. Accurately extrapolating the experimental data to 0 mW/cm^2 was difficult given the non-linearity of the experimental data. For modeling purposes, the lower modeling limit for photocatalytic activity was set at 0.5 mW/cm^2, the mid-point between no light conditions and the lowest light intensity at which photocatalytic activity was observed.

For the base case, surface resistances for uncoated barriers identified during the course of the project were utilized. For the sensitivity studies, the identified surface resistances for coated barriers were implemented only during hours with sunlight; in the absence of sunlight, surface resistances for uncoated barriers were utilized. Surface resistances for ozone for highways were obtained from (Poppendieck et al., 2011): asphalt $R_{s,O3}$ = 990 s/m; concrete $R_{s,O3}$ = 500 s/m; these values were not subject to concentrations of NO and NO_2 described above. Surface resistances from Wesely's (1989) urban land use category for NO and NO_2 were utilized for highways pavements.

Within CAMx, "the continuity equation is numerically marched forward in time over a series of time steps. At each step, the continuity equation is replaced by a time-splitting approach that calculates the separate contribution of each major process (advection, diffusion, chemistry, etc.) to concentration change within each grid cell" (ENVIRON, 2010). Thus the algorithms for major processes are applied sequentially within one time step. The order can influence determination of the switch for low NO and high NO conditions, as defined during the course of the project. Thus, a decision was made to determine the switch based on grid cell average concentrations, not on intermediate concentrations determined between major processes within the CAMx operator splitting execution. The effect of this decision was that the low NO switch was more frequent than the high NO switch regardless of the episode considered.

5.3.1 Determination of solar insolation

The TUV radiative transfer model, originally developed by the National Center for Atmospheric Research (NCAR[5]) was adapted to estimate solar insolation within CAMx. TUV simulates spectral irradiance between 121 and 750 nm and serves as a pre-processor. ENVIRON, the developer of the CAMx model, has a version of the TUV program that calculates photolysis rate for atmospheric chemical reactions as a function of elevation above the ground, solar zenith angle, surface albedo, atmospheric turbidity, and ozone column, and generates an input file for CAMx. At run time, CAMx acquires these five parameters for specific modeling grid cells, accesses TUV calculated photolysis rate under similar conditions through a look-up table, and linearly interpolates the values. The results are adjusted to account for attenuation by clouds to estimate photolysis rates for the grid cell.

For the purposes of this work, the TUV model distributed by ENVIRON was adapted to estimate solar insolation for wavelengths shorter than 380 nm. Direct and diffuse light from above ground level was included in the calculation for the fully illuminated side of the barrier; only diffuse light was included in the calculation for the shaded side of the barrier. Determination of the solar insolation was performed using the same values of zenith angle, albedo, turbidity, ozone column, cloud cover, and cloud energy transmission coefficients as for the calculation of photolysis rates, and the results were exported as a file with same format as the CAMx photolysis rate file. CAMx was modified to read this extra file and store the look up table of solar insolation values in a dedicated array that could be utilized in the dry deposition subroutines. As described above, dark conditions were assumed when the solar insolation dropped below 0.5 mW/cm^2.

5.3.2 Spatial representation of highways and barriers

The locations, areas, and pavement materials of highways in the DFW and HGB areas were determined from the TxDOT PMIS. Each record in the PMIS was associated with a TxDOT managed highway segment defined by (1) a linearly referenced section of highway routes, which are provided as polyline features within a geographic information system (GIS) and (2) one of five types of roadway beds: single main lane road, right main lane road, left main lane road, right frontage road, and left frontage road. Each record also specifies the pavement material—either asphaltic concrete, continuously reinforced concrete, or joined concrete—and total width of road bed. This information was processed in GIS as paved surface area by material type within model grid cells:

$$A\_pvmt = L \times W\_pvmt \tag{5.9}$$

where

A_pvmt	area of pavement
L	longitudinal length of the roadway segment
W_pvmt	width of pavement for a particular road bed (main lane, frontage etc.)

The surface area of highway barriers with photocatalytic stucco coating was estimated using a different method, because these structures were not included in the PMIS. The polyline features of highway routes allowed estimation of their lengths within model grid cells. It was

[5] http://cprm.acd.ucar.edu/Models/TUV/

assumed that all highway routes uniformly had a center barrier with a height of 1.1 meter. Both sides were coated with photocatalytic stucco, regardless of the highway type as long as it was included in the PMIS:

$$A\_paint = L \times h\_barrier \times 2 \quad (5.10)$$

where

A_paint	area of surface on which the photocatalytic paint would be applied
h_barrier	height of the median barrier, i.e., 1.1 m

The factor of two accounted for both sides of the barrier.

Of all highways in the nine-county DFW and eight-county HGB area, only segments within the "Urban Area" or "Urban Cluster" as defined by the U.S. Census Bureau[6] were explicitly represented as described above; this approach assumed that highways in rural area were less likely to be accompanied by structures on which a photocatalytic coating could be applied. These assumptions likely resulted in an over-estimation of the total coated surface area, as not all highway routes have median barriers for example, for traffic safety. However, photocatalytic coatings could potentially be applied to structures other than median barriers, such as road side barrier walls or bridges.

The version CAMx utilized in this work applies the dry deposition of Wesely (1989), which designates land use/land cover within a modeled region as one of 11 land use categories as described above. The total highway pavement area within each grid cell was subtracted from the "urban" category area and established as a twelfth land use category, designated as "highway" in the land use/land cover input file for CAMx. Table 5.2 shows the total surface area for the nine-county DFW and eight-county HGB areas, calculated on the Lambert Conformal projection coordinates used in the CAMx modeling[7].

Table 5.2 Highway and barrier surface area (km^2) within the nine-county DFW and eight-county HGB regions.

	Total Area of Interest	CAMx Urban Area	Asphalt Pavements	Concrete Pavements	Photocatalytic Coating
DFW 9 Counties	18241.4	1344.7	37.5	36.3	5.3
HGB 8 Counties	20422.6	2554.3	17.8	42.9	4.4

Figure 5.4 and Figure 5.5 show the spatial distribution of highways assumed to have barriers in the DFW and HGB areas, respectively.

[6] http://www.census.gov/geo/www/ua/2010urbanruralclass.html

[7] http://www.tceq.texas.gov/airquality/airmod/data/dfw8h2/dfw8idsh2_camx_domain.html

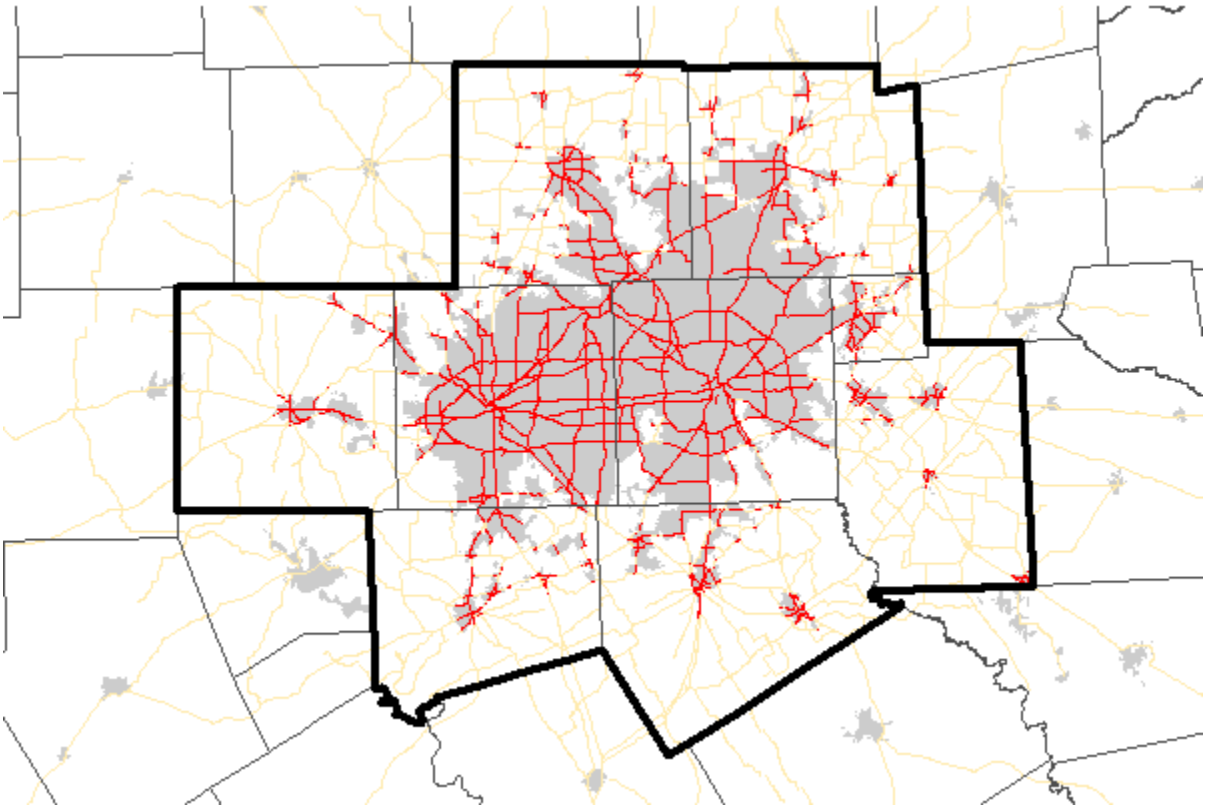

Figure 5.4 The locations of highways in the DFW area (red) assumed to have barriers. Highways not included but with records in the TxDOT PMIS are shown in pale yellow. The "Urban Area" or "Urban Cluster" as defined by the U.S. Census Bureau[8] is shown in gray. The boundary of the DFW nine-county region considered in this study is delineated in black.

[8] http://www.census.gov/geo/www/ua/2010urbanruralclass.html

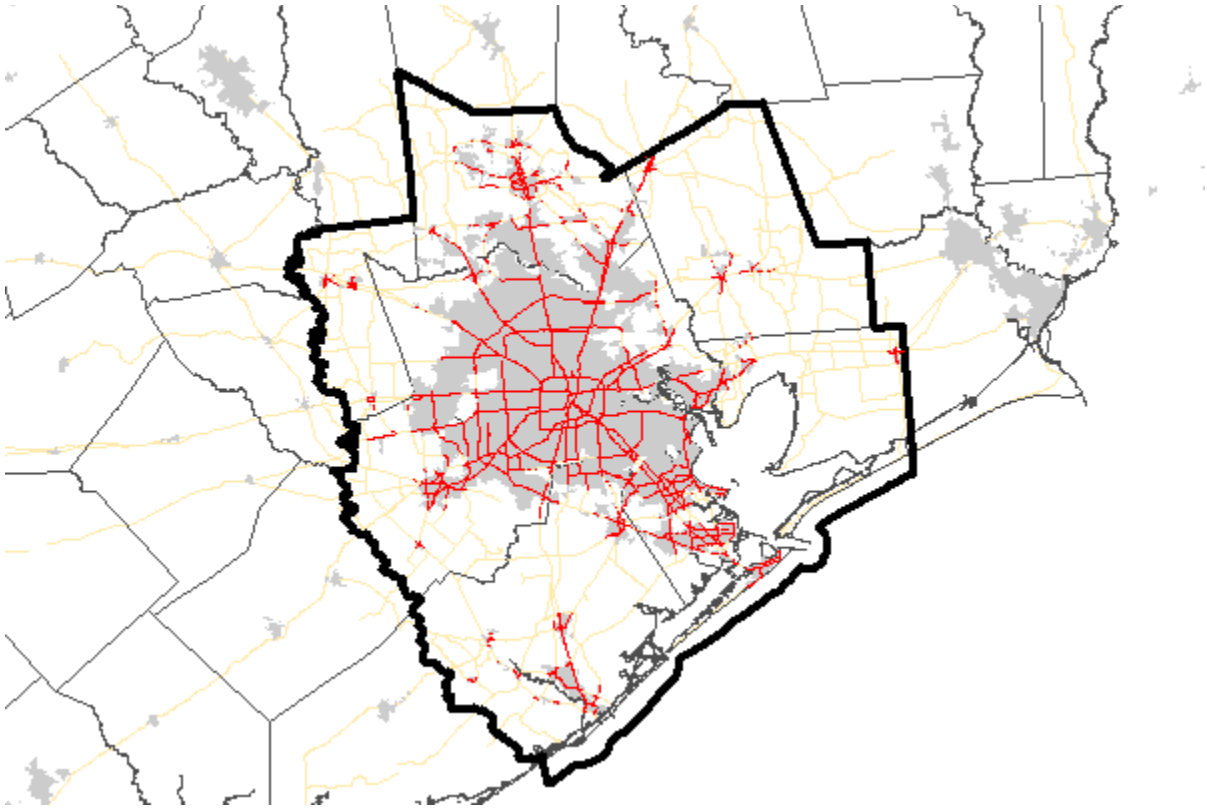

Figure 5.5 The locations of highways in the HGB area (red) assumed to have barriers. Highways not included but with records in the TxDOT PMIS are shown in pale yellow. The "Urban Area" or "Urban Cluster" as defined by the U.S. Census Bureau[9] is shown in gray. The boundary of the HGB eight-county region considered in this study is delineated in black.

5.3.3 Results

For each episode, a base case CAMx simulation was conducted that included explicit consideration of the dry deposition of ozone and NO_x to highways and uncoated barriers. A sensitivity study was conducted for each episode that was the same as the base case, but evaluated the removal of pollutants by photocatalytic stucco-coated (instead of uncoated) barriers during sunlit hours. Figure 5.6 shows daily maximum ozone concentrations averaged over 8 hours for the base case and photocatalytic stucco study within the nine-county DFW and eight-county HGB areas. Figure 5.7 and Figure 5.8 show the differences in daily maximum ozone concentrations averaged over 8 hours and maximum differences in ozone concentrations averaged over 8 hours in the DFW and HGB areas, respectively between the base case and photocatalytic stucco study (base case—stucco). Differences in daily maximum 8-hour averaged ozone concentrations in the DFW area across the episode ranged from -0.0001 to 0.09 ppb. Maximum difference in 8-hour averaged ozone concentrations, regardless of time of day or magnitude, ranged from 0.01 to 0.1 ppb in the DFW area. Differences in daily maximum 8-hour averaged ozone concentrations in the HGB area across the episode ranged from 0.0006 to 0.04 ppb. Maximum difference in 8-hour averaged ozone concentrations, regardless of time of day or magnitude, ranged from 0.004 to 0.1 ppb in the HGB area.

[9] http://www.census.gov/geo/www/ua/2010urbanruralclass.html

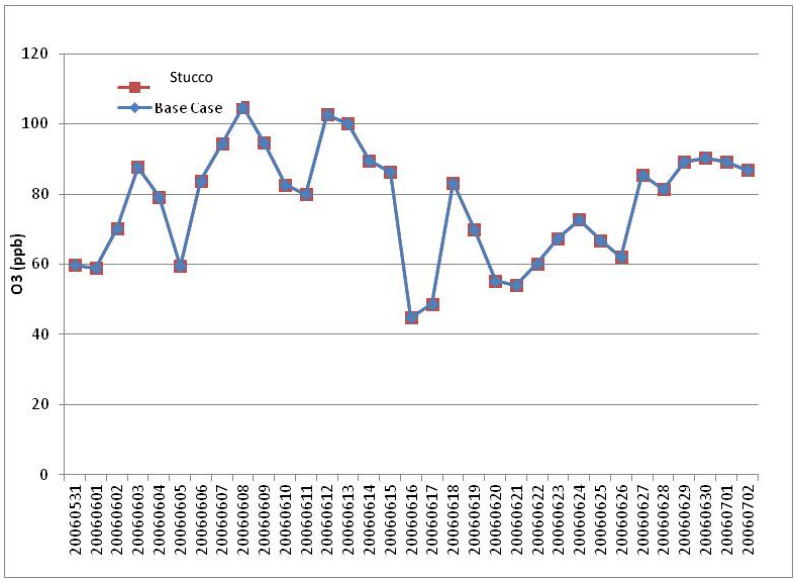

(a)

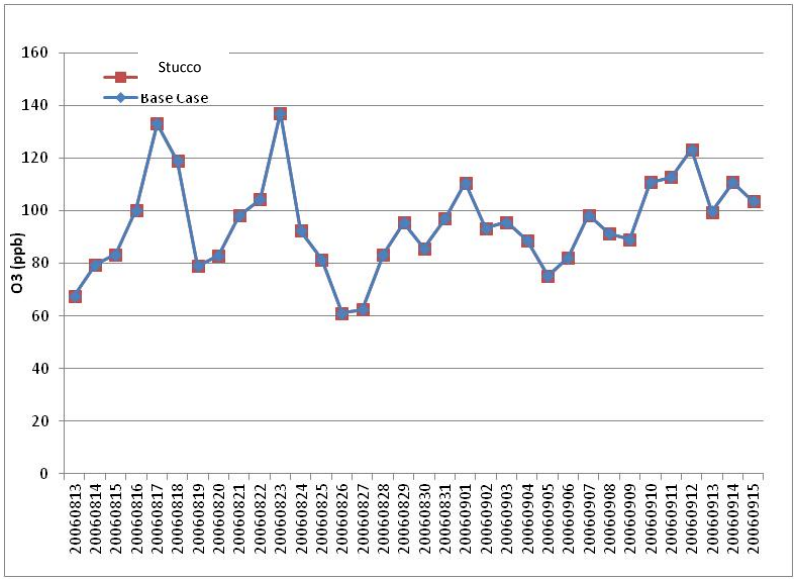

(b)

Figure 5.6 Daily maximum ozone concentrations averaged over 8 hours for the base case and photocatalytic stucco study within the (a) DFW nine-county and (b) HGB eight-county areas

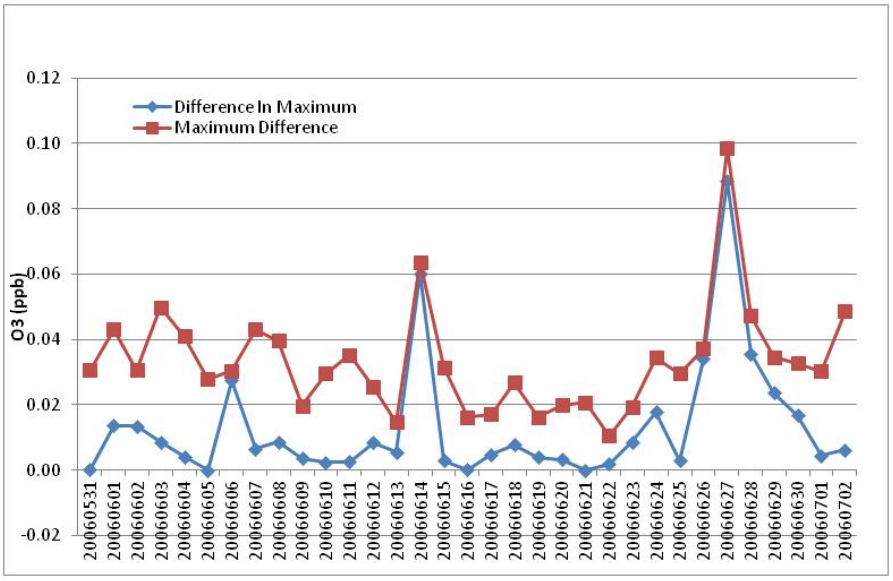

Figure 5.7 Difference in daily maximum ozone concentrations averaged over 8 hours and maximum differences in ozone concentrations averaged over 8 hours in the DFW area between the base case and photocatalytic stucco study (base case—stucco)

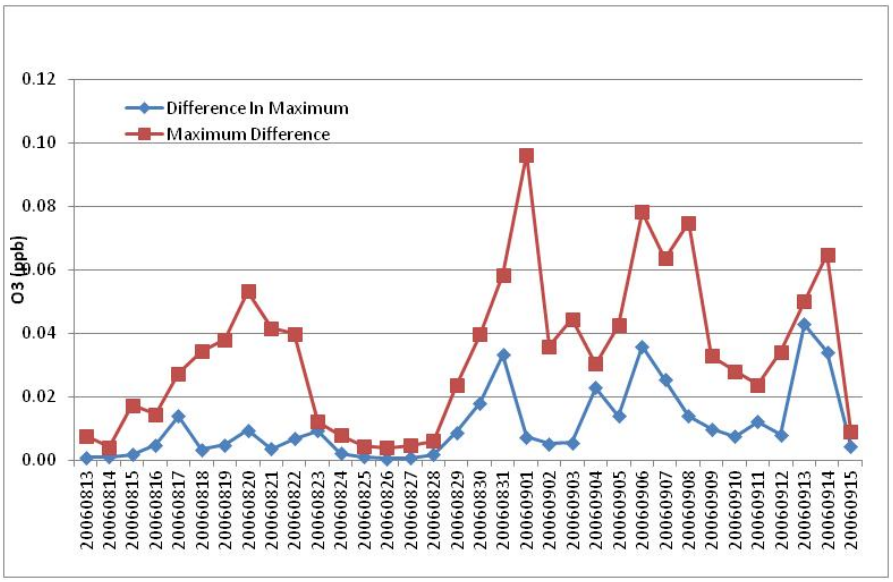

Figure 5.8 Difference in daily maximum ozone concentrations averaged over 8 hours and maximum differences in ozone concentrations averaged over 8 hours in the Houston/Galveston area between the base case and photocatalytic stucco study (base case—stucco)

In order to evaluate the sensitivity of predicted ozone concentrations to the total photocatalytic stucco-coated surface area, two additional CAMx simulations were performed for the DFW region: (1) the surface area of the barrier was tripled while keeping all other conditions the same ("triple barrier" case) and (2) in addition to the barriers, all asphalt and concrete pavements in the base case were converted to photocatalytic stucco-coated concrete ("all coated" case). Figure 5.9 shows the differences in daily maximum ozone concentrations averaged over 8

hours between the base case and each of the three photocatalytic stucco-coated cases. The "original"—or the case in which only barriers were coated with photocatalytic stucco—is identical to the results shown in Figure 5.6. The "triple barrier" case and "all coated" cases resulted in greater ozone reductions than the "original" case. The "triple barrier" and "all coated" cases had three and fifteen times, respectively, greater photocatalytic stucco-coated surface area than the "original" case. Incremental changes in predicted ozone concentrations were not proportional to incremental changes in photocatalytic stucco-coated surface area, especially on days where the "original" case resulted in relatively larger ozone reductions. For example, reductions in daily maximum 8-hour average ozone concentrations on June 27 were 0.089 ppb, 0.102 ppb, and 0.136 ppb for the "original," "triple barrier," and "all coated" cases, respectively, relative to the base case. Thus, adding to the total photocatalytic stucco-coated surface area resulted in ozone reductions (relative to the base case) that exceeded the "original" case by only 15% ("triple barrier) and 50% ("all coated"). For days during which the "original" case exhibited more modest reductions in daily maximum ozone concentrations, the responsiveness to increasing the total photocatalytic stucco surface area was greater. For example, on June 19 the "original," "triple" barrier," and "all coated" cases resulted in reductions in daily maximum ozone concentrations of 0.0039 ppb, 0.011 ppb, and 0.464 ppb, respectively, relative to the base case. The "triple barrier" and "all coated" case increased the reductions in daily maximum 8-hour ozone concentrations by factors of 2.7 and 11.9, respectively, in comparison to the "original" case for this date. Figure 5.10 shows the maximum differences in ozone concentrations averaged over 8 hours in the DFW area, comparing the base case and each of photocatalytic stucco-coated cases. The "original" case is identical to that shown in Figure 5.6. Similar to differences in the daily maximum ozone concentration, the maximum differences in ozone concentrations also increased with the photocatalytic stucco-coated surface area.

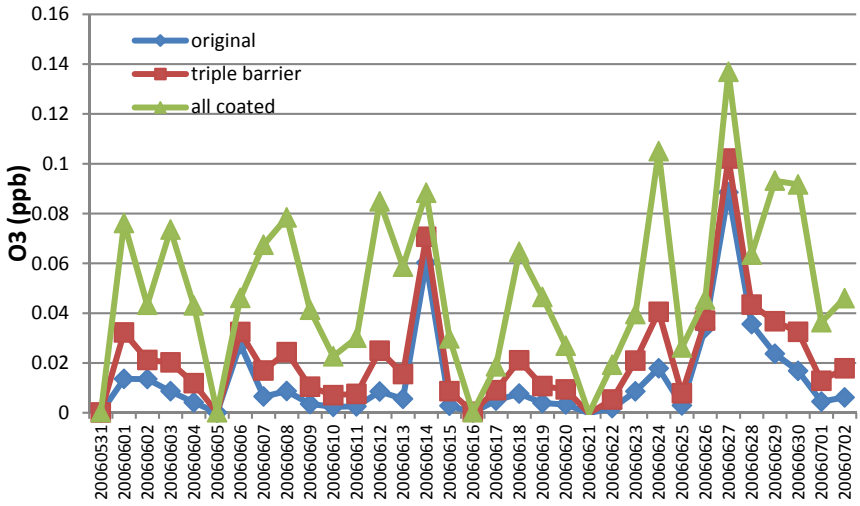

Figure 5.9 Difference in daily maximum ozone concentrations averaged over 8 hours in the DFW area between each of photocatalytic stucco-coated cases and the base case

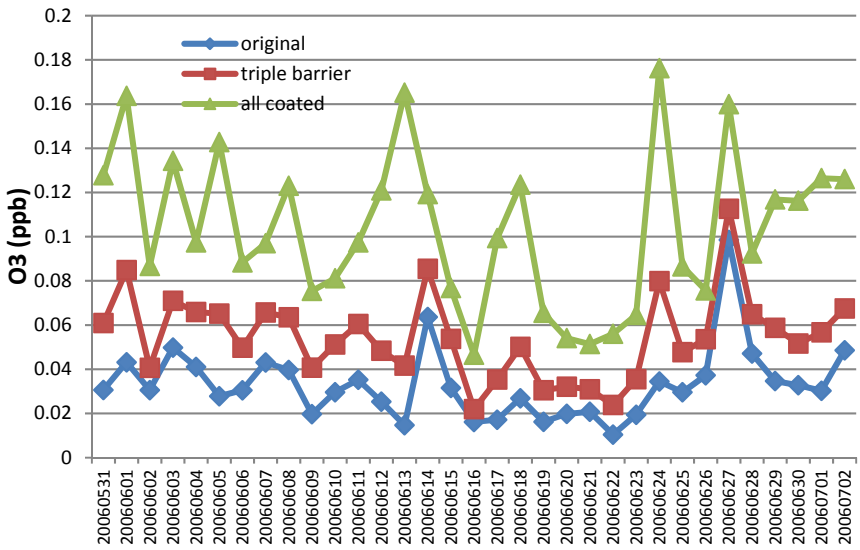

Figure 5.10 Maximum differences in ozone concentrations averaged over 8 hours in the DFW area between each of photocatalytic stucco-coated cases and the base case

5.3.4 Summary and key findings

Reductions in emissions of ozone precursors and improvement and long-term maintenance of air quality are mandated in SIPs for achieving attainment with NAAQS. The photochemical grid model CAMx is used by the State of Texas for attainment demonstrations and air quality planning and, consequently, plays a central role in the design of strategies for achieving reductions of ozone and its precursors. This study evaluated the predicted reductions in ozone concentrations averaged over 8 hours that could be achieved by the application of photocatalytic coatings to portland cement concrete highway barriers in the Houston and DFW areas. The laboratory studies, which were designed to emulate roadway conditions, were used to establish the removal rates of ozone and NO_x by a TiO_2-based material, photocatalytic stucco. These data were applied in CAMx episodes developed to support air quality planning in the Houston and DFW areas, respectively. Three modifications were required for each of the CAMx modeling episodes:

1. Modification of the dry deposition algorithm to account for removal of ozone and NOx by highway surfaces and by uncoated or photocatalytic stucco-coated concrete barriers based on project-generated data;
2. Modification of the land use/land cover data to spatially represent highways and traffic barriers using data from the TxDOT PMIS and U.S. Census Bureau; and
3. Modification of the TUV radiative transfer model, a pre-processor for CAMx to calculate photolysis rates, to output UV solar irradiance.

For each episode, a base case CAMx simulation was conducted that included explicit consideration of the dry deposition of ozone and NO_x to highways and uncoated barriers. A sensitivity study was conducted for each episode that was the same as the base case, but evaluated the removal of pollutants by photocatalytic stucco-coated (instead of uncoated) barriers during sunlit hours. Differences in daily maximum ozone concentrations averaged over 8 hours and

maximum differences in ozone concentrations averaged over 8 hours in the DFW area and HGB areas, respectively were evaluated between the base case and photocatalytic stucco study (base case—photocatalytic stucco). Differences in daily maximum 8-hour averaged ozone concentrations in the DFW area across the episode ranged from -0.0001 to 0.09 ppb. Maximum difference in 8-hour averaged ozone concentrations, regardless of time of day or magnitude, ranged from 0.01 to 0.1 ppb in the DFW area. Differences in daily maximum 8-hour averaged ozone concentrations in the HGB area across the episode ranged from 0.0006 to 0.04 ppb. Maximum difference in 8-hour averaged ozone concentrations, regardless of time of day or magnitude, ranged from 0.004 to 0.1 ppb in the HGB area.

Two additional sensitivity studies evaluated the air quality effects of increasing the total photocatalytic stucco-coated surface area in the DFW area by tripling the coated barrier surface area and replacing all asphalt and concrete pavements with photocatalytic stucco-coated concrete. The "triple barrier" case and "all coated" cases resulted in larger ozone reductions, relative to the base case, than the "original" case, described above, in which only the estimated barrier area had a photocatalytic stucco coating. However, incremental changes in predicted ozone concentrations were not necessarily proportional to incremental changes in photocatalytic stucco-coated surface area. Reductions in maximum daily 8-hour averaged ozone concentrations were at most 0.14 ppb for the "all coated" case relative to the base case. Maximum reductions in 8-hour averaged ozone concentrations regardless of time of day or magnitude were at most 0.18 ppb for the "all coated" case relative to the base case.

Chapter 6. Long-Term Outdoor Exposure Results

6.1 Periodic field testing

6.1.1 Monitoring of field sites

The three field sites were monitored every 3 months using several different techniques. The samples were also thoroughly evaluated prior to exposure and after 1 year of exposure. The stucco specimens were monitored for an additional year. Weather data were recorded to understand how rainfall, solar radiation, and other factors may affect performance of the photocatalytic coatings. Onset Hobo weather stations were placed at the Austin and Houston field sites, and a Campbell Scientific weather station was placed at the J. J. Pickle field site. All of the weather stations recorded rainfall, temperature, RH, solar radiation, wind speed, and wind direction.

Ion Chromatography

Water samples were obtained before, after, and every 3 months throughout exposure by washing the concrete specimens with distilled water. Distilled water was used to ensure no trace amounts of nitrate or nitrite ions were present before contact with the concrete. The distilled water was placed into a clean and unused 2-gallon capacity pump sprayer. Then 2 L of distilled water were pumped and sprayed in a steady stream onto the coated concrete surfaces, as shown in Figure 6.1. This volume was selected because it is approximately equal to a 1 in. (2.5 cm) rainfall over the surface of the specimen.

Figure 6.1 Concrete washing procedure

This process was repeated for each of the four sections of the barrier specimens and each of the slab specimens. Each of the water samples was collected in an aluminum dish and transferred to plastic bottles using a funnel. The samples were then capped. Figure 6.2 shows the collection procedure.

Figure 6.2 Water collection procedure for concrete specimens

The samples were transported back to the lab. Each sample was weighed and then divided in half, and the half-samples were weighed again. One of the halves was stored and the other was uncapped and placed in a vacuum oven. Each sample was evaporated until it reached a volume close to or just above the volume necessary for ion chromatography testing, which was approximately 150 mL. The volume of the samples was reduced to concentrate the nitrogen compounds in the samples to improve detection of any nitrate and nitrite present.

The wash water samples were sent to Water Testing USA in Cleveland, Ohio, for evaluation for the presence of nitrate and nitrite ions using ion chromatography. As described in Chapter 2, the presence of nitrate and nitrite ions can indicate photocatalytic activity. Water Testing USA has a minimum detection limit of 0.5 mg/L for nitrate and nitrite tests.

Spectrophotometry and Photography

Each of the barrier sections and slabs was monitored for changes in color and appearance using two different methods. Color was measured before and after exposure using a Stellar Net EPP2000-HR Portable Spectrophotometer. Ten readings were taken for each specimen and averaged. By converting the transmittance of different wavelengths of light to the International Commission on Illumination (CIE) color space, color could be determined on three scales: red to green (a*), yellow to blue (b*), and black to white (L*). Three spectrophotometer readings were taken for each of the barrier sections and slabs. These readings were then averaged to determine color values. Specimens were also photographed before and after exposure to note any visual changes and the accumulation of visible dirt or discoloration.

Temperature

Temperature of each specimen was recorded during each site visit using an infrared thermometer to determine the effect of coatings on temperature of the concrete.

6.1.2 Exposure site monitoring results

Ion Chromatography

All slab specimens and each of the coated barrier sections were washed with distilled water before exposure and every 3 months until the 1-year outdoor exposure period was complete in the manner described in section 6.1.1. Testing continued on the control and stucco sections for an additional year. For months 0 and 3, the water was collected and analyzed. For months 6 and later, the water washes were collected and evaporated in a vacuum oven to concentrate the amount of nitrate and nitrite ions in solution. No samples were collected for the slab specimens at 12 months for any of the field sites so that they could be returned for air chamber testing in a "dirty" state. The minimum detection limit was 0.5 mg/L for the 0- and 3-month samples, and the effective minimum detection limit for the samples that were concentrated was approximately 0.15 to 0.25 mg/L, depending on the amount evaporated. Results are reported in milligrams per liter of the original, dilute solution. All results were affected by the number of days since the last significant rainfall experienced by the specimen during that period. Rainfall data are not available for the Austin site at 12 months due to a weather station malfunction.

Ion chromatography results for the barrier and slab specimens that were placed at the Houston field site, Austin field site, and lab field site are presented in Appendix C. It is difficult to draw conclusions about the relative effectiveness of the different coatings from these data since the measured concentrations of nitrates and nitrites are generally close to the minimum detection limits. However, in almost all cases, the control specimens showed no measurable nitrates or nitrites in the wash water while many of the coated sections show measureable concentrations, particularly when the measurements were made long after a rain event. It can be concluded from these data that all of the coatings were somewhat effective at photocatalyzing NO_x compared to the control, but relative difference between coating effectiveness are difficult to prove using these data.

Spectrophotometry and Photography

Color was measured before exposure and every 3 months throughout the duration of the first year of exposure using a spectrophotometer. Since photocatalytic pollution removal occurs when the material is exposed to an adequate light source, any covering of the photocatalytic surfaces with dirt, visible pollutants, or other contaminants could compromise pollution removal ability. The spectrophotometer was therefore used to determine if any contaminants were adhering to the surface by measuring any changes in color of the material over time. The most effective way to measure this parameter was through the L* scale of the CIE color space, which indicates brightness on a scale from 0 to 100, with 100 indicating bright white. This scale was particularly applicable for the two white coatings, the stucco and the white paint. The scale was less effective for the gray surfaces (control and clear paint 1) because of the color variation in the surface. Therefore, only the measurements on the white coatings are discussed. The spectrophotometer data for the barrier and slab specimens located at the Houston field site, Austin field site, and lab field site are included in Appendix D.

The coated stucco is highly variable with both bright white spots and dark, shadowed areas. This variability in color may have had an effect on the variability of L* readings recorded for these specimens. In general, however, it was found that the L* readings showed an upward, or whitening trend, with time over the 12-month period of measurement. The L* readings taken after washing were slightly lower than before washing because the wet surface was darker than the dry surface.

It can be concluded that the stucco is self-cleaning and the build-up of contaminants that could darken the surface and possibly block UV radiation was not occurring.

For the white paint specimens, the coatings appeared to darken very slightly over time, with L* readings slightly decreasing over time. This suggests that some of the white painted specimens did collect surface contaminants that caused darkening of the surface. From these data, it can be concluded that the paint is not self-cleaning and photocatalytic activity for this paint may be compromised by the build-up of contaminants.

Temperature

The temperature of each specimen was measured using an infrared thermometer for the duration of the first year of outdoor exposure. This information was used to verify the temperatures used in the environmental chambers were appropriate. The results are presented in Appendix E.

6.2 Materials characterization before and after 1 and 2 years of exposure

Three-in. diameter cores were removed from each of the coated sections of the highway barrier before and after the 1-year exposure period, as described in Chapter 3. Cores were also removed from the stucco specimen after an additional year of exposure. The purpose of removing the cores was to be able to determine whether the exposure period caused a reduction in the amount or distribution of photocatalytic material. Coated sections were compared before and after exposure using SEM and x-ray diffraction (XRD).

6.2.1 X-ray diffraction analysis of field specimens

XRD was used to analyze the composition of coated sections of concrete barriers before and after 12 months of outdoor exposure near major highways. Cores of 3 in. (7.6 cm) diameter and 0.5 in (1.3 cm) depth were obtained using a small coring rig. Each coated section was crushed and analyzed by XRD. XRD data gave information on the presence of TiO_2 and phases in the concrete. Since the exact process was repeated on the concrete barriers after the exposure period, results could be directly compared to determine if any changes in composition had occurred as a result of outdoor exposure. However, since the ratio of amount of coating to concrete could vary between specimens, data were not quantitatively compared.

X-ray diffractograms are included in Appendix F of all specimens, before and after the exposure period, for each of the four coatings tested with major phases identified using Jade 9 software.

There were no significant changes in the surface composition of the control barriers over the 12-month exposure period. Similarly, for the clear paint 1 there were no observable changes over time. Interestingly, for the clear paint 1, TiO_2 was not detected by XRD either before or after exposure, likely because the paint contains only 1% TiO_2. Therefore, XRD data could not be used to determine changes in the presence of TiO_2 over time for this paint.

There were no significant changes in the stucco composition over time, but the presence of the anatase form of TiO_2 was detected both before and after exposure. In the white paint specimen, the rutile form of TiO_2 was detected both before and after exposure. It is clear from these studies that the TiO_2 is not removed from the coatings over time and that the coatings and the photocatalytic activity do not significantly change the composition of the concrete.

6.2.2 XRD analysis of environmental chamber specimens

XRD was also run on samples obtained from the each of the full-size slabs that were tested in the environmental chamber. These samples remained indoors for the duration of the project and were not exposed to the outdoor environment, though they were exposed to repeated laboratory testing. The results of these XRD tests are also shown in Appendix F. The results confirm the outdoor exposure test results, with no qualitative changes in specimen composition over time.

6.2.3 Scanning electron microscopy analysis of field samples

To better understand the spatial distribution of TiO_2 in specimens exposed to outdoor conditions, SEM with EDS was used. Cores were obtained both before and after the 1-year outdoor exposure period in the manner described in Chapter 3; 2-year specimens were only collected on the stucco sections. This technique allowed degradation of the photocatalytic coating to be monitored quite easily and effectively.

Figures 6.3 to 6.10 show SEM/EDS images of the uncoated and coated surfaces and cross sections both before exposure and after exposure at each of the three field sites. The green color represents calcium while the red color represents titanium, which indicates the presence of TiO_2.

Figure 6.3 shows the surface of the uncoated control section of the barrier before and after exposure. The images indicate that there is a small amount of titanium present in the uncoated concrete surface. This could be due to background noise or to a small amount of titanium contained in the concrete materials. The fine aggregate material used in the mix was analyzed by XRF and found to contain 0.11% titanium. Another potential source of titanium on the uncoated section is from contamination during the coating of the adjacent clear paint 1-coated section. There appears to be no significant change in the spatial distribution of TiO_2 on the uncoated section surface for any of these field site locations after exposure.

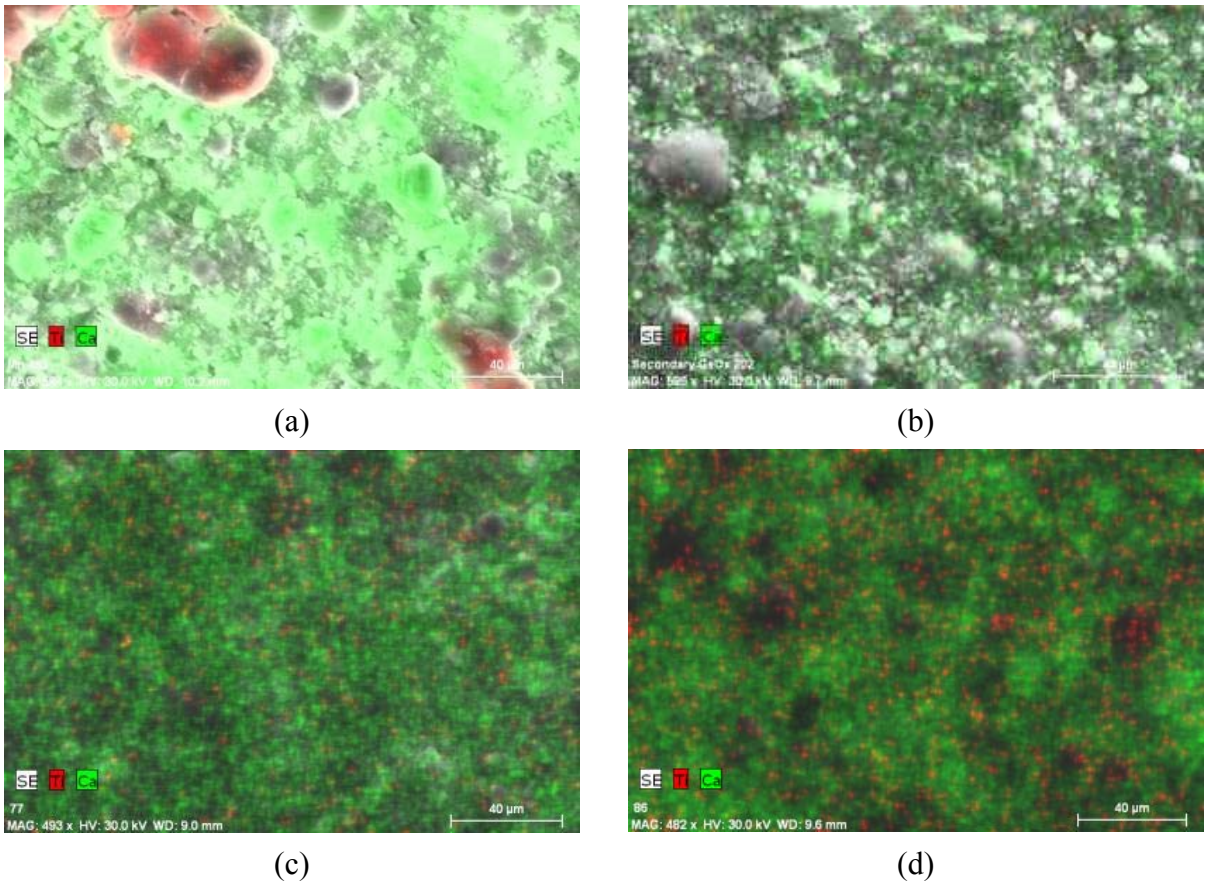

Figure 6.3 SEM images of control surface: (a) before exposure; (b) after exposure in Houston; (c) after exposure in Austin; (d) after exposure at the lab site

Figure 6.4 shows cross sections of the uncoated concrete surface before and after exposure. The image shows that there is an insignificant amount of titanium present at the surface of the sample, which is to be expected since a photocatalytic coating was not applied to this section. Again, any titanium that does appear can likely be attributed to background noise associated with the imaging system.

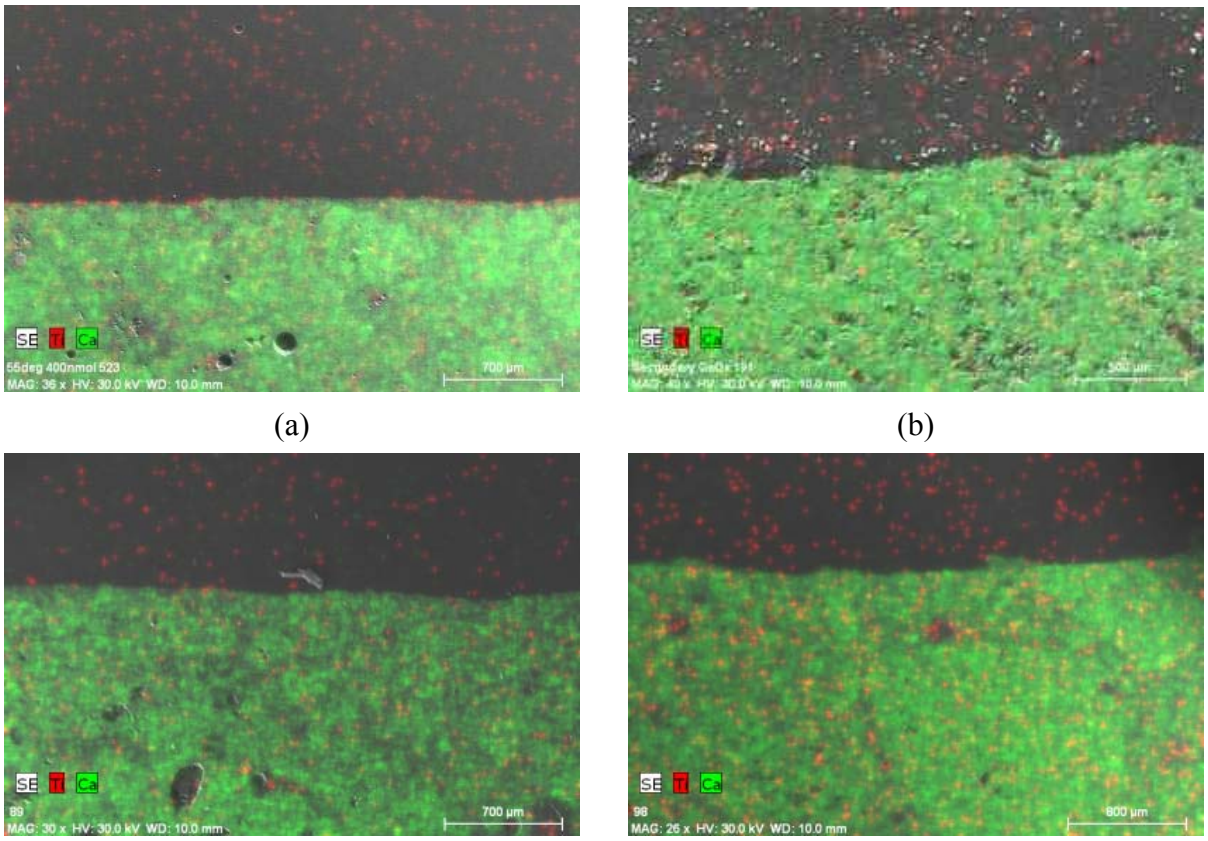

Figure 6.4 SEM images of control cross section: (a) before exposure; (b) after exposure in Houston; (c) after exposure in Austin; (d) after exposure at the lab site

Figure 6.5 and Figure 6.6 show the barrier specimens that were coated with stucco. Figure 6.5 shows the surfaces of the stucco while Figure 6.6 shows cross sections of the coated material. In both cases, the photocatalytic TiO_2 material appears to be interspersed in small agglomerations throughout the stucco matrix, which is largely composed of limestone sand and cement. In Figure 6.6, the sand particles can be viewed as large green sections with titanium interspersed between them. There appears to be no difference in composition between the sections obtained before exposure and those obtained after exposure in any of the three field sites, even after 2 years. This indicates that the stucco did not degrade under outdoor exposure.

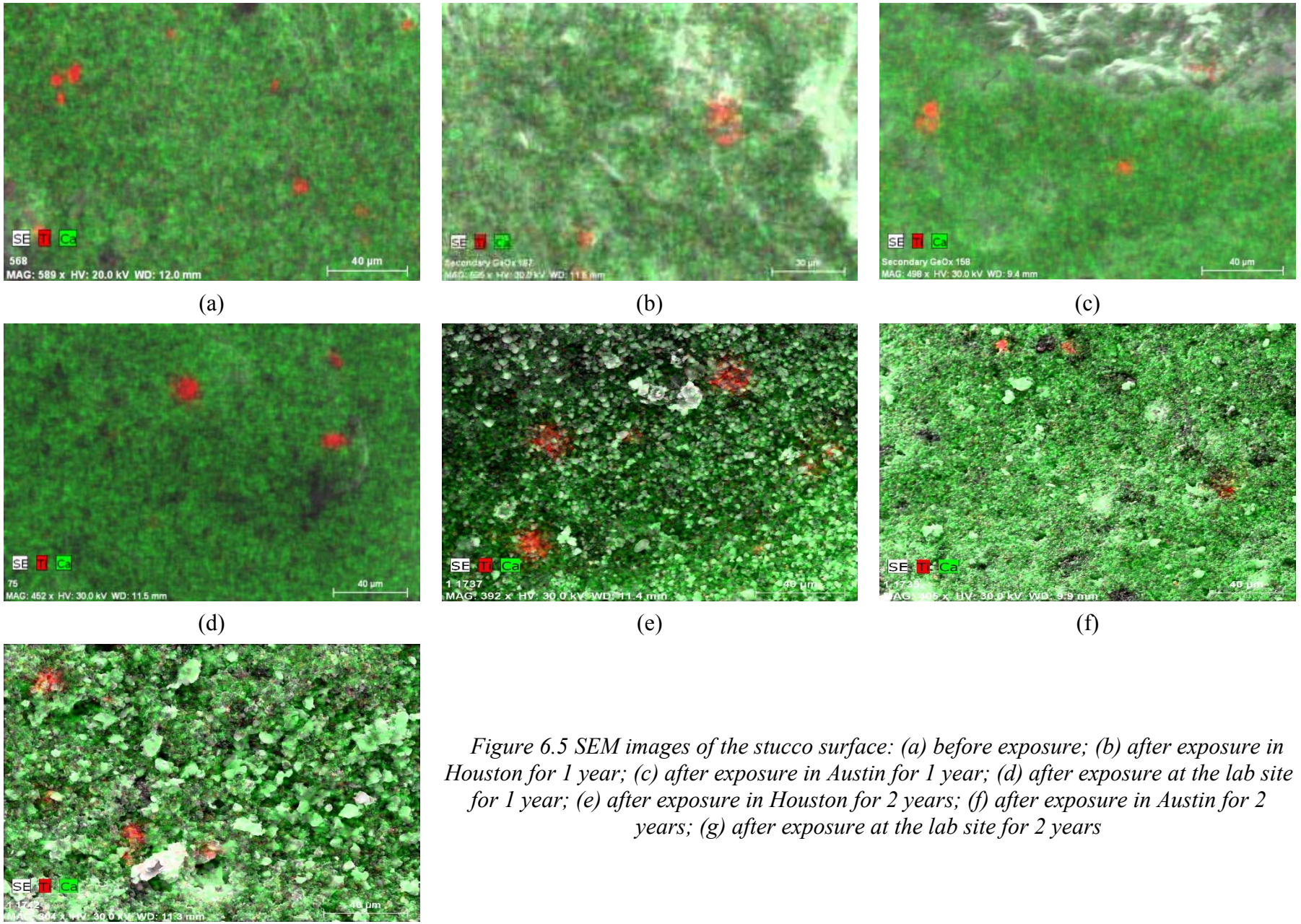

Figure 6.5 SEM images of the stucco surface: (a) before exposure; (b) after exposure in Houston for 1 year; (c) after exposure in Austin for 1 year; (d) after exposure at the lab site for 1 year; (e) after exposure in Houston for 2 years; (f) after exposure in Austin for 2 years; (g) after exposure at the lab site for 2 years

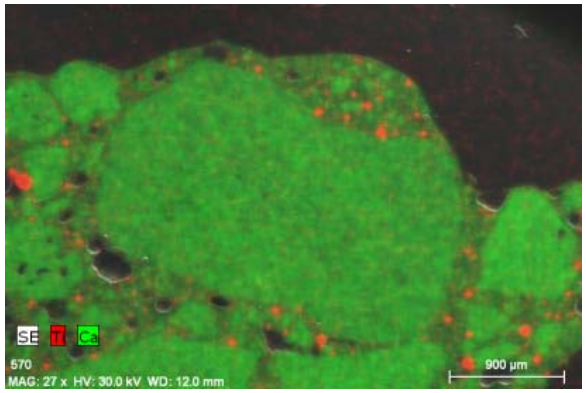

(a)

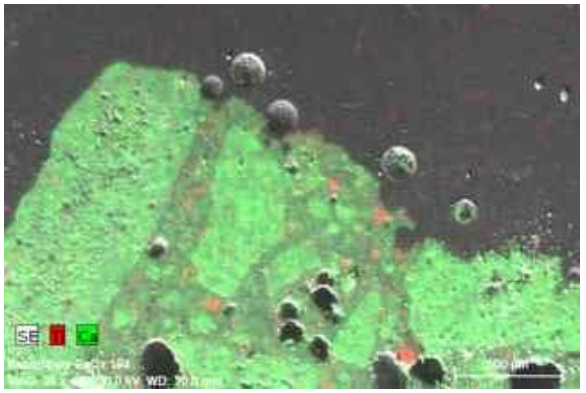

(b)

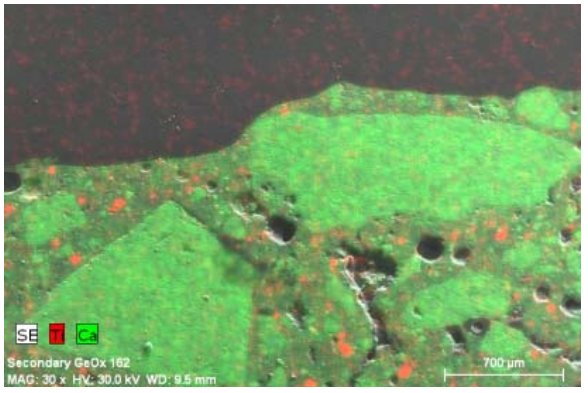

(c)

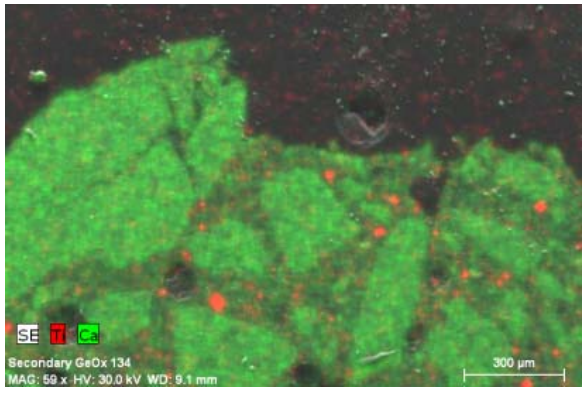

(d)

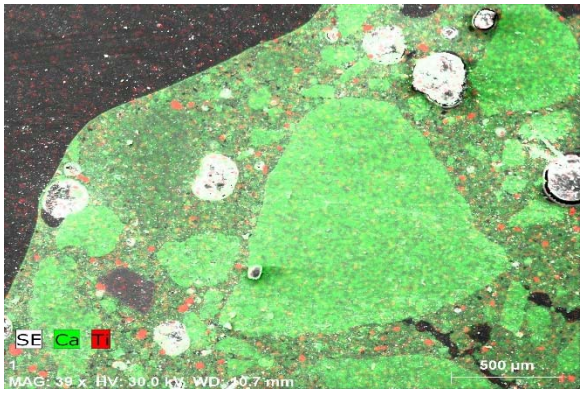

(e)

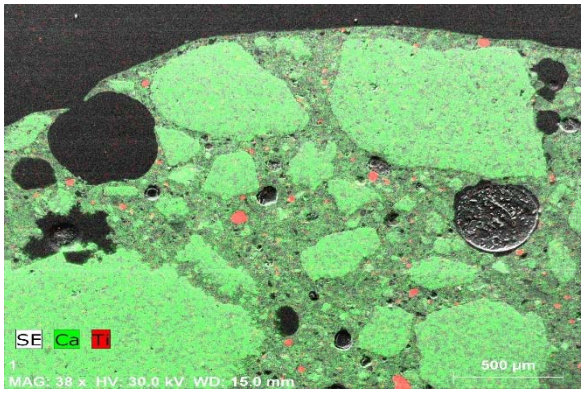

(f)

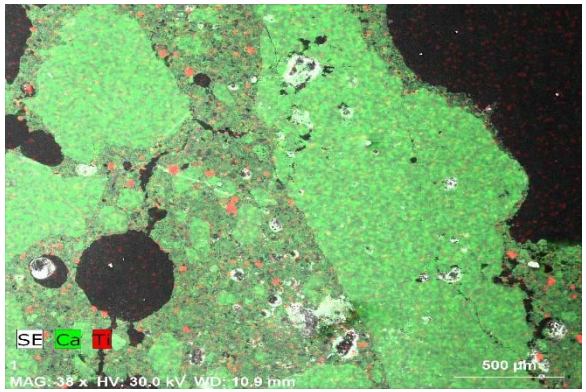

(g)

Figure 6.6 SEM images of the stucco cross sections: (a) before exposure; (b) after exposure in Houston for 1 year; (c) after exposure in Austin for 1 year; (d) after exposure at the lab site for 1 year; (e) after exposure in Houston for 2 years; (f) after exposure in Austin for 2 years; (g) after exposure at the lab site for 2 years

Figure 6.7 shows surfaces of cores obtained from the barrier sections painted with the white paint both before and after exposure outdoors at each of the three field sites. As expected, Figure 6.7 shows that the surface composition is almost entirely titanium. This result is expected because the white paint product is intended to cover the surface and contains no calcium. There appears to be minimal or no degradation of the titanium composition after 1-year outdoor exposure, which may have been indicated by an increase in the calcium that lies directly beneath the painted surface.

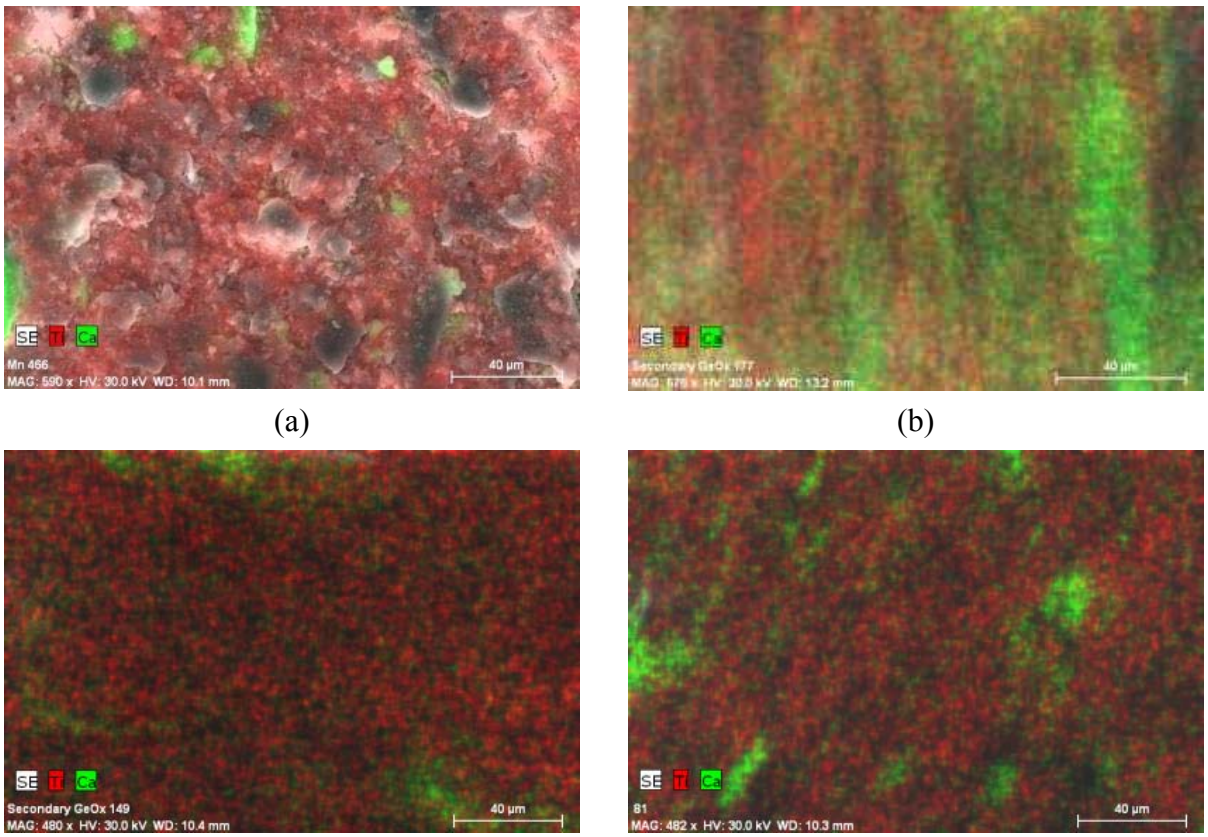

Figure 6.7 SEM images of the white paint surface: (a) before exposure; (b) after exposure in Houston; (c) after exposure in Austin; (d) after exposure at the lab site

Figure 6.8 shows cross sections of the sections coated with white paint. The painted coating appears as a thick layer of titanium. The titanium layer does not appear to decrease in any of the samples taken after exposure. Therefore, the white paint is durable under 1 year of outdoor exposure.

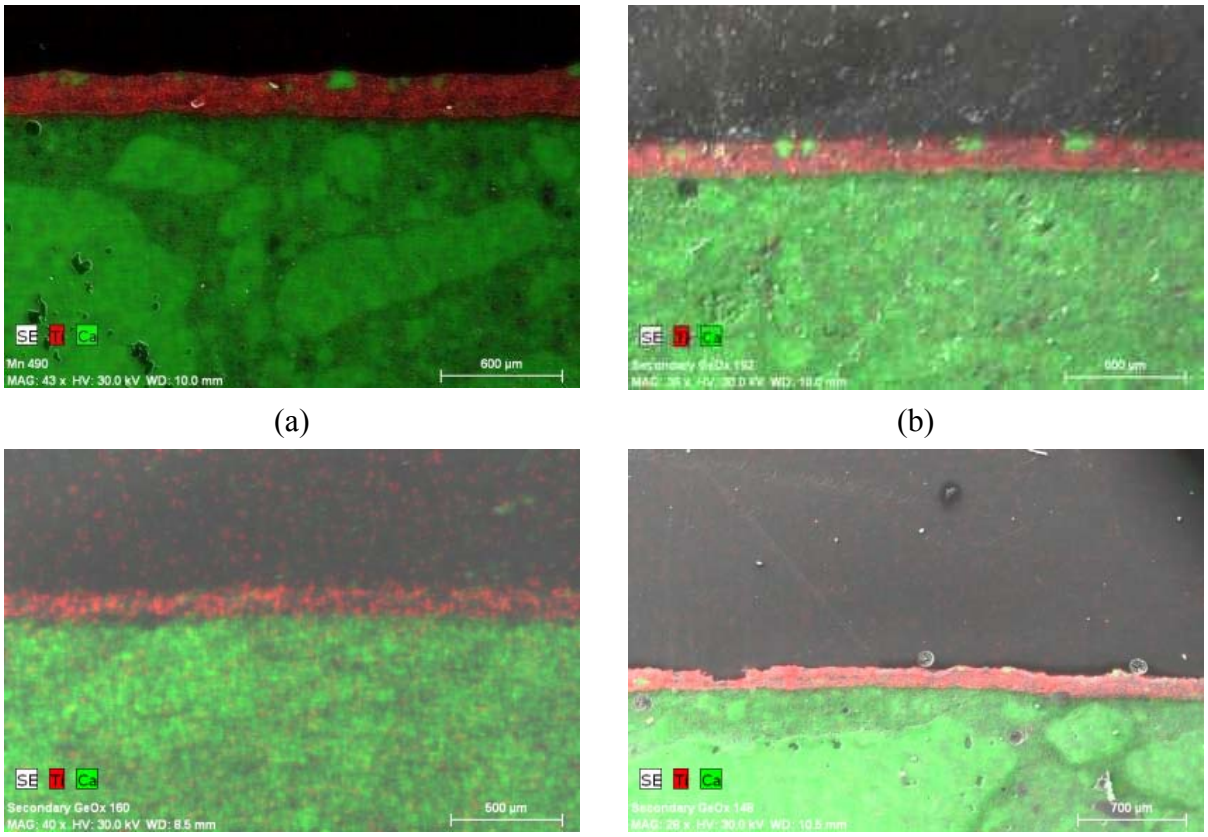

Figure 6.8 SEM images of the white paint cross section: (a) before exposure; (b) after exposure in Houston; (c) after exposure in Austin; (d) after exposure at the lab site

Figure 6.9 shows images of the sections of the barrier that were coated with the clear paint 1. The clear paint 1 is a water-based product that is sprayed on. Its spatial distribution is different from the other coatings since it is sprayed and not painted or toweled in a thick layer. Since the coating is not intended to saturate the entire surface, it is expected that some calcium is present on the surface of the coated section. Drying of the coating may have caused the surface pattern that is shown in Figure 6.9a. It appears that the clear paint 1 degrades during exposure because the patterns or amount of titanium on the surface appear to decrease after exposure, in some cases more than others.

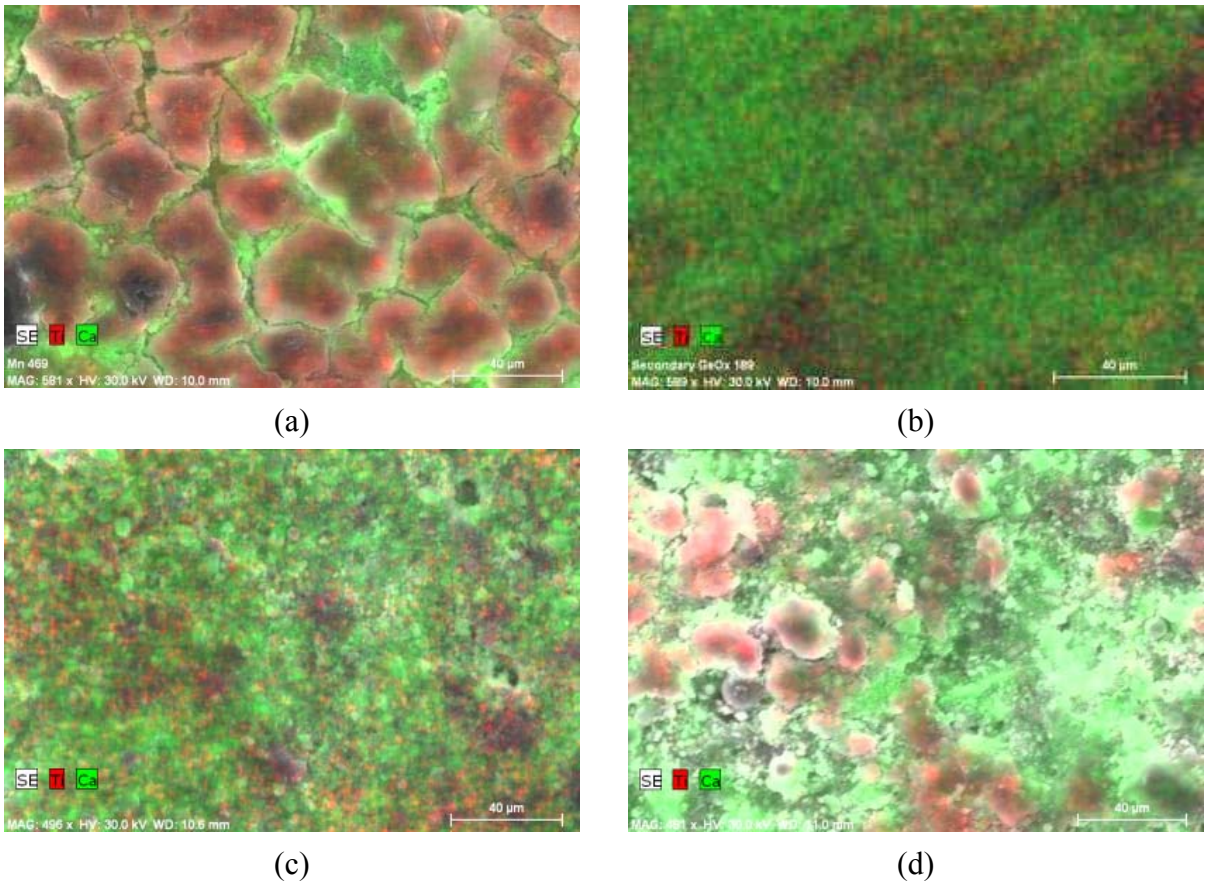

Figure 6.9 SEM images of the clear paint 1 surface: (a) before exposure; (b) after exposure in Houston; (c) after exposure in Austin; (d) after exposure at the lab site

Figure 6.10 shows cross sections of the clear paint 1-coated sections. As expected, there is a thin layer of titanium present on the surface of the material where the coating was applied before the exposure period. However, it appears that the thin layer is diminished for all field sites after 1 year of exposure. Based on these data, it is possible that TiO_2 contained in the clear paint 1 is diminished due to outdoor exposure.

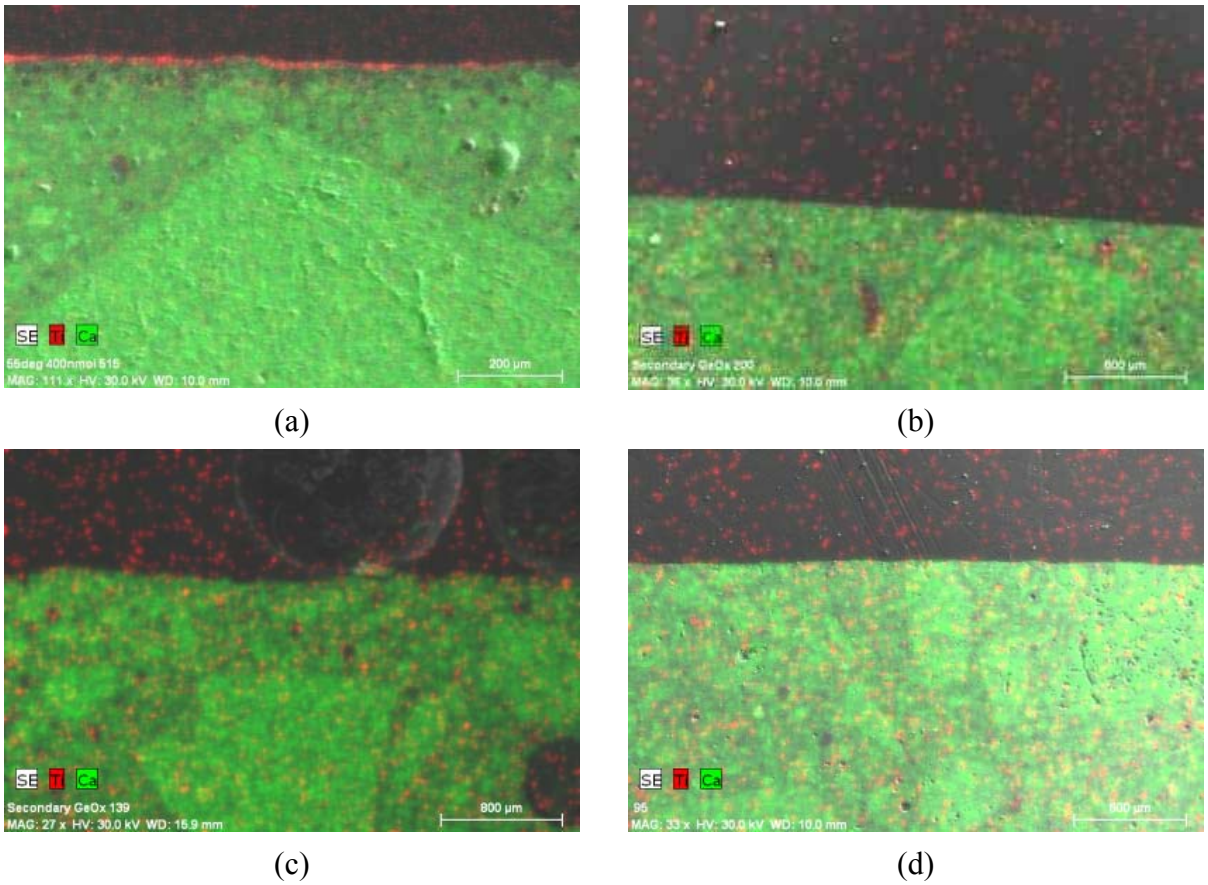

(a) (b)

(c) (d)

Figure 6.10 SEM images of the clear paint 1 cross section: (a) before exposure; (b) after exposure in Houston; (c) after exposure in Austin; (d) after exposure at the lab site

6.2.4 SEM results for environmental chamber specimens

SEM was also run on specimens obtained from each of the full-size slabs that were placed in the environmental chamber for the duration of the project and not exposed outdoors. The results are shown in Figures 6.11 to 6.14 and confirm those from the outdoor exposure tests.

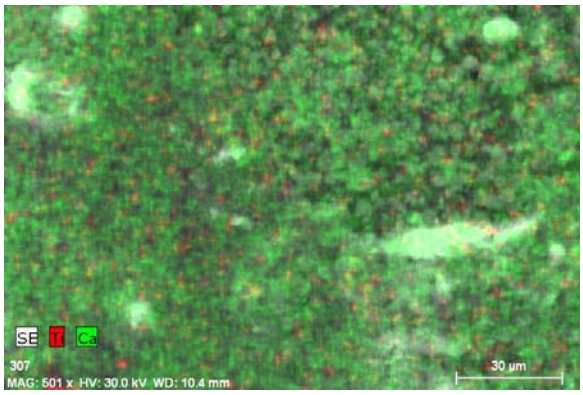

(a)

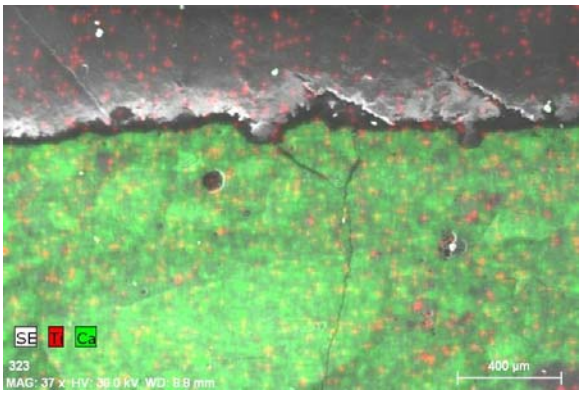

(b)

Figure 6.11 SEM images of uncoated environmental chamber specimen after testing: (a) surface; (b) cross section

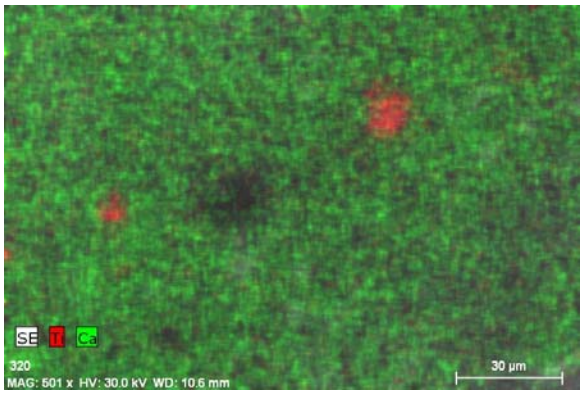

(a)

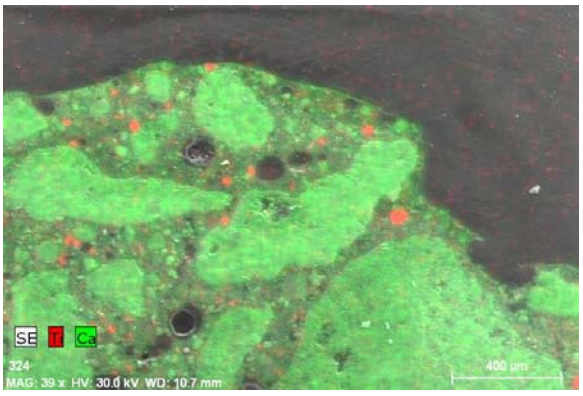

(b)

Figure 6.12 SEM images of the stucco environmental chamber specimen after testing: (a) surface; (b) cross section

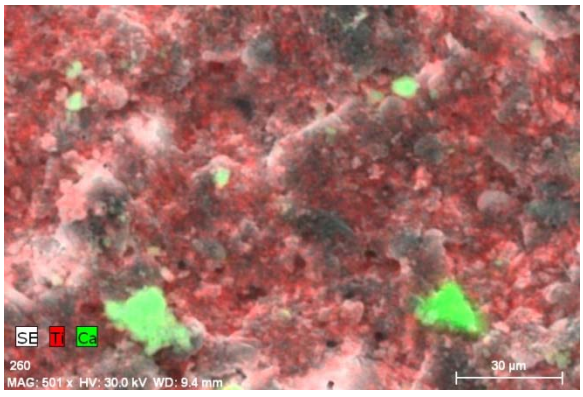

(a)

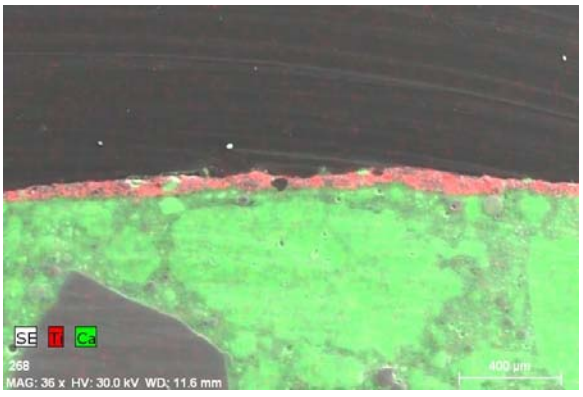

(b)

Figure 6.13 SEM images of the white paint environmental chamber specimen after testing: (a) surface; (b) cross section

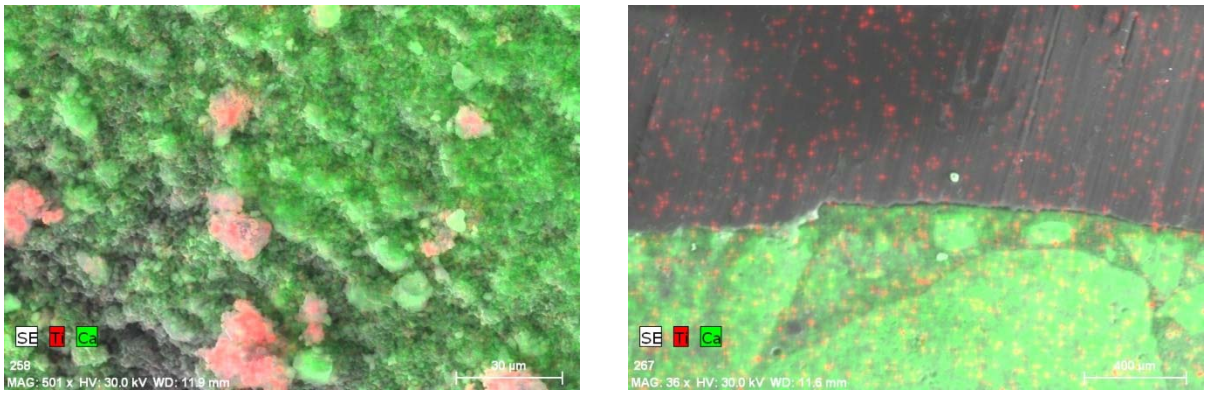

(a) (b)

Figure 6.14 SEM images of the clear paint 1 environmental chamber specimen after testing: (a) surface; (b) cross section

6.3 Pollutant removal testing after 1 and 2 years of exposure

6.3.1 Samples coated and exposed for 1 year

Concrete samples coated with the stucco as well as uncoated samples were brought back from field sites to the laboratory after 1 year of exposure. A detailed discussion of the results can be found in Cros et al. (2015b). Three tests were consecutively run on the samples. First, the sample was tested without any treatment after transport from the field. Then, the sample was washed with distilled water (as described in section 4.2) and tested again. Finally, the sample was washed with soapy water and tested again. Water and soapy water were simply poured onto the samples; no scrubbing took place. The water wash protocol is identical to the one described in section 4.2. The soapy water was made using 30 mL of biodegradable dishwashing liquid (Green Works, Free & Clear) mixed in a gallon (3.78 L) of distilled water. The mixture was poured on the sample while it was horizontal. Then, a gallon (3.78 L) of distilled water was poured on the sample to rinse the soap off while it was still horizontal. A second gallon (3.78 L) of distilled water was poured on the sample after it was tilted at a 30° angle. A baseline test was run on all samples, keeping the environmental conditions constant. These tests were used to compare performance over time and after different types of washes. The conditions were as follows: 50% RH, 35°C, 1.5 minute contact time, low organic pollutants (0.25 ppm propane, 0.05 ppm propylene), high lights (2 mW/cm^2).

The results are shown in Figure 6.15, with the "base case" signifying the performance of a stucco-coated concrete that was not exposed to outdoor conditions. The results show a reduction of performance in NO_x removal for the morning inorganic condition. For the Houston and J. J. Pickle locations, the wash with distilled water did not improve removal efficiency. Treatment of the samples with soapy water wash increased the removal efficiency to 50–75% of the base case removal rate. For the Austin site, the first water wash increases the NO_x removal rates to their initial level. The Austin field samples were retrieved last, in the second half of the month of May 2012. Higher UV light intensities during the month of May compared to earlier in the year might have led to higher oxidation activity at the surface of the catalyst resulting in less non oxidized pollutants adsorbed at the material surface.

For the afternoon inorganics condition, all samples behave in a similar fashion with NO_x removals close to the base case prewash and between 90 and 100% of the base case after the soap wash.

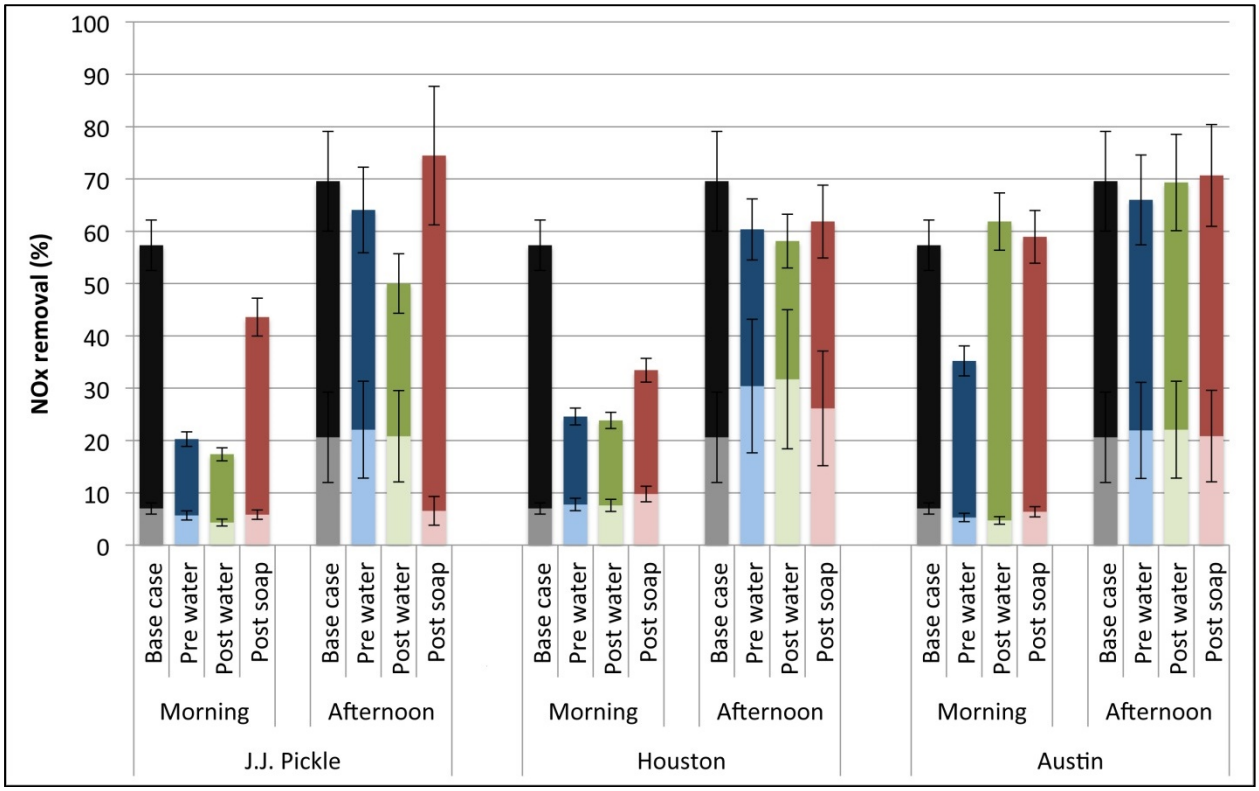

Figure 6.15 NOx removal by the stucco in all three field sites for both morning and afternoon inorganic levels conditions.
The bottom of each bar (lighter shade) represents removal by the uncoated concrete and the top (darker shade) represents the improvement in removal obtained through the use of photocatalytic stucco.

6.3.2 Samples coated and exposed for 2 years

After the first year, the samples were returned to the three field sites for an additional 12 months of exposure. After a total of 24 months of exposure, the samples were returned to the laboratory and tested using the procedures described in section 6.3.1. The results of these tests are presented in Figure 6.16.

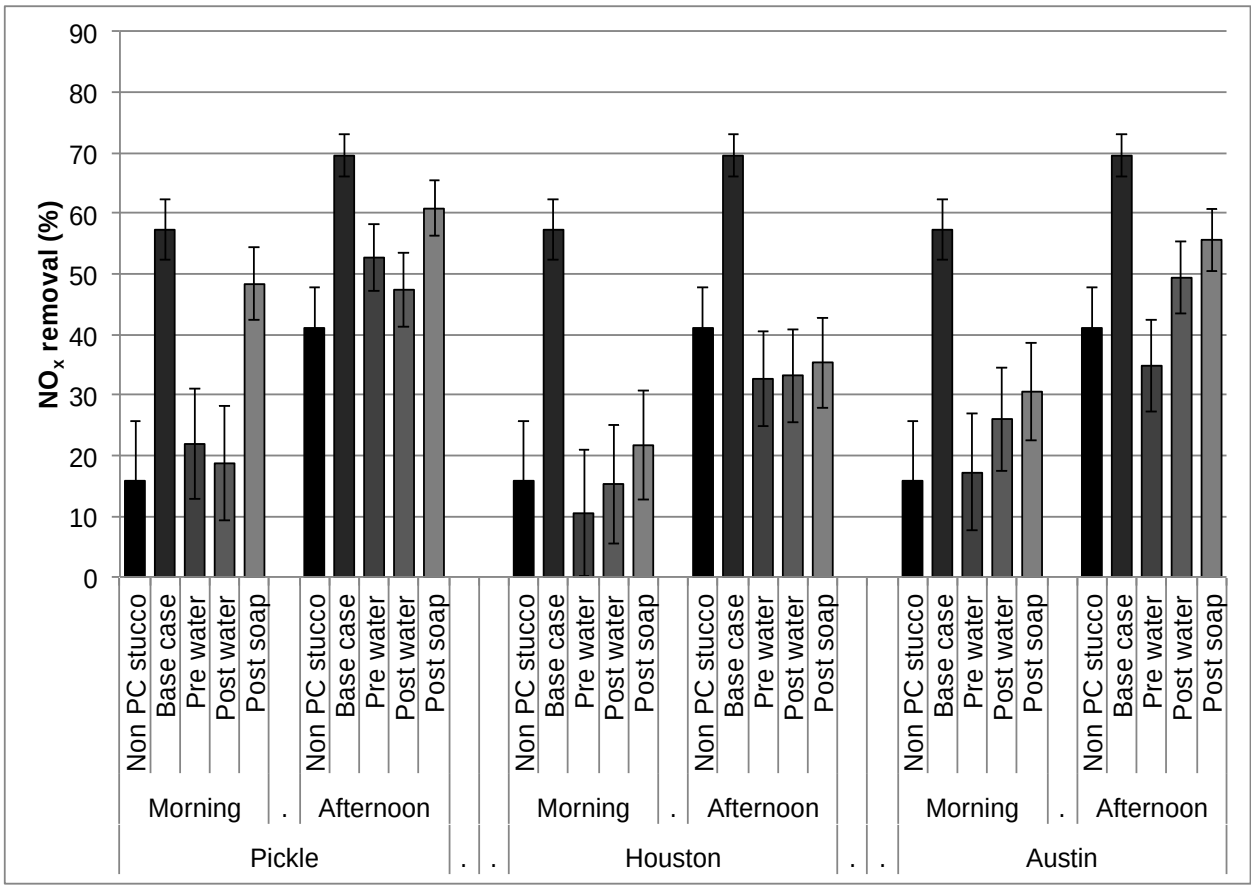

Figure 6.16 NOx removal by the stucco in all three field sites for both morning and afternoon inorganic levels conditions after 2 years of outdoor exposure

Examination of the results presented in Figure 6.16 show that the water rinse had a negligible effect on all of the samples except for the Houston slab under morning conditions. All of the slabs, however, showed improved removal efficiency after the soap and water rinse. These results suggest that non-polar materials such as grease or high molecular weight alkanes may be blocking the active sites, reducing removal efficiencies. The Houston slab showed the lowest removal rates for all conditions, indicating that higher traffic areas may result in faster degradation of photocatalytic performance. Other researchers have reported similar results for high-traffic areas. Petit et al. (Petit, 2009) reported that a high-traffic test site in Vanves, France, lost its catalytic capabilities in approximately 3 months. Various cleaning methods were tried, but photocatalytic activity could not be regenerated. In a similar study conducted in Bergamo, Italy (Guerrini and Peccati, 2007), researchers conducted two data collection campaigns, one each in November 2006 and January 2007. Data collected in 2006 indicated that NO_x concentrations, during daytime, were about 40 to 50% lower above the photocatalytic surface compared to regular non-catalytic asphalt. In January 2007, the difference had dropped to a 20 to 30% reduction of NO_x concentrations above the photocatalytic surface compared to the untreated reference site. Further performance data for this field test site has not been reported.

Figure 6.16 also shows the results of tests performed on a non-photocatalytic stucco that has not been exposed to outdoor conditions for comparison. Compared to the "base case" photocatalytic stucco that has not been exposed to outdoor pollutants, the non-photocatalytic

stucco has lower removals, as expected. These tests were performed to verify that the performance of the photocatalytic stucco was due to the presence of the photocatalyst and not to its rough surface texture compared to the control concrete surface.

Chapter 7. Roadside Field Study

After the completion of the field exposure and laboratory chamber tests, the results were presented to the project management committee (PMC). After reviewing the data developed from the laboratory and outdoor exposure tests, the PMC decided to proceed with a roadside field study.

7.1 Roadside field site selection

The following criteria were used to select the roadside field test site: 1) roadway safety; 2) site orientation to the prevailing summer winds; 3) existing highway barriers for application of the photocatalytic material; 4) sampling points near the roadway; 5) electrical power supply for instrumentation and/or an air conditioner; and 6) site security. These criteria are discussed below.

7.1.1 Roadway safety

Installation of any of the required elements for the test site could not degrade the safety of the roadway for drivers, TxDOT personnel, or University of Texas (UT) personnel during installation, operation, or de-commissioning of the test site.

7.1.2 Site orientation

A wind rose for the prevailing wind during ozone season in Austin is shown in Figure 7.1, demonstrating that the prevailing wind direction during the Austin ozone season is from south to north. To take advantage of the prevailing wind, the field test site would need to be located along an east-west roadway with sample locations on the north side of the road.

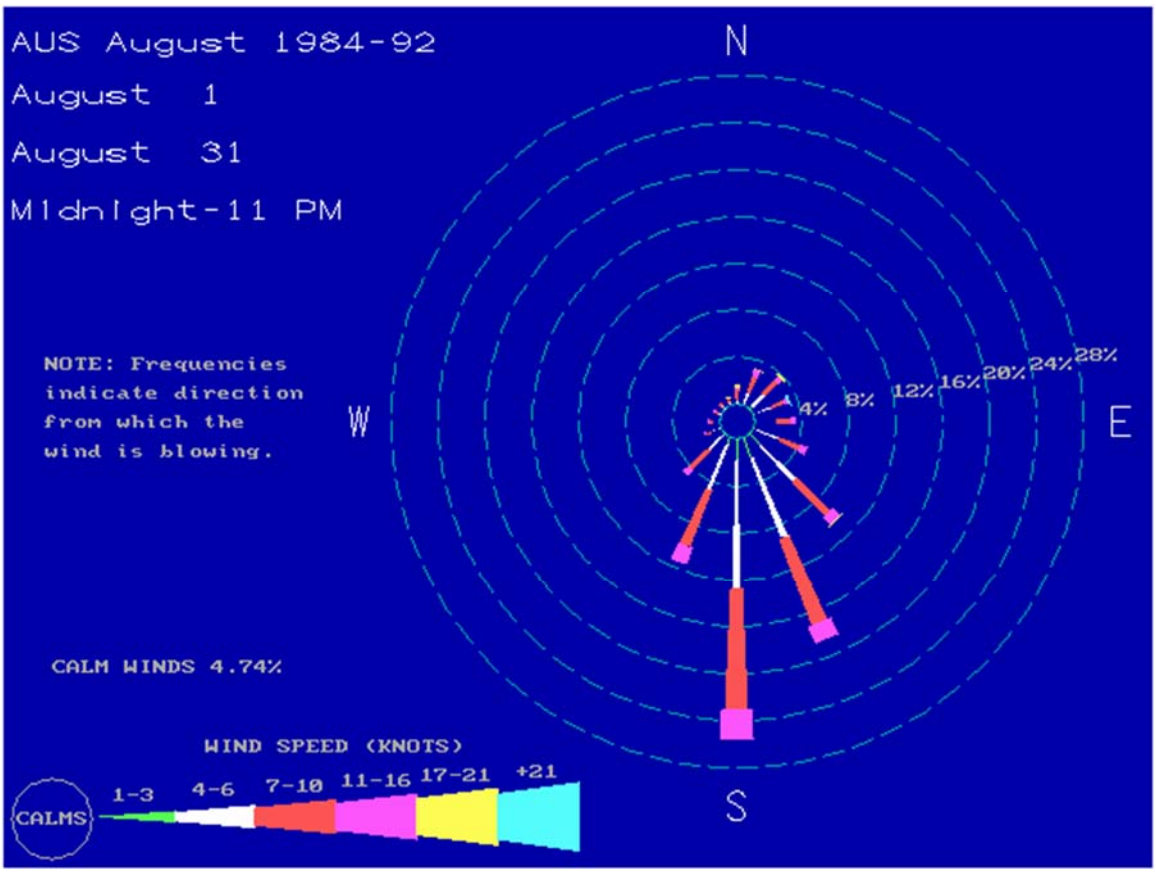

Figure 7.1 Historic wind rose for ozone season in Austin

7.1.3 Existing highway barriers

In pre-project and early project meetings, the PMC decided to limit application of the photocatalytic material to non-roadway concrete surfaces such as highway barriers. To reduce the cost of the roadside field test site and to minimize traffic disruptions, it was important to find a site that was already outfitted with at least some concrete barriers—specifically, barriers that were parallel and evenly spaced across the test site. Keeping the barriers evenly spaced and parallel helped to ensure even distribution of coated and uncoated barriers.

7.1.4 Sampling points

The proximity of the sampling points to the roadway greatly affects the airborne concentration of chemicals emitted by vehicles on the roadway. Olson et al. (2009) reported that increasing the distance from the roadway to the sampling location from 13 m to 92 m decreased the concentration of roadway VOCs by as much as 50%. These results suggested that the two sampling points of the roadside field test site need to be approximately the same distance from the roadway and as close to the roadway as possible.

7.1.5 Electrical power

The analytical instruments, pumps, and communication equipment all require 110-volt AC power. Additionally, the pumps associated with the analytical instruments generate a substantial

amount of heat that must be removed to prevent the instruments from overheating. In general, the local electrical company can easily and relatively inexpensively provide access to electrical power, if there are nearby transmission lines. Alternatively, the instruments could be housed in a building owned by UT or TxDOT already outfitted with electrical power.

7.1.6 Site security

Remote field sites require security to protect the instruments and other equipment located at the site. Typically, field instruments are kept in trailers surrounded by chain-link fencing to secure the equipment. Alternatively, the trailer could be located in a secure facility, such as a TxDOT yard or on UT property. Optionally, the equipment could be kept in a secure building.

7.2 Selected roadside field site location and configuration

Using the selection criteria in section 7.1 and the assistance and input of TxDOT and Toll Operations Division personnel, a field site was selected at the Parmer Lane toll plaza on SH 45 (also known as the Lake Creek Toll Plaza). The roadside field test site GPS coordinates are 30.474515, -97.774839. Figure 7.2 is a Google satellite image of the site. The roadway, as it passes through the field test site, is oriented east/west allowing for the summertime southerly winds to vertically traverse the roadway, maximizing the number of useable sampling days. This orientation allows for the separate analysis of air parcels that pass over uncoated barriers and photocatalyst-coated barriers.

Figure 7.2 Google satellite image of roadway field test site

Figure 7.3 provides a satellite digital image of the roadside field test site modified to show the photocatalytic barrier locations and both sampling ports. There are four rows of concrete barriers over which air passes before reaching the sampling points. The blue lines in the figure outline the air parcel that was considered for sampling in the coated section; only barriers within the triangular region for sampling were coated. The selected field test site required the placement of approximately 1710 ft (521m) of additional concrete highway barriers so that both test sites had four rows of highway barriers. To protect the additional barriers that were placed and ensure safety during the coating application, roadway hazard barrels were added to close a lane as shown in Figure 7.4.

Figure 7.3 Google satellite image of roadside field test site (with callouts)

Figure 7.4 Additional highway barriers and road hazard barrels

The two sampling sites are shown in the schematic drawing in Figure 7.5; the barriers shown run parallel to the roadway. There is a gap between the barriers and the tollbooth to allow access to the median. The sampling points shown in Figure 7.5 were outfitted with "gooseneck" samplers and a 5-micron dust filter. Figure 7.6 provides photos of the gooseneck samplers.

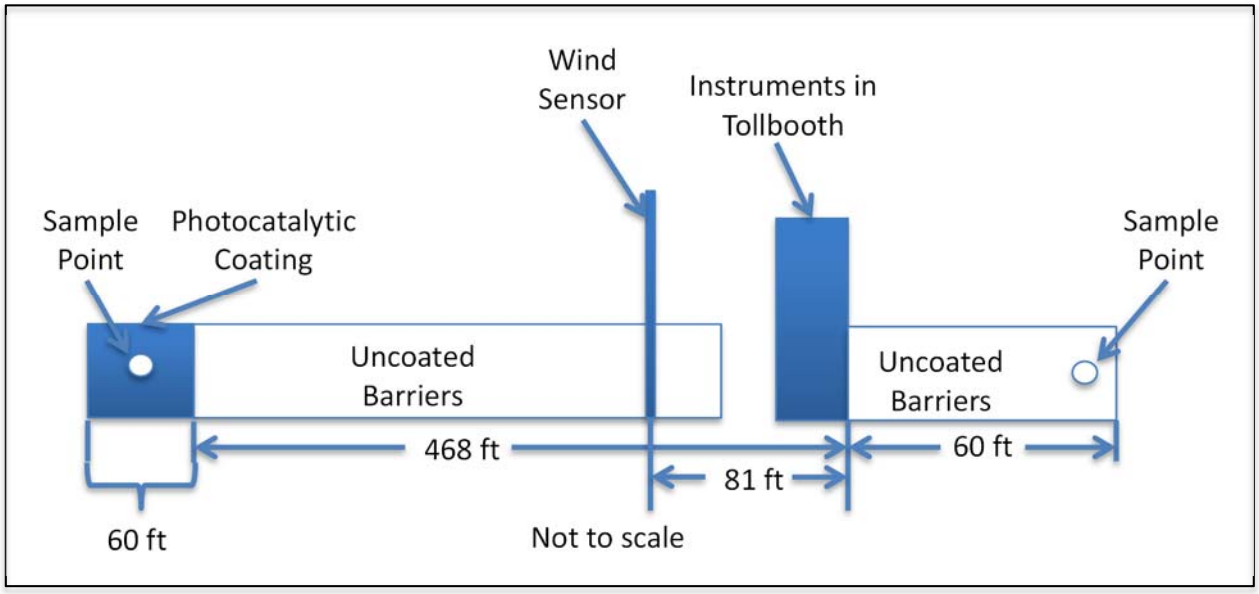

Figure 7.5 Schematic of roadside field test site

Figure 7.6 Sampling goosenecks

The selected field test site also allowed the sampling stations to be placed directly adjacent to a barrier a little more than 50 feet (16 m) from the active roadway of Texas SH 45, maximizing the observed concentrations for roadside O_3 and NO_x (Figure 7.7 and Figure 7.8) while minimizing the other differences between the sampling sites. The distance to the sampling point for the photocatalytic stucco was approximately 500 ft (152 m) from the tollbooth used to house the instrumentation. To ensure that the sample lines for each sampling point were of similar length, the sample line for the control site was run 220 ft (67 m) toward the catalytic sampling point and then turned to run back to the control site, as shown in Figure 7.9. This arrangement generated sampling lines that were approximately 500 ft (152 m) for both the photocatalytic coating sampling point and the control sampling point.

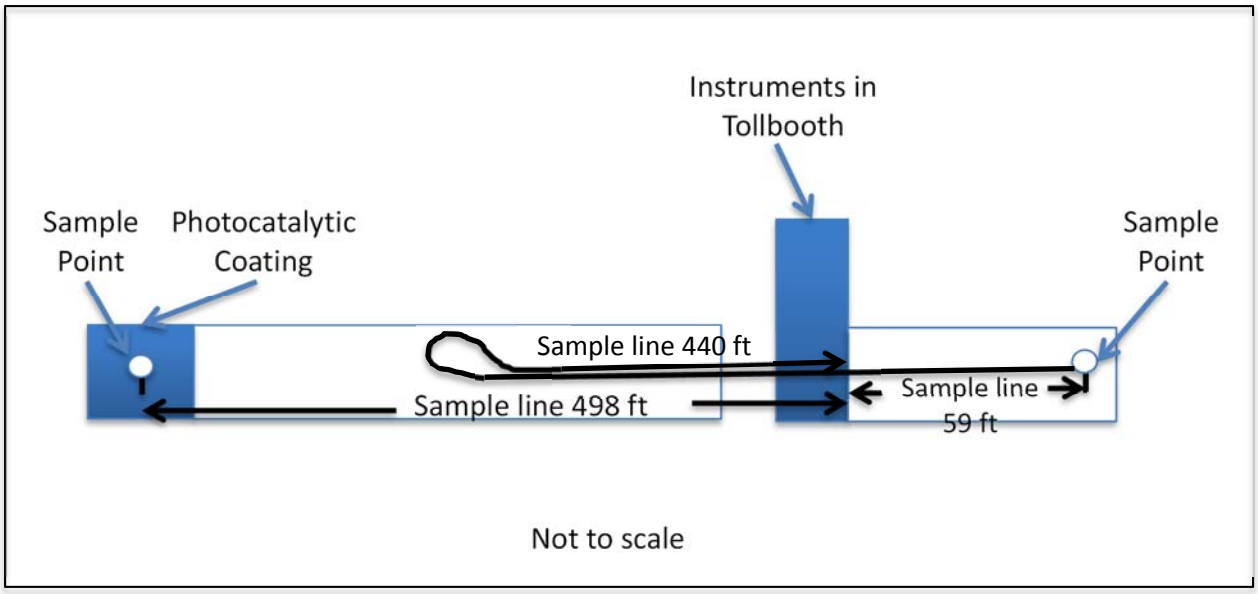

Figure 7.7 Schematic drawing of sample line configuration

Figure 7.8 Photocatalytic sampling port (gooseneck) and proximity to roadway (goosenecks were placed on the northernmost barrier facing south)

Figure 7.9 Uncoated barrier sampling port (gooseneck) and proximity to roadway (goosenecks were placed on the northernmost barrier facing south)

7.3 Preparation and installation of roadside field site photocatalytic stucco

As shown in Figure 7.3, there are four rows of concrete highway barriers that were coated with photocatalytic stucco. The northernmost barrier, at the sampling point, had the shortest coated section, with a length of 60 ft (18m). The other coated sections had lengths of 200 (61m), 360 (110m), and 480 ft (146m). The barriers are 3.5 ft (1.17m) high and both sides were coated; this made for a total coating area of 7700 ft^2 (715 m^2).

The barriers were power washed before the stucco application (River City Power Washing). The stucco was professionally prepared and applied by Waterloo Plastering, Inc. A bonding agent was first applied to the surface, immediately followed by the prepared stucco mixture. Approximately 50 bags (84 lbs/bag (38 kg/bag)) of photocatalytic stucco cement in total were used to coat the barriers, and a stucco cement-to-sand ratio of 1:3 was used.

Not considering the cost to place the additional concrete barriers on site, the total cost of installing the field site was approximately $20,000 ($5,000 for the photocatalytic stucco cement and $15,000 for the other materials and services).

7.4 Roadside test site equipment and analytical instruments

The support equipment and analytical instruments used for this study were selected to be the same or similar to the equipment and instrumentation used by TCEQ at the time of purchase or acquisition, except for the weather station. The roadside test site location did not have adequate

room to install a National Oceanic and Atmospheric Administration standard weather station. A Met One Instrument, 034B Wind Sensor, was selected as a replacement based on its relative accuracy for wind speed and direction and its relatively small size and installation footprint. The manufacturer and model number for the equipment and analytical instrumentation used for this study are presented in Table 7.1.

Table 7.1 Roadside field test site support equipment and analytical instruments

Equipment Type	Manufacturer	Model Number
Zero Air Generator	Teledyne	701
No, NO_2, and NO_X Monitor	Teledyne	200E
O_3 Monitor[1]	Dasibi[1]	1008-AH
O_3 Monitor[2]	Horiba[2]	APOA-370
Multi-gas Dynamic Dilution Calibrator	Teledyne	T700
Wireless Modem	Sierra Wireless	LS300
Wind Sensor	Met One Instruments	
Data Logger	Zeno	3200

[1] O_3 analyzers used in year 1
[2] O_3 analyzers used in year 2

It should be noted that for the first year of the field study, Dasibi model 1008-AH O_3 monitors were used. During weekly inspections of the test site near the end of the first year, it was noted that the instantaneous O_3 values for these analyzers were increasingly unstable even though the instruments were meeting the calibration requirements of Sutron's Leading Environmental Analysis & Display System (LEADS). Bids were accepted for equivalent replacements and the low bid was received from Horiba. The Horiba model APOA-370 is listed as an EPA equivalent method as of July 25, 2006. The Horriba O_3 monitors were used for all year-2 O_3 sampling.

7.5 Data collection results

7.5.1 Data availability year 1

The data availability for 2015, year 1, is presented in Tables 7.2 and 7.3. The Sutron/LEADS software separately maintains the data and statistics for the photocatalytic stucco site and the control site. The calculated percent availability numbers take into account daily calibrations for the O_3 and NO_x monitors as well as system maintenance and outages.

Table 7.2 Percent data availability for photocatalytic stucco site – year 1

Month	NO	NO_2	NO_x	O_3	Wind Speed	Wind Direction	Wind Gust
June	74%	No Data	11.8%	92.1%	100%	100%	100%
July	69%	53.2%	53.2%	70.3%	100%	100%	100%
August	95.3%	95.7%	94.8%	96.5%	100%	100%	99.9%
September	93.5%	93.3%	93.5%	95.6%	100%	100%	100%
October[1]	98.1%	98.1%	98.1%	97.0%	100%	100%	100%

[1] Data available October 1 through midnight October 26

Table 7.3 Data availability for control site – year 1

Month	NO	NO_2	NO_x	O_3
June	76.1%	10.8%	18.8%	97.4%
July	69.9%	44.5%	47.0%	65.6%
August	85.8%	85.8%	85.8%	97.3%
September	81.7%	81.7%	81.7%	84.4%
October[1]	95.1%	95.1%	95.1%	98.4%

[1] Data available October 1 through midnight October 26

There were several warranty repairs made to the NO_x analyzers and the dynamic dilution calibrator that reduced the overall data availability. The warranty repairs included the factory repair of a NO_x analyzer for signal instability and the factory repair of a dynamic dilution calibrator for instability. The most significant repair was the field replacement of the NO_x converters for both analyzers in early July. Replacing the NO_x converters resulted in significant increases in the data availability from the NO_x monitors. Site stability and calibration repeatability was further improved through the use of a single dynamic dilution calibrator for both sites. To maintain calibration for both sites, every 7 days the communication and sample lines connecting dynamic dilution calibrator to one set of analytical instruments were changed to the other set of instruments.

Non-calibration data losses in August are attributable to a power failure for the zero air generator producing failed NO_x calibrations for the control site. Data losses in September resulted from a failed electrical power strip that supplied power to the pumps for both NO_x monitors and the control site ozone monitor. Following restoration of the power to the instruments, additional calibrations were required to restore the instruments to service.

7.5.2 Data availability year 2

The data availability for 2016, year 2, is presented in Tables 7.4 and 7.5.

Table 7.4 Percent data availability for photocatalytic stucco site – year 2

Month	NO	NO_2	NO_x	O_3	Wind Speed	Wind Direction	Wind Gust
March	52.6	53.6	56.0	56.3	100	100	96.4
April	97.9	97.9	97.9	97.7	100	100	100
May	96.1	96.1	95.4	97.6	100	100	100
June	97.9	97.5	97.9	97.5	100	100	100
July	75.8	75.5	76.1	79.0	100	100	100
August	66.1	66.1	66.1	64.7	100	100	100
September 1–6	72.9	73.6	73.6	90.3	100	100	100

Table 7.5 Percent data availability for control site – year 2

Month	NO	NO_2	NO_x	O_3
March	88.6	80.6	80.6	93.8
April	97.8	97.8	97.8	99.7
May	94.8	85.1	85.1	98.5
June	96.8	96.8	96.8	99.0
July	96.8	96.8	96.8	98.9
August	92.1	92.1	92.1	95.7
September 1–6	99.3	99.3	99.3	89.6

The analytical instruments were moved to the roadside test site in March. During that month the instruments required multiple "spans and zeros" to meet the quality assurance limits imposed by Sutron's LEADS software reducing the data availability for the month. In July, the weekly change-over of the dynamic dilution calibrator from one set of instruments to the other was omitted, requiring that the data be marked as out of QA requirements and omitted from the available data. In the month of August, the electrical breaker for the zero air generator tripped, causing a failed calibration. Two subsequent calibrations also failed due to communication difficulties between the Zeno data logger and the dynamic dilution calibrator.

7.6 Analysis of field site data

7.6.1 Analysis of roadway field test site data for year 1

Ambient air at the roadside field test site was monitored continuously, collecting five-minute average data for the concentrations of NO, NO_2, NO_3, and O_3. Data were also collected at the site for the five-minute averages of the wind speed, wind direction, and wind gusts. The data were collected and stored using Sutron's LEADS software. After the end of the "ozone season" in November, an independent statistician was given access to the data (a complete copy of the report can be found in Appendix H). The analysis of the data was single-blinded, in that the information was withheld from the statistician regarding which dataset was collected from the photocatalytic test site. Analysis was restricted to the days with at least 18 hours of complete data. Because the analysis is a comparison of the data collected from both the control and photocatalytic sites, only days for which both sites have complete data can be considered. Using these criteria there are 90 days of data for analysis of NO, NO_2, and NO_x and 95 days for comparison of O_3 data. Figure 7.10 compares the cumulative distributions of the daily maximum one-hour measurements for NO_2 at

the two sites for the 90 days from August 1 to November 10. Excluding the 90-day extrema (maxima and minima), the difference between the control site (Site 1) and photocatalytic site (Site 2) values at the same percentiles (10 percent to 90 percent) ranges from -2.1 to –1.1 ppb, averaging -1.8 ppb. The results indicate that the observed maximum NO_2 concentration at sampling station 2 (photocatalytic site) exceeded the observed maximum NO_2 concentration at the sampling station 1 (control site) by an average value of 1.8 ppb.

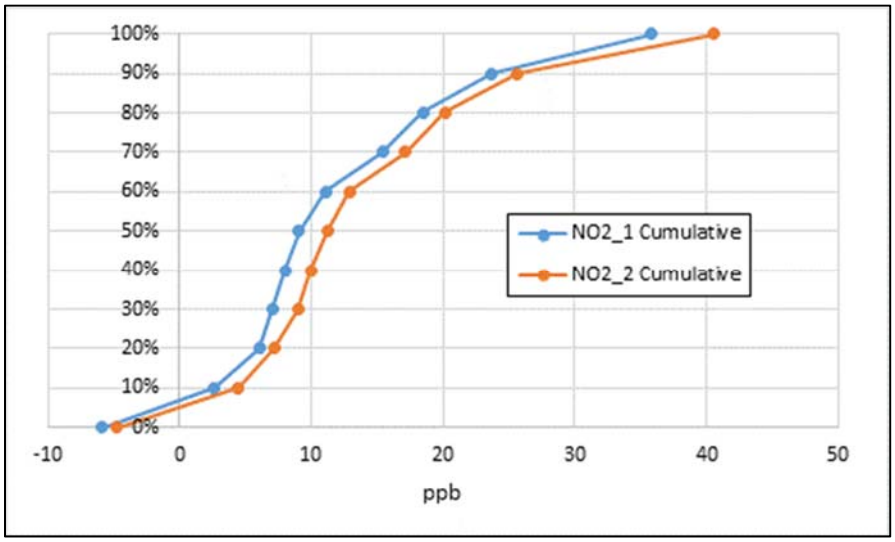

Figure 7.10 Cumulative distributions of the daily maximum one-hour NO_2. NO2_1 is the photocatalytic site and NO2_2 is the control.

Figure 7.11 is a cumulative distribution plot of the maximum one-hour O_3 concentration at the two sites for the 95 days of comparable data. Once again excluding the extrema (maxima and minima), the Site 1 and Site 2 values differ by 2.2 to 3.6 ppb, averaging 2.9 ppb. Thus, sample Site 1 (control site) maximum O_3 ozone concentration is greater than the photocatalytic site by an average of 2.9 ppb.

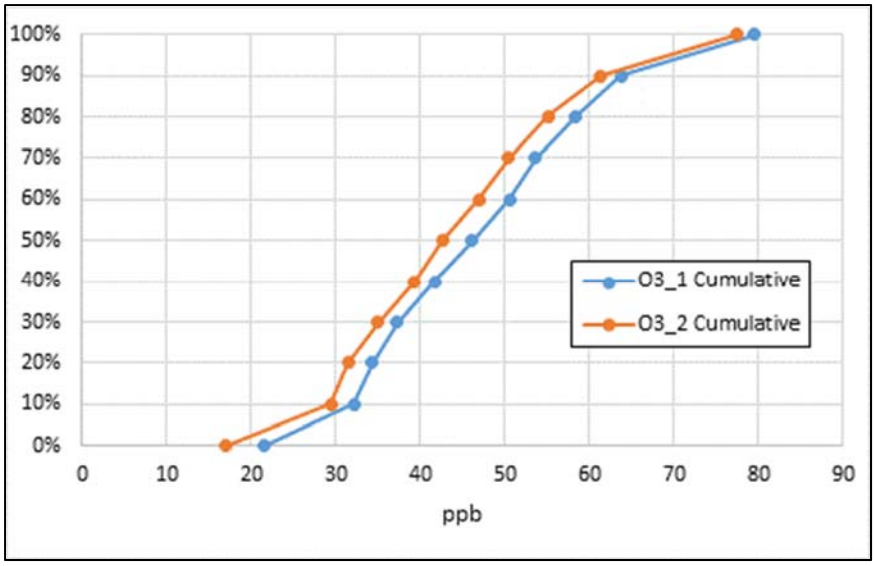

Figure 7.11 Cumulative distributions of the daily maximum one-hour O_3 values. O3_1 is the control site and O3_2 is the photocatalytic site.

Linear regressions were also conducted to examine the differences between the observed concentrations at the two sites. Figures 7.12 through 7.15 are the outputs from a series of linear regressions for NO, NO_2, NO_x, and O_3.

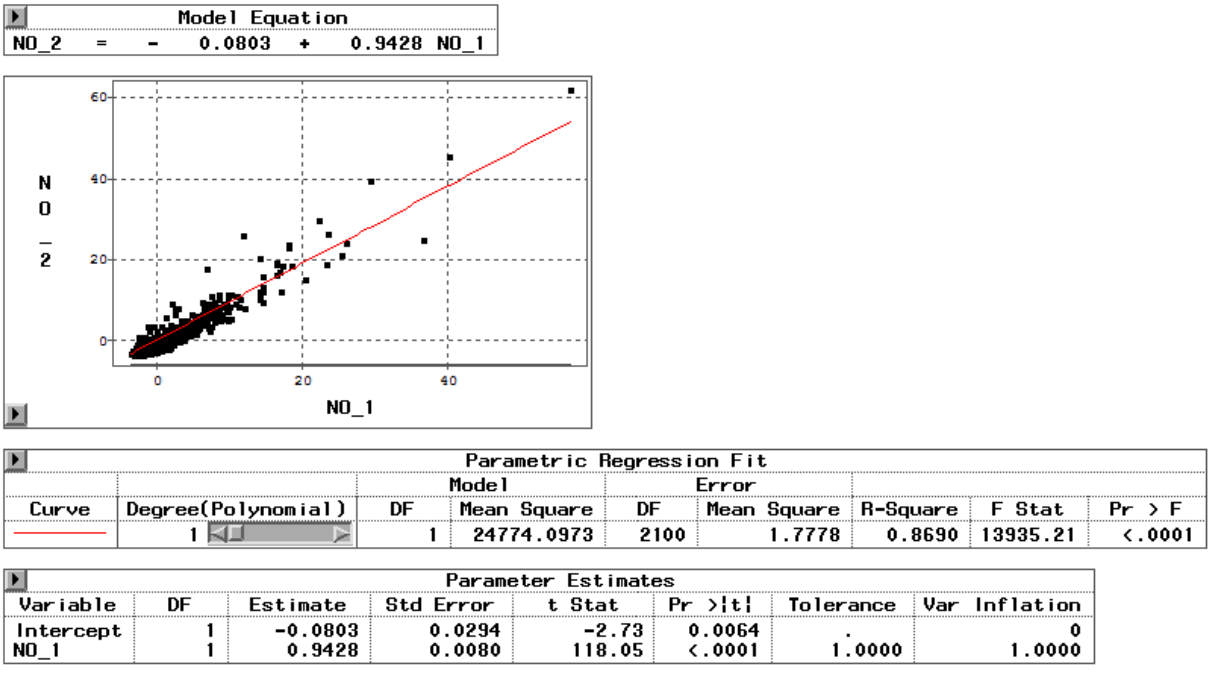

Model Equation

NO_2 = - 0.0803 + 0.9428 NO_1

Parametric Regression Fit

Curve	Degree(Polynomial)	Model DF	Model Mean Square	Error DF	Error Mean Square	R-Square	F Stat	Pr > F
	1	1	24774.0973	2100	1.7778	0.8690	13935.21	<.0001

Parameter Estimates

Variable	DF	Estimate	Std Error	t Stat	Pr >|t|	Tolerance	Var Inflation
Intercept	1	-0.0803	0.0294	-2.73	0.0064	.	0
NO_1	1	0.9428	0.0080	118.05	<.0001	1.0000	1.0000

Figure 7.12 Linear regression for NO

Model Equation

NO2_2 = 1.4985 + 1.0009 NO2_1

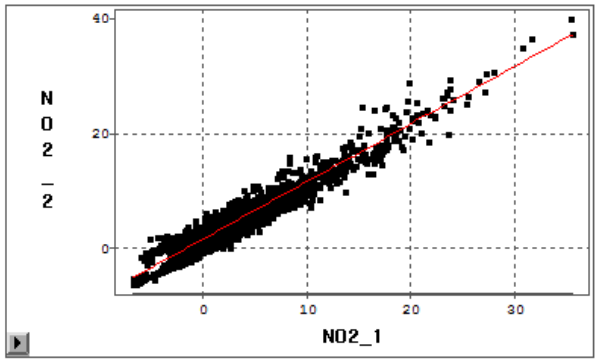

Parametric Regression Fit

Curve	Degree(Polynomial)	Model DF	Model Mean Square	Error DF	Error Mean Square	R-Square	F Stat	Pr > F
	1	1	67191.9485	2100	2.3054	0.9328	29145.19	<.0001

Parameter Estimates

Variable	DF	Estimate	Std Error	t Stat	Pr >|t|	Tolerance	Var Inflation
Intercept	1	1.4985	0.0382	39.26	<.0001	.	0
NO2_1	1	1.0009	0.0059	170.72	<.0001	1.0000	1.0000

Figure 7.13 Linear regression for NO_2

Model Equation

NOx_2 = 0.1027 + 1.0078 NOx_1

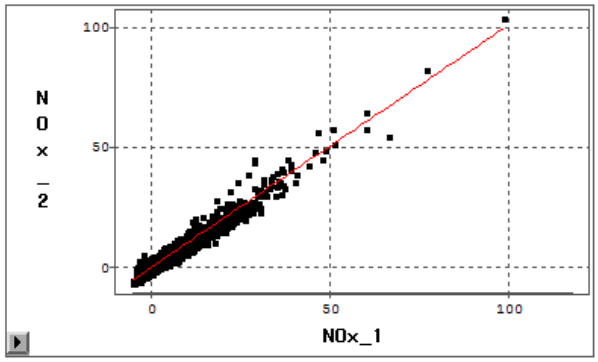

Parametric Regression Fit

Curve	Degree(Polynomial)	Model DF	Model Mean Square	Error DF	Error Mean Square	R-Square	F Stat	Pr > F
	1	1	144446.883	2100	3.9176	0.9461	36871.73	<.0001

Parameter Estimates

Variable	DF	Estimate	Std Error	t Stat	Pr >|t|	Tolerance	Var Inflation
Intercept	1	0.1027	0.0554	1.86	0.0637	.	0
NOx_1	1	1.0078	0.0052	192.02	<.0001	1.0000	1.0000

Figure 7.14 Linear regression for NO_x

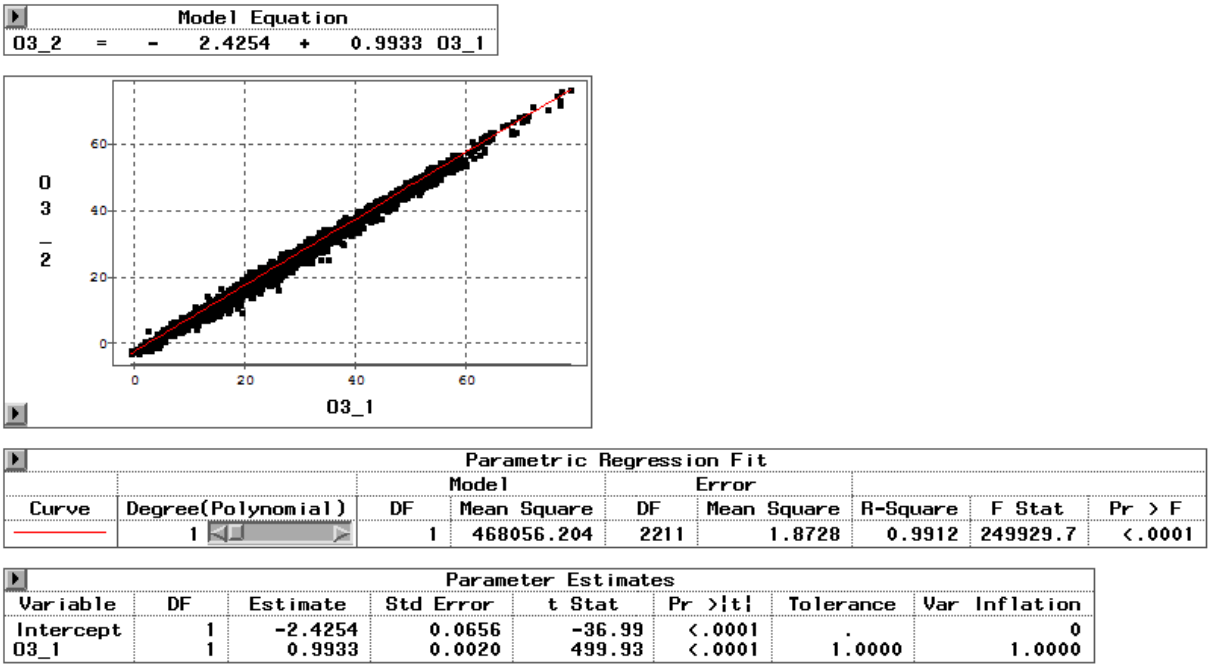

Model Equation

O3_2 = - 2.4254 + 0.9933 O3_1

Parametric Regression Fit

Curve	Degree(Polynomial)	Model DF	Model Mean Square	Error DF	Error Mean Square	R-Square	F Stat	Pr > F
	1	1	468056.204	2211	1.8728	0.9912	249929.7	<.0001

Parameter Estimates

Variable	DF	Estimate	Std Error	t Stat	Pr >|t|	Tolerance	Var Inflation
Intercept	1	-2.4254	0.0656	-36.99	<.0001	.	0
O3_1	1	0.9933	0.0020	499.93	<.0001	1.0000	1.0000

Figure 7.15 Linear regression for O_3

All of the regressions are statistically significant at $p < 0.0001$. Considering all of the complete data for both O_3 and NO_2, the slopes are practically equal to 1.0 and the y-intercepts are statistically significant: -2.43±0.13 ppb for O_3 and +1.50±0.01 ppb for NO_2. This suggests a consistent 2.4 ppb bias for the control site (*O3_1 > O3_2)* and a consistent 1.5 ppb bias for photocatalytic site (*NO_2_2 > NO_2_1)*. If concentrations of *O_3_1* below 40 ppb are excluded, the *O_3_1 > O_3_2* bias is still approximately the same at -2.62±0.80. If concentrations of *NO_2_1* below 5 ppb are excluded, the y-intercept shrinks to 1.10±0.31 ppb and the slope increases to 1.04±0.03.

To further investigate the differences between the test sites, the diurnal variation of the NO_2 and O_3 concentrations were examined. Representative plots of the diurnal variation in the concentration of these pollutants are shown in Figures 7.16 and 7.17.

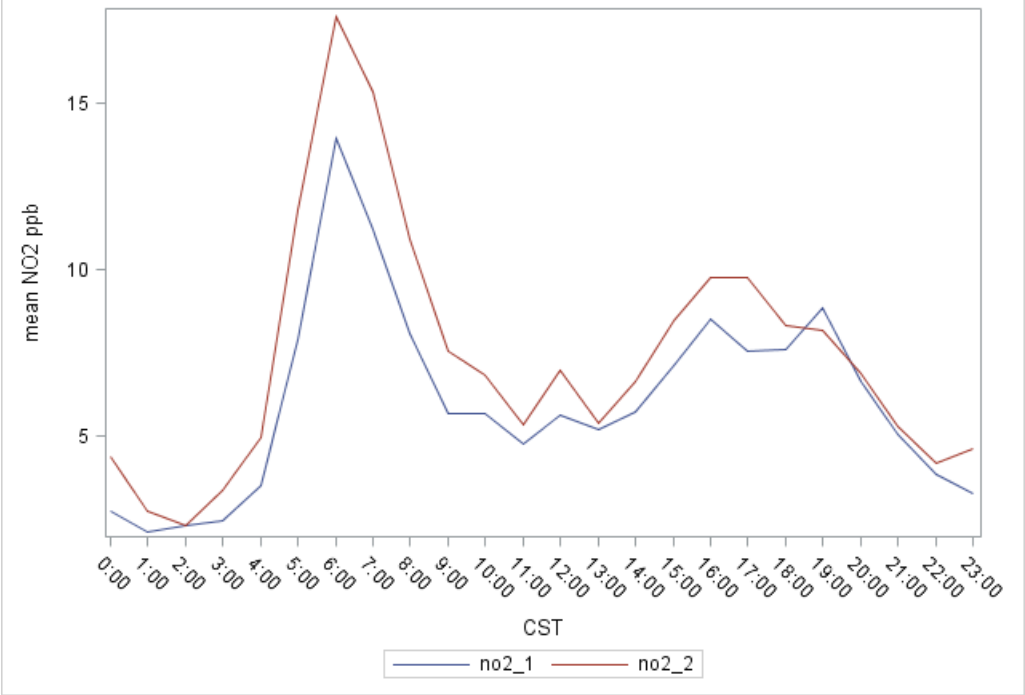

Figure 7.16 Diurnal pattern for mean hourly concentration for NO_2 for Aug. 22–28

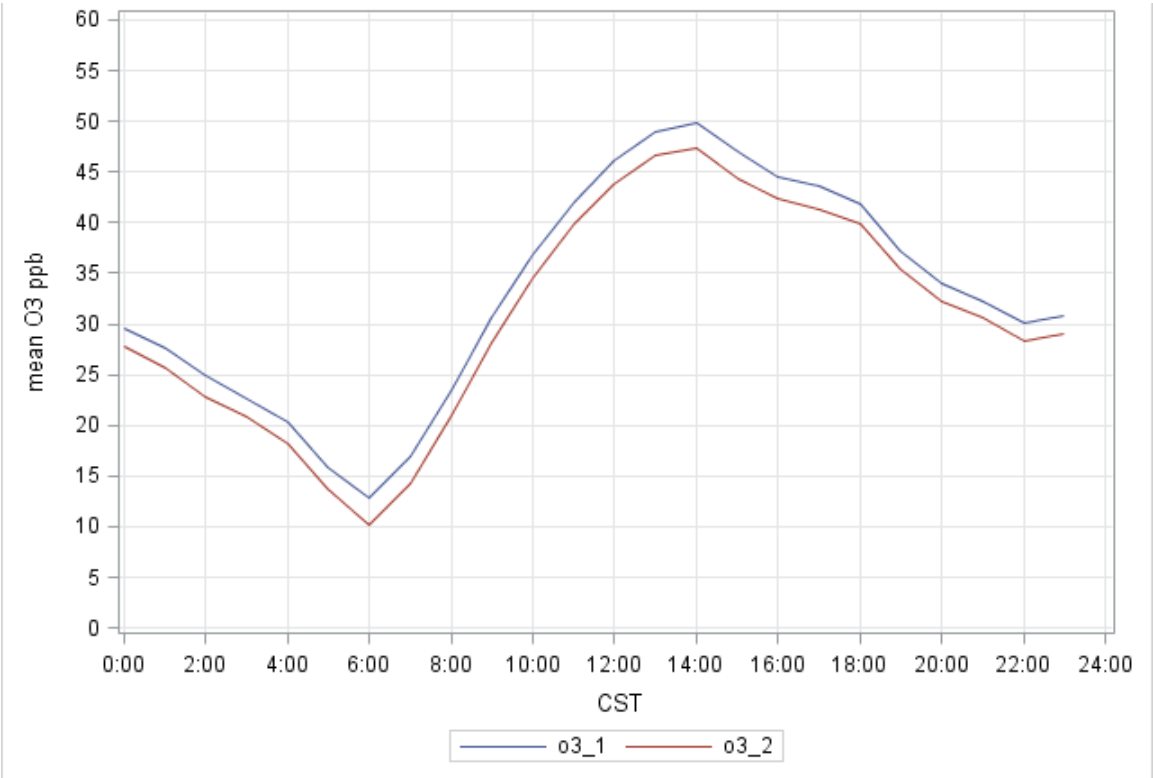

Figure 7.17 Diurnal pattern for mean O_3 concentration for August 2015

Examination of the NO_2 diurnal pattern shows a variable difference between the two sites. However, during daylight hours the relative difference between the NO_2 concentrations increases. In other words, the NO_2 in close proximity to the photocatalyst goes up compared to the control site. This observation is in direct conflict with the postulated function of the photocatalytic surface.

The diurnal plot for O_3 shows an almost constant offset between the two sites, independent of the time of day. These O_3 results suggest that the differences between the sites observed in year 1 may be the result of an "offset" between the two instruments and not the result of photocatalytic processes, which should be lower at night in the absence of sunlight.

The calculated differences produced by the regression analysis are within the uncertainty associated with the analytical instruments and the calibrator. They are also within the quality assurance requirements imposed by the LEADS software. Further, the values for the observed concentrations are relatively low, particularly for NO_2. As the observed concentrations approach zero, the relative uncertainty associated with the measurements increases, also suggesting that the observed differences may be due to small differences in the analytical instruments and typical instrument drift.

All three methods of evaluating the data from the first year of the roadway field test site indicate that the O_3 concentration observed at the control site was higher compared to the photocatalytic site. Further, all three methods indicate that the NO_x concentration observed at the photocatalytic site was greater compared to the control site. These findings are at odds with the results from the chamber tests that showed a decrease in both NO_x and O_3 concentrations in the presence of the photocatalyst. The conflicting results suggest that the differences between the test sites may not be the result of photocatalysis, but are caused by other factors, such as small differences in the analytical equipment or drift in the calibration process that are within the specified quality control limits of LEADS.

7.6.2 Analysis of roadway field test site data for year 2

Following the completion of the analysis for year 1, several efforts were made to reduce the inherent differences between the two sets of instruments used in this study. These efforts included replacing the Daisbi 1008-AH ozone monitors with two Horiba ozone analyzers (model 1008-AH); adding O_3 calibration values to the dynamic dilution calibrator that correspond to the O_3 concentrations generated for instrument calibration; and conducting the manufacturers' annual maintenance for the NO_x analyzers, zero air generator, and dynamic dilution calibrator. Following these efforts, the instruments were configured exactly as they were during the field study. The instruments were located in the "high bay" at the Center for Energy and Environmental Studies at the University of Texas at Austin. The air in the high bay is greatly influenced by outdoor air, generating NO_x and O_3 levels higher than typical for indoor air. The LEADS system was used to perform routine calibrations and record the data. For these measurements the instruments were "co-located" in that the sampled air was pulled through a single tube that was split into two streams using a "T" just prior to entering the manifolds for the analytical instruments.

Figure 7.18 contains graphs of the differences between the one-hour averages for NO_x and O_3 concentrations measured by the analyzers. The dots are the differences between the five-minute averages recorded in LEADS for both instruments. The vertical linear groupings are a single day's worth of data. Examining the graph for O_3 from left to right, the data on the left side of the graph appear to indicate that the instruments differ by approximately 0.5 ppb and that difference "bounces" between the instruments, with both instruments having the highest value from time to time. Moving to the right side of the graph, the delta appears to shift with the control site analyzer,

producing the larger values a greater percentage of the time. While both of the instruments were within the calibration limits of LEADS, the shift in the plotted data is noticeable.

Examining the graph for NO_2 beginning at the left side of the graph, the first week of data exhibits a difference between the two instruments of 1 to almost 2.5 ppb and absolute shift of between -1.5 and -2 ppb from zero. To address this issue, the instruments were zeroed and spanned before collecting the next week's data. After adjusting the instruments, the range of differences between the two NO_x analyzers for a single day varied from approximately +0.3 to -0.75 to +0.75 to -1.8. Producing overall differences between the analyzers of approximately 1 ppb to 2.5 ppb centered around zero. The variation observed between the O_3 analyzers was less, averaging approximately 1 ppb and typically centered about zero. However, as was the case for the NO_X analyzers, the center of the distribution for the difference between the O_3 analyzers did drift away from zero. The differences in the analytical instruments are associated with machine drift, calibration uncertainties, and the uncertainty associated with the relatively low absolute concentrations observed. It should also be noted that these instruments were calibrated using the same instruments and procedures employed at the test site and, therefore, similar variance should be expected in the analytical instruments at the roadside field test site.

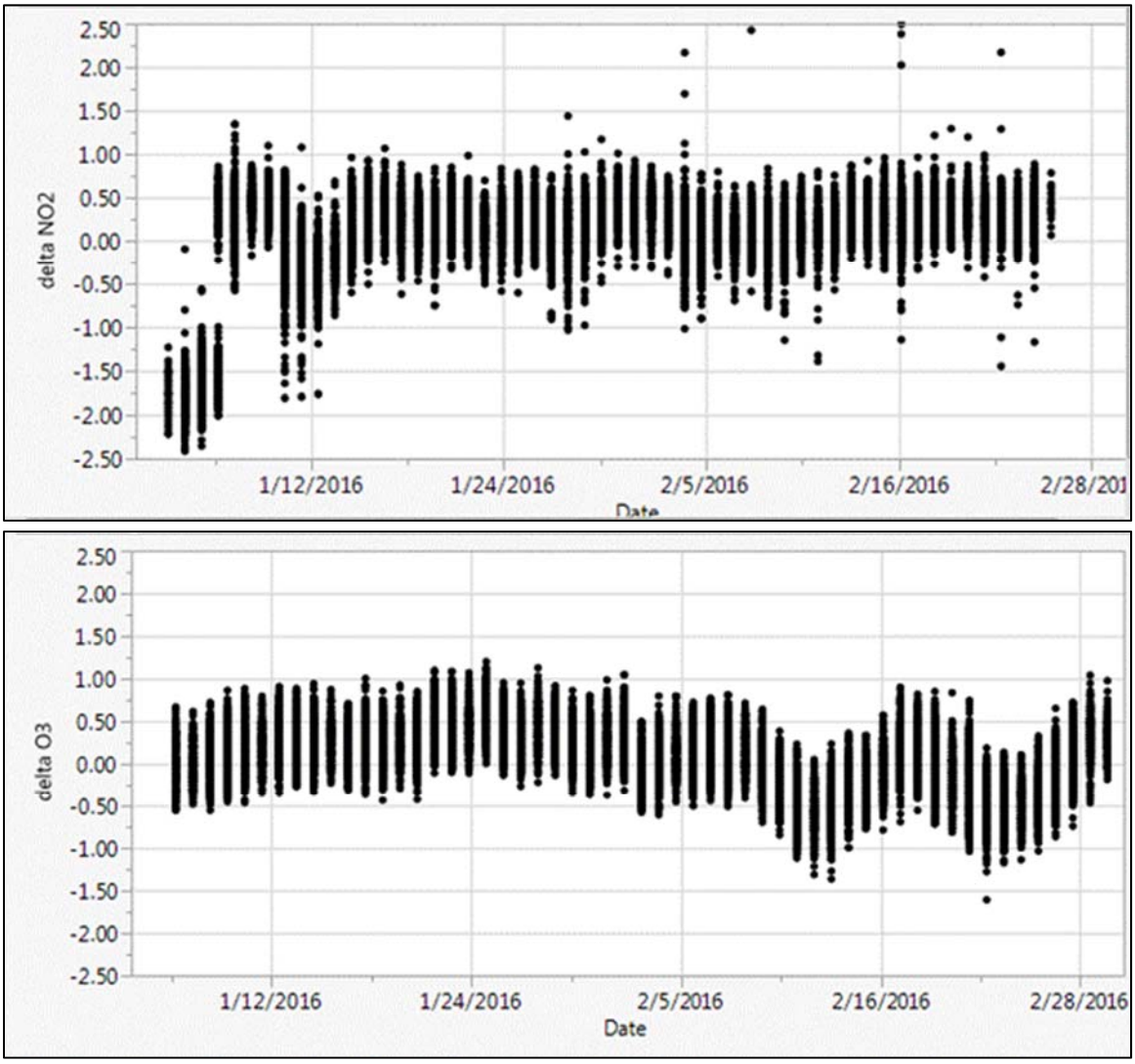

Figure 7.18 Plots of the difference between the outputs for the NO_x and O_3 analyzers used for this study sampling the same air parcels

In year 2, the ambient air and metrological conditions at the roadside field test site were monitored and stored as described in section 7.6.1. In September the site was decommissioned and the data made available to an independent statistician for analysis. Again the analysis of the data was single-blinded, in that the information was withheld from the statistician regarding which dataset was collected from the photocatalytic test site (the complete report can be found in Appendix I). Analysis was restricted to the days with at least 18 hours of complete data for NO_x and O_3. Using these criteria, there are 167 days of data for O_3 analysis and 157 days for NO_x analysis. The NO_2 and O_3 data were examined by comparing the diurnal patterns between the two sites. The comparison was conducted by first averaging all of the raw 5-minute averages from the LEADS system by hour. The hourly values were then averaged for seven-day periods. The difference in the average pollutant concentrations between the two sites was calculated by subtracting Site 1 (control site) from Site 2 (photocatalytic site). The hourly averages were then averaged into 3-hour groups. The data for NO_2 are presented in Table 7.6.

Table 7.6 Mean difference in NO_2 concentrations Site 2 (photocatalytic) minus Site 1 (control)[1,2]

Week	Week	00-02	03-05	06-08	09-11	12-14	15-17	18-20	21-23	Average
1	Mar. 23-Mar.	-1.11	-1	-0.41	-0.92	-0.37	-0.26	-0.61	-0.73	-0.68
2	Mar. 30-Apr. 5	-2.2	-2.02	-2.66	-2.62	-2.57	-1.92	-2.90	-3.27	-2.52
3	Apr. 6-Apr. 12	-2.23	-1.67	-1.94	-1.84	-0.90	-0.96	-1.62	-1.64	-1.60
4	Apr. 13-Apr.	-2.09	-1.72	-1.30	-1.21	-0.91	-0.48	-1.12	-1.59	-1.3
5	Apr. 20-Apr.	-1.89	-1.70	-0.56	-1.00	-1.14	-1.15	-1.73	-1.96	-1.39
6	Apr. 27-May 3	-2.05	-2.29	-1.74	-1.16	-1.05	-1.05	-1.15	-1.62	-1.51
7	May 4-May10	0.05	-0.10	0.46	0.78	0.75	0.55	0.03	0.42	0.37
8	May 11-May	-0.23	-0.24	-0.19	0.36	0.57	0.67	-0.37	-0.22	0.04
9	May 18-May	0.22	0.24	1.04	1.27	1.08	1.60	0.75	0.51	0.84
10	May 25-May	1.78	1.50	1.74	1.47	1.55	1.56	1.30	1.23	1.52
11	Jun. 1-Jun. 7	1.75	2.21	3.68	4.01	3.79	3.86	3.24	2.76	3.16
12	Jun. 8-Jun. 14	3.83	4.14	3.60	3.59	3.52	4.12	3.18	3.46	3.68
13	Jun. 15-Jun.	2.96	3.31	2.74	2.74	2.84	2.97	2.59	2.82	2.87
14	Jun. 22-Jun.	1.49	1.41	1.13	1.69	1.64	1.63	0.88	1.34	1.40
15	Jun. 29-Jul. 5	1.18	1.38	1.90	2.24	2.21	1.80	1.62	1.66	1.75
16	Jul. 6-Jul. 12	2.43	2.33	2.03	2.08	2.13	1.97	1.84	2.07	2.11
18	Jul. 20-Jul. 26	2.53	2.73	2.28	2.65	2.47	2.67	2.59	2.29	2.53
19	Jul. 27-Aug. 2	0.44	0.17	-0.18	-0.21	-0.09	-0.43	-0.33	-0.12	-0.09
20	Aug. 3-Aug. 9	-1.79	-1.66	-1.82	-1.59	-1.55	-1.34	-1.68	-1.77	-1.65
21	Aug. 10-Aug.	0.69	0.66	1.20	1.67	0.91	1.30	1.15	1.02	1.07
22	Aug. 17-Aug.	1.25	1.54	1.78	1.92	2.00	1.74	1.66	1.54	1.68
24	Aug. 31-Sep. 6	0.08	0.28	0.99	0.87	0.99	1.17	0.64	0.19	0.65
26	Sep. 14-Sep.	2.53	2.88	3.19	4.11	4.08	3.15	2.81	2.59	3.17
Grand Total		0.42	0.54	0.74	0.91	0.96	1.01	0.56	0.48	0.70

[1] Green indicates Site1 > Site2 and red find indicates Site2 > Site1

[2] Based on 157 days from March 23 to September 18, 2016

Examination of the data in Table 7.6 shows that for only 8 of the 23 weeks analyzed in the field was the NO_2 concentration observed at the photocatalytic site lower compared to the control site.

The results shown in Table 7.6 can also be viewed graphically. Figures 7.19 and 7.20 contain representative diurnal plots selected from 2 sample weeks (March 30–April 5 and May 25–31).

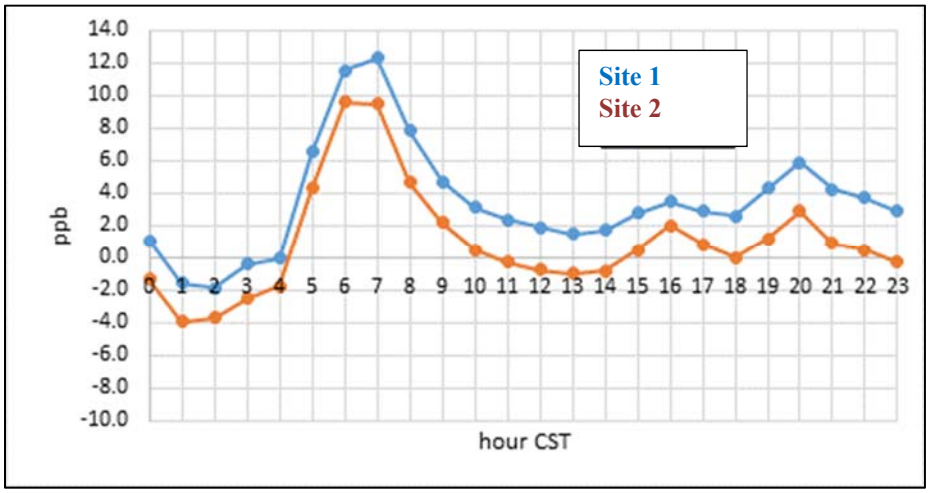

Figure 7.19 NO_2 diurnal pattern for March 30 through April 5

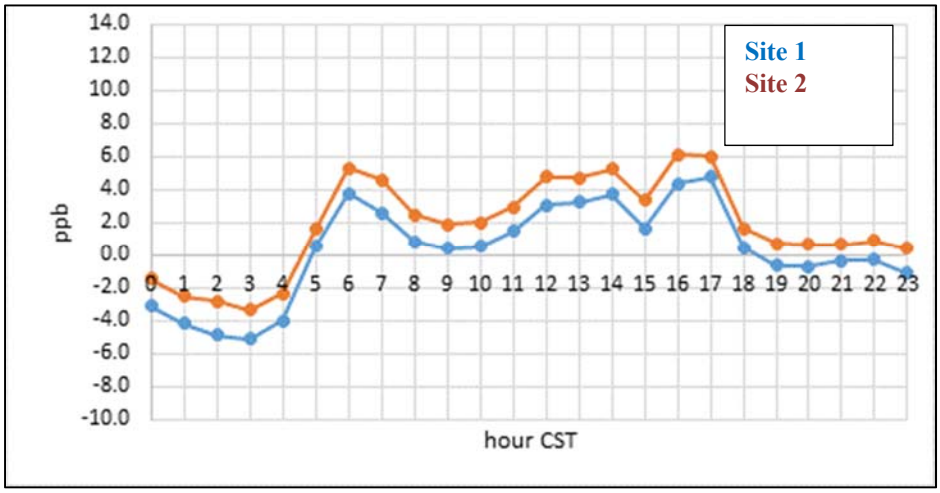

Figure 7.20 O_3 diurnal pattern for May 25 through May 31

The mean difference between O_3 concentrations for the two test sites is presented in Table 7.7.

Table 7.7 Mean difference in O_3 concentrations Site 2 (photocatalytic) minus Site 1 (control)[12]

Week Index	Week	00-02 CST	03-05 CST	06-08 CST	09-11 CST	12-14 CST	15-17 CST	18-20 CST	21-23 CST	Grand Total
1	Mar. 23-Mar. 29	-0.98	-1.01	-0.95	-0.63	-1.10	-0.86	-0.47	-0.41	-0.80
2	Mar. 30-Apr. 5	0.18	0.28	0.54	-0.23	-0.43	-0.79	-0.02	0.26	-0.03
3	Apr. 6-Apr. 12	0.45	0.28	0.22	0.18	-0.24	-0.14	0.55	0.56	0.23
4	Apr. 13-Apr. 19	0.25	0.26	-0.37	-0.69	-1.06	-1.21	-0.40	0.08	-0.39
5	Apr. 20-Apr. 26	0.48	0.59	-0.78	-0.16	-0.76	-0.74	0.24	0.38	-0.10
6	Apr. 27-May 3	-0.32	-0.38	-1.06	-1.71	-1.53	-1.28	-0.64	-0.04	-0.87
7	May 4-May10	-0.09	0.58	-0.10	-0.13	-0.94	-0.98	-0.43	-0.33	-0.30
8	May 11-May 17	-1.04	-0.97	-0.93	-1.21	-1.42	-1.78	-0.52	-0.98	-1.11
9	May 18-May 24	-0.49	-0.61	-0.74	-0.59	-0.65	-1.01	-0.44	0.04	-0.56
10	May 25-May 31	0.00	-0.09	-0.22	0.09	0.24	-0.21	0.02	0.02	-0.02
11	Jun. 1-Jun. 7	-0.34	-0.20	-0.46	0.03	-0.05	-0.64	-0.02	0.10	-0.20
12	Jun. 8-Jun. 14	0.85	0.58	0.39	0.46	0.31	-0.32	0.70	0.73	0.46
13	Jun. 15-Jun. 21	0.64	0.60	0.83	0.72	0.05	0.32	0.82	0.68	0.58
14	Jun. 22-Jun. 28	1.16	0.97	1.07	0.33	0.61	0.47	1.25	1.24	0.89
15	Jun. 29-Jul. 5	0.84	0.86	0.34	0.99	-0.01	0.15	0.86	0.79	0.60
16	Jul. 6-Jul. 12	0.73	0.79	0.71	0.63	0.54	1.24	1.26	0.79	0.84
18	Jul. 20-Jul. 26	0.57	0.56	0.79	0.47	0.03	0.11	0.25	0.41	0.40
19	Jul. 27-Aug. 2	0.11	0.11	0.43	0.70	0.10	0.65	0.58	0.36	0.38
20	Aug. 3-Aug. 9	0.52	0.47	0.95	0.98	1.03	1.19	1.01	1.25	0.92
21	Aug. 10-Aug. 16	2.47	2.35	2.03	1.46	1.96	1.95	2.02	2.27	2.07
22	Aug. 17-Aug. 23	2.87	2.78	3.21	3.53	2.66	2.80	2.81	2.78	2.93
24	Aug. 31-Sep. 6	0.50	0.81	0.55	-0.61	-0.98	-0.64	-0.50	-0.76	-0.20
25	Sep. 7-Sep. 13	-0.99	-0.79	-1.42	-2.05	-1.45	-1.02	-0.62	-0.68	-1.13
26	Sep. 14-Sep. 19	-0.48	-0.22	-0.96	-1.93	-1.93	-1.01	-0.65	-0.50	-0.96
Grand Total		0.33	0.36	0.17	0.03	-0.21	-0.16	0.32	0.38	0.15

[1] Green indicates Site1 > Site2 and red indicates Site2 > Site, [2] Based on 167 days from March 23 to September 18, 2016

Examination of the data in Table 7.7 indicates that the differences between the O_3 measurements are smaller compared to the differences between the NO_2 measurements. However, the O_3 data are similar to NO_2 data in that the site with the highest O_3 concentration is inconsistent. In fact, for 13 of the 24 weeks analyzed in Table 7.7, the O_3 concentration was higher for the control site, and for the other 11 weeks the higher O_3 concentration was observed for the photocatalytic site. Two representative diurnal patterns for this data are presented in Figure 7.21 and 7.22.

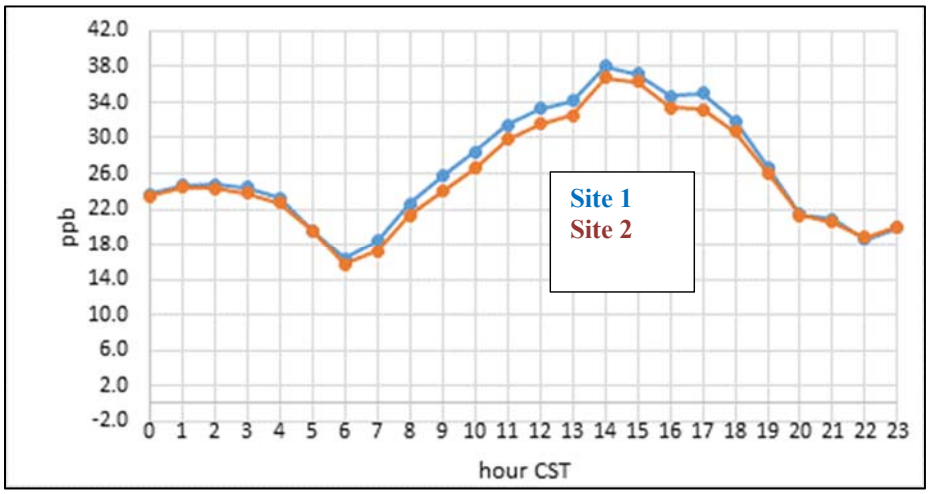

Figure 7.21 O_3 diurnal pattern for April 27 to May 3

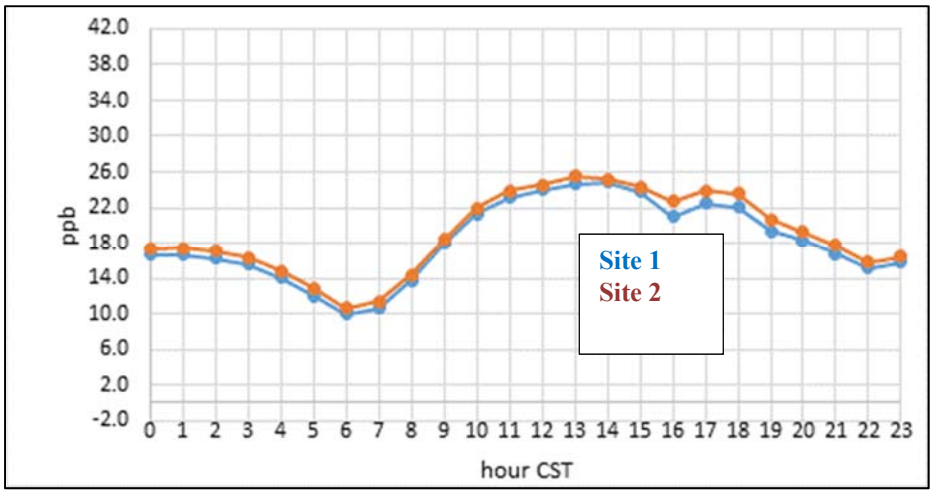

Figure 7.22 O_3 diurnal pattern for July 6 to July 12

The relationship between the observed concentrations and the meteorological data was also investigated. For this analysis the wind speed and direction collected at the roadside field test site were merged with metrological data collected by two nearby TCEQ continuous ambient monitoring station (CAMS) sites, CAMS 3 and CAMS 38 (the details for merging these data and a detailed analysis of the effect of weather on this study are presented in the report in Appendix I). The correlation between six variables—east-west wind, north-south wind, ambient temperature, solar intensity, differences in NO_2 concentrations, and differences in O_3 concentrations—were

considered. Analysis of the Pearson Correlations produced no assignable cause for the wind direction or rainfall associations with the differences in O_3 concentrations or wind direction association with differences in NO_2 concentrations.

7.7 Quality assurance for roadway field test site

The quality assurance protocol used for the roadway field test site is described in detail in Appendix G, which contains the Quality Assurance Project Plan developed for and followed in this project. In general, the quality assurance methods and calibrations limits employed in the Sutron/LEADS software for this project are the same as the ones used by the TCEQ for environmental monitoring. The only exception was the use of a single dynamic dilution calibrator for both sets of analytical equipment as described in section 7.4.1 of this report. The protocol for the use of a single calibrator required that the calibrator be switched from one set of analytical instruments to the other every 7 days. In the event that an instrument was not calibrated at least every 7 days, the data from that instrument were excluded from consideration.

Chapter 8. Conclusions and Recommendations

8.1 Summary and conclusions

This study investigated the use of TiO_2 as an abatement method for atmospheric NO_x and ground level O_3. The study consisted of four parts: laboratory chamber studies evaluating several commercially available TiO_2-containing photocatalytic coatings; outdoor exposure studies to evaluate the environmental stability of the coatings; modeling to determine the potential effect of a photocatalytic coating on non-attainment areas in Houston and Dallas; and a field study to evaluate the "real world" effectiveness and durability of the coating found most effective in the first two parts of the study, a stucco.

Laboratory chamber studies consisted of screening tests, a full factorial experiment to determine the factors influencing the photocatalytic activity of TiO_2, and kinetic studies to measure input parameters for modeling of the photocatalytic effect in the Houston and Dallas metropolitan areas. Four commercial TiO_2-containing photocatalytic coatings were examined and, following the screening tests, a stucco containing TiO_2 and a commercial clear paint containing TiO_2 were selected for further testing based on their effectiveness at removing NOx and non-methane hydrocarbons. Full factorial testing revealed that NOx removal was sensitive to temperature, RH, light intensity, and contact time. The results from the full factorial experiments indicated that the stucco consistently removed more NO_x compared to the clear paint, and the photocatalytic stucco was selected for modeling and field studies.

Three of the commercial coatings (a clear paint, a white paint, and the stucco) were tested in outdoor exposure studies in three locations, adjacent to highways in Austin and Houston and at the J. J. Pickle Research Campus in Austin. Concrete samples that were of the appropriate size for laboratory chamber tests (i.e., test coupons) were placed on these sites. In addition, a concrete highway barrier was partitioned into coated and uncoated sections and left at the sites for monitoring. Samples were monitored on-site for surface temperature and color changes. Further, the surfaces were "washed" periodically with water that was collected and analyzed for nitrate and nitrite content. After 1 year, small cores were removed and analyzed for composition using x-ray diffraction and scanning electron microscopy. Coupons were returned to the laboratory for chamber testing. The control and stucco-coated samples were exposed and tested for an additional year. Test results suggested that the white paint was ineffective at NOx removal and that the clear paint was washed off following rain or water washing. Therefore, the stucco is the only effective and environmentally stable coating of those examined.

Chamber tests conducted on the field coupons showed that after 1 year of outdoor exposure, the Houston-area stucco-coated coupon retained only 50 to 75% of its original NO_x removal capacity. Chamber tests conducted after 2 years of outdoor exposure in Houston found that the photocatalyst had retained approximately 30 to 50% of its original NO_x removal capacity. Test slabs exposed to the Houston roadways showed the lowest removal rates for all conditions, indicating that higher traffic areas may result in faster degradation of photocatalytic performance.

Kinetic data derived from the laboratory chamber experiments were integrated into the Comprehensive Air Quality Model with extensions (CAMx; ENVIRON, 2010). Modeled simulations showed a reduction of the daily 8-hour maximum average ozone concentrations in the DFW area ranging from -0.0001 to 0.09 ppb. Differences in daily maximum 8-hour average ozone concentrations in the HGB area ranged from 0.0006 to 0.04 ppb.

A roadside field test site was established at the Parmer Lane toll plaza on SH 45 (also known as the Lake Creek Toll Plaza). The test site GPS coordinates are 30.474515, -97.774839. The test site consisted of a series of concrete highway barriers coated with the photocatalytic stucco and a similar set of uncoated barriers. In all, 1100 linear feet (7700 ft^2) of barriers were coated, at a cost of $20,000, including materials and labor. Sampling stations were placed on the northern side of the roadway in the direction of the prevailing summer winds in the Austin area. The sampling stations were outfitted with matching O_3 and NO_x analyzers. The data from the analyzers and the quality assurance procedures were maintained by Sutron's LEADS software, the same software used by TCEQ to maintain their continuous ambient monitoring stations (CAMs). The test site was composed of two sections. Site 1 was the control site composed of untreated barriers. Site 2 was the photocatalytic site comprising barriers coated with photocatalytic stucco. The test site was operated from March 2015 to October 2015 and again from March 2016 to September 2016. The two field campaigns produced more than 240 days for comparison of the effect of the two test sites.

The data collected for year 1 indicated that, in general, the O_3 concentrations associated with the photocatalytic site were lower compared to the control site. Conversely, the NO_2 concentrations associated with the photocatalytic site were higher compared to the control site. The observed differences are within the error of the instruments. Additionally, the results contradict the chamber tests and the published literature, suggesting that the results are not conclusive.

The data collected for year 2 showed no consistent correlation between the sites and the concentration of O_3 or NO_x. Over the course of the second year, the site with the highest concentration changed several times. An independent analysis of the data collected for both years found no statistical correlation between the difference in pollutant concentrations and the use of photocatalytic coating. Further, additional statistical analysis found no statistical correlation between metrological conditions and the differences observed in the pollutant concentrations between the test sites.

Utilization of photocatalytic materials to reduce ground levels of O_3 depends on a reliable, durable catalytic material. Further, the material must be relatively inexpensive given that the interstate highway system that TxDOT supports covers thousands of miles—not to mention the other roadways TxDOT maintains, such as the U.S. highways, state highways, farm-to-market roads, tollways, etc. Without a statistically significant reduction in ground level NOx or O3, use of the selected photocatalytic stucco, at the current cost, cannot be considered an option for air pollution abatement.

8.2 Recommendations

Over the course of the data analysis, these recommendations were developed for similar future projects:

- While there was no statistically significant reduction in NOx or O_3 concentrations associated with the photocatalytic treatment investigated in this study, it is possible that the Texas Commission on Environmental quality (TCEQ) and/or TxDOT will investigate other roadside pollution control techniques to mitigate vehicular pollution. Beginning in 2014, the TCEQ initiated a near-roadway monitoring program in Houston, Dallas, and San Antonio. The traffic patterns in these so-called "hot spots" generate significant concentrations of NOx, up to 20 times greater than

observed in this study. It is understood that the logistics of using these high-volume traffic areas as test sites present significant challenges; however, the elevated pollutant levels would increase confidence in the measured concentrations, improving the chances of generating statistically significant results.

- The calibration routines employed in the LEADS data collection and monitoring systems were developed when the ambient concentration of NOx and O_3 were higher than they are today. Projects evaluating pollution control technologies should consider updating the calibration procedures to reflect current ambient pollution levels when appropriate.

References

Agrios, A.G., Pichat, P., 2005. State of the art and perspectives on materials and applications of photocatalysis over TiO2. J Appl Electrochem 35, 655–663.

Alberici, R., Jardim, W., 1997. Photocatalytic destruction of VOCs in the gas-phase using titanium dioxide. Applied Catalysis B: Environmental 14, 55–68.

Allen, N.S., Edge, M., Sandoval, G., Verran, J., Stratton, J., Maltby, J., 2005. Photocatalytic coatings for environmental applications. Photochem. Photobiol. 81, 279–290.

Ao, C.H., Lee, S.C., Mak, C.L., Chan, L., 2003. Photodegradation of volatile organic compounds (VOCs) and NO for indoor air purification using TiO2: promotion versus inhibition effect of NO. Applied Catalysis B: Environmental 42, 119–129.

Auvinen, J., Wirtanen, L., 2008. The influence of photocatalytic interior paints on indoor air quality. Atmospheric Environment 42, 4101–4112.

Ballari, M.M., Hunger, M., Husken, G., H, B.H.J., 2010a. Modelling and experimental study of the NOx photocatalytic degradation employing concrete pavement with titanium dioxide. Catal Today 151, 71–76.

Ballari, M.M., Hunger, M., Husken, G., H, B.H.J., 2010b. NOx photocatalytic degradation employing concrete pavement containing titanium dioxide. Applied Catalysis B: Environmental 95, 245–254.

Ballari, M.M., Yu, Q.L., H, B.H.J., 2011. Experimental study of the NO and NO2 degradation by photocatalytically active concrete. Catal Today 161, 175–180.

Beeldens, A., Van Gemert, D., 2004. Experimental Investigation of Efficiency of TiO2-cement Coating for Self-cleaning and Air Purification, in: Presented at the RILEM International Symposium on Environment-Conscious Materials and Systems for Sustainable Development, pp. 353–359.

Bengtsson, N., Castellote, M., 2010. Photocatalytic Activity for NO Degradation by Construction Materials: Parametric Study and Multivariable Correlations. J Adv Oxid Technol 13, 341–349.

Bouazza, N., Lillo-Rodenas, M.A., Linares-Solano, A., 2008. Photocatalytic activity of TiO2-based materials for the oxidation of propene and benzene at low concentration in presence of humidity. Applied Catalysis B: Environmental 84, 691–698.

Bowering, N., Croston, D., Harrison, P., Walker, G., 2007. Silver modified Degussa P25 for the photocatalytic removal of nitric oxide. International Journal of Photoenergy.

Brigden, C.T., Poulston, S., Twigg, M.V., Walker, A.P., Wilkins, A.J.J., 2001. Photo-oxidation of short-chain hydrocarbons over titania. Applied Catalysis B: Environmental 32, 63–71.

Brunekreef, B., Holgate, S., 2002. Air pollution and health. The Lancet 360, 1233–1242.

Chaloulakou, A., Mavroidis, I., Gavriil, I., 2008. Compliance with the annual NO2 air quality standard in Athens. Required NOx levels and expected health implications. Atmospheric Environment 42, 454–465.

Chen, J., Kou, S., Poon, C.-S., 2011. Photocatalytic cement-based materials: Comparison of nitrogen oxides and toluene removal potentials and evaluation of self-cleaning performance. Building and Environment 46, 1827–1833.

Chen, J., Poon, C.-S., 2009a. Photocatalytic construction and building materials: From fundamentals to applications. Building and Environment 44, 1899–1906.

Chen, J., Poon, C.-S., 2009b. Photocatalytic Cementetious Materials: Influence of the

Microstructure of Cement Paste on Photocatalytic Pollution Degradation. Environ. Sci. Technol 43, 8948–8952.
Chen, W., Zhang, J., 2008. UV-PCO device for indoor VOCs removal: Investigation on multiple compounds effect. Building and Environment 43, 246–252.
Ching, W., Leung, M., Leung, D., 2004. Solar photocatalytic degradation of gaseous formaldehyde by sol–gel TiO2 thin film for enhancement of indoor air quality. Solar Energy 77, 129–135.
Cros, C.J., Terpeluk, A.L., Crain, N.E., Juenger, M.C.G., Corsi, R.L., 2015a. Influence of environmental factors on removal of oxides of nitrogen by a photocatalytic coating, Journal of the Air & Waste Management Association 65, 937-947.
Cros, C.J., Terpeluk, A.L., Burris, L.E., Crain, N.E., Corsi, R.L., Juenger, M.C.G., 2015b. Effect of weathering and traffic exposure on removal of nitrogen oxides by photocatalytic coatings on roadside concrete structures. Materials and Structures 48, 3159–3171.
Dalton, J., Janes, P., Jones, N., Nicholson, J., Hallam, K., Allen, G., 2002. Photocatalytic oxidation of NOx gases using TiO2: a surface spectroscopic approach. Environmental Pollution 120, 415–422.
Dehn, F., Bahnemann, D., Bilger, B., 2004. Development of photocatalytically active coatings for concrete substrates, in:. Presented at the RILEM International Symposium on Environment-Conscious Materials and Systems for Sustainable Development, pp. 347–352.
Devahasdin, S., Fan, C., Li, K., Chen, D.H., 2003. TiO2 photocatalytic oxidation of nitric oxide: transient behavior and reaction kinetics. J Photoch Photobio A 156, 161–170.
Diamanti, M., Ormellese, M., Pedeferri, M., 2008. Characterization of photocatalytic and superhydrophilic properties of mortars containing titanium dioxide. Cement and Concrete Research 38, 1349–1353.
Dylla, H., Hassan, M.M., Mohammad, L.N., Rupnow, T.S., Wright, E., 2010. Evaluation of Environmental Effectiveness of Titanium Dioxide Photocatalyst Coating for Concrete Pavement. Transportation Research Record: Journal of the Transportation Research, Board 2164, 46–51.
Einaga, H., Futamura, S., Ibusuki, T., 2002. Heterogeneous photocatalytic oxidation of benzene, toluene, cyclohexene and cyclohexane in humidified air: comparison of decomposition behavior on photoirradiated TiO2 catalyst. Applied Catalysis B: Environmental 38, 215–225.
Fernandez, A., Lassaletta, G., Jimenez, V.M., Justo, A., Gonzalez-Elipe, A.R., Herrmann, J.M., Tahiri, H., Ait-Itchou, Y., 1995. Preparation and characterization of TiO2 photocatalysts supported on various rigid supports (glass, quartz, and stainless steel). Comparative studies of photocatalytic activity in water purification. Applied Catalysis B: Environmental 7, 49–63.
Folli, A., Strøm, M., Pilegaard Madsen, T., Henriksen, T., Lang, J., Emenius, J., Klevebrant, T., Nilsson, A., 2015. Field Study of air purifying paving elements containing TiO2. Atmospheric Environment, 107, 44-51.
Fujishima, A., Honda, K., 1972. Electrochemical photolysis of water at a semiconductor electrode. Nature 238, 37–38.
Fujishima, A., Zhang, X., Tryk, D.A., 2008. TiO2 photocatalysis and related surface phenomena. Surface Science Reports 63, 515–582.
Guerrini, G., Peccati, E., 2007. Photocatalytic Cementetious Roads for Depollution, in:. Presented at the International RILEM Symposium on Photocatalysis, Environment and Construction Materials, Florence, Italy, pp. 179–186.

Gustafsson, R.J., Orlov, A., Griffiths, P.T., Cox, R.A., Lambert, R.M., 2006. Reduction of NO2 to nitrous acid on illuminated titanium dioxide aerosol surfaces: implications for photocatalysis and atmospheric chemistry. Chem. Commun. (Camb.) 37, 3936–3938.
Hashimoto, K., Wasada, K., Toukai, N., Kominami, H., Kera, Y., 2000. Photocatalytic oxidation of nitrogen monoxide over titanium(IV) oxide nanocrystals large size areas. J Photoch Photobio A 136, 103–109.
Hassan, M., Dylla, H., Mohammad, L.N., Rupnow, T., 2010. Evaluation of the durability of titanium dioxide photocatalyst coating for concrete pavement. Construction and Building Materials 24, 1456–1461.
Hoffmann, M.R., Martin, S.T., Choi, W., Bahnemann, D.W., 1995. Environmental Applications of Semiconductor Photocatalysis. Chem. Rev. 95, 69–96.
Huang, C.H., Chen, D.H., Li, K., 2003. Photocatalytic oxidation of butyraldehyde over titania in air: By-product identification and reaction pathways. Chemical Engineering Communications 190, 373–392.
Hunger, M., Husken, G., H, B.H.J., 2010. Photocatalytic degradation of air pollutants - From modeling to large scale application. Cement and Concrete Research 40, 313–320.
Husken, G., Hunger, M., H, B.H.J., 2009. Experimental study of photocatalytic concrete products for air purification. Building and Environment 44, 2463–2474.
Imoberdorf, G., Irazoqui, H., Cassano, A., Alfana, O., 2005. Photocatalytic degradation of tetrachloroethylene in gas phase on TiO2 films: A kinetic study. Ind. Eng. Chem. Res. 44, 6075–6085.
Jayapalan, A.R., Lee, B.Y., Fredrich, S.M., Kurtis, K.E., 2010. Influence of additions of anatase TiO2 nanoparticles on early-age properties of cement-based materials. Transportation Research Record: Journal of the Transportation Research, Board 2141, 41–46.
Jia, C., Batterman, S.A., Godwin, C., 2008. VOCs in industrial, urban and suburban neighborhoods, Part 1: Indoor and outdoor concentrations, variation, and risk drivers. Atmospheric Environment 42, 2083–2100.
Kawakami, M., Furumura, T., Tokushige, H., 2007. NOx removal effects and physical properties of cement mortar incorporating titanium dioxide powder, in:. Presented at the International RILEM Symposium on Photocatalysis, Environment and Construction Materials, pp. 163–170.
Kimura, Y., McDonald Buller, E., Poppendieck, D.G., Darling, E.K., Corsi, R.L., 2011. Dry Deposition of Ozone to Built Environment Surfaces. Center for Energy and Environmental Resources, University of Texas at Austin.
Kleffman, J., 2015. Disscussion on "field study of air purification paving elements containing TiO2," by Folli et al. (2015). Atmospheric Environment, 126, 95-97.
Lackhoff, M., Prieto, X., Nestle, N., Dehn, F., Niessner, R., 2003. Photocatalytic activity of semiconductor-modified cement—influence of semiconductor type and cement ageing. Applied Catalysis B: Environmental 205–216.
Langridge, J.M., Gustafsson, R.J., Griffiths, P.T., Cox, R.A., Lambert, R.M., Jones, R.L., 2009. Solar driven nitrous acid formation on building material surfaces containing titanium dioxide: A concern for air quality in urban areas? Atmospheric Environment 43, 5128–5131.
Laufs, S., Burgeth, G., Duttlinger, W., Kurtenbach, R., Maban, M., Thomas, C.E.S., Thomas, C., Wiesen, P., Kleffman, J., 2010. Conversion of nitrogen oxides on commercial photocatalytic dispersion paints. Atmospheric Environment 44, 2341–2349.
Lee, B.Y., Thomas, J.J., Treager, M., Kurtis, K.E., 2010. Influence of TiO2 nanoparticles on

early C3S hydratation. Journal of the American Ceramic Society 93, 3399–3405.
Lichtin, N., Sadeghi, M., 1998. Oxidative photocatalytic degradation of benzene vapor over TiO2. J Photoch Photobio A 113, 81–88.
Lim, T., Jeong, S., Kim, S., Gyenis, J., 2000. Photocatalytic decomposition of NO by TiO2 particles. J Photoch Photobio A 134, 209–217.
Lin, Y.-M., Tseng, Y.-H., Huang, J.-H., Chao, C.C., Chen, C.-C., Wang, I., 2006. Photocatalytic Activity for Degradation of Nitrogen Oxides over Visible Light Responsive Titania-Based Photocatalysts. Environ. Sci. Technol 40, 1616–1621.
Lippmann, M., 1989. Health effects of ozone. A critical review. Journal of the Air Pollution Control Association 39, 672–695.
Liu, H., Ye, X., Lian, Z., Wen, Y., Shangguan, W., 2006. Experimental study of photocatalytic oxidation of formaldehyde and its by-products. Res Chem Intermediat 32, 9–16.
Lothenbach, B., Scrivener, K., Hooton, R.D., 2011. Supplementary Cementitious Materials. Cement and Concrete Research 41, 1244-1256
Lu, K., Zhang, Y., Su, H., Brauers, T., Chou, C.C., Hofzumahaus, A., Liu, S.C., Kita, K., Kondo, Y., Shao, M., Wahner, A., Wang, J., Wang, X., Zhu, T., 2010. Oxidant (O3+ NO2) production processes and formation regimes in Beijing. J. Geophys. Res. 115, 1–18.
Maggos, T., Bartzis, J.G., Leva, P., Kotzias, D., 2007a. Application of photocatalytic technology for NOx removal. Appl Phys A-Mater 89, 81–84.
Maggos, T., Bartzis, J.G., Liakou, M., Gobin, C., 2007b. Photocatalytic degradation of NOx gases using TiO2-containing paint: A real scale study. J Hazard Mater 146, 668–673.
Maggos, T., Plassais, A., Bartzis, J.G., Vasilakos, C.H., Moussiopoulos, N., Bonafous, L., 2008. Photocatalytic degradation of NOx in a pilot street canyon configuration using TiO2-mortar panels. Environmental Monitoring and Assessment 136, 35–44.
Marsili-Libelli, S., 1996. Simplified kinetics of tropospheric ozone. Ecological modelling 84, 233–244.
Maynard, R., 2004. Key airborne pollutants—the impact on health. Science of the total environment 334-335, 9–13.
Monge, M.E., George, C., D'Anna, B., Doussin, J.-F., Jammoul, A., Wang, J., Eyglunent, G., Solignac, G., Daële, V., Mellouki, A., 2010. Ozone Formation from Illuminated Titanium Dioxide Surfaces. Journal of the American Chemical Society 132, 8234–8235.
Motohashi, K., Inukai, T., 2007. Self-cleaning performance evaluation of commercial photocatalyst coating materials through 5 years of outdoor exposure, in:. Presented at the International RILEM Symposium on Photocatalysis, Environment and Construction Materials, pp. 307–313.
Motohashi, K., Inukai, T., Konishi, T., 2004. Performance evaluation of self-cleaning effect for photocatalyst-applied exterior finishing materials through outdoor exposure test and laboratory test. RILEM International Symposium on Environment-Conscious Materials and Systems for Sustainable Development 27–34.
Muggli, D.S., McCue, J.T., Falconer, J., 1998. Mechanism of the Photocatalytic Oxidation of Ethanol on TiO2. Journal of Catalysis 173, 470–483.
Murata, Y., Kamitani, K., Takeuchi, K., 2000. Air purifying blocks based on photocatalysis, in:. Presented at the JIPEA World Congress, pp. 570–578.
Obee, T.N., Brown, R.T., 1995. TiO2 Photocatalysis for Indoor Air Applications: Effects of Humidity and Trace Contaminant Levels on the Oxidation Rates of Formaldehyde, Toluene, and 1,3-Butadiene. Environ. Sci. Technol 29, 1223–1231.

Obuchi, E., Sakamoto, T., Nakano, K., 1999. Photocatalytic decomposition of acetaldehyde over TiO2/SiO2 catalyst. Chem Eng Sci 54, 1525–1530.
Ohko, Y., Nakamura, Y., Negishi, N., Matsuzawa, S., Takeuchi, K., 2009. Photocatalytic oxidation of nitrogen monoxide using TiO2 thin films under continuous UV light illumination. J Photoch Photobio A 205, 28–33.
Ohko, Y., Nakamura, Y., Negishi, N., Matsuzawa, S., Takeuchi, K., 2010. Unexpected release of HNO3 and related species from UV-illuminated TiO2 surface into air in photocatalytic oxidation of NO2 . Environmental Chemistry Letters 8, 289–294.
Ollis, D.F., Pelizzetti, E., Serpone, N., 1991. Photocatalyzed destruction of water contaminants. Environ. Sci. Technol 25, 1522–1529.
Olson, D., Hammond, D., Seila, R., Burke, J., Norris, G., 2009. Spatial gradients and source apportionment of volatile organic compounds near roadways. Atmospheric Environment 43 5647-5653.
Ozawa, T., Iwasaki, M., Tada, H., Akita, T., Tanaka, K., Ito, S., 2005. Low-temperature synthesis of anatse-brookite composite nanocrystals: the junction effect on photocatalytic activity. Journal of Colloid and Interface Science 281, 510–513.
Pepe, C., Amadelli, R., Pimpinelli, N., Cassar, L., 2004. Doped-TiO2/Cement matrices photoactive materials, in:. Presented at the RILEM International Symposium on Environment-Conscious Materials and Systems for Sustainable Development, pp. 331–336.
Petit, J., 2009. Chaussée dépolluante par photocatalyse de Vanves. Laboratoire Régional de l'Ouest Parisien.
Poon, C.S., Cheung, E., 2007. NO removal efficiency of photocatalytic paving blocks prepared with recycled materials. Construction and Building Materials 21, 1746–1753.
Poppendieck, D.G., Darling, E.K., McDonald Buller, E., Kimura, Y., Corsi, R.L., 2011. Dry Deposition of Ozone to Built Environment Surfaces. Center for Energy and Environmental Resources, University of Texas at Austin.
Poulston, S., Twigg, M.V., Walker, A.P., 2009. The Effect of nitric oxide on the photocatalytic oxidation of small hydrocarbons over titania. Applied Catalysis B: Environmental 89, 335–341.
Puzenat, E., 2009. Photo catalytic self-cleaning materials: Principles and impact on atmosphere. Eur. Phys. J. Conferences 1, 69–74.
Rachel, A., Subrahmanyam, M., Boule, P., 2002. Comparison of photocatalytic efficiencies of TiO2 in suspended and immobilized form for the photocatalytic degradation of nitrobenzenesulfonic acids. Applied Catalysis B: Environmental 37, 301–308.
Ramirez, A.M., Demeestere, K., De Belie, N., Mantyla, T., Levanen, E., 2010. Titanium dioxide coated cementetious materials for air purifying purposes: preparation, characterization, and toluene removal potential. Building and Environment 45, 832–838.
Rhead, D., Panesar, D.K., 2012. Photocatalytic Concrete Field Trial Along Ontario's Freeways Ministry of Transportation Ontario, in:. Presented at the ACI Fall Convention, Toronto, Canada, pp. 1–13.
Rousseau, P., 2010. The NOxer process: from developments to in-situ depollution measurements, in:. Presented at the International Road Federation World Meeting, Lisbon, Portugal.
Ruot, B., Plassais, A., Oliva, F., Guillot, L., Bonafous, L., 2009. TiO2-containing cement pastes and mortars: measurements of the photocatalytic efficiency using a rhodamine B-based colourimetric test. Solar Energy 83, 1794–1801.

Shiraishi, F., Ohkubo, D., Toyoda, K., Yamaguchi, S., 2005. Decomposition of gaseous formaldehyde in a photocatalytic reactor with a parallel array of light sources:: 1. Fundamental experiment for reactor design. Chemical Engineering Journal 114, 153–159.
Simms, G., 2010. Email interview.
Stone, W., 2010. Telephone interview.
Strini, A., Cassese, S., Schiavi, L., 2005. Measurement of benzene, toluene, ethylbenzene, and o-xylene gas phase photodegradation by titanium dioxide dispersed in cementetious materials using a mixed flow reactor. Applied Catalysis B: Environmental 61, 90–97.
Toma, F., Bertrand, G., Klein, D., Coddet, C., 2004a. Photocatalytic removal of nitrogen oxides via titanium dioxide. Environmental Chemistry Letters 2, 117–121.
Toma, F., Guessasma, S., Klein, D., Montavin, G., Bertrand, G., Coddet, C., 2004b. Neural computation to predict TiO2 photocatalytic efficiency for nitrogen oxides removal. J Photoch Photobio A 165, 91–96.
Toulan, E., 2006. Le mur dépollueur NOxer, in:. Presented at the Réduction du bruit de transports terrestres, Aix-les-Bains, France.
Walmsley, J.L., Wesely, M.L., 1996. Modification of coded parametrizations of surface resistances to gaseous dry deposition. Atmospheric Environment 30, 1181–1188.
Wang, W., Ku, Y., 2003. Photocatalytic degradation of gaseous benzene in air streams by using an optical fiber photoreactor. J Photoch Photobio A 159, 47–59.
Wesely, M.L., 1989. Parametrization for surface resistances to gaseous dry deposition in regional-scale numerical models. Atmospheric Environment 23, 1293–1304.
Wesely, M.L., Hicks, B.B., 1977. Some factors that affect the deposition rates of sulfur dioxide and similar gases on vegetation. Journal of the Air Pollution Control Association 27, 1111–1116.
Wesely, M.L., Hicks, B.B., 2000. A review of the current status of the knowledge on dry deposition. Atmospheric Environment 34, 2261–2282.
Ye, X., Chen, D., Li, K., Shah, V., Kesmez, M., Vajifdar, K., 2007. Photocatalytic Oxidation of Aldehydes/PCE Using Porous Anatase Titania and Visible-Light-Responsive Brookite Titania. Chemical Engineering Communications 194, 368–381.
Ye, X., Chen, D.H., Gossage, J., Li, K., 2006. Photocatalytic oxidation of aldehydes: Byproduct identification and reaction pathway. J Photoch Photobio A 183, 35–40.
Yu, J., 2003. Deactivation and regeneration of environmentally exposed titanium dioxide based products (No. E183413). Prepared for the environmental protection department, HKSAR.
Zhang, M., 2011. Strength properties of pavement concrete containing nano-particles, in:. Presented at the International Conference on Electric Technology and Civil Engineering.
Zhang, M., Li, H., 2011. Pore structure and chloride permeability of concrete containing nano-particles for pavement. Construction and Building Materials 25, 608–616.
Znaidi, L., Seraphimova, R., Bocquet, J.F., Colbeau-Justin, C., Pommier, C., 2001. A semi-continuous process for the synthesis of nanosize TiO2 powders and their use as photocatalysts. Materials Research Bulletin 36, 811–825.

Appendix A

Table A.1: Absorption and Specific Gravity of Aggregates

Aggregate Type	Absorption (%)	Specific Gravity
Limestone Coarse	1.86	2.59
Limestone Fine	1.84	2.61

Table A.2: Tricon Precast Concrete Barrier Mixture Design Sheet

AGGREGATE CHARACTERISTICS					Revised Date	00/20/09
Aggregate	**SP Gravity**	**SSD Unit Wt LBS / Cu. Ft.**	**% Solids**	**Source**		**F.M./Grade**
Fine [FA]	2.62	106.90	65.49%	Hanson Servtex		3.05
Coarse [CA]	2.59	96.30	59.68%	Hanson Servtex		4

DESIGN FACTORS							
			w/cm Ratio	**0.34**	**CA% of Total Agg. by Vol.**	**50.92%**	
CA Factor [CAF]	0.650		**Air Factor [AF]**	2.0%	**Theor. Unit Wt of Conc.**	**150.33**	
Cement Factor [CF]	6.00	sks/cy	**Cement Source / Type**	Capitol Cement Type III			
Water Factor [WF]	3.75	gal/sk	**Water Source**	Garden Ridge Municipal Water			
SCM 1 Percent	25.0%		**SCM 1 Source/Type**	Headwaters - Limestone Class F	**SP.GR.**	2.36	
SCM 2 Percent			**SCM 2 Source/Type**		**SP.GR.**		

Batch Design [One Sack]	Volume: 1-Sk Batch [Cu Ft]		Vol to Wt [Lb] Vol x 62.5 x Sp Gr	1-Sack Batch Wt	Full Size Batch Factor	Full Size Batch Wts
1. Concrete Yield = CuFt per CuYd / CF	27 / 6.0	4.500				
2. Volume CA = Yield x CAF x Solids	4.500 x 0.65 x 0.597	**1.727**	x 62.4 x 2.59	279.11	6.00	* **1,675**
3. Volume Mortar = Yield - Vol CA	4.500 - 1.727	2.773				
4. Volume Water = WF / Gals Wat per CuFt	3.8 / 7.5	**0.500**	x 62.4 x 1.00	31.20	6.00	* **187**
5. Volume SCM 1	94 x 25% / 62.4 x 2.36	**0.160**	x 62.4 x 2.36	23.50	6.00	**141**
6. Volume SCM 2	94 x 0% / 62.4 x 0.00	**0.000**	x 62.4 x 0	0.00	6.00	-
7. Volume One Sk Cement	94 x 75% / 62.4 x 3.15	**0.359**	x 62.4 x 3.10	69.44	6.00	**423**
8. Volume Entrained Air = Yield x AF	4.500 x 0.020	**0.090**				
9. Volume Paste = Vol Cem+Water+Air	0.518 + 0.500 + 0.090	1.108				
10. Volume FA = Vol Mortar - Paste	2.773 - 1.108	**1.665**	x 62.4 x 2.62	271.10	6.00	* **1,627**
11. Yield [Summation of 2, 4, 5, 6, 7, 8, & 10 to Check Number 1 above]		**4.501**		TOTAL Batch Wts		* **4,053**
12. FA Factor = Vol FA / FA Solids x Vol Mortar	1.665 / 0.655 x 2.773	1.665 / 1.816 = 0.92			* Correct for Free Moisture & Absorption	

Table A.3: Tricon Precast Concrete Barrier Mixture Cylinder Strength Results & Admixture Information

Cyl No	Age	Area	Load	Stress	Cyl No	Age	Area	Load	Stress
1	19 Hours	12.50	65,680	5,250	3	3 day	12.50	79,410	6,350
2	19 Hours	12.50	64,540	5,160	4	3 day	12.50	82,700	6,620
			19 Hours Hr Avg	**5,210**				**3 Day Avg**	**6,490**
Cyl No	**Age**	**Area**	**Load**	**Stress**	**Cyl No**	**Age**	**Area**	**Load**	**Stress**
5	7 day	12.50	92,220	7,380	7	14 day	12.50	101,640	8,130
6	7 day	12.50	90,290	7,220	8	14 day	12.50	99,260	7,940
			7 Day Avg	**7,300**				**14 Day Avg**	**8,040**
Cyl No	**Age**	**Area**	**Load**	**Stress**	**Remarks**				
9	28 day	12.50	104,310	8,340					
10	28 day	12.50	105,630	8,450					
			28 Day Avg	**8,400**	Entrained Air Content	2.9	Initial Set (hrs)	n/a	

Slump	6.50	Admixture	Type	Sika 2110	Dosage (oz/100 lbs)	7	% solids	40
Air Temperature	89	Admixture	Type	Plastiment	Dosage (oz/100 lbs)	2	% solids	33
Concrete Temperature	89	Admixture	Type		Dosage (oz/100 lbs)		% solids	
Actual Unit Weight	148.80	Admixture	Type		Dosage (oz/100 lbs)		% solids	

Table A.4: Mixture Design Used in the Laboratory-Mixed Slab Specimens

MATERIALS PROPERTIES

Material	BSG* (SSD)	AC** (OD)	Description
Cement	3.1	NA	
Fly Ash	2.36		
Other:			
Water	1	NA	
Rock	2.59	1.84	
Sand	2.61	1.8	

* BSG = Bulk Specific Gravity
** AC = Absorption Capacity

THEORETICAL MIX PROPORTIONS PER CU. YD.

Material	Weight, lb.	Volume, cu. ft.	Dosage, fluid ounces
Cement	423	2.18672457	
Fly Ash	141	0.95746415	
Other:			
Water	187	2.99679487	
Rock (SSD)	1675	10.3640729	
Sand (SSD)	1627	9.98993025	
Air	2.00%	0.54	
		27.03	
Admixtures:			
Sika 2110			7.0
Plastiment			2.0

BATCHING INFORMATION

Batch Size = 2.577372129 cu.ft.

Appendix B

Photocatalytic stucco coated concrete barrier with solar insolation ≥ 0.5mW/cm^2

- $R_{s,NO}(s/m) = \left(\frac{1}{v_{d,NO,chamber}} - \frac{1}{22.43}\right) \times 3600$ if $0 < v_{d,NO,chamber} < 22.43$

  $= 0$ if $22.43 \le v_{d,NO,chamber}$

  $= 9999999$ if $v_{d,NO,chamber} \le 0$

  where

  $v_{d,NO,chamber}(m/h) = 5.4083 \times UV^{0.5893} - 9.20 \times 10^{-2} \times (T - 35) - 2.97 \times 10^{-4} \times ([H_2O] - 27754)$

  UV Solar insolation (mW cm^{-2})

  T Temperature ($°C$)

  [H_2O] Water vapor concentration (ppm)

- $R_{s,NO2}$ is dependent on the NO/NO_2 ratio:

  When [NO] > [NO_2], $R_{s,NO2}$ = 9999999. Laboratory data from Task 7 indicated that NO_2 was actually released during the interaction of NO with photocatalytic stucco coated concrete in the absence of ozone. In this case, the release of NO_2 was included by modifications to CAMx. NO removal by dry deposition was partitioned by land use type during each model time step to determine the amount associated with photocatalytic stucco coated barriers. The following relationship for NO_2 production was implemented in CAMx according to the findings of Task 7:

  NO_2 produced (tons) = (-0.304 UV +0.6848)*NO removed (tons)

  Photocatalytic stucco coating was present on both sides of barriers. Consequently, the NO_2 flux was proportional to the surface resistance for NO on each side, which varied with solar insolation. The release of NO_2 was only associated with photocatalytic stucco coated highway barriers and occurred within the first vertical layer of affected grid cells upon exit from the CAMx dry deposition algorithm. NO_2 removal by dry deposition to other land use types within CAMx was unaffected.

  When [NO] < [NO_2]

  $R_{s,NO_2}(s/m) = \left(\frac{1}{v_{d,NO_2,chamber}} - \frac{1}{18.13}\right) \times 3600$ if $0 < v_{d,NO_2,chamber} < 18.13$

  $= 0$ if $18.13 \le v_{d,NO_2,chamber}$

  $= 9999999$ if $v_{d,NO_2,chamber} \le 0$

  where

  $v_{d,NO_2,chamber}(m/h) = 6.1313 \times UV^{0.5503} - 0.407 \times (T - 35) - 2.16 \times 10^{-4} \times ([H_2O] - 27754)$

- $R_{s,O_3}(s/m) = \left(\frac{1}{v_{d,O_3,chamber}} - \frac{1}{19.43}\right) \times 3600$ if $0 < v_{d,O_3,chamber} < 19.43$

  $= 0$ if $19.43 \le v_{d,O_3,chamber}$

  $= 9999999$ if $v_{d,O_3,chamber} \le 0$

  where

  $v_{d,O_3,chamber}(m/h) = 9.78 - 0.165 \times (T - 35) - 5.12 \times (UV - 2)$

Uncoated concrete barrier (regardless of solar insolation) and photocatalytic stucco coated concrete barrier with solar insolation < 0.5 mW/cm^2

- $R_{s,NO}(s/m) = \left(\frac{1}{v_{d,NO,chamber}} - \frac{1}{22.43}\right) \times 3600$ if $0 < v_{d,NO,chamber} < 22.43$

  $= 0$ if $22.43 \le v_{d,NO,chamber}$

  $= 9999999$ if $v_{d,NO,chamber} \le 0$

  where

  $v_{d,NO,chamber}(m/h) = 0.1001 - 6.13 \times 10^{-6} \times ([H_2O] - 27754)$

- $R_{s,NO2}$ is dependent on the NO/NO_2 ratio:

  When [NO] > [NO_2]

  $R_{s,NO_2}(s/m) = \left(\frac{1}{v_{d,NO_2,chamber}} - \frac{1}{18.13}\right) \times 3600$ if $0 < v_{d,NO_2,chamber} < 18.13$

  $= 0$ if $18.13 \le v_{d,NO_2,chamber}$

  $= 9999999$ if $v_{d,NO_2,chamber} \le 0$

  where

  $v_{d,NO_2,chamber}(m/h) = 0.9647 + 2.87 \times 10^{-5} \times ([H_2O] - 27754)$

  When [NO] < [NO_2], $R_{s,NO2} = 9999999$.

- $R_{s,O_3}(s/m) = \left(\frac{1}{v_{d,O_3,chamber}} - \frac{1}{19.43}\right) \times 3600$ if $0 < v_{d,O_3,chamber} < 19.43$

  $= 0$ if $19.43 \le v_{d,O_3,chamber}$

  $= 9999999$ if $v_{d,O_3,chamber} \le 0$

  where

  $v_{d,O_3,chamber}(m/h) = 1.8915 + 4.97 \times 10^{-6} \times ([H_2O] - 27754)$

Appendix C

Table C.1: Nitrate and Nitrite Concentrations of Wash Water from the Houston Field Site

Specimen Description	Testing Date	Days since Rainfall	Nitrate Concentration (mg/L)	Nitrite Concentration (mg/L)
Control Barrier	Initial	-	0	0
	3 month	17	0	0
	6 month	2	0	0
	9 month	5	0	0
	12 month	3	0	0
	16 month	4	1.5	0
	20 month	13	0	0
	24 month	8	0	0
Control Slab	Initial	-	0	0
	3 month	17	0	0
	6 month	2	0.4	0
	9 month	5	0	0
	12 month	3	0	0
	16 month	4	2.3	0
	20 month	13	0	0
	24 month	8	6.5	0
Clear Paint 1 Barrier	Initial	-	0	0
	3 month	17	0	0
	6 month	2	0.3	0.7
	9 month	5	0.3	0.0
Clear Paint 1 Slab	Initial	-	0	0
	3 month	17	0	0
	6 month	2	0.5	0
	9 month	5	0	0
Stucco Barrier	Initial	-	0	0
	3 month	17	0	0
	6 month	2	0.9	0.6
	9 month	5	0.4	0.0
	12 month	3	0.8	0
	16 month	4	0	0
	20 month	13	0	0
	24 month	8	0	0

Specimen Description	Testing Date	Days since Rainfall	Nitrate Concentration (mg/L)	Nitrite Concentration (mg/L)
Stucco Slab	Initial	-	0	0
	3 month	17	0	0
	6 month	2	0.6	0.7
	9 month	5	0	0
	12 month	3	0	0
	16 month	4	0	0
	20 month	13	-	0
	24 month	8	8.2	0
White Paint Barrier	Initial	-	0	0
	3 month	17	0	0
	6 month	2	0.4	0.6
	9 month	5	0	0
White Paint Slab	Initial	-	0	0
	3 month	17	0	0
	6 month	2	1.2	0
	9 month	5	0.2	0.0

Table C.2: Nitrate and Nitrite Concentrations of Wash Water from the Austin Field Site

Specimen Description	Testing Date	Days since Rainfall	Nitrate Concentration (mg/L)	Nitrite Concentration (mg/L)
Control Barrier	Initial	-	0	0
	3 month	20+	0	0
	6 month	2	0	0
	9 month	2	0	0
	12 month	5	0	0
	16 month	4	0	0
	20 month	6	0	0
	24 month	1	0	0
Control Slab	Initial	-	0	0
	3 month	20+	0	0
	6 month	2	0	0
	9 month	2	0	0
	12 month	5	0	0
	16 month	-	-	-
	20 month	-	-	-
	24 month	7	0	0
Clear Paint 1 Barrier	Initial	-	0	0
	3 month	20+	0	0
	6 month	2	0	0
	9 month	2	0	0
Clear Paint 1 Slab	Initial	-	0	0
	3 month	20+	0	0
	6 month	2	0	0
	9 month	2	0	0
Stucco Barrier	Initial	-	0	0
	3 month	20+	0.6	0
	6 month	2	0	0
	9 month	2	0	0
	12 month	5	0	0
	16 month	4	0	0
	20 month	6	1.2	0
	24 month	1	0.7	0

Specimen Description	Testing Date	Days since Rainfall	Nitrate Concentration (mg/L)	Nitrite Concentration (mg/L)
Stucco Slab	Initial	-	0	0
	3 month	20+	0	0
	6 month	2	0	0
	9 month	2	0	0
	12 month	5	0	0
	16 month	-	-	-
	20 month	-	-	-
	24 month	7	0.8	0
White Paint Barrier	Initial	-	0	0
	3 month	20+	0.6	0
	6 month	2	0	0
	9 month	2	0	0
White Paint Slab	Initial	-	0	0
	3 month	20+	0	0
	6 month	2	0	0
	9 month	2	0	0

Table C.3: Nitrate and Nitrite Concentrations of Wash Water from the Lab Field Site

Specimen Description	Testing Date	Days since Rainfall	Nitrate Concentration (mg/L)	Nitrite Concentration (mg/L)
Control Barrier	Initial	-	0	0
	3 month	20+	0.9	0
	6 month	6	0	0
	9 month	5	0	0
	12 months	5	0	0
	16 months	-	-	-
	20 months	6	0	0
	24 months	1	0	0
Control Slab	Initial	-	0	0
	3 month	20+	0	0
	6 month	6	0	0
	9 month	5	0	0
	12 months	5	0	0
	16 months	-	-	-
	20 months	-	-	-
	24 months	1	0	0
Clear Paint 1 Barrier	Initial	-	0	0
	3 month	20+	0.7	0
	6 month	6	0	0
	9 month	5	0	0
Clear Paint 1 Slab	Initial	-	0	0
	3 month	20+	0	0
	6 month	6	0	0
	9 month	5	0	0
Stucco Barrier	Initial	-	0	0
	3 month	20+	0.7	0
	6 month	6	0	0
	9 month	5	0	0
	12 months	5	1.4	0
	16 months	-	-	-
	20 months	6	0	0
	24 months	1	0	0

Specimen Description	Testing Date	Days since Rainfall	Nitrate Concentration (mg/L)	Nitrite Concentration (mg/L)
Stucco Slab	Initial	-	0	0
	3 month	20+	0.8	0
	6 month	6	0	0
	9 month	5	0	0
	12 months	5	0	0
	16 months	-	-	-
	20 months	-	-	-
	24 months	-	-	-
White Paint Barrier	Initial	-	0	0
	3 month	20+	0.5	0
	6 month	6	0	0
	9 month	5	0	0
White Paint Slab	Initial	-	0	0
	3 month	20+	1.2	0
	6 month	6	0	0
	9 month	5	0	0

Appendix D

Table D.1: Average L* Values of Specimen Surfaces for the Houston Field Site

	L* value (average ± standard deviation)					
Exposure time (mo)	0	3	9		12	
Time since rain (d)	-	17	5		3	
Pre- or Post-wash	-	Prewash	Prewash	Postwash	Prewash	Postwash
Control Barrier	73.267 ± 2.757	88.340 ± 3.421	66.787 ± 9.642	98.546 ± 0.332	98.807 ± 0.295	98.373 ± 0.727
Control Slab	73.267 ± 2.757	81.020 ± 0.552	98.244 ± 0.989	73.134 ± 9.858	98.807 ± 0.295	-
Clear Paint 1 Barrier	80.557 ± 0.908	86.813 ± 2.782	71.894 ± 4.188	96.915 ± 4.458	98.977 ± 0.098	90.283 ± 7.072
Clear Paint 1 Slab	80.557 ± 0.908	82.540 ± 1.796	97.739 ± 1.459	62.454 ± 1.918	98.824 ± 0.214	-
Stucco Barrier	80.810 ± 1.938	83.460 ± 11.144	97.312 ± 1.990	96.320 ± 4.061	99.173 ± 0.504	-
Stucco Slab	80.801 ± 1.938	74.243 ± 4.560	65.768 ± 24.985	92.638 ± 6.335	98.894 ± 1.093	97.923 ± 1.908
White Paint Barrier	100.657 ± 0.226	98.480 ± 0.148	98.080 ± 5.689	99.839 ± 0.249	99.775 ± 0.054	99.908 ± 0.021
White Paint Slab	100.657 ± 0.226	98.523 ± 0.021	99.914 ± 0.101	98.016 ± 1.720	90.626 ± 28.480	-

Table D.2: Average L* Values of Specimen Surfaces for the Austin Field Site

	L* value (average ± standard deviation)					
Exposure time (mo)	0	3	9		12	
Time since rain (d)	-	20+	2		N/A	
Pre- or Post-wash	-	Prewash	Prewash	Postwash	Prewash	Postwash
Control Barrier	73.267 ± 2.757	90.497 ± 0.762	95.091 ± 1.246	80.353 ± 3.248	99.035 ± 0.259	74.540 ± 21.741
Control Slab	73.267 ± 2.757	81.935 ± 17.869	80.405 ± 4.886	78.505 ± 2.595	87.378 ± 11.313	87.245 ± 13.954
Clear Paint 1 Barrier	80.557 ± 0.908	86.857 ± 12.750	96.580 ± 0.469	87.437 ± 5.839	98.903 ± 0.173	90.333 ± 8.653
Clear Paint 1 Slab	80.557 ± 0.908	66.560 ± 10.112	91.470 ± 7.113	72.525 ± 4.716	97.512 ± 1.968	90.828 ± 16.407
Stucco Barrier	80.810 ± 1.938	72.985 ± 13.866	82.993 ± 27.655	85.057 ± 11.694	98.366 ± 1.330	91.531 ± 11.097
Stucco Slab	80.810 ± 1.938	87.037 ± 1.434	81.785 ± 23.285	79.720 ± 0.382	97.969 ± 2.146	81.284 ± 21.569
White Paint Barrier	100.657 ± 0.226	100.257 ± 0.086	100.360 ± 0.026	100.713 ± 0.761	100.031 ± 0.043	99.953 ± 0.400
White Paint Slab	100.657 ± 0.226	99.040 ± 1.245	100.275 ± 0.064	99.550 ± 0.127	99.886 ± 0.040	99.723 ± 0.374

Table D.3: Average L* Values of Specimen Surfaces for the Lab Field Site

	L* value (average ± standard deviation)					
Exposure time (mo)	0	3	9		12	
Time since rain (d)	-	20+	5		3	
Pre- or Post-wash	-	Prewash	Prewash	Postwash	Prewash	Postwash
Control Barrier	73.267 ± 2.757	85.827 ± 1.421	98.511 ± 0.322	96.177 ± 2.021	98.750 ± 0.730	98.680 ± 0.340
Control Slab	73.267 ± 2.757	68.952 ± 1.414	94.900 ± 5.296	57.404 ± 14.175	93.420 ± 2.930	-
Clear Paint 1 Barrier	80.557 ± 0.908	89.247 ± 0.633	99.235 ± 0.148	91.650 ± 8.941	98.770 ± 0.210	98.570 ± 0.830
Clear Paint 1 Slab	80.557 ± 0.908	83.600 ± 0.750	98.757 ± 0.588	90.800 ± 4.859	98.530 ± 0.710	-
Stucco Barrier	80.801 ± 1.938	88.877 ± 17.239	94.760 ± 10.148	73.091 ± 22.867	99.380 ± 0.460	98.650 ± 0.630
Stucco Slab	80.810 ± 1.938	95.025 ± 12.155	85.618 ± 24.794	88.577 ± 7.754	99.560 ± 1.190	-
White Paint Barrier	100.657 ± 0.226	104.823 ± 1.176	100.032 ± 0.119	99.959 ± 0.072	100.480 ± 0.470	99.870 ± 0.020
White Paint Slab	100.657 ± 0.226	104.680 ± 5.812	100.250 ± 0.030	99.948 ± 0.076	99.940 ± 0.030	-

Appendix E

Table E.1: Temperature Data for Houston Site

	3 Months				6 Months				9 Months				12 Months			
Date	8/16/11				11/17/11				1/30/12				4/4/12			
Time	10:30 AM				9:30 AM				9:30 AM				9:30 AM			
Weather	Sunny and hot with sparse clouds				Sunny				Sparse clouds							
	PURETi	TxActive	Control	KEIM	PURETi	TxActive	Control	KEIM	PURETi	TxActive	Control	KEIM	PURETi	TxActive	Control	KEIM
Temp: Barrier (°F)	Unavailable				75	63	74.5	60.8	70.2	62.6	69.1	63.8	73.3	71.8	73.2	71.9
Temp: Slab (°F)					63.1	49.9	61.3	49.9	69.1	62.7	69.4	63	72.1	70.9	69.8	70.4

Table E.2: Temperature Data for Austin Site

	3 Months				6 Months				9 Months				12 Months			
Date	8/30/11				12/1/11				2/9/12				3/23/12			
Time	9:15 AM				2:30 PM				9:30 AM				1:00 PM			
Weather	Sunny and hot				Sunny, few clouds				Sunny, few clouds				sunny and hot			
	PURETi	TxActive	Control	KEIM	PURETi	TxActive	Control	KEIM	PURETi	TxActive	Control	KEIM	PURETi	TxActive	Control	KEIM
Temp: Barrier (°F)	74.9	76.5	77.3	76.7	68.5	66.2	67.3	65.7	45.5	42.8	44.6	41.7	57	53	57	50
Temp: Slab (°F)	63.3	62.2	64.4	63.9	75.6	70.2	77.4	68	55.6	50.7	56.8	48.1	86	70	90	65

Table E.3: Temperature Data for Lab Site

	3 Months				6 Months				9 Months				12 Months			
Date	9/1/11				12/10/11				2/8/12				3/22/12			
Time	9:00 AM				9:00 AM				12:30 PM				1:00 PM			
Weather	Sunny and hot				overcast				Partly cloudy				sunny and clear			
	PURETi	TxActive	Control	KEIM	PURETi	TxActive	Control	KEIM	PURETi	TxActive	Control	KEIM	PURETi	TxActive	Control	KEIM
Temp: Barrier (°F)	93.6	84.2	101.7	84.4	45.2	45.2	45.7	45	63	55.1	71.4	55	83.7	74.5	84.7	74.8
Temp: Slab (°F)	100.2	90.3	101.2	89.6	45.6	45.6	46.6	44.8	64.1	55.8	71.9	56.1	95.5	83.7	101.4	84

Appendix F

XRD analysis of field specimens

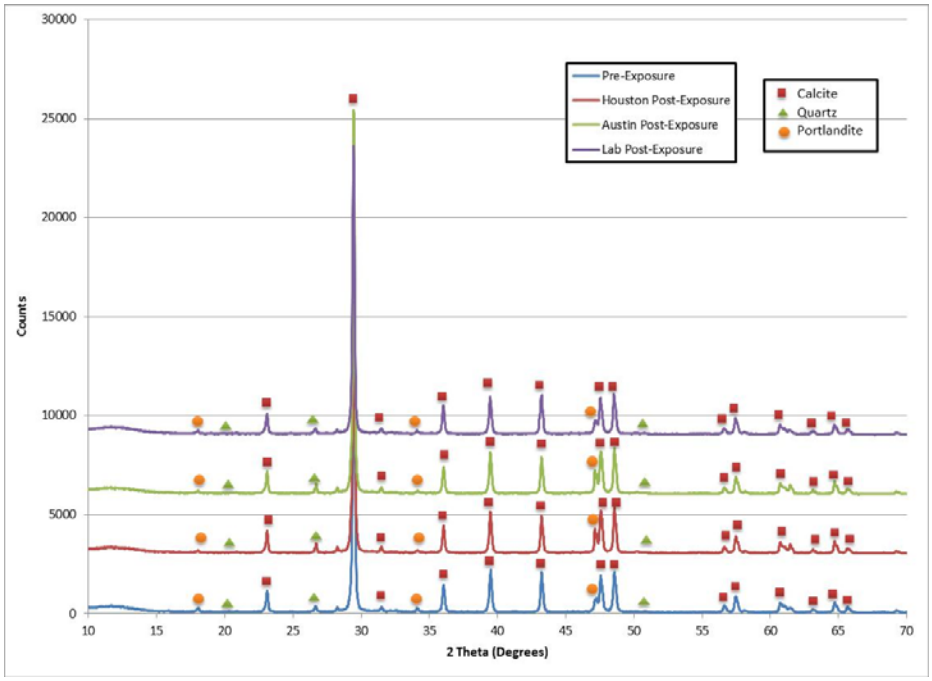

Figure F.1: XRD analysis of uncoated control barrier core before exposure and after exposure in Houston, Austin, and the lab sites

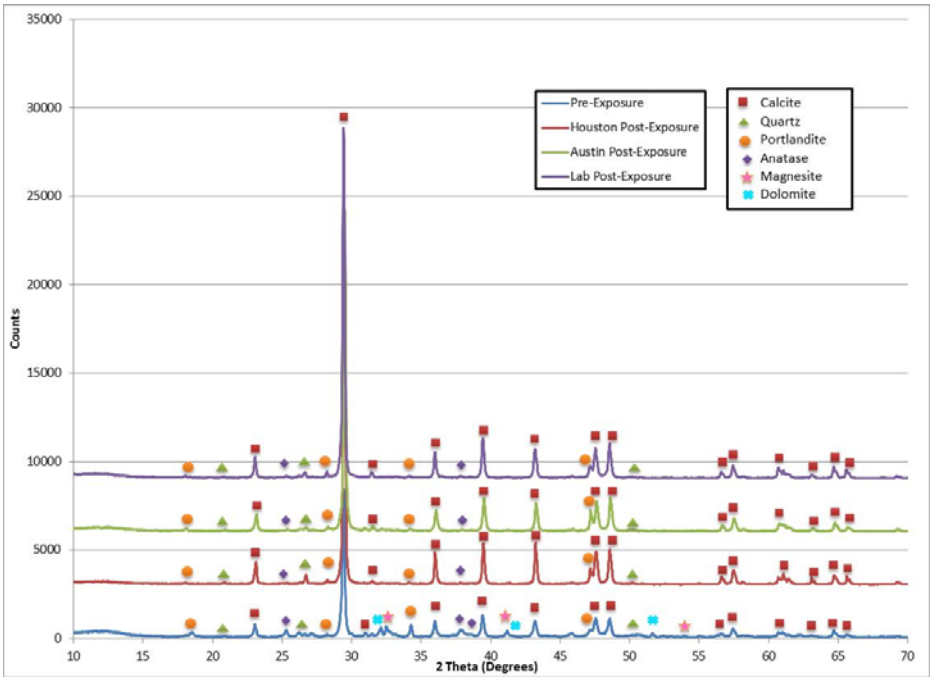

Figure F.2: XRD analysis of the stucco barrier core before exposure and after exposure in Houston, Austin, and the lab sites

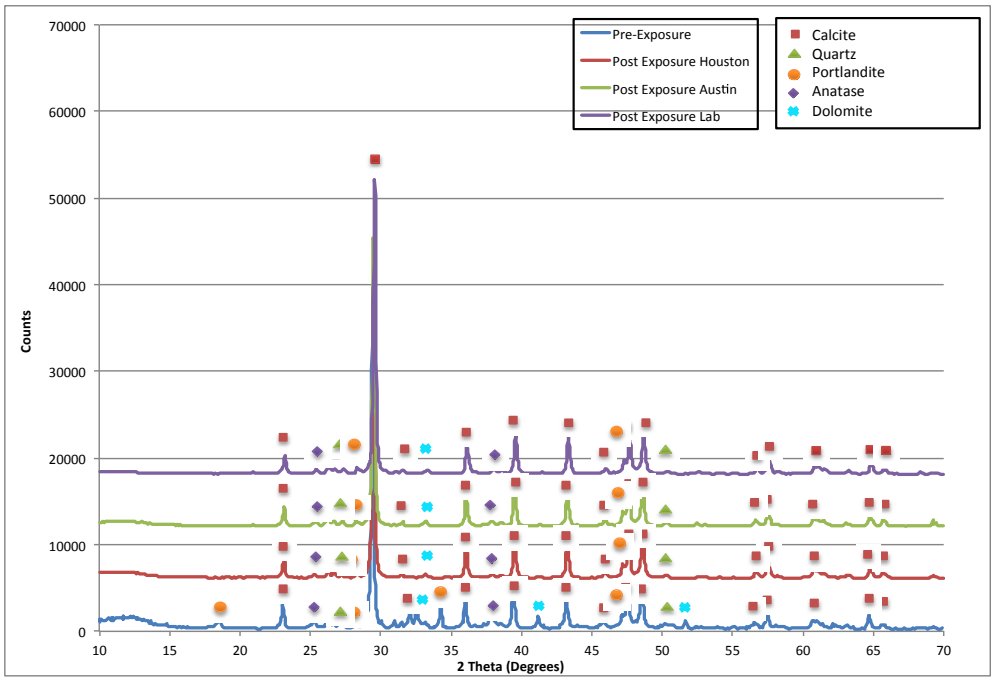

Figure F.3: XRD analysis of the stucco barrier core before exposure and after 2 years of exposure in Houston, Austin, and the lab sites

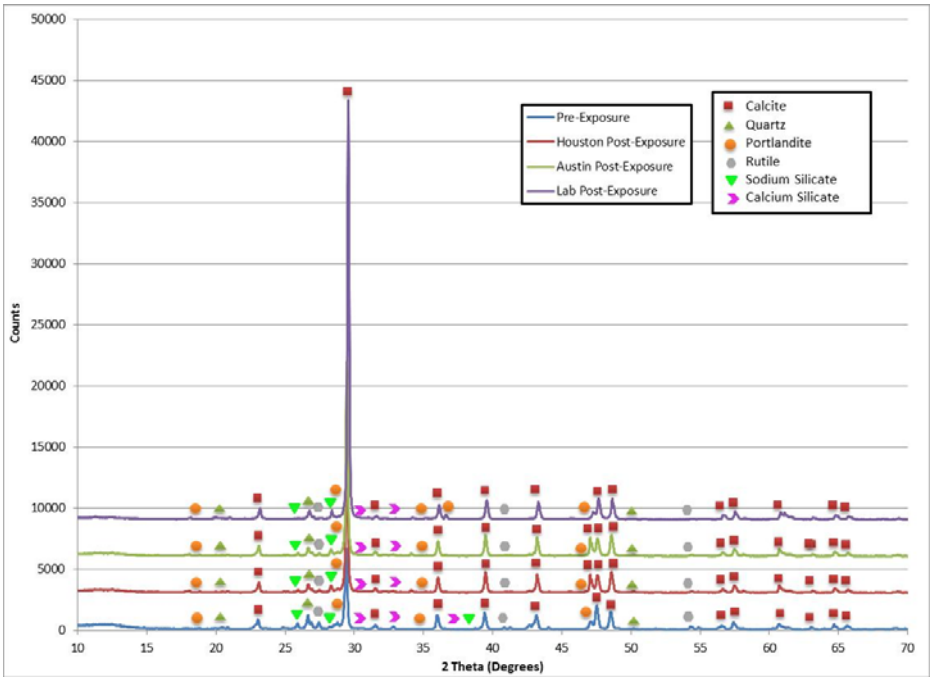

Figure F.4: XRD analysis of the white paint barrier core before exposure and after exposure in Houston, Austin, and the lab sites

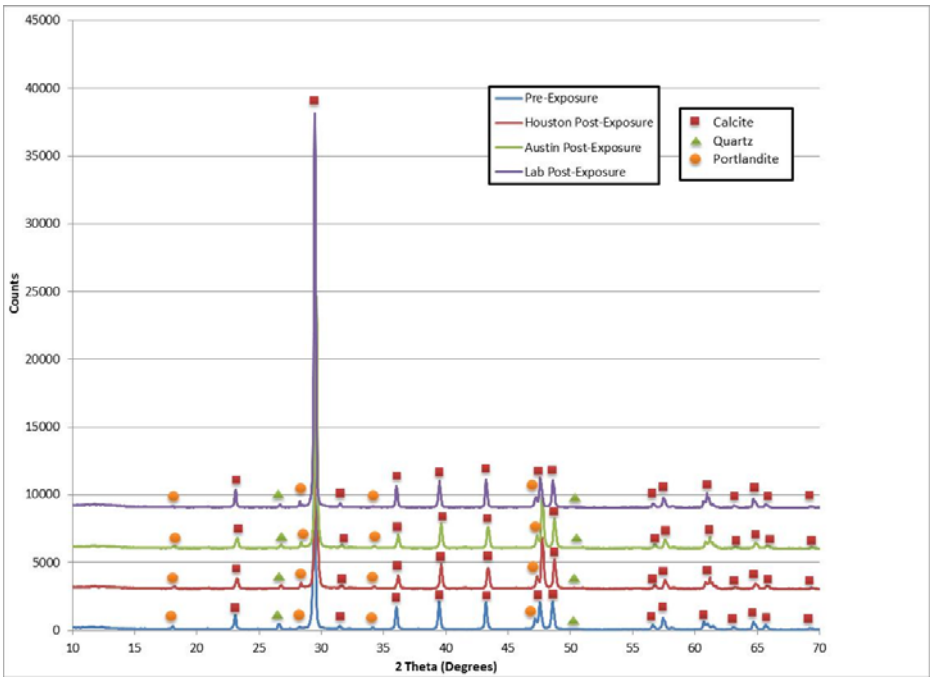

Figure F.5: XRD Analysis of the clear paint 1 barrier core before exposure and after exposure in Houston, Austin, and the lab sites

XRD Analysis of Environmental Chamber Specimens

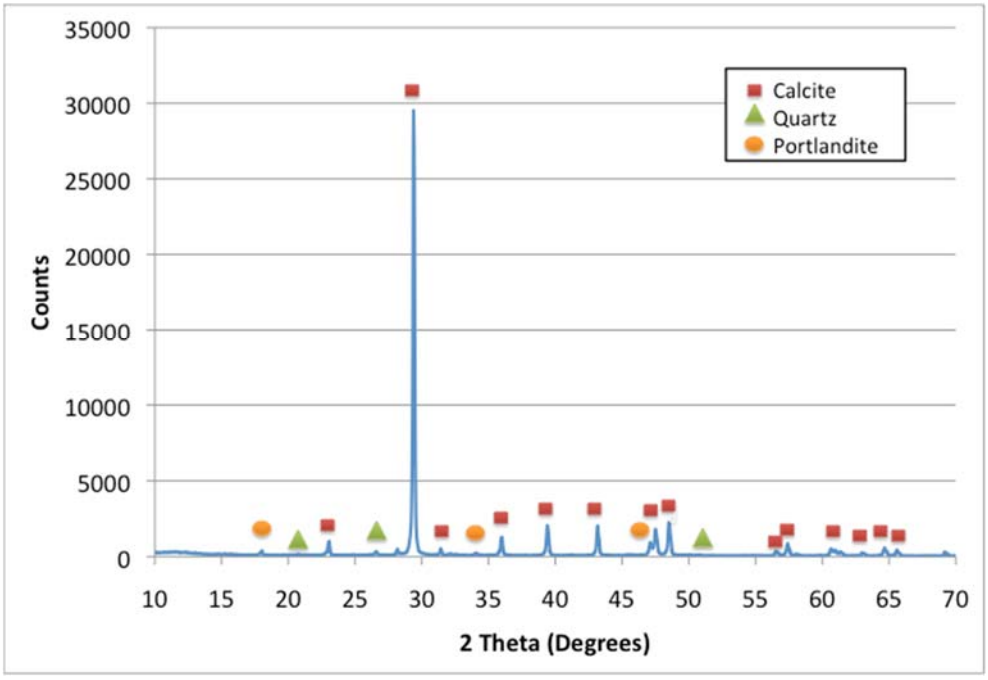

Figure F.6: XRD analysis of uncoated control environmental chamber specimen core

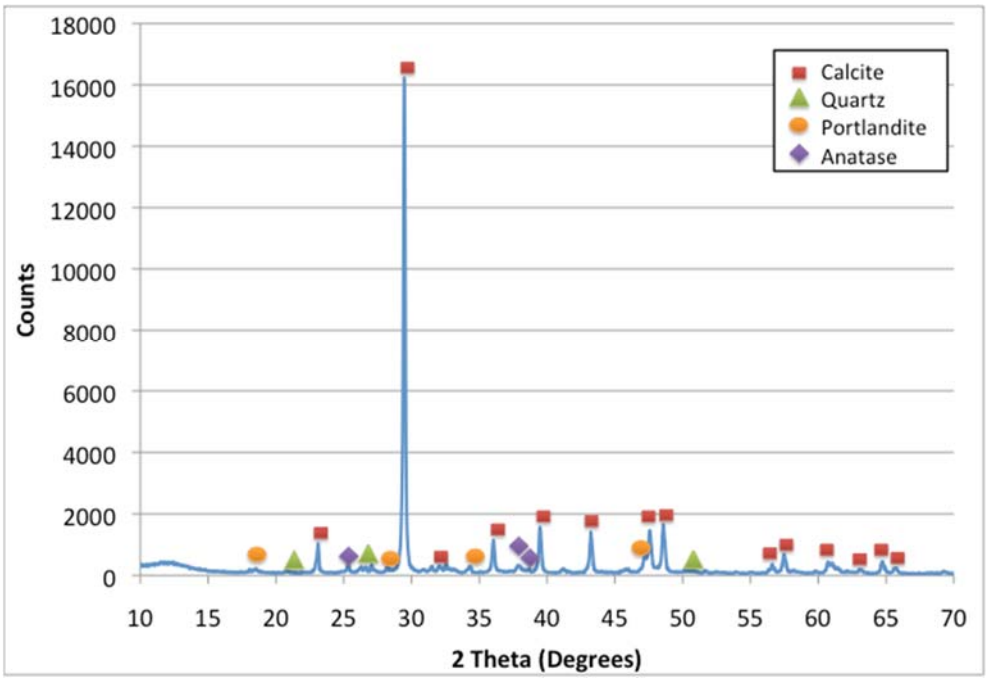

Figure F.7: XRD Analysis of the stucco environmental chamber specimen core

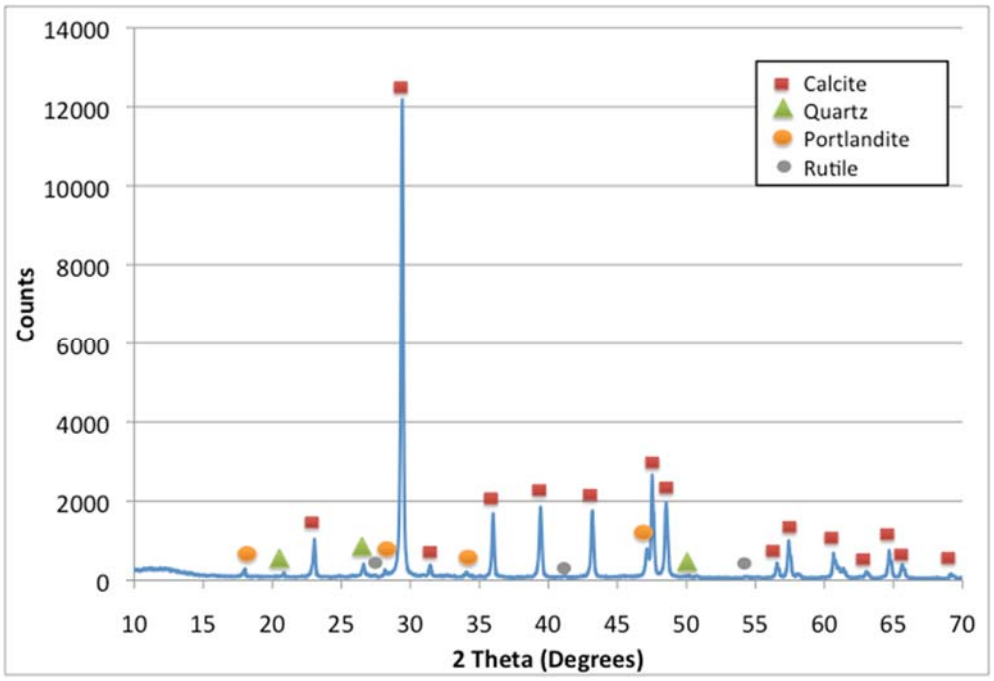

Figure F.8: XRD Analysis of the white paint environmental chamber specimen core

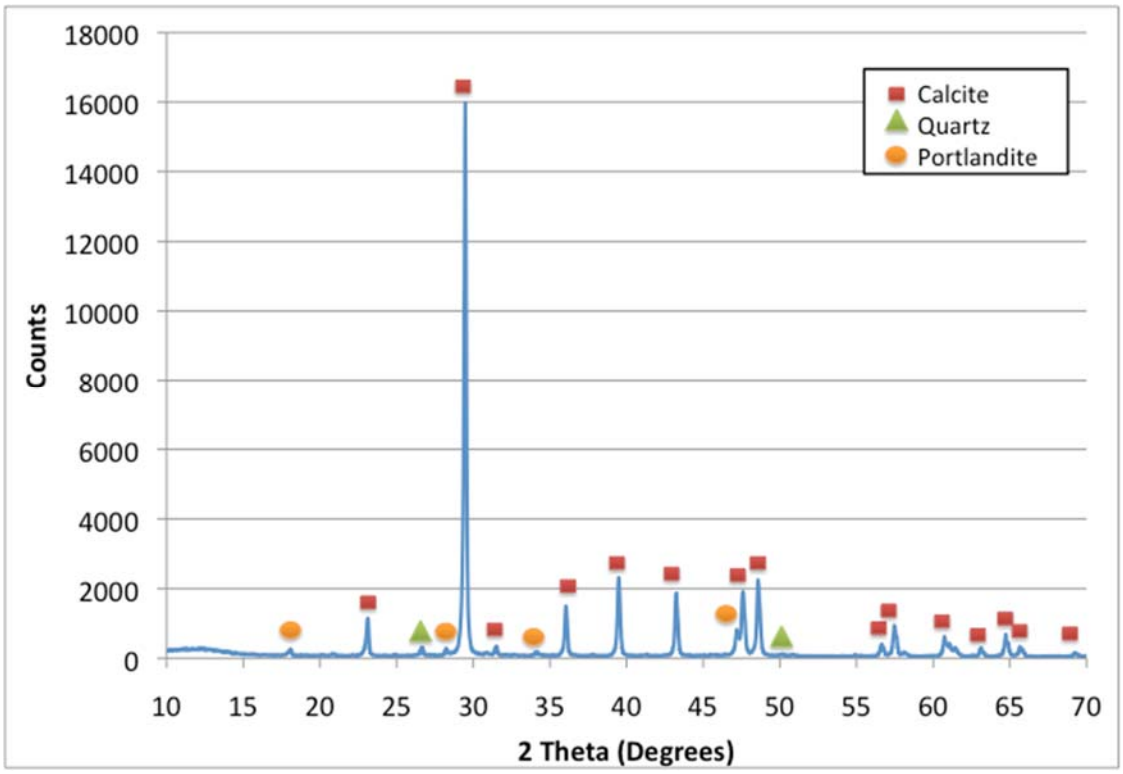

Figure F.9: XRD Analysis of clear paint 1 environmental chamber specimen core

Appendix G

Project Quality Assurance Project Plan (QAPP)

A1.1 Preface

This Quality Assurance Project Plan (QAPP) is submitted in support of Project No. 0-6636 "Photocatalytic NOx/HRVOC/O3 Removal in Transportation Applications"

Contact:
Dr. Neil Crain (512/923-7999)
Project Manager
Project No. 0-6636 "Photocatalytic NOx /HRVOC/O3 Removal in Transportation Applications"
Mailing Address:

The University of Texas at Austin
Center for Energy & Environmental Resources (R7100)
10100 Burnet Road, EME (Bldg 133)
Austin, TX 78758

A1.2 Approval Page

Project Manager Wade Odell Texas Department of Transportation	Wade Odell	Date
Principal Investigator Project No. 0-6636 Photocatalytic NOx/HRVOC/O3 Removal in Transportation Applications" The University of Texas at Austin Austin, Texas	Maria Juenger, Ph.D.	Date
Project Manager Project No. 0-6636 Photocatalytic NOx/HRVOC/O3 Removal in Transportation Applications" The University of Texas at Austin Austin, Texas	Neil Crain, Ph. D.	Date
Project Quality Assurance Officer Project No. 0-6636 Photocatalytic NOx/HRVOC/O3 Removal in Transportation Applications" The University of Texas at Austin Austin, Texas	Cyril Durrenberger	Date

TABLE OF CONTENTS

Section	Title	Pages	Revision	Date
	PROJECT MANAGEMENT			
A1	Title and Approval Sheets	2	0	10/12
	A1.1 Preface			
	A1.2 Approval Page			
A2	Table of Contents	10	0	10/12
	A2.1 List of Figures			
	A2.2 List of Tables			
	A2.3 List of Appendices			
A3	Distribution List	1	1	07/15
A4	Project/Task Organization	3	1	07/15
	A4.1 Project Sponsor			
	A4.2 Texas Commission on Environmental Quality (TCEQ)			
	A4.3 Principal Investigator and Project Manager			
	A4.4 Project Quality Assurance (QA) Officer			
	A4.5 Monitoring Station Operations and Maintenance			
	A4.6 VOC Canister Analysis			
	A4.7 Monitoring Data Management and Validation			
	A4.8 Statistical Support			
	A4.9 Subcontractors			
A5	Problem Definition/Background	2	0	10/12
	A5.1 Overview			
	A5.2 Conclusions to be Made			
	A5.3 Uses of Data			
	A5.4 Decision Makers			
	A5.5 Principal Customers for the Results			
A6	Project/Task Description	2	1	07/15
	A6.1 Project Overview			
	A6.2 Sampling Activities			
	A6.3 Standards and Screening Levels			
	A6.3.1 NAAQS			
	A6.3.2 Effects Screening Levels (ESL)			
	A6.4 Assessment Tools			
	A6.4.1 Technical Systems Audits			
	A6.4.2 Performance Evaluations			
	A6.5 Project Reports			
A7	Data Quality Objectives (DQO) for Measurement Data	4	0	10/12
	A7.1 General Project Objective			
	A7.2 Network Specific Objectives			
	A7.3 Conclusions to be Made			
	A7.4 Uses of Data			
	A7.5 Measurement Quality Objectives			
	A7.5.1 Detection Limits			
	A7.5.2 System Contribution to the Measurement			
	A7.5.3 Precision			
	A7.5.4 Accuracy			
	A7.5.5 Completeness			

TABLE OF CONTENTS

Section	Title	Pages	Revision	Date
	A7.5.6 Representativeness			
	A7.5.7 Comparability			
A8	Special Training Requirements/Certification	1	0	10/12
A9	Documentation and Records	2	3	08/16
	A9.1 Mechanisms for Documentation of Procedures and Objectives			
	A9.2 Mechanisms for Record Keeping			
	A9.3 Data Reporting Turnaround Time			
	A9.4 Data Storage			
	MEASUREMENT/DATA ACQUISITION			
B1	Sampling Process Design (Experimental Design)	1	1	03/15
	B1.1 Network Design			
	B1.2 Network Design Rationale			
	B1.3 Measurement Validation			
B2	Sampling Methods Requirements	3	1	01/16
	B2.1 Continuous Methods			
	B2.1.1 Sulfur Dioxide (SO_2)			
	B2.2.2 Hydrogen Sulfide (H_2S)			
	B2.1.3 Time Lapse Video			
	B2.1.4 Meteorological Measurement Systems			
	B2.1.5 Volatile Organic Compound (VOC) Continouous Gas Chromatograph (GC) Sampling			
	B2.1.6 Continuous FID Methane/Non-methane			
	B2.2 Noncontinuous Methods			
	B2.2.1 VOC Canister Sampling			
	B2.3 Corrective Actions			
B3	Sample Handling and Custody	2	0	10/12
	B3.1 Documentation and Custody Requirements			
	B3.1.1 Sulfur Dioxide (SO_2)			
	B3.1.2 Hydrogen Sulfide (H_2S)			
	B3.1.3 Meteorological Measurement Systems			
	B3.1.4 Continuous Gas Chromatograph			
	B3.1.5 Continuous FID Methane/Non-methane			
	B3.1.6 Volatile Organic Compounds (VOCs), Canister Samples			
	B3.1.6.1 Transfer from the UT Austin CEER Laboratory to Subcontractor's Field Office			
	B3.1.6.2 Return from Subcontractor's Field Office to UT Austin CEER Laboratory			
	B3.1.7 Time Lapse Video			
	B3.2 Sample Handling Procedures			
	B3.2.1 SO_2			
	B3.2.2 H_2S			
	B3.2.3 Meteorological Measurement Systems			

TABLE OF CONTENTS

Section	Title	Pages	Revision	Date
	B3.2.4 Continuous GC			
	B3.2.5 Continuous FID Methane/Non-methane			
	B3.2.6 VOCs, Canister Samples			
	B3.2.7 Time Lapse Video			
B4	Analytical Methods Requirements	2	1	03/15
	B4.1 Analytical Procedures			
	B4.1.1 Sulfur Dioxide (SO_2)			
	B4.1.2 Hydrogen Sulfide (H_2S)			
	B4.1.3 Meteorological Measurement Systems by U.S. Environmental Protection Agency (EPA) *Quality Assurance Handbook Volume IV* Methodology			
	B4.1.4 Continuous Gas Chromatograph (GC) (Perkin Elmer GC/Flame Ionization Detector [FID]) for Volatile Organic Compounds (VOCs)			
	B4.1.5 Continuous FID Methane/Non-methane			
	B4.1.6 EPA Method TO-15 Canisters for VOCs Collected in Glass-Lined Stainless Steel Canisters			
	B4.1.7 Time Lapse Video			
	B4.2 Corrective Actions			
B5	Quality Control (QC)	3	3	08/16
	B5.1 Sulfur Dioxide (SO_2)			
	B5.2 Hydrogen Sulfide (H_2S)			
	B5.3 Meteorology			
	B5.4 Continuous Gas Chromatograph (GC)			
	B5.5 Continuous FID Methane/Non-methane			
	B5.6 TO-15 Canister Volatile Organic Compounds (VOCs)			
	B5.6.1 Sampler QC Checks			
	B5.6.2 Analytical QC Checks in the UT Austin CEER Laboratory			
	B5.5.2.1 Blank Analysis			
	B5.5.2.2 MS Performance Check			
	B5.5.2.3 Calibration Check			
	B5.5.2.4 Analytical Precision			
	B5.7 Time Lapse Video			
	B5.8 Precision			
	B5.9 Accuracy			
B6	Instrument/Equipment Testing, Inspection, and Maintenance Requirements	2	1	03/15
	B6.1 Instrument Testing/Inspection			
	B6.2 Preventive Maintenance Procedures			
	B6.2.1 Sulfur Dioxide (SO_2)			
	B6.2.2 Hydrogen Sulfide (H_2S)			
	B6.2.3 Time Lapse Video			
	B6.2.4 Meteorological Measurement Systems			
	B6.2.5 Continuous Gas Chromatograph (GC)			
	B6.2.6 Continuous FID Methane/Non-methane			

TABLE OF CONTENTS

Section	Title	Pages	Revision	Date
	B6.2.7 Volatile Organic Compounds (VOC) Canister Samples			
	B6.2.8 Canister VOC Analysis			
	B6.3 Corrective Maintenance Procedures			
	B6.3.1 SO_2			
	B6.3.2 Time Lapse Video			
	B6.3.3 Meteorological Measurement Systems			
	B6.3.4 Automated GC			
	B6.3.5 Continuous FID Methane/Non-methane			
	B6.3.6 VOC Canister Samplers			
	B6.3.7 VOC Canister Analysis			
	B6.4 Availability of Spare Parts			
B7	Instrument/Equipment Calibration and Frequency	5	2	03/15
	B7.1 Calibration			
	B7.1.1 Sulfur Dioxide (SO_2)			
	B7.1.2 Hydrogen Sulfide (H_2S)			
	B7.l.3 Meteorological Equipment			
	B7.1.4 Continuous Gas Chromatograph (GC)			
	B7.1.5 Continuous FID Methane/Non-methane			
	B7.1.6 Canister VOC Sampler			
	B7.1.7 VOC Canister Samples			
	B7.2 Traceability			
	B7.2.1 SO_2			
	B7.2.2 Hydrogen Sulfide (H_2S)			
	B7.2.3 Meteorological Equipment			
	B7.2.4 Continuous GC			
	B7.2.5 Continuous FID Methane/Non-methane			
	B7.3 Documentation			
B8	Inspection/Acceptance Requirements for Supplies and Consumables	1	0	10/12
	B8.1 Sampling Supplies			
	B8.2 Standards			
	B8.3 Spare Parts			
B9	Data Acquisition Requirements (Non-Direct Measurements)	1	0	10/12
B10	Data Management	3	2	08/16
	B10.1 Sulfur Dioxide (SO_2)			
	B10.2 Hydrogen Sulfide (H_2S)			
	B10.3 Meteorological Data			
	B10.4 Continuous Gas Chromatograpgh			
	B10.5 Continuous FID Methane/Non-methane			
	B10.6 Canister Volatile Organic Compound (VOC) Data			
	B10.7 Time Lapse Video			
	B10.8 Acceptability of the Hardware/Software Configuration			
	B10.9 Data to Users			

ASSESSMENT/OVERSIGHT

TABLE OF CONTENTS

Section	Title	Pages	Revision	Date
C1	Assessments and Response Actions	4	1	10/12
	C1.1 Technical Systems Audit			
	C1.1.1 Field Technical Systems Audit			
	C1.1.1.1 Assessment of Sulfur Dioxide (SO_2)			
	C1.1.1.2 Assessment of Hydrogen Sulfide (H_2S)			
	C1.1.1.3 Assessment of Meteorological Equipment			
	C1.1.1.4 Assessment of Continuous Gas Chromatograph (GC)			
	C1.1.1.5 Assessment of Continuous FID Methane/Non-methane			
	C1.1.1.6 Assessment of Volatile Organic Compound (VOC) Canister Samples			
	C1.1.1.7 Assessment of Time Lapse Video			
	C1.1.2 Field Inspections			
	C1.1.3 Laboratory Technical Systems Audit			
	C1.2 Performance Evaluations			
	C1.2.1 Field Assessment			
	C1.2.1.1 SO_2			
	C1.2.1.2 H_2S			
	C1.2.1.3 Meteorological Equipment			
	C1.2.1.4 Continuous GC			
	C1.2.1.5 Continuous FID Methane/Non-methane			
	C1.2.1.6 VOC Canister Analysis			
	C1.2.1.7 Time Lapse Video			
	C1.2.2. Laboratory Assessment			
	C1.3 Assessment of Data Quality Indicators			
	C1.3.1 Specific Procedures to Assess Data Quality			
	C1.3.1.1 Data Precision Assessment			
	C1.3.1.1.1 SO_2			
	C1.3.1.1.2 H_2S			
	C1.3.1.1.3 Meteorological Equipment			
	C1.3.1.1.4 Continuous GC			
	C1.3.1.1.5 Continuous FID Methane/Non-methane			
	C1.3.1.1.6 VOC Canister Analysis			
	C1.3.1.1.7 Time Lapse Video			
	C1.3.1.2 Data Accuracy Assessment			
	C1.3.1.2.1 SO_2			
	C1.3.1.2.2 H_2S			
	C1.3.1.2.3 Meteorological Monitors			
	C1.3.1.2.4 Continuous GC and Canister VOC Sampling			
	C1.3.1.2.5 Continuous FID Methane/Non-methane			
	C1.3.1.3 Data Completeness Assessment			
	C1.4 Audits of Data Quality			
	C1.5 Corrective Actions			

TABLE OF CONTENTS

Section	Title	Pages	Revision	Date
C2	Reports to Management	1	1	10/12
	C2.1 Quality Assurance (QA) Status Report			
	C2.2 Annual Project QA Report			
	C2.3 Data Reports			
	C2.3.1 Field Activity Reports			
	C2.3.2 Laboratory Activity Reports			
	C2.4 Reporting Schedule			
	DATA VALIDATION AND USABILITY			
D1	Data Review, Validation, and Verification Requirements	2	3	08/16
	D1.1 Data Validation			
	D1.1.1 SO_2			
	D1.1.2 H_2S			
	D1.1.3 Continuous FID Methane/Non-methane			
	D1.1.4 Time Lapse Video			
	D1.1.5 Meteorological Measurement Systems			
	D1.2 Data Custody			
	D1.2.1 SO_2			
	D1.2.2 H_2S			
	D1.2.3 Continuous FID Methane/Non-methane			
	D1.2.4 Time Lapse Video			
	D1.2.5 Meteorological Measurement Systems			
	D1.2.6 UT Austin CEER Laboratory			
D2	Validation and Verification Methods	1	1	10/12
	D2.1 Sulfur Dioxide (SO_2)			
	D2.1.1 Quality Control Test Results Performed by the MeteoStar Computer			
	D2.1.2 Laboratory Control Checks (LCC)			
	D2.2 Hydrogen Sulfide (H_2S)			
	D2.2.1 Quality Control Test Results Performed by the MeteoStar Computer			
	D2.2.2 Laboratory Control Checks (LCC)			
	D2.3 Meteorological Equipment			
	D2.4 Continuous Gas Chromatograph (GC)			
	D2.5 Continuous FID Methane/Non-methane			
	D2.5.1 Quality Control Test Results Performed by the MeteoStar Computer			
	D2.5.2 Laboratory Control Checks (LCC)			
	D2.6 Volatile Organic Compound (VOC) Canister Samples			
	D2.7 Time Lapse Video			
	D2.8 Data Review			
D3	Reconciliation with User Requirements	3	2	03/15
	D3.1 Detection Limits			
	D3.2 Precision			
	D3.2.1 Sulfur Dioxide (SO_2)			
	D3.2.2 Hydrogen Sulfide (H_2S)			
	D3.2.3 Meteorological Equipment			
	D3.2.4 Continuous GC			

TABLE OF CONTENTS

Section	Title	Pages	Revision	Date
	D3.2.5 Continuous FID Methane/Non-methane			
	D3.2.6 Canister Volatile Organic Compounds			
	D3.2.7 Time Lapse Video			
D3.3	Accuracy			
	D3.3.1 SO_2			
	D3.3.2 H_2S			
	D3.3.3 Meteorological Equipment			
	D3.3.4 Continuous GC			
	D3.3.5 Continuous FID Methane/Non-methane			
	D3.3.6 Canister Volatile Organic Compounds			
	D3.3.7 Time Lapse Video			
D3.4	Completeness			

LIST OF FIGURES

Section		Title	Pages	Revision	Date
A4	Figure A4.A	Organizational Structure for Project 0-66-36 "Photocatalytic NOx/HRVOC/O3 Removal in Transportation Applications"	1	1	07/15
	Figure A4.B	TCEQ Organization (October 1, 2005)	1	0	10/12
B10	Figure B10	Sample/Data Flows and Storage	1	2	08/16

LIST OF TABLES

Section		Title	Pages	Revision	Date
A6	Table A6.2.A	Overview of Sampling Matrix	1	2	07/15
A6	Table A6.3.B	National Ambient Air Quality Standards (NAAQS)	1	0	10/12
A7	Table A7.5.7.A	Reporting Units of Measurements	1	0	10/12
B2	Table B2.1.A	Criteria Pollutants	1	3	01/16

LIST OF APPENDICES

Appendix	Title	Pages	Revision	Date
A	Table A6.2B Sampling Station Status	1	2	03/15
B	Not used for this project	1	1	10/12
C	Table A7 Measurement Data Quality Objectives	1	2	03/15
D	Figure 1. LEADS Data Collection Model	2	2	03/15
E	Gas Standard Acceptance Test Limits	1	1	10/12
F	Quality Control Activities	8	2	03/15
G	Not used for this project	1	1	10/12
H	Not used for this project	1	1	10/12
I	Not used for this project	1	1	10/12
J	Processing of CAMS QC Data	30	1	10/12
K	Not used for this project	1	1	10/12
L	MetroStar LEADS Web Primer	17	1	10/12
M	Validation Codes for CAMS Data	1	1	10/12
N	Data Validation Procedure for MeteoStar	1	1	10/12

A3 DISTRIBUTION LIST

Texas Department of Transportation

Wade Odell,

The University of Texas at Austin
Maria Juenger, Ph. D., Principal Investigator
Neil Crain, Ph.D., Project Manager
Cyril Durrenberger, PE, Project Quality Assurance Officer

A4 PROJECT/TASK ORGANIZATION

Project No. 0-6636 "Photocatalytic NOx /HRVOC/O3 Removal in Transportation Applications" is performed by The University of Texas at Austin (UT). The project organization is shown in Figure A4.A. The interrelationships and responsibilities of the participants in these projects are listed below:

A4.1 Project Sponsor, The Texas Department of Transportation (TXDOT)

Wade Odell, Texas Department of Transportation

- Sets the preliminary objectives for the project.
- Allocates adequate resources to ensure completion of the project in compliance with the stated objectives.
- Determines the ultimate use of the data set developed from the project activities.

A4.2 Texas Commission on Environmental Quality (TCEQ)

Doug Boyer, Texas Commission on Environmental Quality

- Project Advisor.

A4.3 Principal Investigator and Project Manager

Maria Juenger Ph.D., and Neil Crain Ph.D., The University of Texas at Austin

- Coordinate the monitoring operations of the project and is the primary contact person.
- Coordinate air monitoring activities between the TCEQ and the project.
- Provide project planning and coordinates the preparation of reports to the Project Sponsor.
- Prepare the QAPP for the project for review and approval by the TCEQ.

A4.4 Project Quality Assurance (QA) Officers

Cyril Durrenberger, PE, and Jarret Spinhirne M.S., The University of Texas at Austin

- Coordinate the QA activities for the project including QA activities with external agencies and non-agency groups.
- Participate in the development, approval, implementation, and maintenance of written quality assurance documents (e.g, QMPs, SOPs, QAPPs).
- Perform project and laboratory technical systems audits.
- Participate in the preparation of quality reports.
- Determine conformance with project quality system requirements.
- Review and approve proposed corrective actions and verifications.
- Monitor the implementation of corrective actions.
- Report on the status of corrective action programs.
- Assess the effectiveness of project quality systems.

- Coordinate the identification, disposition, and reporting to management of nonconforming items and activities.
- Prepare and distribute annual quality assurance assessment schedules.

A4.5 Monitoring Station Operations and Maintenance

Jarret Spinhirne, M.S. and Neil Crain, Ph.D., The University of Texas at Austin

- Maintain the site, both inside the shelter and outside, clean, orderly and presentable to the public.
- Provides support to operate, maintain and repair the monitoring equipment.
- Review and certify that all new equipment meets manufacturer's specifications.
- Monitor automated quality control checks and take corrective action when indicated.
- Perform scheduled quality control checks on samplers, sampling equipment, and meteorological equipment.
- Perform scheduled preventive maintenance procedures.
- Record data/information as required in appropriate field/monitoring site logs.
- Calibrate field samplers and meteorological equipment.
- Perform calibration verification checks.
- Maintain calibration equipment.
- Participate in the development of updates and revisions to written quality assurance standards (e.g., QMPs, SOPs, QAPPs).

A4.6 Monitoring Data Management and Statistical Support,

Jarett Spinhirne, M.S., and Dave Sullivan Ph. D., The University of Texas at Austin,

- Provide statistical evaluation of NOx and ozone analytical data to assist in investigating air pollution removal efficiencies .
- Provide statistical evaluation of site analytical data to quality assure data.

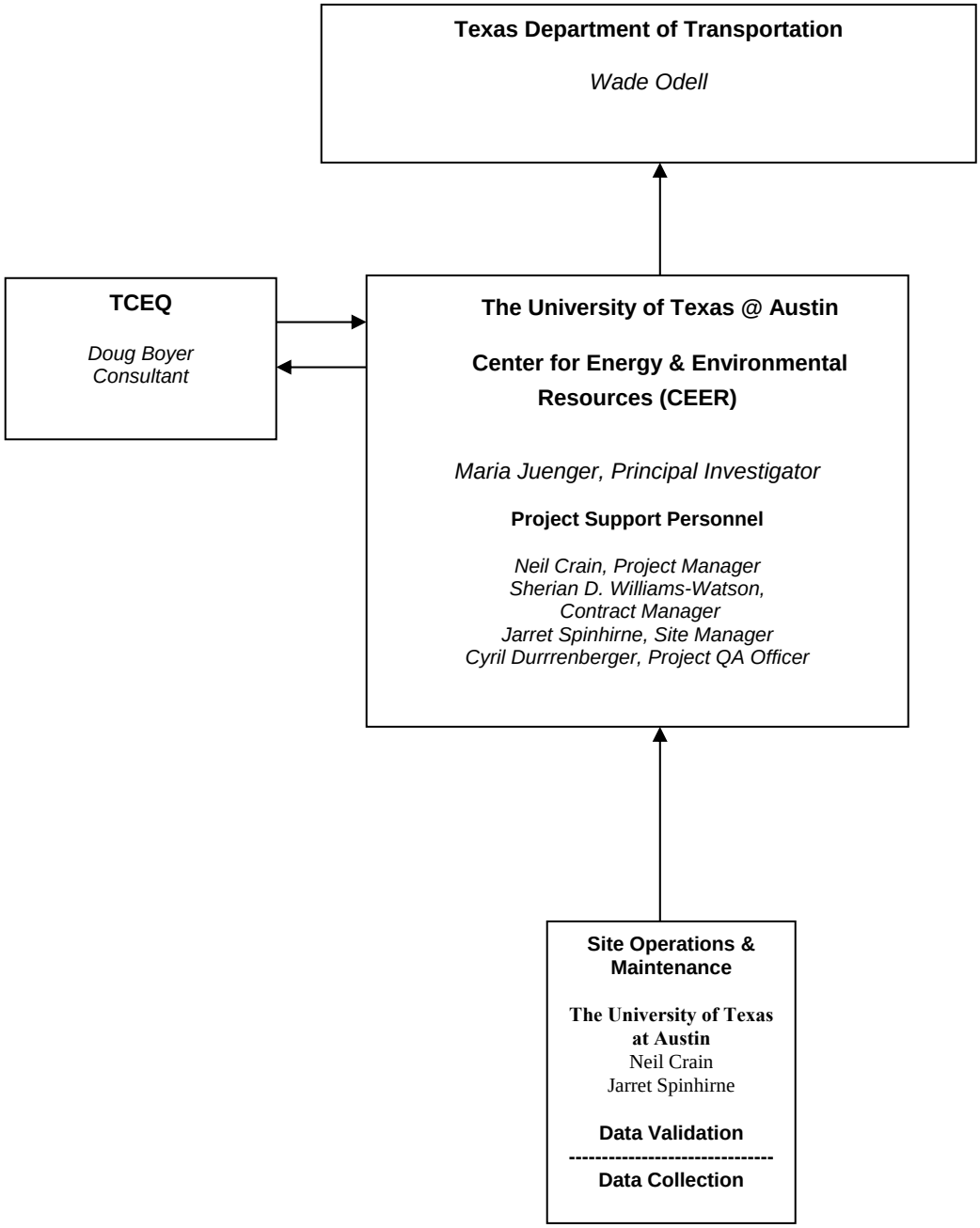

Figure A4.A Organizational Structure for Project No. 0-6636
"Photocatalytic NOx/HRVOC/O3 Removal in Transportation Applications"

A5 PROBLEM DEFINITION/BACKGROUND

A5.1 Overview

The Texas Department of Transportation awarded The University of Texas at Austin's Project No. 0-6636 "Photocatalytic NOx/HRVOC/O3 Removal in Transportation Applications". This project was developed to investigate the use of photocatalytic coatings to reduce the elevated outdoor concentration of oxides of nitrogen (NO, NO_2, and NO_X) where high ozone is observed. Laboratory tests conducted for this project showed significant reduction in both NO_X and ozone concentrations as a result of the photocatalytic activity of one of the test coatings. However, there are several important issues such as life expectancy of the coating in a actual application and pollutant removal efficiencies that must be investigated before wide spread use of the catalytic coatings can be considered. To address these issues a modification to the original project was developed. The modification focuses on a field test of the photocatalytic coatings applied to traffic barriers along a Texas highway. The field test will take place over two ozone seasons and will include NO_X and ozone concentrations upwind and downwind of the test site. The test site will include both coated and uncoated traffic barriers. Near simultaneous measurements will be made of the NO_X and ozone concentrations in the ambient air passing over the coated and uncoated barriers. Removal rates for the catalytic coating will be determined by comparing the ambient NO_X and ozone concentrations for the two different test sections.

A5.2 Conclusions to be Made

1. Data collected from this field study will be used to determine the efficacy of the photocatalytic coating applied to traffic barriers along a Texas highway.
2. The NO_X and ozone removal rates will be monitored over time to establish the effective life expectancy of the coating when used in close proximity to a roadway.
3. Data collected from this field study will be used to validate the ozone reductions predicted by atmospheric photochemical grid models.

A5.3 Uses of Data

The potential uses of the data are listed below:

- To determine the NO_X and ozone removal rates associated with the selected catalytic coating.
- Estimation of the life expectancy of the photocatalytic coating when applied to traffic barriers along a Texas highway.
- Validation of the reduction in NO_X and ozone concentrations predicted by atmospheric photochemical grid models.

A5.4 Decision Makers

- Wade Odell, Texas Department of Transportation
- Dr. Maria Juenger, The University of Texas at Austin

A5.5 Principal Customers for the Results

- Texas Department of Transportation
- TCEQ
- The University of Texas at Austin
- Texas citizens

A6 PROJECT/TASK DESCRIPTION

This section provides a description of the work to be done, an overall view of the project objectives, activities, assessments, and outputs of the project, identification of applicable ambient air quality regulations and standards, and an implementation schedule for the project. The measurements to be made during the project are identified in Table A6.2.A. Measurements are expected to be made in compliance with the current guidance where it exits. This guidance includes but is not limited to the U.S. Environmental Protection Agency (EPA) *Quality Assurance Handbook for Air Pollution Measurement Systems* (Volumes I, II, and IV).

The data collection period for this project will be approximately two years. Sampling periods for each method are indicated in Table A6.2.A.

A6.1 Project Overview

UT will install, maintain and operate an air-monitoring station along Texas Toll way 45 at a site that in Northwest Austin to record the concentrations of specific air pollutants. The sampling station will record concentrations of NO_X and ozone and meteorological data.

Dr. Maria Juenger, UT, will serve as the Principal Investigator for this Project. Essential to the performance of the project is the involvement of the Texas Department of Transportation (TXDOT). TXDOT will review project plans and consult on project implementation, including the selection of the exact monitoring location and implementation schedules.

A6.2 Sampling Activities

The general sampling activities of the project are detailed in Table A6.2.A.

Table A6.2.A Overview of Sampling Matrix

Target Compound/Group	Analytical Method	Sampling Period	Frequency
Nitrogen Compounds			
Nitric Oxide (NO)	Chemiluminescence	5 min	Continuous
Nitrogen dioxide (NO_2)	Chemiluminescence	5 min	Continuous
Oxygen Compounds			
Ozone (O_3)	Photometric	5 min.	Continuous
Meteorology			
Wind Direction*	Single Potentiometer Vane	5 min	Continuous
Wind Speed*	Cup Anemometer	5 min	Continuous

A6.3 Standards and Screening Levels

NO_2 and O_3 are regulated by the EPA.

A6.3.1 NAAQS

The NAAQS listed in Table A6.3.A are health-based standards promulgated by the EPA. The levels are established such that concentrations below them are not expected to cause adverse health impacts.

Table A6.3.A National Ambient Air Quality Standards (NAAQS)

Pollutant Parameter	Standard	Averaging Time
O_3	0.075 ppm*	8 hours
NO_2	0.100 ppm*	1 hour
	0.053 ppm*	Annual mean

* ppm on volume basis

A6.4 Assessment Tools

Assessment tools that will be used are described in this section.

A6.4.1 Performance Evaluations

Performance evaluations are to be performed on critical parts of the monitoring systems in order to assess the accuracy of the data as stated in Section C1.2 of this plan. Performance evaluations of the continuous monitors are to be performed at least once at the beginning of the project and once at the end of the project

A7 DATA QUALITY OBJECTIVES (DQO) FOR MEASUREMENT DATA

This section presents the data quality objectives for the project. The formal data quality objectives process as described in the U. S. Environmental Protection Agency (EPA) document *Guidance for Planning the Data Quality Objectives (DQO) Process, EPA QA/G-4* has not been applied to this project, but the project DQOs have been established by other means.

The results of the DQO process include:

- clarify the intended use of the data
- define the type of data needed to support the decision
- identify the conditions under which the data should be collected
- specify tolerable limits on the probability of making a decision error due to uncertainty in the data

The quantitative objectives for measurement data for each parameter are listed in Table A.7 in Appendix C. The objectives reflect the overall (total) measurement error expected for measurements made during this project. This includes media preparation, sampling, analysis, data reduction/reporting, etc. The quality control program has been developed with control of the measurement processes with these objectives in mind.

A7.1 General Project Objectives

- Provide measurements of NO_X and ozone to be used in evaluating the effect of photocatalytic coatings.
- Provide information regarding the life expectancy of photocatalytic materials exposed to near roadway conditions along a Texas highway.
- Provide data for the validation of results obtained from atmospheric models based on laboratory data.

A7.2 Project Specific Objectives

- Verify laboratory results for removal rates of NO_X and ozone using photocatalytic coatings.
- Support development of a NO_X and ozone control strategy utilizing photocatalytic coatings and materials.

A7.3 Conclusions to be Made

Conclusions to be made are presented in Section A5.2.

A7.4 Uses of Data

The potential uses of the data are provided in Section A5.3.

A7.5 Measurement Quality Objectives

The approaches used to assess data uncertainty and the measurement quality objectives for each type of measurement are addressed in this section. Section D3 details the methods of computation.

A7.5.1 Detection Limits

Detection limits are expressed in units of concentration and reflect the smallest concentration of a compound that can be measured with a defined degree of certainty. Criteria pollutants are measured using EPA designated reference or equivalent methods. The detection limits for these methods are specified in 40 *CFR* Part 53.

A7.5.2 System Contribution to the Measurement

A blank or "zero air" level is part of each automatic calibration and span check of the automated methods for NO_2, NO, and O_3. As part of the calibration, this zero level is used along with the upscale concentrations to establish the monitor's calibration curve. As part of the span check, this level is used as a quality control check for monitor zero drift. Automated calibration and span check procedures are described in Appendix H.

A7.5.3 Precision

Precision is a measure of the repeatability of analytical results. Estimates of precision are assessed in different ways for different measurement technologies. Refer to Table A7 in Appendix C for the DQOs. Specific activities designed to collect precision data are given in Section C1.

- Precision for measurements from continuous monitors for O_3 and oxides of nitrogen (NO, NO_2, and NO_X) will be estimated by analysis of a test atmosphere containing the target compound being monitored in accordance with 40 *CFR* Part 58, Appendix A. Precision for O_3 and oxides of nitrogen (NO, NO_2, and NO_X) will be estimated from precision checks that are done as part of routine span checks of the monitors. This precision check consists of introducing a known concentration of the pollutant into the monitor in the concentration range required by 40 *CFR* Part 58, Appendix A. The resulting measured concentration is then compared to the known concentration. These measurements will be processed into upper and lower 95 percent probability limits for each ozone season. These precision estimates will then be compared to the precision goals.

  The precision goals in Table A7 of Appendix B are given in terms of upper and lower 95 percent probability intervals where the center of these intervals is assumed to be 0 percent error. These goals represent the expectation that for repeated measurements of the same atmosphere, there should be a 95 percent probability that any single measurement error, expressed as the percent difference from the mean measurement, should fall within the 95 percent probability interval goal.
- Precision for the meteorological measurements will not be directly evaluated. Measurements will be compared with those from nearby sites using the same or similar equipment.

A7.5.4 Accuracy

Accuracy is the closeness of a measurement to a reference value, and reflects elements of both bias and precision. Specific activities designed to collect accuracy data are given in Section C1.

- The accuracy for O_3 and oxides of nitrogen (NO, NO_2, and NO_X) monitors, will be estimated from independent performance evaluations. A performance audit consists of introducing a known concentration of the pollutant into the monitor. The resulting measured concentration is then compared to the known concentration.

  These measurements are processed into upper and lower 95 percent probability limits for each ozone season. These accuracy estimates will then be compared to the accuracy goals.

  The accuracy goals in Table A7 of Appendix B are given in terms of upper and lower 95 percent probability intervals where the center of these intervals is assumed to be 0 percent error. These goals represent the expectation that there should be a 95 percent probability that any single measurement error, expressed as the percent difference from the true value, should fall within the 95 percent probability interval goal.
- Meteorological measurement accuracy will be assessed by comparing the results with those from nearby sites using the same or similar equipment.

A7.5.5 Completeness

Data completeness for all pollutants is calculated on the basis of the number of valid samples collected out of the total possible number of measurements. All possible measurements for continuous monitoring for O_3 and oxides of nitrogen (NO, NO_2, and NO_X) and wind direction mean 24 hours a day throughout the ozone season. Data completeness is calculated as follows:

$$\% \text{ Completeness} = \frac{\text{Number of valid measurements}}{\text{Total possible measurements}} \times 100$$

A7.5.6 Representativeness

Representativeness is the extent to which a set of measurements reflects actual conditions for a specific application. The representativeness objective for the data is not stated numerically as a quality assurance objective because quantization is generally not possible. Criteria in 40 *CFR* Part 58 are met where possible. The extent to which these criteria are met should be reflected in site documentation files and technical system audit reports.

A7.5.7 Comparability

Comparability is achieved when the results are reported in standard units to facilitate comparisons between the data from this project and other similar programs. In order to accomplish this objective, the reporting units for the measurements are listed in Table A7.5.7.A.

Wind direction and wind speed data are recorded as one-hour averaged resultant vectors from the start to the end of an hour, with the data being referenced as the hour at which data

collection started. The wind direction standard deviation and the wind speed arithmetic average for the hour are also computed. These figures are compared with data received from the National Weather Service that are two-minute averages of wind direction and wind speed taken at an unspecified time within an hour. The difference between the vector average and the arithmetic average is small, with the vector average never exceeding the arithmetic average.

Table A7.5.7.A Reporting Units of Measurements

Parameter	Units*	Conditions
NO	parts per billion (ppb)	Ambient
NO_2	parts per billion (ppb)	Ambient
Ozone	parts per billion (ppb)	Ambient
Wind Direction	degrees azimuth	Ambient
Wind Speed	miles per hour	Ambient
Temperature	degrees Fahrenheit	Ambient

* ppm, ppmc, ppb on a volume basis

A8 SPECIAL TRAINING REQUIREMENTS/CERTIFICATION

Specialized training and use of standard operating procedures is required for personnel who audit, calibrate, or operate the criteria pollutant monitors and the meteorological equipment at the sampling station to be in compliance with this QAPP. Instrument manuals are available at each site for reference.

A9 DOCUMENTATION AND RECORDS

All personnel working on this project are expected to maintain records that include sufficient information to reconstruct each final reported measurement from the variables originally gathered in the measurement process. This includes but is not limited to information (raw data, electronic files, and/or hard copy printouts) related to media preparation, sampler calibration, sample collection, measurement instrument calibration, quality control checks of sampling or measurement equipment, "as collected" measurement values, an audit trail for any modifications made to the "as collected" measurement values, and traceability documentation for reference standards.

Difficulties encountered during sampling or analysis need to be documented in narratives that clearly indicate the affected measurements. All electronic versions of data sets should reflect the limitations associated with individual measurement values.

A9.1 Mechanisms for Documentation of Procedures and Objectives

- EPA *Quality Assurance Handbooks*
- Method Specific Standard operating procedures
- Instrument manufacturer's technical support manuals
- TCEQ Ambient Air Quality Network Field Quality Control Manual

A9.2 Mechanisms for Record Keeping

The following electronic or hard copy documents are maintained by the analysts, field operators (e.g. activity logs), or data managers (e.g. electronic logs). All hard copy documentation will be recorded in non-erasable ink, with any changes denoted by a single line through the entry, the initials of the person making the change, and the date.

- Instrument calibration data forms
- Electronic and manual daily activity logs
- Electronic and manual data processing and validation logs
- Electronic and manual data management activity logs
- Records of assessment, such as performance evaluation records

A9.3 Data Reporting Turnaround Time

After the end of the ozone season, all data shall have a turnaround time of 90 days from collection through analysis, validation, and reporting.

A9.4 Data Storage

- Continuous and quality assurance data from the sampling station are available in Sutron's LEADs system throughout the duration of the project.
- Meteorological data are stored in the Sutron's LEADs system throughout the duration of the project.
- Audit reports are stored on CDs and in hardcopies at the UT for 7 years after the end of the project.

Table A6.2.B Sampling Station Status

Location	O_3	NO_X	Met	Status	Remarks
TX TW 45 Northwest Austin	N	N	X	↑	

Appendix B is not used for this project

Table A7 Measurement Data Quality Objectives

Parameter	Method Name or Published Reference	Analytical Technique	Sample Period (minutes)	Detection Limit (ppbv unless otherwise stated)	Precision (95% Probability Limits)	Accuracy (95% Probability Limits unless otherwise stated)	Complete-ness *
Ozone	40 CFR 58 (network)	UV Photometry	5	3	±15%	Network ±20%; monitor ±20% as % difference	80%
Nitrogen Oxide	40 CFR 58 (network)	Chemilu-minescence	5	2	±15%	Network ±20%; monitor ±20% as % difference	80%
Nitrogen Dioxide	40 CFR 58 (network)	Chemilu-minescence	5	2	±15%	Network ±20%; monitor ±20% as % difference	80%
Total Oxides of Nitrogen	40 CFR 58 (network)	Chemilu-minescence	5	2	±15%	Network ±20%; monitor ±20% as % difference	80%
Meteorological Parameters							
						Absolute Diff.	
Wind Direction		Single Potentiometer Vane	5	1 Degree	NA	±5 degrees azimuth (±30 degrees, collocated)	90%
Wind Speed		Cup Anemometer	5	0.5 mph	NA	±5% above 11.2 mph and within 0.56 mph below 11.2 mph	90%

NA = Not Applicable
Precision numbers represent precision estimates at or near the detection limit.
* Completeness is defined as the number of valid measurements divided by the number of possible measurements (which excludes QA/QC activities) for the monitoring period.

SUTRON

METEOSTAR/LEADS DATA COLLECTION MODEL

LEADS Data Collection Model

MeteoStar/LEADS uses a multi-tier data collection system as shown in Figure 1. This reduces the communications load on any single computer. Extra benefits include the ability to rapidly reconfigure the communications network in the event of a hardware failure, and multi-stage archival of measurements. It is possible to retrieve data from any of the archive locations and reintroduce it into the system.

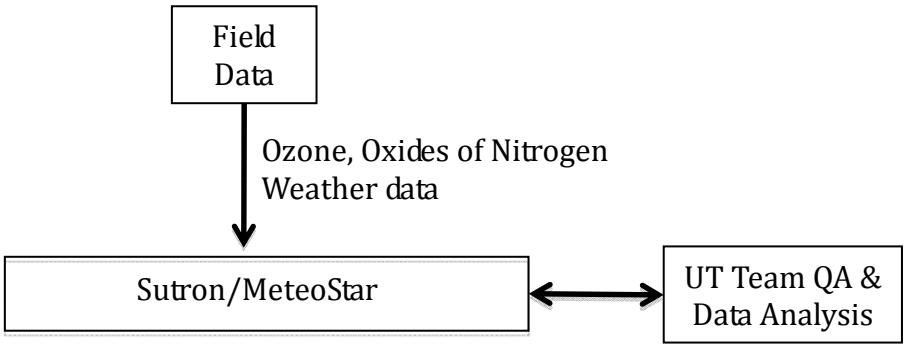

Figure 1. Sutron/MeteoStar LEADS Data Collection Model

A Zeno datalogger is installed at the sampling site. The Zeno collects data, monitors the output of the automatic calibration system, performs initial data flagging, and stores operator logs. The Zeno is capable of storing one to three weeks of data (depending upon the number of parameters being monitored). This is the first of the multi-stage data archival locations.

The CFEP is responsible for ingesting and distributing to the proper computer(s) or processes the measurements and operator logs from the Zeno dataloggers, conventional surface weather observations, upper air weather observations, and the National Weather Service model forecast grids. For pollution data (i.e., all data measured via a Zeno datalogger), the CFEP ingests the data from all the regional hub computers and distributes it into the correct input-processing directory on the LEADS Central Processor where it is decoded and placed into a database. The final data archival stage is actually performed by the Central Processor. As pollution data is being decoded, a copy is written to an electro-optical disk for long-term storage.

GAS STANDARD ACCEPTANCE TEST LIMITS

E.1 Primary Gas Standards

Primary gas standard for nitric oxide (NO) in the form of Standard Reference Materials (SRMs) is obtained from the National Institute for Standards and Technology (NIST) and do not require testing for acceptance by the Texas Commission on Environmental Quality (TCEQ). The TCEQ purchases SRMs containing 100 and 50 ppm concentrations of NO in nitrogen. Ozone (O_3) is generated as required and measured with a Primary Ozone Photometer. Nitrogen dioxide (NO_2) is prepared by the gas phase titration of NO with O_3 and is referenced to the change in NO concentration.

E.2 Secondary or Transfer Gas Standards

Secondary gas standard for NO in the form of NIST traceable certified gases are obtained from vendors. These gases are tested in the Calibration Laboratory. To meet terms of the gas contract, the analytical accuracy must be within ±1 percent and the gas must be traceable to a NIST SRM. The NO gas concentration must be within ±5 percent of the contract specified concentration and the NO gas must contain no more than 1 ppm NO_2 as an impurity.

E.3 Sampling Station Gas Standards

Cylinder gases located in the Sampling Station consist of NO (50 ppm in nitrogen). The acceptance criteria for the gases is the same as described in E.2 above.

E.4 Test Results

Cylinder gases that fail to pass the tests described in E.2 and E.3 are returned to the supplier for replacement.

Appendix F Supplement

There is a separate calibration limits file in Sutron's MeteoStar/LEADS System for each Air Quality System (AQS) site. Each of these files has the limits used for each parameter, parameter occurrence code (POC), and for each quality control (QC) test for any point in time. In other words, each monitor can have its own unique set of limits and a record of changes in these limits can be kept in the file. Listed below are the current set of limits from the Test Continuous Ambient Monitoring Station 90 cal limits file.

The default limits for ozone (O_3), nitric oxide (NO), oxides of nitrogen (NO_x), and nitrogen dioxide (NO_2), operating at .5 parts per million (ppm). The actual limits being used may be tailored to each individual monitor. In general, the QC limits must be tailored to the full-scale setting.

DATE 19971024000000

#PARM **O_3**	POC	NAME	IDENTIFIER	VALUE	DESCRIPTION
44201	1	O_3	1	20	G-level outlier (mv)
44201	1	O_3	2	20	T-level outlier (mv)
44201	1	O_3	3	20	S-level outlier (mv)
44201	1	O_3	4	30	R-level outlier (mv)
44201	1	O_3	5	40	M-level outlier (mv)
44201	1	O_3	6	20	Default outlier (mv)
44201	1	O_3	7	0.006	All levels Conc. Outlier (ppm)
44201	1	O_3	8	10	Concentration Warning (% ideal)
44201	1	O_3	9	15	Concentration Control (% ideal)
44201	1	O_3	10	200	Slope Warning (scalar)
44201	1	O_3	11	400	Slope Control (scalar)
44201	1	O_3	12	25	Intercept Warning (scalar)
44201	1	O_3	13	50	Intercept Control (scalar)
44201	1	O_3	14	0.5	Full Scale PPM
44201	1	O_3	15	15	Precision Warning (mv)
44201	1	O_3	16	30	Precision Control (mv)
44201	1	O_3	17	15	Zero Warning (mv)
44201	1	O_3	18	30	Zero Control (mv)
44201	1	O_3	19	60	Span Warning (mv)
44201	1	O_3	20	120	Span Control (mv)
44201	1	O_3	21	23	Linearity Warning (mv)
44201	1	O_3	22	46	Linearity Control (mv)
44201	1	O_3	35	0	G-level ideal conc. (ppm)
44201	1	O_3	36	0.09	T-level ideal conc. (ppm)
44201	1	O_3	37	0.2	S-level ideal conc. (ppm)
44201	1	O_3	38	0.3	R-level ideal conc. (ppm)
44201	1	O_3	39	0.4	M-level ideal conc. (ppm)

Appendix F Supplement (Continued)

#PARM NO	POC	NAME	IDENTIFIER	VALUE	DESCRIPTION
42601	1	NO	1	20	G-level outlier (mv)
42601	1	NO	2	20	T-level outlier (mv)
42601	1	NO	3	20	S-level outlier (mv)
42601	1	NO	4	30	R-level outlier (mv)
42601	1	NO	5	40	M-level outlier (mv)
42601	1	NO	6	20	Other levels outlier (mv)
42601	1	NO	7	0.006	All levels Conc. Outlier (ppm)
42601	1	NO	8	10	Concentration Warning (% ideal)
42601	1	NO	9	15	Concentration Control (% ideal)
42601	1	NO	10	200	Slope Warning (scalar)
42601	1	NO	11	400	Slope Control (scalar)
42601	1	NO	12	25	Intercept Warning (scalar)
42601	1	NO	13	50	Intercept Control (scalar)
42601	1	NO	14	0.5	Full Scale PPM
42601	1	NO	15	15	Precision Warning (mv)
42601	1	NO	16	30	Precision Control (mv)
42601	1	NO	17	15	Zero Warning (mv)
42601	1	NO	18	30	Zero Control (mv)
42601	1	NO	19	60	Span Warning (mv)
42601	1	NO	20	120	Span Control (mv)
42601	1	NO	21	23	Linearity Warning (mv)
42601	1	NO	22	46	Linearity Control (mv)
42601	1	NO	35	0	G-level ideal conc. (ppm)
42601	1	NO	36	0.16	T-level ideal conc. (ppm)
42601	1	NO	37	0.27	S-level ideal conc. (ppm)
42601	1	NO	38	0.37	R-level ideal conc. (ppm)
42601	1	NO	39	0.47	M-level ideal conc. (ppm)

Appendix F Supplement (Continued)

#PARM **NOx**	POC	NAME	IDENTIFIER	VALUE	DESCRIPTION
42603	1	NOx	1	20	G-level outlier (mv)
42603	1	NOx	2	20	T-level outlier (mv)
42603	1	NOx	3	20	S-level outlier (mv)
42603	1	NOx	4	30	R-level outlier (mv)
42603	1	NOx	5	40	M-level outlier (mv)
42603	1	NOx	6	20	Other levels outlier (mv)
42603	1	NOx	7	0.006	All levels Conc. Outlier (ppm)
42603	1	NOx	8	10	Concentration Warning (% ideal)
42603	1	NOx	9	15	Concentration Control (% ideal)
42603	1	NOx	10	200	Slope Warning (scalar)
42603	1	NOx	11	400	Slope Control (scalar)
42603	1	NOx	12	25	Intercept Warning (scalar)
42603	1	NOx	13	50	Intercept Control (scalar)
42603	1	NOx	14	0.5	Full Scale PPM
42603	1	NOx	15	15	Precision Warning (mv)
42603	1	NOx	16	30	Precision Control (mv)
42603	1	NOx	17	15	Zero Warning (mv)
42603	1	NOx	18	30	Zero Control (mv)
42603	1	NOx	19	60	Span Warning (mv)
42603	1	NOx	20	120	Span Control (mv)
42603	1	NOx	21	23	Linearity Warning (mv)
42603	1	NOx	22	46	Linearity Control (mv)
42603	1	NOx	35	0	G-level ideal conc. (ppm)
42603	1	NOx	36	0.16	T-level ideal conc. (ppm)
42603	1	NOx	37	0.27	S-level ideal conc. (ppm)
42603	1	NOx	38	0.37	R-level ideal conc. (ppm)
42603	1	NOx	39	0.47	M-level ideal conc. (ppm)

Appendix F Supplement (Continued)

#PARM NO_2	POC	NAME	IDENTIFIER	VALUE	DESCRIPTION
42602	1	NO_2	1	20	G-level outlier (mv)
42602	1	NO_2	2	20	T-level outlier (mv)
42602	1	NO_2	3	20	S-level outlier (mv)
42602	1	NO_2	4	30	R-level outlier (mv)
42602	1	NO_2	5	40	M-level outlier (mv)
42602	1	NO_2	6	20	Other levels outlier (mv)
42602	1	NO_2	7	0.006	All levels Conc. Outlier (ppm)
42602	1	NO_2	8	10	Concentration Warning (% ideal)
42602	1	NO_2	9	15	Concentration Control (% ideal)
42602	1	NO_2	10	200	Slope Warning (scalar)
42602	1	NO_2	11	400	Slope Control (scalar)
42602	1	NO_2	12	25	Intercept Warning (scalar)
42602	1	NO_2	13	50	Intercept Control (scalar)
42602	1	NO_2	14	0.5	Full Scale PPM
42602	1	NO_2	15	15	Precision Warning (mv)
42602	1	NO_2	16	30	Precision Control (mv)
42602	1	NO_2	17	15	Zero Warning (mv)
42602	1	NO_2	18	30	Zero Control (mv)
42602	1	NO_2	19	60	Span Warning (mv)
42602	1	NO_2	20	120	Span Control (mv)
42602	1	NO_2	21	23	Linearity Warning (mv)
42602	1	NO_2	22	46	Linearity Control (mv)
42602	1	NO_2	23	25	Balance Warning (mv)
42602	1	NO_2	24	75	Balance Control (mv)
42602	1	NO_2	25	5	Efficiency Warning (%)
42602	1	NO_2	26	10	Efficiency Control (%)
42602	1	NO_2	35	0	G-level ideal conc. (ppm)
42602	1	NO_2	36	0.09	T-level ideal conc. (ppm)
42602	1	NO_2	37	0.2	S-level ideal conc. (ppm)
42602	1	NO_2	38	0.3	R-level ideal conc. (ppm)
42602	1	NO_2	39	0.4	M-level ideal conc. (ppm)

O_3, NO, NO_2, NO_X

Assessment Parameter	Quality Control Procedure	Minimum Frequency	Acceptance Criteria	Corrective Action
Sampling system contribution	Intercept test	During calibration	*	Check zero air supply. Check for leaks. Replace desiccant if needed.
Measurement system contribution - Calibration	Precision/Linearity test – Multipoint calibration	Following installation, repair, or adjustment of equipment or at least every six months	*	Check calibrator settings. Recalibrate or repair.
Measurement system contribution –Span Check	Concentration spacing test	Daily, every other week	*	Check calibrator settings. Recalibrate or repair.
Measurement system contribution	Linearity test-span checks	Once, each year at beginning of measurement season	*	Check calibrator settings. Recalibrate or repair.
Measurement system contribution	Concentration outlier check	Daily, every other week	*	Check calibrator settings. Recalibrate or repair.
Qualitative performance	Slope test (five-point calibration)	Following installation, repair, or adjustment of equipment or at least every 28 days	*	Check calibrator settings. Recalibrate or repair.
Qualitative performance	Instrument voltage outlier test	Daily, every other week	*	Check calibrator settings. Recalibrate or repair.
Quantitative performance	Span drift test	Daily, every other week	Agreement within ±15% difference	Retest. Recalibrate or repair.
Quantitative performance	NO_2/NO Converter efficiency test	Once per week	*	Retest. Recalibrate or repair.
Precision	Replicate analysis at 2nd level	Once per week	Agreement within ±15% difference	Reaudit. Recalibrate or repair.
Accuracy (Bias)	Multipoint audit	Once, each year at beginning of measurement season	Agreement within ±20% difference	Recalibrate, repair or replace sensor.

*See Appendix J, "MeteoStar/LEADS Processing of CAMS Quality Control Data, 4/5/2000," for automated data processing information.
See supplement for default values.
See Appendix P for complete list of acronyms.

Wind Direction by Single Potentiometer Vane

Assessment Parameter	Quality Control Procedure	Minimum Frequency	Acceptance Criteria	Corrective Action
Sampling system contribution - Detection limit (DL)		Vendor provided	Graphical resolution: ±22.5°	Replace bearings if start threshold is too high. Remeasure start threshold. Repair or replace sensor.
Qualitative Performance	Visual inspection	During each site visit	Position of vane corresponds to current conditions	Repair or replace sensor.
Precision	NA	NA	NA	NA
Accuracy (bias)	EPA QA Handbook Vol IV, 1995 - Comparison to co-located sensor or direct reading sensor	Once per year	Graphical resolution: ±22.5°	Repair or replace sensor.

See Appendix P for a complete list of acronyms.

Wind Speed by Cup Anemometer

Assessment Parameter	Quality Control Procedure	Minimum Frequency	Acceptance Criteria	Corrective Action
Sampling system contribution - Detection limit (DL)	EPA QA Handbook Vol IV, 1995	Vendor provided	±10%	Replace.
Qualitative Performance	Visual inspection	During each site visit	Cups spinning and undamaged	Repair or replace sensor.
Precision	NA	NA	NA	NA
Accuracy (bias)		Once per year	±10%	Repair or replace sensor.

Note: 1 m s-1 = 2.237 mph.
See Appendix P for a complete list of acronyms.

Appendix G is not used for this project

Appendix H is not used for this project

Appendix I is not used for this project

SUTRON'S METEOSTAR/LEADS PROCESSING OF SAMPLING STATION QC DATA 4/5/00

FROM APPENIDIX D OF THE

TCEQ METEOSTAR/LEADS CONTRACT

NOTE: This is the original specification that was the basis of how Lockheed programmed LEADS to process and automatically validate SAMPLING STATION calibration and Span Check data. Several details were implemented differently and there have been a few additions. For example the data logger does not control the calibrator as described in this specification, H_2S cals and spans are processed differently and processing of NOy monitor data has been added. The specification for processing H_2S and NOy data are given in latter contracts with Lockheed. Also, this document does not cover the processing and automatic validation of weather data.

Most of the contract specifications written after the first Lockheed contract are written in terms of corrections or additions to, at that time, current software. Because of this, there is currently no one unified document that describes how LEADS processes SAMPLING STATION data. [Note that a permanent change in the concentrations of nitric oxide (NO) used in calibrations, referenced on page 7 (Calibration Sequence for GPT Channels) and page11 (Ideal Concentrations (ppm); and in span checks, referenced on page 8 (Span Check Sequence for GPT Channels); has occurred. These concentrations have been reduced by 0.020 ppm at each concentration level.]

Alternate Processing of Pollutant Measurements:

As of January1, 2003 an alternate method of processing raw voltage measurements from pollutant monitors into concentration units was implemented in the MeteoStar system. A description of this alternate processing method (APM-2) has been added to section D.6 of this Appendix. Reasons for this change in processing method are as follows:

The traditional approach to data processing for continuous measurements for criteria pollutants involves adjustment of the measured 5-minute average of raw voltage response. The 5-minute raw voltage response is converted to millivolts then adjusted by the factors derived from linear regression of the measurement system responses to the last 5-point performance assessment (zero + 4 upscale values up to 80% of full scale, aka. a calibration using G,T,S,R,M levels in TCEQ terminology). Each 5-minute average (in volts) is multiplied by 1000 (now in millivolts), the y-intercept (factor developed from the linear regression of the 5-point calibration data) is subtracted, and the result is divided by the slope (factor developed from the linear regression of the 5-point calibration data). The adjusted 5-minute values that occur during a given hour (12

per hour) are then used to develop the hourly average. If the hourly average is negative (below zero), the hourly average value is set to zero (0). This approach tends to optimize the system performance near the NAAQS levels of interest (typically greater than 10% of full scale (e.g 50 ppb for NO-NOx) and provides a cleaner looking baseline (no negative values).

As the use of measurement data from the NAMS/SLAMS targeted measurement systems has changed from simply NAAQS compliance or non-compliance to understanding the chemistry involved in ozone formation and visibility impairment, it has become evident that the traditional TCEQ approach has two shortcomings relative to measurements near zero. First, y-intercept factors may not always be representative of the measurement system performance at zero (G level) so the adjusted measurements near the baseline (less than 10 ppb) may not be representative of true system performance. Second, the systematic censoring of negative hourly values to 0 removes useable information about the true measurements near the baseline, or 0. If the y-intercept used for adjustment is +, and the true system performance is 0, the resulting adjusted 5 -minute measurement values will be lower than they should be. If the y-intercept used for adjustment is -, and the true system performance is 0, the resulting adjusted 5 -minute measurement values will be higher than they should be. While adding or subtracting 3 -5 ppb to measurement values greater than 50 ppb has a relatively small impact on the resulting value (8-10%) , adding or subtracting 3 -5 ppb to measurement values near 10 ppb has a much large affect on the resulting value (30 - 50%). As the measurement value approaches zero, the adverse impact on the representativeness of the measurement value increase to where adding or subtracting 3 -5 ppb to measurement values of 3 - 5 ppb has an impact on the resulting value (of> + /- 100%). For example, in a system where the true performance at zero is 0, a true measured response of 3 ppb could become an adjusted measured response of 8 ppb by application of a y-intercept, of -5 ppb. The same 3 ppb could become -2 ppb if the y -intercept was +5 ppb. In this latter case, the ability to discerne a distant plume (typically indicated by a rise from baseline of 3 - 5 ppb) would be lost.

This change will immediately improve the representativeness of the measurements near zero and minimize the occurrence of NO measurements that are greater than NOx. The slope, from the least squares regression of the most recent 5-point calibration, would continue to be applied, after adjustment for the measured response at zero.

Appendix D
MeteoStar/LEADS Processing of SAMPLING STATION Quality Control Data

April 5, 2000
(Adapted from "Quality Assurance Plan for
NAMS and SLAMS Monitoring in Texas," Section 2.D)

Prepared by
Robert Brewer
MeteoStar/LEADS Data Collection Sub team
Texas Comission on Environmental Quality

Appendix D
MeteoStar/LEADS Processing of SAMPLING STATION
Quality Control Data
April 5, 2000

Table of Contents

D.1 General Description
- **D**.1.1 Scope
- **D**.1.2 Data Acquisition System (DAS) Data Logging and Status Coding
- **D**.1.3 General Data Handling Description

D.2 Calibration System Data

D.3 Calibration and Span Check Sequences and Calculating Pollutant Concentration Generated by the Calibration System (done by the SAMPLING STATION DAS)
- **D**.3.1 Calibration and Span Check Sequences for non-GPT Channels (CO, O_3, SO_2)
- **D**.3.2 Calibration and Span Check Sequences for GPT Channels (NO, NO_2, and NO_x)

D.4 Multipoint Calibration
- **D**.4.1 Completeness Test
- **D**.4.2 Outlier Test and Average Instrument Response Calculations
- **D**.4.3 Concentration Outlier and Spacing Tests
  - **D**.4.3.1 Concentration Outlier Test
  - **D**.4.3.2 Concentration Spacing Test
- **D**.4.4 Slope and Intercept Calculation
- **D**.4.5 Slope and Intercept Tests
  - **D**.4.5.1 Slope Test
  - **D**.4.5.2 Intercept Test
- **D**.4.6 Precision/Linearity Test
- **D**.4.7 Zero and Span Tests
  - **D**.4.7.1 Zero Test
  - **D**.4.7.2 Span Test
- **D**.4.8 NOx Monitor Channel Balance Test
- **D**.4.9 NOx Monitor Converter Efficiency Test

D.5 Span Check
- **D**.5.1 Completeness Test (Instrument Response)
- **D**.5.2 Outlier Test and Average Instrument Response Calculations
- **D**.5.3 Concentration Outlier and Spacing Tests
- **D**.5.4 Zero and Span Tests
- **D**.5.5 Linearity Tests
- **D**.5.6 NOx Monitor Channel Balance Test
- **D**.5.7 NOx Monitor Converter Efficiency Test

D.6 Calculating Ambient Concentrations (done by the central computer)

D.7 Data Flow and Logic
- **D**.7.1 Processing Multipoint Calibration Data
- **D**.7.2 Processing Span Check Data
- **D**.7.3 Overall Data Processing

D.8 List of Symbols

Appendix D
MeteoStar/LEADS Processing of SAMPLING STATION Quality Control Data

D.1 General Description

D.1.1 Scope

The intent of this document is to described in detail the automatic data processing of data from the SAMPLING STATION data acquisition system (DAS). The pollutants covered in this description are: CO, O_3, SO_2, NO, NO_2, and NO_X. Only those data processing and validation activities involved in calibrations or span checks are detailed.

D.1.2 DAS Data Logging and Status Coding

The response of each pollutant monitor is sampled once a second by the DAS. These one-second samples are averaged into 5 min. average voltages. These averages are logged on output channels of the DAS every 5 min. in units of millivolts. There is one output channel for each parameter being logged.

An additional output channel is logged when the calibration system is being used to introduce a known concentration of pollutant gas into a pollutant monitor. The DAS logs the 5 min. average concentration being generated into this channel in units of parts per million volume ratio (ppm).

Each logged value has a corresponding status code. These codes are used to identify the status of the DAS, calibrator, and monitor. The following letter codes are used:

K - code used to identify that the monitor is sampling ambient air. This code indicates that valid air quality data was collected.

M, R, S, T, G - codes used to identify that the monitor is sampling calibration gas rather than ambient air. These codes are assigned by the DAS during a calibration or span check and are assigned to both the pollutant channel affected and the concentration channel.

M - calibration gas at 80% of monitor full-scale concentration (except for NO & NO_X).

R - calibration gas at 60% of monitor full-scale concentration (except for NO & NO_X).

S - calibration gas at 40% of monitor full-scale concentration (except for NO & NO_X).

T - calibration gas at 18% of monitor full-scale concentration (except for NO & NO_X).

G - calibration gas at 0% of monitor full-scale concentration (zero gas).

J, P, Q - codes used to indicate that the monitor is not collecting valid air quality data or calibration data.

J - Indicates that the monitor has malfunctioned. This code can only be assigned by the DAS operator. A new monitor calibration is required before data from this monitor will be considered valid.

P - Indicates that preventive maintenance or other testing is being done in the SAMPLING STATION that would invalidate the data being collected for as long as the code is in effect. This code can be assigned by the DAS operator and is assigned by the DAS for 15 min. following a code change to "K" from any code other than "P." The P code is also assigned by the DAS if a full 300 one second samples are not collected during the 5 min. averaging period. This code is also assigned to the 5 min. average concentration channel during a calibration or span check if any of the 300 concentration readings are missing or invalid.

Q - Indicates that a quality assurance procedure is being done in the SAMPLING STATION that would invalidate the data being collected as long as the code is in effect. This code can only be assigned by the DAS operator.

D.1.3 General DAS Data Handling Description

There are three kinds of data collected from the SAMPLING STATION DAS that are involved in calculating and partially validating the air quality data. These data are collected and processed by the central MeteoStar/LEADS system. These are:

-- Multipoint calibration data
-- Ambient air quality data
-- Span check data

In addition there are calibration system data stored in the DAS that are used by the DAS to calculate the concentrations being generated by the SAMPLING STATION calibration system. These calibration system data are reported to the central MeteoStar/LEADS system by the DAS whenever a value is changed. The Meteostar/LEADS system will report the calibration system data being used in the SAMPLING STATION at the request of the MeteoStar/LEADS user.

During a calibration or a span check, the DAS commands the calibration system to generate a series of concentrations of the target gas corresponding to the monitor being calibrated. At the beginning of this process the DAS actuates the "span" valve for the monitor to introduce the calibration gas into it.

Each concentration level is generated for 35 min. to allow the monitor response to stabilize. This time interval per concentration level should be user selectable by the DAS operator on a pollutant-by-pollutant basis.

For each concentration level commanded, the DAS calculates the actual concentration generated or request this information from the calibration system. These concentrations are logged on an output channel of the DAS as 5 min. averages corresponding to the 5 min. average voltage responses of the pollutant monitor.

The multipoint calibration data is used by the central computer to determine the instrument's response curve. The ambient data is converted to pollutant concentration using the response curve derived from the multipoint calibration data. And, the span check data is used to ensure that the instrument is holding its calibration. In addition, the low level concentration from the span check data is used by the central computer as a precision check to assess instrument precision as required by federal regulations.

D.2 Calibration System Data

The SAMPLING STATION calibration system is connected to the DAS via a serial cable. The DAS controls the calibration system and receives information from it. All interactions with the calibration system, including entering calibration data, are accomplished through the DAS.

The calibration system has a gas port for zero air and a number of ports for connecting span gas cylinders. The system also contains an ozone generator for the production of known concentrations of ozone. Known concentrations of pollutant gas are generated by accurately diluting known concentrations and flows of span gas from the gas cylinders with known flows of zero air. The system can also generate known concentrations of NO_2 by the Gas Phase Titration (GPT) of NO from a gas cylinder with ozone from the ozone generator. This method is used because NO_2 can not at this time be reliably stored in gas cylinders at the concentrations needed for this application.

The calibration system data includes the following information for each span gas from a cylinder:

-- Pollutant identification
-- Gas cylinder concentration (ppm)
-- Calibration system span gas port number
-- Span gas flow controller calibration information
-- Zero air flow controller calibration information
-- Date and time any of these data were last changed

For ozone, the calibration system data includes information on the calibration of the ozone generator.

D.3 Calibration and Span Check Sequences and Calculating Pollutant Concentration Generated by the Calibration System (done by the SAMPLING STATION DAS)

The calibration system is used during multipoint calibrations and span checks to produce and introduce into the air monitor up to five different concentrations of pollutant gas. One calibration system is used for all monitors. Only one monitor is calibrated at a time. The DAS reports the concentration being generated to the MeteoStar/LEADS system as a 5 min. average concentration on an output channel.

D.3.1 Calibration and Span Check Sequences for non-GPT Channels (CO, O_3, SO_2)

These pollutant concentrations are calculated by the DAS or retrieved from the calibrator by the DAS and reported on the concentration channel in units of ppm. The following sequences are used for calibrations and span checks:

Calibration Sequence for Non-GPT Channels

Step	Span Valve	Time Interva (min.)	Pollutant Channel Code	Conc.* Channel Code & %FS
1	on	25	M	M, 80
2	on	25	R	R, 60
3	on	25	S	S, 40
4	on	25	T	T, 18
5	on	25	G	G, 0
6	off	5	Q	none

Span Check Sequence for Non-GPT Channels

Step	Span Valve	Time Interva (min.)	Pollutant Channel Code	Conc.* Channel Code & %FS
1	on	25	M	M, 80
2	on	25	T	T, 18
3	on	25	G	G, 0
4	off	5	Q	none

*NOTE: The concentrations in these tables are expressed in terms of a percentage of the full-scale range (FS) of the monitor channel being calibrated or checked. The actual concentrations in units of ppm are logged in the concentration channel by the DAS.

D.3.2 Calibration and Span Check Sequences for GPT Channels (NO, NO_2, and NO_x)

Gas Phase Titration ,GPT, is used to generate known concentrations of NO_2 by titrating known concentrations of NO with O_3. The drop in response of the NO channel of the NOx monitor due to the O_3 titration is used to calculate the concentration of NO_2 being generated. The following reaction occurs during this process:

$NO + O_3 \text{ ---> } NO_2 + O_2$

This procedure establishes tracability of the NO_2 channel calibration to the NO gas cylinder.

The concentrations of NO are retrieved from the calibrator by the DAS. The concentration reported on the concentration channel (i.e. NO or NO_2) is dependent on the step in the calibration or span check sequence. Concentrations are logged in units of ppm. The following sequences are used for calibrations and span checks:

Calibration Sequence for GPT Channels

Step	Span Valv	Time Interva (min.)	NO Ch. Code (1)[1]	NO_2 Ch. Code (2)	NO_x Ch. Code (3)	NO_x Conc. (ppm) (4)	NO_2 Conc. (ppm) (5)[2]	O_3 Conc. (ppm) (6)	Conc.[3] Ch. Code & Param. (7)
1	on	25	G	G	G	0	0	0	G, NO
2	on	25	M	M*	M	.470	NA	0	M, NO
3	on	25	M*	M*	M	.470	calc.	.400	M, NO_2
4	on	25	R	R*	R	.370	NA	0	R, NO
5	on	25	R*	R*	R	.370	calc.	.300	R, NO_2
6	on	25	S	S*	S	.270	NA	0	S, NO
7	on	25	S*	S*	S	.270	calc.	.200	S, NO_2
8	on	25	T	T*	T	.160	NA	0	T, NO
9	on	25	T*	T*	T	.160	calc.	.090	T, NO_2
10	off	5	Q	Q	Q	NA	NA	NA	NA

Notes:
1. Table column number
2. The concentrations in this column are calculated from GPT.
3. This column gives the code assigned to the concentration channel and the pollutant whose concentration is being logged. The actual concentrations for this pollutant, in units of ppm, are logged in the concentration channel by the DAS.

Span Check Sequence for GPT Channels

Step	Span Valv	Time Interva (min.)	NO Ch. Code (1)[1]	NO_2 Ch. Code (2)	NO_x Ch. Code (3)	NO Conc. (ppm) (4)	NO_2 Conc. (ppm) (5)[2]	O_3 Conc. (ppm) (6)	Conc.[3] Ch. Code & Param. (7)
1	on	25	G	G	G	0	0	0	G, NO
2	on	25	M	M	M	.470	NA	0	M, NO
3	on	25	M*	M*	M*	.470	calc.	.400	M, NO_2
4	on	25	T	T	T	.160	NA	0	T, NO
5	on	35	T*	T*	T*	.160	calc.	.090	T, NO_2
6	off	15	Q	Q	Q	NA	NA	NA	NA

Notes:
1. Table column number
2. The concentrations in this column are calculated from GPT.
3. This column gives the code assigned to the concentration channel and the pollutant whose concentration is being logged. The actual concentrations for this pollutant, in units of ppm, are logged in the concentration channel by the DAS.

In these calibration and span check sequences, step 1 is used as the zero (G) level for NO, NO_2, & NO_x channels. The untitrated NO steps (i.e. 2, 4, 6, 8 and 2, 4 respectively) are used to calibrate both the NO and the NO_x channels of the NOx monitor. The titrated steps (i.e. 3, 5, 7, 9 and 3, 5 respectively) are used to calibrate the NO_2 channel.

The concentration of NO2 generated during these sequences is calculated by the DAS for each 5 min. period as follows:

Let: $VI_{step,col}$ = 5 min. instrument average response (mv) for columns (col) 1, 2, or 3 in the calibration or span check sequence tables.

$C_{step,col}$ = 5 min. average concentration (ppm) for columns (col) 4, 5, or 7 in the calibration or span check sequence tables.

then: $C_{step,7}$ = $C_{step,4}$ for steps 1, 2, 4, 6, & 8 during a calibration or steps 1, 2, & 4 during a span check.

$C_{step,7}$ = $C_{step,5}$ for steps 3, 5, 7, & 9 during a calibration or steps 3 & 5 during a span check.

$$C_{step,5} = \frac{C_{(step-1),4}\left(VI_{(step-1),1} - VI_{step,1}\right)}{VI_{(step-1),1} - VI_{1,1}} + C\left[NO_2 \text{ from Cyl.}\right]_{(step-1)}$$

for steps 3, 5, 7, & 9 during a calibration or steps 3 & 5 during a span check.

where: $C[NO_2$ from Cyl.] = the concentration of NO_2 calculated by the DAS due to the NO_2 impurity in the NO span gas cylinder.

D.4 Multipoint Calibration (done by the central computer)

The multipoint calibration consists of finding the instrument's response to five equally spaced levels of pollutant gas from the calibration system. The results of this calibration are then used to convert the instrument's response to concentration. To ensure that the calibration is meaningful, several tests need to be made on the data. The central computer performs these tests.

D.4.1 Completeness Test

For each concentration level coded M, R, S, T, or G, there should be seven consecutive, correctly coded (i.e. no "P" codes) five-minute updates of instrument response data and concentration data. If this is not true, the test is failed and the multipoint calibration data cannot be processed.

D.4.2 Outlier Test and Average Instrument Response Calculations (Completeness Test Passed)

The outlier test requires that no one five-minute update used to form an average instrument response is more than an allowed deviation from the average. This test should detect problems such as long instrument rise-time and erratic instrument response.

Let: VI_i = instrument response (mv) for any update, i = 1 to 7 of any code M, R, S, T, or G

$\overline{VI}$ = average instrument response for any code M, R, S, T, or G (mv)

d2 = allowed deviation of any VI_i from the mean (mv).

Do: $$D_i = VI_i - \frac{\sum_{j=4}^{7} VI_j}{4} \quad \text{for i = 4 through 7.}$$

Let: D_m = the maximum deviation of D_i from zero.

If: $|D_m| \leq d2$

then: $\overline{VI} = \frac{\sum_{j=4}^{7} VI_j}{4}$

If not: VI_m = value which failed, subscript m.

Do: $D_i = VI_i - \frac{\sum_{j=4}^{7} VI_j - VI_m}{3}$ for i = 4 through 7 not m.

Let: D_n = the maximum deviation of D_i from zero.

If: $|D_n| \leq d2$

then: $\overline{VI} = \frac{\sum_{j=4}^{7} VI_j - VI_m}{3}$

If not, then the outlier test is failed and the calibration as a whole is failed.

D.4.3 Concentration Outlier and Spacing Tests

These tests check the stability and spacing of the concentration levels generated by the SAMPLING STATION calibration system.

D.4.3.1 Concentration Outlier Test

The concentration outlier test requires that no one five-minute update used to form an average concentration is more than an allowed deviation from the average. This test should detect problems such as an unstable calibration system.

Let: c_i = concentration for any update, i = 1 to 7 of any code M, R, S, T, or G

C = average concentration for any code M, R, S, T, or G (mv)

d1 = allowed deviation of any c_i from the mean (mv).

$$\text{Do:} \quad D_i = c_i - \frac{\sum_{j=4}^{7} c_j}{4} \quad \text{for i = 4 through 7.}$$

Let: D_m = the maximum deviation of D_i from zero.

If: $|D_m| \leq d1$

$$\text{then:} \quad C = \frac{\sum_{j=4}^{7} c_j}{4}$$

If not: c_m = value which failed, subscript m.

$$\text{Do:} \quad D_i = c_i - \frac{\sum_{j=4}^{7} c_j - c_m}{3} \quad \text{for i = 4 through 7 not m.}$$

Let: D_n = the maximum deviation of D_i from zero.

If: $|D_n| \leq d1$

$$\text{then:} \quad C = \frac{\sum_{j=4}^{7} c_j - c_m}{3}$$

If not, then the outlier test is failed and the calibration is invalid.

D.4.3.2 Concentration Spacing Test

In order to get a good multipoint calibration, the five pollutant concentrations generated by the calibration system need to be evenly spaced throughout the instrument's range. The ideal concentration for each pollutant and each level is given in the following table.

Ideal Concentrations (ppm)

Level	NO & NOx only	O_3, NO_2, SO_2	CO
M	.470	.4	40.0
R	.370	.3	30.0
S	.270	.2	20.0
T	.160	.09	9.0
G	0	0	0

To assure even spacing, each pollutant concentration generated by the calibration system should be required to be within the following limits:

Let: dw1 = warning limit for the generated concentration from ideal (ppm)

dc1 = control limit for the generated concentration from ideal (ppm)

$Ideal_i$ = Ideal concentration (ppm) for the i'th level and pollutant of interest where i = 1 to 5 corresponding to data coded M, R, S, T, and G, respectively.

C_i = the i'th calibration gas concentration (ppm) where i = 1 to 5 corresponding to data coded M, R, S, T, and G, respectively.

Do: $D_i = C_i - Ideal_i$, for i = 1 through 4.

Let: D_P = maximum deviation of D_i from zero where i = 1 through 4.

If: $|D_p| > dc1$

then the concentration test is failed and the calibration is invalid. If not, then continue.

If: $|D_p| > dw1$

then the warning limit is exceeded but the calibration is valid. If not, then the concentration test is passed with no warning.

D.4.4 Slope and Intercept Calculation

All instruments considered in this document are assumed to be linear with a response given by:

$$\overline{VI} = A \times C + B$$

Where: $\overline{VI}$ = average instrument response (mv) to any concentration, C (ppm), between zero and instrument full scale

A = slope of line (mv/ppm)

B = the y intercept (mv) of the line.

Using the method of least squares, the slope, A, and intercept, B, of the instrument response curve is calculated from the calibration data as follows:

Let: C_i = the average concentration of pollutant gas (ppm) from the calibration system where i = 1 through 5 corresponding to data coded M, R, S, T, or G respectively

$\overline{VI}_i$ = the average instrument response (mv) corresponding to the pollutant input, C_i

N = number of calibration points (5).

Then: $$A = \frac{N\sum_{i=1}^{N} C_i \overline{VI}_i - \left(\sum_{i=1}^{N} C_i\right)\left(\sum_{i=1}^{N} \overline{VI}_i\right)}{N\sum_{i=1}^{N} C_i^2 - \left(\sum_{i=1}^{N} C_i\right)^2}$$

and $$B = \frac{\left(\sum_{i=1}^{N} \overline{VI}_i\right)\left(\sum_{i=1}^{N} C_i^2\right) - \left(\sum_{i=1}^{N} C_i \overline{VI}_i\right)\left(\sum_{i=1}^{N} C_i\right)}{N\sum_{i=1}^{N} C_i^2 - \left(\sum_{i=1}^{N} C_i\right)^2} .$$

D.4.5 Slope and Intercept Tests

These tests are designed to determine if the instrument is operating within its design specifications.

Let:
dw2 = warning limit for slope (mv/ppm)
dc2 = control limit for slope (mv/ppm)
dw3 = warning limit for intercept (mv)
dc3 = control limit for intercept (mv)
CFS = instrument full-scale concentration (ppm)
DS = the difference between the measured slope, A, and the ideal slope = (A - 1000/CFS) (mv/ppm).

D.4.5.1 Slope Test

If: $|DS| > dc2$

then the slope test is failed and the calibration as a whole is failed. If not, then continue:

If: $|DS| > dw2$

then the warning limit is exceed but the calibration is valid. If not, then the slope test is passed with no warning.

D.4.5.2 Intercept Test

If: $|B| > dc3$

then the intercept test is failed and the calibration as a whole is failed. If not, then continue:

If: $|B| > dw3$

then the warning limit is exceed but the calibration is valid. If not, then the intercept test is passed with no warning.

D.4.6 Precision/Linearity Tests

This test is designed to determine if the instrument has a stable, linear response curve by measuring the distance of each calibration point from the regression line.

Let: dw4 = warning limit for precision/linearity (mv)
dc4 = control limit for precision/linearity (mv)

Do: $D_i = [VI_i - (A\ C_i + B)]$ for i = 1 through 5.

Let: DI = maximum deviation of D_i from zero.

If: $|DI| > dc4$

then the precision/linearity test is failed and the calibration as a whole is failed. If not, then continue:

If: $|DI| > dw4$

then the warning limit is exceeded but the calibration is valid. If not, then the test is passed with no warning.

D.4.7 Zero and Span Tests

These two tests are designed to see if the instrument's calibration is holding since the last calibration or span check.

Provision will need to be made to disable these tests or put in dummy past values if this is the first calibration for a given instrument and SAMPLING STATION. If not, the failure of either or both of these tests would require the central computer to reject ambient data that is not yet in existence.

Let: dw5 = warning limit for zero test (mv)

dc5 = control limit for zero test (mv)

$\overline{VI}_5'$ = average instrument response to G level concentration during the previous calibration (mv)

DZ = the difference between the current G level voltage and the previous calibration's G level voltage (mv)

$= \overline{VI}_5 - \overline{VI}_5'$

dw6 = warning limit for span test (mv)

dc6 = control limit for span test (mv)

$\overline{VI}_1'$ = average instrument response to M level concentration during the previous calibration (mv)

C_i' = M level concentration during the previous calibration (ppm)

DR = the difference between the current M level voltage (mv) and the previous calibration's M level voltage corrected for M level concentration changes

$$= \overline{VI}_1 - \frac{(\overline{VI}_1' - \overline{VI}_5')C_i}{C_i'} - \overline{VI}_5' .$$

D.4.7.1 Zero Test

If: $|DZ| > dc5$

then the zero test is failed and the ambient data back to the last good span check or calibration should be rejected. If not, then continue:

If: $|DZ| > dw5$

then the warning limit is exceeded but no data should be rejected. If not, then the zero test is passed with no warning.

D.4.7.2 Span Test

If: $|DR| > dc6$

then the span test is failed and the ambient data back to the last good span check or calibration should be rejected. If not, then continue:

If: $|DR| > dw6$

then the warning limit is exceeded but no data should be rejected. If not, then the span test is passed with no warning.

D.4.8 NO_x Monitor Channel Balance Test

This test is done only when processing NO_x monitor calibrations or span checks. The test measures the electronic and flow balance between the NO and the NO_x channels of chemiluminescence type NO_x monitors. This test affects the validity of only the NO_2 channel calibration.

Let: $\overline{VI}_{step,col}$ = average instrument response (mv) for columns 1, 2, or 3 in the calibration or span check sequence tables (section **D**.3.2). Averages are calculated in section **D**.4.2

dw8 = warning limit for balance test (mv)

dc8 = control limit for balance test (mv)

Bal_{step} = an index for NOx monitor channel balance.

Do: $Bal_{step} = 1000\frac{\left(VI_{step,2} - VI_{1,2}\right)}{\left(VI_{step,1} - VI_{1,1}\right)}$ for steps 2, 4, 6, & 8.

Let: Dbal = maximum deviation of Bal_{step} from zero.

If: $|Dbal| > dc8$

then the balance test is failed and the calibration of the NO_2 channel is failed. If not, then continue:

If: $|Dbal| > dw8$

then the warning limit is exceeded but the calibration is valid. If not, then the test is passed with no warning.

D.4.9 NO_x Monitor Converter Efficiency Test

This test is done only when processing NO_x monitor calibrations or span checks. The test measures the efficiency of the NO_2 to NO converter used in chemiluminescence type NO_x monitors. This test affects the validity of the NO_2 and NO_x channel calibrations.

Let: $\overline{VI}_{step,col}$ = average instrument response (mv) for columns 1, 2, or 3 in the calibration or span check sequence tables (section **D**.3.2). Averages are calculated in section **D**.4.2

dw9 = warning limit for efficiency test (mv)

dc9 = control limit for efficiency test (mv)

E_{step} = efficiency of the NOx converter.

$$E_{step} = 100 \times \left[1 - \left(\frac{\overline{VI}_{step-1,1} - \overline{VI}_{1,1}}{\overline{VI}_{step-1,1} - \overline{VI}_{step,1}}\right) \times \left(\frac{\overline{VI}_{step-1,3} - \overline{VI}_{step,3}}{\overline{VI}_{step-1,3} - \overline{VI}_{1,3}}\right)\right]$$

for steps 3, 5, 7, &9.

Do: D_{step} = $(100 - E_{step})$ for steps 3, 5, 7, &9.

Let: De = maximum deviation of D_{step} from zero.

If: $|De| > dc9$

then the efficiency test is failed and the calibrations of the NO_2 and NO_x channels are failed. If not, then continue:

If: $|De| > dw9$

then the warning limit is exceeded but the calibration is valid. If not, then the test is passed with no warning.

D.5 Span Check (done by the central computer)

The span check is a quality control activity that is performed by the DAS as scheduled by the DAS operator. This check is used to ensure that the previous calibration of the instrument is still good. The span check consists of admitting M, T, and G coded gas

concentrations into the instrument and performing the following tests on the instrument's response. These tests are performed by the central computer.

D.5.1 Completeness Test

This test is the same as in Part **D**.4.1. If this test is failed, then the span check data cannot be processed.

D.5.2 Outlier Test and Average Instrument Response Calculations (Completeness Test Passed)

This test is the same as in Part **D**.4.2. If this test is failed, then the span check as a whole fails.

D.5.3 Concentration Outlier and Spacing Tests

These tests are the same as in Part **D**.4.3, except only concentrations coded M and T are tested. This corresponds to i = 1 and 4. If this test is failed, the span check is invalid.

D.5.4 Zero and Span Tests

These tests are the same as in Part **D**.4.7.

D.5.5 Linearity Test

This test is designed to determine if the instrument is linear at the time of the span check. This is done by calculating the deviation of the instrument response to the T coded concentration, C_4, from the response predicted by interpolation between the span check data points (C_5, $\overline{VI}_5$) and (C_1, $\overline{VI}_1$).

Let: dw7 = warning limit for linearity test (mv)
dc7 = control limits for linearity test (mv)
DL = the difference between the T level voltage (mv) and the interpolated T level voltage at the T level concentration

$$= \overline{VI}_4 - \frac{(\overline{VI}_1 - \overline{VI}_5)C_4}{C_1} - \overline{VI}_5 .$$

If: $|DL| > dc7$

then the linearity test is failed and ambient data should be rejected back to the last good span check or calibration and forward to the next good calibration. If not, then continue:

If: $|DL| > dw7$

then the warning limit is exceeded but no data should be rejected. If not, then the linearity test is passed with no warning.

D.5.6 NOx Monitor Channel Balance Test

This test is the same as in Part **D**.4.8, except only step = 2 and 4 are used in the calculation of Bal_{step}.

D.5.7 NOx Monitor Converter Efficiency Test

This test is the same as in Part **D**.4.9, except only step = 3 and 5 are used in the calculation of E_{step} and D_{step}.

D.6 Calculating Ambient Concentration (ppm)

TCEQ original Method:

Given the calibration curve derived during the most recent calibration:

$$\overline{VI} = A C + B$$

where the symbols are defined as in **D**.4.4. Solving for the concentration:

$$C = \frac{\overline{VI} - B}{A}$$

Equation (2): APM-2 Method

C = concentration

$\overline{VI}$ = measured voltage
A = mathematically calculated slope established by a calibration
B = mathematically calculated intercept established by a calibration
V_G = measured response at zero level (clean air)

$$C = \frac{\overline{VI} - V_G}{A}$$

APM-2 will use V_G from either a 5-point calibration or a 3-point span check and adjust the intercept in the equation above.

D.7 Data Flow and Logic

This section details what the central computer does, based on the results of the various tests described above. The data flow and logic given applies individually to every pollutant considered in this document.

First, the tests already described are summarized, numbered, and located :

Test No.	Test	Found
T1	Instrument response & conc. data completeness	D.4.1, D.5.1
T2	Instrument response data outlier	D.4.2, D.5.2
T3	Concentration Outlier	D.4.3.1, D.5.3.1
T4	Concentration Spacing	D.4.3.2, D.5.3.2
T5	Slope	D.4.5.1
T6	Intercept	D.4.5.2
T7	Precision/Linearity	D.4.6
T8	Zero	D.4.7.1, D.5.4
T9	Span	D.4.7.2, D.5.4
T10	Linearity	D.5.5
T11	NOx Monitor channel balance	D.4.8, D.5.6
T12	NOx Monitor converter efficiency	D.4.9, D.5.7

Assume that the central computer has received all of the data from the microcomputer from one calibration to the next. Also, let the following flags be set (1) or removed (0) based on the results of the tests. The computer will then take action based on the condition of the flags at the end of processing each set of calibration or span check data.

F1 (1) Reject ambient data back to last good calibration or span check.
F1 (0) Accept ambient data back to the last span or calibration.
F2 (1) Reject ambient data forward to the next good calibration.
F2 (0) Accept ambient data forward to the next good span or calibration.
F3 (1) Calibration or Span check results invalid.
F3 (0) Calibration or Span check results valid.

The central computer makes decisions affecting the ambient data based only on whether or not a test is failed (i.e., the control limit is exceeded). The warning limit is part of a test only to signal appropriate personnel that the parameter tested is drifting outside of its expected operating limits and that something should be done to correct the problem. With this in mind, the following data flowchart will consider if a test is passed or failed based on the control limits.

D.7.1 Process Multipoint Calibration Data

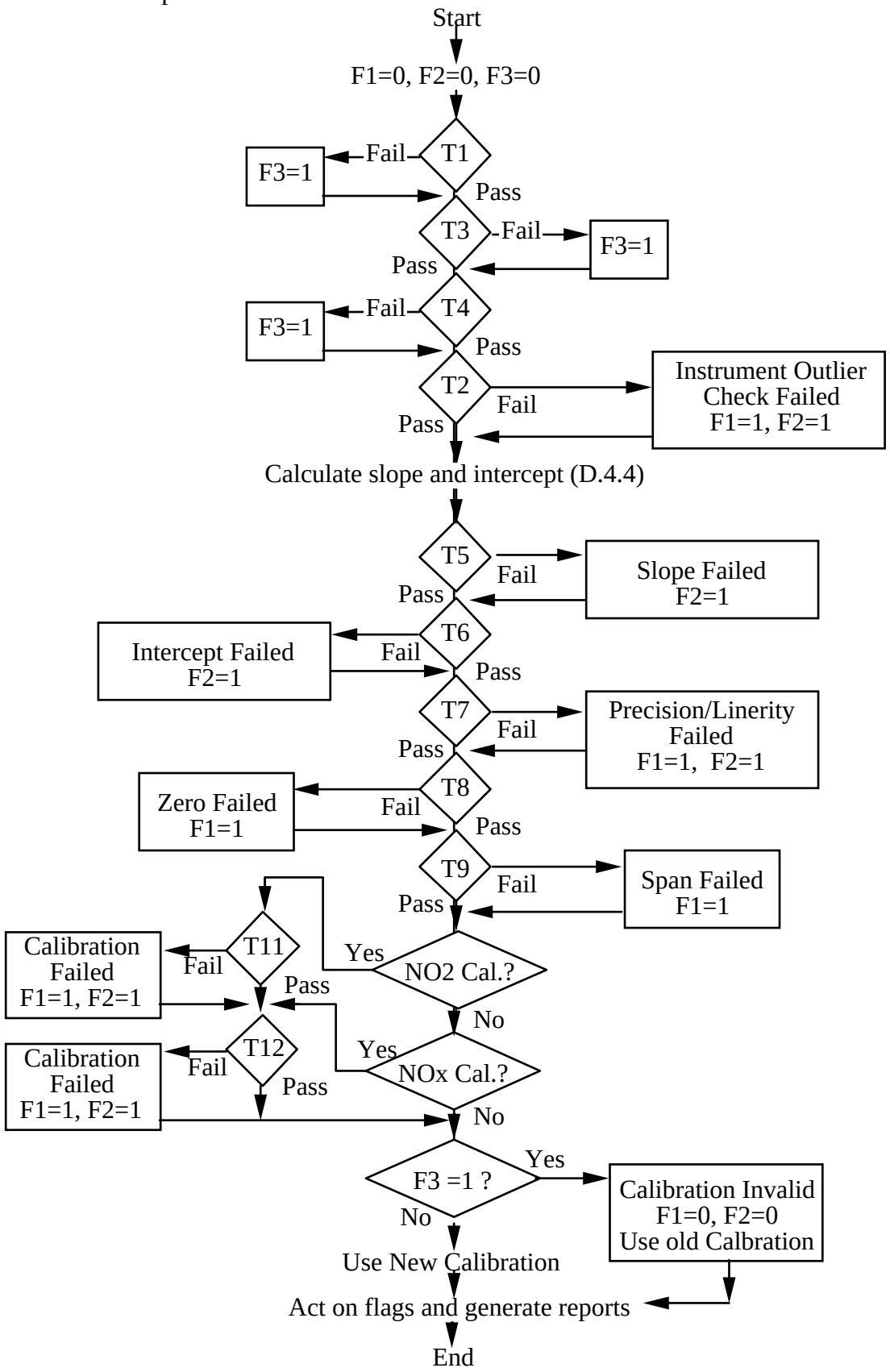

D.7.2 Process Span Check Data

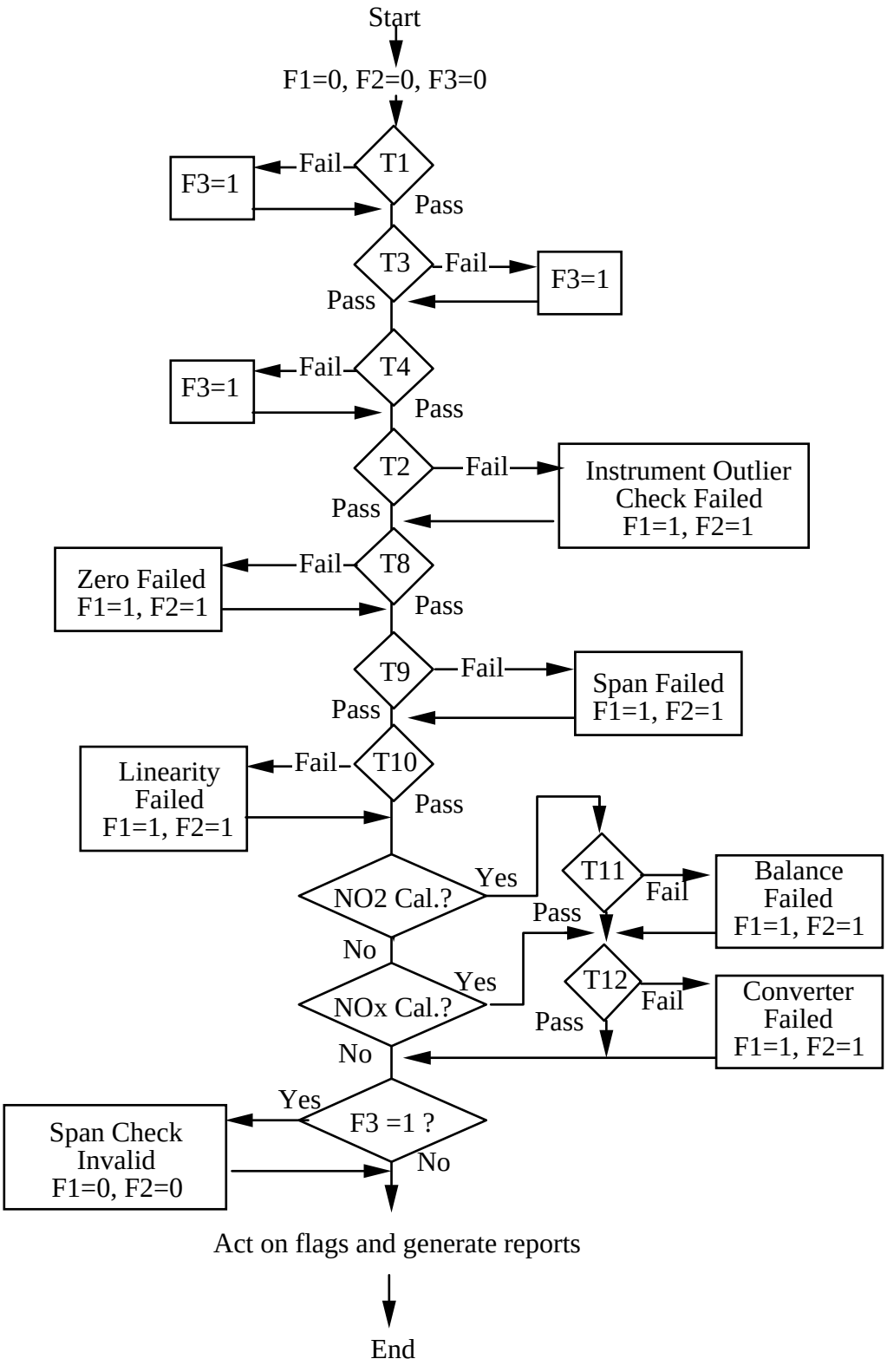

D.7.3 Overall Data Processing

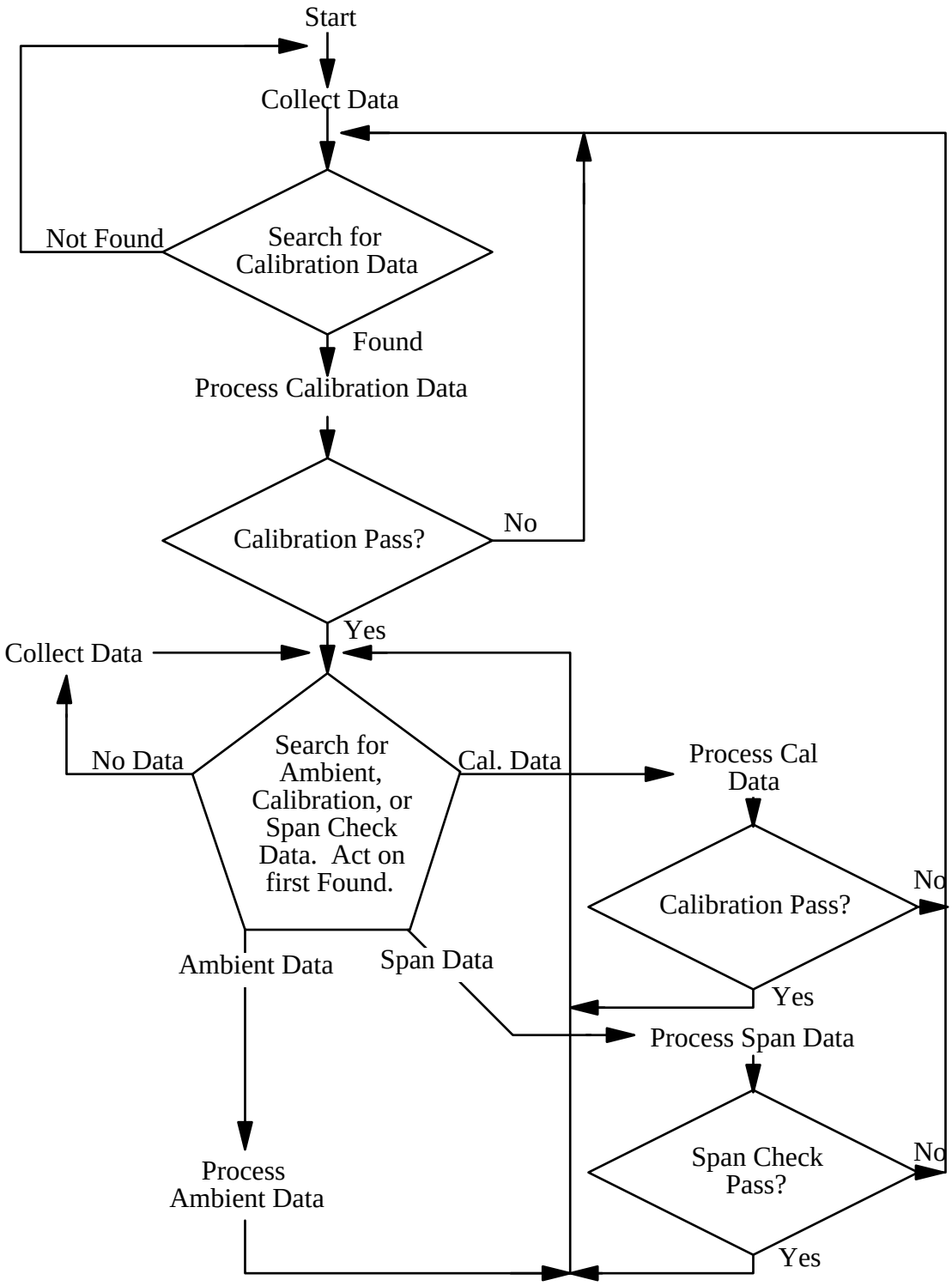

D.8 List of Symbols

Symbol	Description	Section
M, R, S, T, G	Instrument response and concentration data letter codes corresponding to a different pollutant concentration for each code	D.3.4
VI_i	Instrument response (mv) for any update, i = 1 through 7, of any code M, R, S, T, or G	D.4.2
$\overline{VI}$	Average instrument response (mv) for any update, i = 1 through 7, of any code M, R, S, T, or G	D.4.2
d2	Allowed deviation of any VI_i from the mean (mv)	D.4.2
D_m	The maximum instrument deviation using four updates	D.4.2
D_n	The maximum instrument deviation using three updates	D.4.2
dw1	Warning limit for generated concentration from ideal (ppm)	D.4.3
dc1	Control limit for generated concentration from ideal (ppm)	D.4.3
Dp	Maximum concentration difference of C_i from ideal	D.4.3
A	Slope of calibration line (mv/ppm)	D.4.4
B	Intercept of calibration line (mv)	D.4.4
C	Any concentration between zero and instrument full scale	D.4.4
$\overline{VI}_i$	Average instrument response (mv) corresponding to C_i	D.4.4
N	Number of calibration points	D.4.4
dw2	Warning limit for slope (mv/ppm)	D.4.5
dc2	Control limit for slope (mv/ppm)	D.4.5
dw3	Warning limit for intercept (mv)	D.4.5
dc3	Control limit for intercept (mv)	D.4.5
CFS	Instrument full scale concentration (ppm)	D.4.5

DS	Deviation of slope from ideal (mv/ppm)	D.4.5
dw4	Warning limit for precision/linearity test (mv)	D.4.6
Symbol	Description	Section
dc4	Control limit for precision/linearity test (mv)	D.4.6
DI	Maximum precision/linearity difference measured (mv)	D.4.6
dw5	Warning limit for zero test (mv)	D.4.7
dc5	Control limit for zero test (mv)	D.4.7
DZ	Measured deviation of zero from ideal (mv)	D.4.7
dw6	Warning limit for span test (mv)	D.4.7
dc6	Control limit for span test (mv)	D.4.7
DR	Measured deviation of span from ideal (mv)	D.4.7
dw7	Warning limit for linearity test (mv)	D.5.5
dc7	Control limit for linearity test (mv)	D.5.5
DL	Measured nonlinearity (mv)	D.5.5

Appendix K is not used for this Project

SUTRON'S

METEOSTAR/LEADS WEB PAGE PRIMER

This is a quick introduction to the statewide Continuous Ambient Monitoring Station (SAMPLING STATION) monitoring network information that is available via the Internet.

System Requirements

Basic requirements to get to the web pages are: a computer, an Internet connection, and a web browser.

The complete set of web pages is currently available only from within the Sutron's firewall. -

In order to properly view the web pages, you will need Netscape Navigator 3.0 or higher. Versions 4.51 or 4.7x are preferred. The web pages make extensive use of tables and cell shading which are not supported in earlier versions of the web browsers. Microsoft Internet Explorer 3.0 or higher works, but has not been extensively tested. MSIE 5.0 **CANNOT** display some of the internal pages correctly – there is a bug (feature?) in the browser that causes it to time out before the page is displayed.

Web Page Locations

The internal Sutron MeteoStar web pages (behind the firewall) are all accessed from one main page. The URL (Uniform Resource Locator) for the main web page is:

```
http://longhorn.tx.sutron.local
```

Enter this in the "date and time" entry window in Netscape. The main Sutron MeteoStar web page will be loaded. This page is called "UT CEER Special Study"

Web Page Background

The web pages were developed jointly by Tracor and IPS MeteoStar. IPS MeteoStar developed and installed the MeteoStar system that collects and processes the raw pollution information. IPS MeteoStar has taken over maintenance and further development of the database and web pages initially developed by Tracor. Information from the MeteoStar system is transferred to a database that is maintained on the web server. The web pages use data from this database as well as the primary MeteoStar databases to produce reports.

The fundamental difference between web pages developed by the two companies is the timeliness of the data available. The Tracor-developed web pages are based on data that is transferred once a day (early in the morning) - with the exception of the Air Quality Index (AQI) report, which is real-time. The IPS MeteoStar web pages access system data as soon as it becomes available in real-time. The Tracor-developed web pages allow thorough review and analysis of historical data spanning arbitrary time spans. The IPS MeteoStar web pages allow real-time review of data and system performance monitoring. IPS MeteoStar is currently in the process of transforming all of the non-real-time web pages into real-time web pages.

The external web pages offer the public access to much of the same information available internally. However, due to security considerations and the firewall implementation, the underlying data that the external web pages is based on is only updated once every thirty minutes outside the firewall. There can be significant delays between what is available externally and what is visible inside the firewall. For instance, MeteoStar exports hourly averages once an hour at 15 minutes past the hour. These averages are available immediately inside the firewall. These same averages eventually make their way outside the firewall during the scheduled data transfer at 30 minutes past the hour. This data transfer can take 10 to 15 minutes to complete due to the huge volume of data that must be transferred (not just MeteoStar data). This means the hourly averages on the external web pages are almost always 30 to 45 minutes older than what is available internally.

Synopsis of Available Reports

LEADS Network Status Reports - Non-real-time data. This is a family of reports that provide a variety of information about Sutron's MeteoStar monitoring network. This is the primary tool used for reviewing calibrations and spans. This report can span any arbitrary time period. The reports available under this include:

Calibration Results - A highly detailed calibration report for a specific pollutant. All the measurements and tests performed on the measurements are summarized. You can view previous calibrations to catch instrument drift trends.

Span Check Results - A highly detailed span check report for a specific pollutant. All the measurements and tests performed on the measurements are summarized. You can view previous span checks to catch instrument drift trends.

Span-Zero Results - A highly detailed span-zero report for a specific pollutant. All the measurements and tests performed on the measurements are summarized. You can view previous span-zeros to catch instrument drift trends.

High Values - A summary of any high values measured for a specific pollutant. This report covers the time period and stations you initially selected.

Data Loss - A summary of all data lost and the reason for the data loss. This report covers the time period and stations you initially selected.

Cal/Span Acceptance - A summary of all the calibrations and span checks performed for all pollutants covering the time period you initially selected. From this report, you can select to view detailed reports. This is especially useful when trying to track down instrument problems.

SAMPLING STATION Average Sum Pollutant Summary - Non-real-time data. This produces a very detailed report with many statistics about the data. You select a time range and a pollutant. This report can take a very long time to create if you select a large time span or a large number of sites.

Data Return - Non-real-time data. This report produces a detailed report with statistics about selected pollution and meteorological parameters and is based on the same data used to generate the Data Loss report. You select a time range and stations to report over. This is useful for tracking required data return rates.

Data Loss - Non-real-time data. This is the same report available under the LEADS Network Status Web Pages. Produces a very detailed report with many statistics about data loss and is based on the same data use to generate the Data Return report. You select a time range and stations to report over. This is useful for tracking required data return rates.

High Values – Non-real-time data. This is the same report available under the LEADS Network Status Web Pages. A summary of any high values measured for a specific pollutant. This report covers the time period and stations you initially selected.

Ozone Exceedance - Real-time data. This produces a detailed report of all one-hour Ozone exceedances for a specified year. (The current year is reported as year-to-date). The maximum

values for each day of exceedance and the number of hours of exceedance are tabulated. You may sort this report by various columns.

AQS Precision Transactions File - Non-real-time data. This produces an AQS Precision Transaction file suitable for submittal to the EPA. This file is a measure of the precision accuracy of the instruments based on the "T" level measurements during span checks. Summaries of precision tests are also generated.

Cal/Span History – Non-real-time data. Produces a report similar to the Cal/Span Acceptance web page that displays pertinent information about cals, spans, and span-zeros. You can specify any arbitrary date range, pick which sites to report over, and restrict the report to specific parameters or types of calibrations.

Last Cal/Span Report – Real-time data. Produces a report showing the last cals or spans performed. You can limit the report to a specific region or types of sites. Currently provides a subset of the cal/span data shown on the Cal/Span Acceptance Report or the Cal/Span History page.

Graphical SAMPLING STATION Data – Real-time data. Produces graphical displays of one-hour averages of any parameter. You can graph data over any date range you desire – a day, a week, a month, a year, several years. The only real limitation on how much data you can graph is the computer you use to view the data. All processing is done on your computer – so viewing lots of data can take a while on older, slower machines.

Current Hourly Averages By Parameter - Real-time data. This report is based on the hourly averages automatically created by MeteoStar. Hourly averages are created at 15 minutes past the hour. The Current Hourly Average Report covers one parameter (either a pollutant or a weather parameter) for one day (user specified). This allows quick review of the entire network of sensors. The maximum value for the day is highlighted and a table of the previous day's maximum value and when it occurred is attached.

SAMPLING STATION Hourly Averages By Site - Real-time data. This report is also based on the hourly averages created by MeteoStar. This report covers all parameters at a particular SAMPLING STATION (user specified) for one day (user specified). This allows a quick review of all instruments at a particular site. It is also possible to spot interactions such as strange Ozone readings caused by extreme internal station temperature (either too hot or too cold). This is called "Data by Day by Site (all parameters)" on the external web page.

AQI (Air Quality Index) Ratings - Real-time data. AQI is the new EPA incarnation of the Pollutant Standards Index (PSI). Each hour, MeteoStar calculates the maximum one-hour Ozone average, the maximum running eight-hour average of Ozone for each day, the maximum running eight-hour average of CO for each day, and the maximum daily average of Sulfur Dioxide, PM_{10} and $PM_{2.5}$ at each site where these parameters are measured. The values for the current day represent data from midnight to the current time. This report summarizes and groups this information into metropolitan areas. The concentrations are converted to AQI values (an AQI of 100 corresponds to the EPA exceedance value for a particular pollutant). This report is

extremely useful during Ozone season. It is also useful as a quick check of the status of the data ingest processing of MeteoStar. From this web page you can access historical AQI information as well. This is called "Peak Air Pollutant Concentrations (The AQI Report)" on the external web page. *This report only uses data provided by the MeteoStar system.* This web page will also produce a summary report by individual site within a region.

Pollution Data By Parameter Report - Real-time data. Through this web page you can view either 5-minute averages or hourly averages for a single parameter at a site. This is essentially a dump of the MeteoStar database and contains many parameter flags that cannot be viewed directly by other tools. This report can be output in a comma-delimited format for pasting into spreadsheets.

SAMPLING STATION Data Printout - Real-time data. Through this web page you can view either 5-minute averages or hourly averages for all parameters measured at a site. This is essentially a dump of the MeteoStar database. This report does not contain the level of detail that the Pollution Data by Parameter Report does. This report can be output in a comma-delimited format for pasting into spreadsheets.

Monthly Summary Report - Real-time data. Provides a monthly summary of any or all parameters measured at a site for a selected month. The web page allows you to select a variety of statistical values that can be included in the report. This report can be output in a comma-delimited format for pasting into spreadsheets or as a Rich Text Format (RTF) stream that will feed directly into a word processor. This is called "Data by Month by Site by Parameter" on the external web page.

Five-Minute Quick Look – Real-time data. The Five-Minute Quick Look covers one parameter (either a pollutant or a weather parameter) for 2 to 6 hours (user specified). This allows quick review of the entire network of sensors. If you select ozone (the default), any five-minute averages greater than 125 ppb are highlighted in red.

Ozone Action Day Forecast - Just what it claims to be. A summary of forecasted ozone action days. The current day's (up to current time) and previous day's eight-hour peak ozone concentrations and one-hour peak ozone concentrations are also shown.

Missing/Unexpected Data – Real-time data. Allows you to see several different things related to missing data – which sites are not reporting any data at all and/or which parameters are not flagged ambient (failed cals, spans, maintenance, etc.). The Unexpected data option will highlight system configuration problems – channel definitions missing, Zeno programming errors, etc.

AutoGC Data – Real-time data. A family of reports for viewing AutoGC data.

> Current Hourly Averages by Parameter - Real-time data. This report is based on the values reported by the automated gas chromatograph sites. These are reported once an hour. The Current Hourly Averages by Parameter report covers one parameter (any of the AutoGC components) for one day (user specified). This allows quick review of the entire network of sensors. The maximum value for the day is highlighted and any values exceeding odor or health thresholds are also highlighted.

Hourly Averages by Site - Real-time data. This report is based on the values reported by the automated gas chromatograph sites. These are reported once an hour. The Hourly Averages by Site report covers one site (user selected) for one day (user specified). This allows quick review of any or all of the compounds measured at that site. The maximum value for the day for each compound is highlighted and any values exceeding odor or health thresholds are also highlighted.

Monthly Summary - Real-time data. This report is based on the values reported by the automated gas chromatograph sites. These are reported once an hour. Monthly Summary report covers one site (user selected) for one month (user specified). Any or all of the compounds measured at the site can be included in the report. The maximum value for the day for each compound is highlighted and any values exceeding odor or health thresholds are also highlighted. Daily and monthly statistics are also calculated

Data Extractor. Real-time data. A tool for retrieving data spanning large date ranges. This report tool is very flexible and user configurable.

Ozone 8-Hour 4 Highest - A report spanning from the beginning of the year (that you select) to either the end of the year, or the current date (for the current year). This report shows the 4 highest 8-hour running averages calculated at each site and the date and time they occurred. Any average that is above 85 ppb is highlighted. The data this report is based on is automatically generated each hour. This report is called "Four highest eight-hour ozone concentrations" and is accessed from the "Eight-Hour Ozone Information and Data" link on the external web page.

Ozone 8-Hour Monthly Summary - A monthly summary of the peak daily 8-hour ozone averages calculated at each site that monitors ozone. Any average that is above 85 ppb is highlighted. The data this report is based on is automatically generated each hour. This report is called "Monthly summaries of daily 8-hr maximum ozone concentrations" and is accessed from the "Eight-Hour Ozone Information and Data" link on the external web page.

Ozone 8-Hour High Value Days - A summary of any daily 8-hour ozone averages that are above 85 ppb. The date and time of the high values are shown. The data this report is based on is automatically generated each hour. This report is called "Eight-hour ozone concentrations that meet or exceed 85 parts per billion" and is accessed from the "Eight-Hour Ozone Information and Data" link on the external web page. You can sort by various columns.

8-Hour Ozone Attainment - A summary that shows how each site that measures ozone is doing compared to the 8-hour EPA standard. The fourth highest 8-hour ozone average at each site for three years is displayed along with the three-year average of these.

Ozone Warnings - A web page that summarizes the current status of Ozone Warnings that have been issued by the TCEQ. Currently only Houston and Dallas-Fort Worth participate in the ozone warning program.

Map of Current Ozone Levels – Real-time data. Tied to the Ozone Warning system. A set of images created once an hour for almost all regions that measure ozone. The colors used to highlight the latest hourly averages are identical to the Ozone Warning colors.

Peak One-Hour Ozone – Non-real-time data. Produces a monthly summary report of the peak one-hour averages of ozone reported at each the test site. You can specify the month and year the report covers.

Ozone Summary – Real-time data. Produces a yearly summary report of the any one-hour averages of ozone that exceed 125 ppb and any eight-hour averages of ozone that exceed 85 ppb. The highest one-hour and eight-hour averages are shown along with the date/time of occurrence.

Data Connections - Real-time data. A family of reports that provide detailed information about communications (both modem and network) within the MeteoStar system.

Comms Problems – This web page displays any site that has not reported data within the last 2 – 3 hours. It attempts to analyze and suggest remedies for any problems it finds. This report can pinpoint comms problems to either a modem at a site or a modem at one of the regional computers.

Comms Report - A summary of the phone communications from the regional office to each monitoring site. The phone communications data is gathered from the regional offices and requires the wide area network to be up. The MeteoStar system makes 96 phone calls to each site per day (once every 15 minutes).

Detailed Comms Report – A closer view of the phone communications from the regional office to each monitoring site. This report can be used to pinpoint comms problems to within a 15-minute window.

Connectivity – A snapshot of the modem connectivity parameters and settings on the hub computers that is generated the moment you select this page. Used by MeteoStar support personnel in Austin to maintain and tweak the modems and phone numbers.

Network Status – A near real-time connectivity report that details the wide area network (used to transfer data from each regional office to Austin). This status is automatically checked once an hour.

Instant Net Status – A snapshot of the network connectivity for the wide-area network that is generated the moment you select this page. Used by MeteoStar support personnel in Austin to monitor the health of MeteoStar. The advantage of this over the "Wide-Area Network Status" web page is the timeliness of the data.

Raw Comms Log – The raw data file that is rolled up into the Comms Report. Primarily of use to system support personnel when troubleshooting phone line problems.

Log Files - Real-time data. A family of reports that allow viewing of the various log files generated in the MeteoStar system.

Hub Error Logs – The regional hub computers examine each 5-minute sample that is gathered from the Zeno dataloggers. A database of detected errors is maintained on each regional hub computer. This web page produces a report from this database. The regional hub computer can detect data sequencing problems (gaps in the data stream or data received out of order), and also decodes the 32-Bit error word the Zeno datalogger attaches to each data sample.

Operator Logs – The Zeno dataloggers installed at the monitoring sites contain an electronic operator log. This can be used by the SAMPLING STATION operators to send messages to the validators or to explain extenuating circumstances (such as a calibration cylinder ran dry, etc.). Operator log entries can be entered locally at the station (via a terminal interface) or remotely from anywhere via modem. You can view the operator logs from any SAMPLING STATION. The web page also supports direct entry of operator logs.

Validator Notes – Real-time data. This web page allows you to view the validator notes for any site/parameter/date combination that you select. The validator notes are contained in the audit trail files that are automatically updated whenever data is validated. Validators can also manually insert validator notes at any time.

Error Word Decoder. This web page allows you to type in an error word as reported by the Zeno datalogger. The web page will display which BITs are set in the entered error word.

MeteoStar Configuration - Real-time data. A family of reports that show the contents of the MeteoStar system configuration files. In order for MeteoStar to ingest and store data, it is necessary to have a series of site definition files.

Zeno Channels - The Zeno Channel Assignment Files are a series of files that map Zeno channel numbers (which are embedded in the input data stream) to EPA parameter numbers. Again, this is so the data can be properly tagged for later retrieval.

> Note: Data from the Zeno dataloggers is received with a SAMPLING STATION number, a date/time stamp, an error word, and a series of data triplets consisting of a channel number, a value, and a flag. No other information is available. One of the primary functions of the automatic cal/val processing is to map this information into EPA parameters at an EPA site. This is accomplished via the MeteoStar site definition files.

Cal Limits – This web page allows you to view the calibration limits set up for each parameter at each site. The calibration limits control the various tests performed during automatic calibrations and span checks.

NEG/MUL Tests – This web page allows you to view the NEG/MUL test definitions set up for each parameter at each site. The NEG/MUL test definitions control the NEG (sets data

that is slightly negative to zero and very negative data is flagged non-ambient) and MUL (checks to make sure $NO + NO_2 = NO_X$) tests.

Site Info - A family of reports that displays site-related information.

Monitor Status – Non-real-time data. A status page showing the first date and hour data was collected at each monitor (met or pollution) at each SAMPLING STATION. The first date and hour of valid data (data flagged as "K-Valid") as well as the shutdown date and hour of each monitor is also shown. This data is used when calculating the data return and data loss pages.

Monitor Summary – Non-real-time data. A status page showing which parameters are monitored at each site. This report is based on the same data that goes into the Monitor Status web page.

Site Summary – Non-real-time data. A status page showing which SAMPLING STATION are tied to which EPA sites. This report is based on the same data that goes into the EPA Site File and SAMPLING STATION Definitions web pages.

MeteoStar Software – Real-time data. A family of reports that displays information specific to the health and well-being of the MeteoStar system software.

Process Status - This web-based tool is designed to allow system maintainers rapid access to the status of MeteoStar processes running on each Unix box. There are also web-based tools (tied to specific IP addresses) that allow system maintainers to kill processes or to restart processes as needed.

Who Is Logged In - This web-based tool is designed to allow system maintainers to see who is currently logged in and utilizing the MeteoStar analysis tools. This is helpful for system maintenance.

Cal/Val Log - Used primarily by the MeteoStar system support personnel. Provides detailed information about the automatic ingest processing of pollution data. It is possible to determine why calibrations and span checks fail even when there is no information available on the other web pages.

Model Grids – Displays which specific forecast fields from the various meteorological forecast models currently reside in the MeteoStar database. This is useful for determining if there is missing model data or if all the data for a particular model run has been received.

Support Data – Real-time data. A family of reports that displays information that is not specific to collection or processing of data.

Contact Manager – A web-based tool for entering and maintaining contact information. Users can add themselves to the contact manager database and then maintain their own information. You can use the Contact Manager to find who is responsible for a variety of things – site maintenance, site validation, repair and maintenance of specific pieces of hardware, etc.

File Status - This provides a synopsis of all the support files used by the other web pages. Most of these support files are updated hourly, some update only once a day. Generally, the support files contain a year's worth of data. Only the current year updates automatically. Changes to older data will necessitate running the compilation programs manually – this page lets you see why the changes you made to data from 1997 are not reflected in the web pages until the support files are updated.

Audit Status – Synopsis of the status of all audit trail files. Each time a validator validates data, there is an entry automatically made into an audit trail file for each site that is affected. There is one audit trail file for each site collecting data in the system. This web page allows you to see the last time each file was updated, and how many entries are in each file. This page can be used to track down error messages generated in Manual Validation referring to the inability to open a file.

Permissions – A web page that shows the contents of the Manual Validation password file. This file contains all the user and group definitions and permissions used to control change permissions under Manual Validation. Shows which group each defined user belongs to. The permissions for each user group can also be viewed. The group permissions directly control whether or not group members can validate (save changed data), produce AQS reports, etc.

Op Log Status – Synopsis of the status of all operator log files. There is one operator log file for each site collecting data in the system. Operator log entries can be made directly on the data logger or through many of the web pages. This web page allows you to see the last time each file was updated, and how many entries are in each file. This page can be used to track down errors referring to the inability to open a file.

Ozone Seasons – Displays the ozone season definitions used in the Ozone Forecast web page.

Air Conditioner Study – A family of reports displaying data about the air conditioner study conducted in Houston last year. These reports are designed to help visualize the amount of ozone reduction produced by the special coating under test on the air conditioner coils.

On-Line Documentation - All of the training material that has been developed for the MeteoStar system is available on-line.

> NOTE WELL: The on-line documentation lags the development of new web pages and implementation of new software features. Training material is always updated and posted to the web page before formal training classes are held. Formal training classes occur once or twice a year depending upon need.

Training Material – The latest training material is available for download on this page. The documents are in PDF (portable data format) and require an Adobe PDF viewer (this viewer is normally installed on agency computers). Once you download one of these documents, you can print it locally or view it in the viewer.

Operating Procedures – Copies of selected Standard Operating Procedure documents relating to the MeteoStar system and many of the sensors and other instruments used in the system.

AQI Calculator – A web-based tool that allows you to calculate the Air Quality Index (AQI) for any criteria pollutant. You enter a concentration for one or more pollutants, and the web page calculates the corresponding AQI.

Modem Setup – A web-based tool that walks you through the steps necessary to set up a modem for use in the MeteoStar system.

SAMPLING STATION Time Syncronization - A family of tools designed to keep the system time synchronized throughout the MeteoStar system. The MeteoStar system normally issues time-sync commands automatically twice a week. This insures that the Zeno datalogger and Dasibi calibrator clocks are properly synchronized. If a datalogger or calibrator is swapped out, a time-sync command must be sent manually before a calibration can be successfully completed. These web pages allow operators to initiate the time-sync command.

SAMPLING STATION Time Sync - A tool that easily allows time-sync commands to be sent directly to a monitoring site. This command is protected by an authorization code. There is a different authorization code for each region. If you don't know the authorization code for your region and you feel like you should, please contact David Stroud (512) 239-2033 Logs of all time-sync commands initiated (failed or successful) are logged and available via web pages.

Hub Time Sync Log - The status of time sync commands that are generated via the web page cannot be determined by the "SAMPLING STATION Time Sync" web page. This is due to the mechanism used to get the time sync command to the datalogger. The "SAMPLING STATION Time Sync" web page actually starts a program on the hub computer to send the time sync command. Fortunately, the hub computer logs both the standard time sync commands (that are sent twice a week) and any time sync commands initiated via the web page. This allows you to review the "real" status of the time sync command. The report is formatted exactly like the comms summary report. You should be able to see the time sync command you initiated via the web page. If the summary shows no errors, it is safe to assume the time sync was successful. The definitive method of telling if a time sync was successful is to be at the station when the time sync is sent and watch the front panel of the Dasibi for changes.

Time Sync Log - A tool that allows you to view time sync commands that are initiated via the web page. We use this in conjunction with the "Hub Time Sync Log" to monitor time sync commands. We can tell which computer you initiated the command from.

Time Sync Errors - A tool that allows MeteoStar system support personnel to monitor who is attempting to send time sync commands. We can tell which computer you initiated the command from and what authorization code(s) you attempted to use.

Hub Log - The status of canister sampling commands that are generated via the web page cannot be determined by the Command Log web page. This is due to the mechanism used to get the canister sampling command to the datalogger. The Command Log web page actually starts a program on the hub computer to send the canister sampling command. The hub computers log communication information for these commands that are initiated via the web page. This allows you to review the "real" status of the canister sampling command. The report is formatted exactly like the Comms Report. You should be able to see the canister sampling command you initiated via the web page. If the summary shows no errors, it is almost safe to assume the sampling command was successful.

Command Log – A tool that allows you to view canister sampling commands that are initiated via the web page.

Errors - A tool that allows MeteoStar system support personnel to monitor who is attempting to send canister sampling commands. We can tell which computer you initiated the command from and what authorization code(s) you attempted to use.

External Web Page	URL
Airborne Particulates	http://www.TCEQ.state.tx.us/cgi-bin/monops/particulates
Air Quality in Texas	http://www.TCEQ.state.tx.us/cgi-bin/monops/texas_aqi
AQI (Air Quality Index) Ratings	http://www.TCEQ.state.tx.us/cgi-bin/monops/psi_rpt
SAMPLING STATION Hourly Averages By Site	http://www.TCEQ.state.tx.us/cgi-bin/monops/select_summary
Current Hourly Averages By Parameter	http://www.TCEQ.state.tx.us/cgi-bin/monops/daily_average
Current PM-2.5 Levels in Texas	http://www.TCEQ.state.tx.us/cgi-bin/monops/texas_pm25
Fuel Cell Demo	http://www.TCEQ.state.tx.us/cgi-bin/monops/fuel_cell
Map of Current Ozone Levels	http://www.TCEQ.state.tx.us/cgi-bin/monops/select_curlev
Monitors	http://www.TCEQ.state.tx.us/cgi-bin/monops/monitors
Monthly Summary Report	http://www.TCEQ.state.tx.us/cgi-bin/monops/select_month
Ozone 8-Hour 4 Highest	http://www.TCEQ.state.tx.us/cgi-bin/monops/8hr_4highest
Ozone 8-Hour High Value Days	http://www.TCEQ.state.tx.us/cgi-bin/monops/8hr_exceed
Ozone 8-Hour Monthly Summary	http://www.TCEQ.state.tx.us/cgi-bin/monops/8hr_monthly
Ozone Action Day Forecast	http://www.TCEQ.state.tx.us/cgi-bin/monops/ozone_actionday
Ozone Animations	http://www.TCEQ.state.tx.us/cgi-bin/monops/ozone_animation
Ozone Exceedance	http://www.TCEQ.state.tx.us/cgi-bin/monops/ozone_exceedance
Ozone Summary	http://www.TCEQ.state.tx.us/cgi-bin/monops/ozone_summary
Ozone Warnings	http://www.TCEQ.state.tx.us/cgi-bin/monops/warning_status
Peak One-Hour Ozone	http://www.TCEQ.state.tx.us/cgi-bin/monops/peak_monthly
Site Information	http://www.TCEQ.state.tx.us/cgi-bin/monops/site_info
Site Photos	http://www.TCEQ.state.tx.us/cgi-bin/monops/site_photo
Water Hourly Averages by Site	http://www.TCEQ.state.tx.us/cgi-bin/monops/select_water_daily
Water Monthly Averages	http://www.TCEQ.state.tx.us/cgi-bin/monops/select_water_month

Internal Web Page	URL
8-hr Ozone Attainment	http://dsr.TCEQ.state.tx.us/cgi-bin/lsr/8hr_attainment
Air Conditioner Study	http://dsr.TCEQ.state.tx.us/O3ReducStudy2.html
Air Quality in Texas	http://dsr.TCEQ.state.tx.us/cgi-bin/lsr/texas_aqi
AQS Precision Transactions File	http://dsr.TCEQ.state.tx.us/cgi-bin/lsr/select_precision
AQI (Air Quality Index) Ratings	http://dsr.TCEQ.state.tx.us/cgi-bin/lsr/psi_rpt
AQI Calculator	http://dsr.TCEQ.state.tx.us/cgi-bin/lsr/aqi_calc
Audit Status	http://dsr.TCEQ.state.tx.us/cgi-bin/lsr/audit_status
AutoGC Current Hourly Averages by Parameter	http://dsr.TCEQ.state.tx.us/cgi-bin/lsr/agc_daily_average
AutoGC Data	http://dsr.TCEQ.state.tx.us/agc.html
AutoGC Hourly Averages by Site	http://dsr.TCEQ.state.tx.us/cgi-bin/lsr/agc_daily_summary
AutoGC Monthly Summary	http://dsr.TCEQ.state.tx.us/cgi-bin/lsr/agc_monthly_summary
Cal Limits	http://dsr.TCEQ.state.tx.us/cgi-bin/lsr/cal_limits
Cal/Span Acceptance	http://dsr.TCEQ.state.tx.us/cgi-bin/lsr/select_msr
Cal/Span History	http://dsr.TCEQ.state.tx.us/cgi-bin/lsr/cal_span_history
Cal/Val Log	http://dsr.TCEQ.state.tx.us/cgi-bin/lsr/calval_report
Calibration Results	http://dsr.TCEQ.state.tx.us/cgi-bin/lsr/select_msr
SAMPLING STATION Average Sum Pollutant Summary	http://dsr.TCEQ.state.tx.us/cgi-bin/lsr/average_summary
SAMPLING STATION Data Printout	http://dsr.TCEQ.state.tx.us/cgi-bin/lsr/dataout
SAMPLING STATION Definitions	http://dsr.TCEQ.state.tx.us/cgi-bin/lsr/LEADS_sites?Sampling Station
SAMPLING STATION Hourly Averages By Site	http://dsr.TCEQ.state.tx.us/cgi-bin/lsr/daily_summary
SAMPLING STATION Time Sync	http://dsr.TCEQ.state.tx.us/cgi-bin/lsr/time_sync
Comm Problems	http://dsr.TCEQ.state.tx.us/cgi-bin/lsr/comm_problems
Comms Report	http://dsr.TCEQ.state.tx.us/cgi-bin/lsr/comms_report
Contact Manager	http://dsr.TCEQ.state.tx.us/cgi-bin/lsr/contacts
Connectivity	http://dsr.TCEQ.state.tx.us/cgi-bin/lsr/connectivity
CS-10 Command Log	http://dsr.TCEQ.state.tx.us/cgi-bin/lsr/view_sync_logs?canister
CS-10 Control	http://dsr.TCEQ.state.tx.us/cgi-bin/lsr/start_canister
CS-10 Errors	http://dsr.TCEQ.state.tx.us/cgi-bin/lsr/view_sync_logs?bad_can
CS-10 Hub Log	http://dsr.TCEQ.state.tx.us/cgi-bin/lsr/can_report
CS-10 Tracker	http://dsr.TCEQ.state.tx.us/cgi-bin/lsr/track_canister
Current Hourly Averages By Parameter	http://dsr.TCEQ.state.tx.us/cgi-bin/lsr/daily_average
Current PM-2.5 Levels in Texas	http://dsr.TCEQ.state.tx.us/cgi-bin/lsr/texas_pm25
Data Extractor	http://dsr.TCEQ.state.tx.us/cgi-bin/lsr/data_extract
Data Loss	http://dsr.TCEQ.state.tx.us/cgi-bin/lsr/data_loss
Data Return	http://dsr.TCEQ.state.tx.us/cgi-bin/lsr/data_return
Detailed Comms Report	http://dsr.TCEQ.state.tx.us/cgi-bin/lsr/comms_report
E-Mail Signup	http://dsr.TCEQ.state.tx.us/cgi-bin/lsr/email_signup
EPA Site File	http://dsr.TCEQ.state.tx.us/cgi-bin/lsr/LEADS_sites?epa
Error Word Decoder	http://dsr.TCEQ.state.tx.us/cgi-bin/lsr/error_word
File Status	http://dsr.TCEQ.state.tx.us/cgi-bin/lsr/compiled_files
Five-Minute Quick Look	http://dsr.TCEQ.state.tx.us/cgi-bin/lsr/quick_look
Fuel Cell Demo	http://dsr.TCEQ.state.tx.us/cgi-bin/lsr/fuel_cell
Graphical SAMPLING STATION Data	http://dsr.TCEQ.state.tx.us/cgi-bin/lsr/graph_data
Grid Status	http://dsr.TCEQ.state.tx.us/cgi-bin/lsr/grid_data
H/W Tracker	http://dsr.TCEQ.state.tx.us/cgi-bin/lsr/config_change
High Values	http://dsr.TCEQ.state.tx.us/cgi-bin/lsr/high_value
Hub Error Logs	http://dsr.TCEQ.state.tx.us/cgi-bin/lsr/hub_errorlog
Hub Time Sync Log	http://dsr.TCEQ.state.tx.us/cgi-bin/lsr/sync_report
Individual SAMPLING STATION Summary	http://dsr.TCEQ.state.tx.us/cgi-bin/lsr/select_msr
Instant Net Status	http://dsr.TCEQ.state.tx.us/cgi-bin/lsr/netstatus
Last Cal/Span Report	http://dsr.TCEQ.state.tx.us/cgi-bin/lsr/last_cal_span
LEADS Network Status Reports	http://dsr.TCEQ.state.tx.us/cgi-bin/lsr/select_msr
Listserver Status	http://dsr.TCEQ.state.tx.us/cgi-bin/lsr/listserv_status
Map of Current Ozone Levels	http://dsr.TCEQ.state.tx.us/cgi-bin/lsr/select_curlev
Missing/Unexpected Data	http://dsr.TCEQ.state.tx.us/cgi-bin/lsr/missing_data
Model Grids	http://dsr.TCEQ.state.tx.us/cgi-bin/lsr/mg_elements
Modem Setup	http://dsr.TCEQ.state.tx.us/cgi-bin/lsr/modem_info
Monitor Status	http://dsr.TCEQ.state.tx.us/cgi-bin/lsr/monitor_status
Monitor Summary	http://dsr.TCEQ.state.tx.us/cgi-bin/lsr/monitor_summary
Monitors	http://dsr.TCEQ.state.tx.us/cgi-bin/lsr/monitors
Monthly Summary Report	http://dsr.TCEQ.state.tx.us/cgi-bin/lsr/monthly_summary
Near Real-Time Cameras	http://dsr.TCEQ.state.tx.us/cgi-bin/lsr/site_camera

Internal Web Page	URL
NEG/MUL Tests	http://dsr.TCEQ.state.tx.us/cgi-bin/lsr/neg_mul_test
Network Status	http://dsr.TCEQ.state.tx.us/cgi-bin/lsr/netsummary
Op Log Status	http://dsr.TCEQ.state.tx.us/cgi-bin/lsr/oplog_status
Operating Procedures	http://dsr.TCEQ.state.tx.us/cgi-bin/lsr/procedure_docs
Operator Logs	http://dsr.TCEQ.state.tx.us/cgi-bin/lsr/oplog_report
Overall SAMPLING STATION Summary	http://dsr.TCEQ.state.tx.us/cgi-bin/lsr/select_msr
Ozone 8-Hour 4 Highest	http://dsr.TCEQ.state.tx.us/cgi-bin/lsr/8hr_4highest
Ozone 8-Hour High Value Days	http://dsr.TCEQ.state.tx.us/cgi-bin/lsr/8hr_exceed
Ozone 8-Hour Monthly Summary	http://dsr.TCEQ.state.tx.us/cgi-bin/lsr/8hr_monthly
Ozone Action Day Forecast	http://dsr.TCEQ.state.tx.us/cgi-bin/lsr/ozone_actionday
Ozone Animations	http://dsr.TCEQ.state.tx.us/cgi-bin/lsr/ozone_animation
Ozone Comparison	http://dsr.TCEQ.state.tx.us/cgi-bin/lsr/external/direct_reduct3
Ozone Exceedance	http://dsr.TCEQ.state.tx.us/cgi-bin/lsr/ozone_exceedance
Ozone Reduction	http://dsr.TCEQ.state.tx.us/cgi-bin/lsr/external/direct_reduct1
Ozone Reduction Study	http://dsr.TCEQ.state.tx.us/cgi-bin/lsr/external/direct_reduct4
Ozone Reduction Test Site	http://dsr.TCEQ.state.tx.us/cgi-bin/lsr/external/direct_reduct2
Ozone Seasons	http://dsr.TCEQ.state.tx.us/cgi-bin/lsr/ozone_season
Ozone Summary	http://dsr.TCEQ.state.tx.us/cgi-bin/lsr/ozone_summary
Ozone Warnings	http://dsr.TCEQ.state.tx.us/cgi-bin/lsr/warning_status
Peak One-Hour Ozone	http://dsr.TCEQ.state.tx.us/cgi-bin/lsr/peak_monthly
Permissions	http://dsr.TCEQ.state.tx.us/cgi-bin/lsr/permissions
Pollution Data By Parameter	http://dsr.TCEQ.state.tx.us/cgi-bin/lsr/database_print
Process Status	http://dsr.TCEQ.state.tx.us/cgi-bin/lsr/leads_monitor
Raw Comms Log	http://dsr.TCEQ.state.tx.us/cgi-bin/lsr/comms_log
Site Info	http://dsr.TCEQ.state.tx.us/cgi-bin/lsr/site_info
Site Photos	http://dsr.TCEQ.state.tx.us/cgi-bin/lsr/site_photo
Site Summary	http://dsr.TCEQ.state.tx.us/cgi-bin/lsr/site_summary
SO2/H2S 30 Minute Running Averages	http://dsr.TCEQ.state.tx.us/cgi-bin/lsr/30min_average
SO2/H2S 30-Minute Exceedances	http://dsr.TCEQ.state.tx.us/cgi-bin/lsr/30min_exceed
SO2/H2S 30-Minute Monthly Summary	http://dsr.TCEQ.state.tx.us/cgi-bin/lsr/30min_monthly
Span Check Results	http://dsr.TCEQ.state.tx.us/cgi-bin/lsr/select_msr
Span-Zero Results	http://dsr.TCEQ.state.tx.us/cgi-bin/lsr/select_msr
Span Check Results	http://dsr.TCEQ.state.tx.us/cgi-bin/lsr/select_msr
Time Sync Errors	http://dsr.TCEQ.state.tx.us/cgi-bin/lsr/view_sync_logs?errors
Time Sync Log	http://dsr.TCEQ.state.tx.us/cgi-bin/lsr/view_sync_logs?log
Training Material	http://dsr.TCEQ.state.tx.us/cgi-bin/lsr/training_docs
Upcoming/Overdue Cals	http://dsr.TCEQ.state.tx.us/cgi-bin/lsr/cal_schedule
Validator Notes	http://dsr.TCEQ.state.tx.us/cgi-bin/lsr/audit_log
Water Web Pages	http://dsr.TCEQ.state.tx.us/water.html
Water Hourly Averages by Site	http://dsr.TCEQ.state.tx.us/cgi-bin/lsr/select_water_daily
Water Monthly Averages	http://dsr.TCEQ.state.tx.us/cgi-bin/lsr/select_water_month
Who Is Logged In	http://dsr.TCEQ.state.tx.us/cgi-bin/lsr/logins
Zeno Channels	http://dsr.TCEQ.state.tx.us/cgi-bin/lsr/zeno_channels

SUTRON'S

VALIDATION CODES FOR SAMPLING STATION DATA

Flag Definition

Flag	Meaning
NOL	Station or instrument not on-line (does not count for or against data return).
LST	Data were collected but lost and could not be recovered.
CAL	Data missing because instrument calibration was in progress for the indicated parameter.
SPN	Data lost because a span check was in progress for at least four five-minute periods in an hour.
LIM	Calibration or span check was out of limits.
QAS	Quality assurance audit in progress (Q code initiated in the station).
PMA	Preventative maintenance operation in progress (P code set in the station).
FEW	Data lost because there were less than nine five-minute updates in an hour, and there was at least one update present.
NEG	Hourly value rejected because it is below the preset range limit. Slightly negative values are recorded as zeroes.
MUL	Data lost because of improper relationships between parameters on a multi-parameter instrument.
QRE	Data rejected as a result of QA results.
AQI	Data determined not to be representative of ambient conditions.

DATA VALIDATION PROCEDURE FOR METEOSTAR

STANDARD OPERATING PROCEDURE
Title: METEOSTAR 010 Data Validation
Unit leader:_____ Date: _____
Quality Control Review:_____ Date: _____
Section Manager:_____ Date: _____
Effective Date: _____

Revision 02/03

1.0 PURPOSE

This SOP describes the procedures for validating pollutant and meteorological data from the Sampling Station operated under the MeteoStar system.

2.0 SCOPE AND APPLICABILITY

2.1 Pollution Section

Pollution data from the Sampling Station includes: ozone, sulfur dioxide, hydrogen sulfide, nitric oxide, nitrogen dioxide, total oxides of nitrogen, and carbon monoxide. The automated procedures are performed by the MeteoStar computer system (paragraph 11.1), and the manual procedures are performed by the Sampling Station Data Validators.

2.2 Meteorological Section

These procedures are applicable for validating wind speed resultants, wind direction resultants, and ambient air temperatures. Wind speed averages and solar radiation are not being validated at this time, but may at some time in the future. The automated procedures are performed by the MeteoStar computer system (paragraph 11.2), and the manual procedures are performed by the meteorologists.

3.0 METHOD OR PROCEDURAL SUMMARY

3.1 Pollution Section

Oversee the collection and processing of the data to facilitate data completeness and to ensure all the correct factors are input for the automatic processing. Verify that cals and spans are current and passed. Investigate any high values and data loss. Examine the data for unusual values and patterns. Review operator logs for routine and unusual events. Notify the appropriate staff of any problems encountered to facilitate instrument repair and to determine the effects on the

validity of data. Investigate anomalies and if necessary, correct the data, or flag it invalid. Document any edits of the data. See that reports reflect the appropriate data.

3.2 Meteorological Section

3.2.1 Evaluate the validity of Sampling Station weather data by comparing AQS data files retrieved from MeteoStar against Texas airport weather observations retrieved from WXBase.

3.2.2 Manually validate data on MeteoStar Pollution Interface.

3.2.3 Notify the Sampling Station operators and appropriate staff when a problem is discovered.

4.0 LIMITATIONS

4.1 Pollution Section

4.1.1 The automated data validation checks do not evaluate ambient air pollution data. Only quality control data is evaluated automatically.

4.1.2 Validation depends on the quality of field observations and the reporting of events in the Operator Log.

4.1.3 The Operator Log is not available through MeteoStar. This log is available through LabView.

4.1.4 MeteoStar is a developing system. The software tools used to validate data may contain defects that may or may not be identified. This may necessitate checking one tool against another.

4.2 Meteorological Section

4.2.1 Only a daily spot check of Sampling Station weather data is evaluated against weather data received from Texas and Mexican airports and buoys over WXBase system.

4.2.2 Validating weather observations is very subjective because winds and temperatures may vary significantly from site to site in an area. Various factors come into play such as terrain, vegetation, proximity to the gulf, and equipment mast height to mention a few.

4.2.3 The weather reports received from airports and buoys around the state are spot observations. The Sampling Station data that is being validated against these observations are hourly averages.

4.2.4 Until all Sampling Station sites are being processed by MeteoStar, data validation will be accomplished on the Macintosh, because Datkon files and Zeno files will be mixed for the weekly check.

4.2.5 An experienced meteorologist is required to validate meteorological data because value judgments are involved.

5.0 SAFETY

No specific safety issues are associated with this SOP. Monitoring Operations maintains a required safety training program that covers all health and safety related aspects of the office environment and computer equipment usage.

6.0 EQUIPMENT

Computer Hardware

486PC, 8MB RAM, 80 MB hard-drive or 68040 Macintosh, 8MB RAM 80 MB hard-drive
MeteoStar hardware
MeteoStar UNIX computer system, HP 715 workstation
Data logger, data communication hardware,
SCO UNIX computer system, 16 MB RAM, 500 MB hard-drive
Modem
Central office HP Computer
Ethernet Connection
GTE satellite system

Computer Software (Validation Tools)

HP UNIX
SCO UNIX
HP View Light
Exceed for PC
Exodus for Macintosh
MeteoStar pollution user interface
MeteoStar user interface
Microsoft Excel menu
(see Appendix A, Figure 2.)
Microsoft Word
Monthly Air Quality Report
Netscape
Labview/Zeno datalogger application
WXPlot
AQPlot
Power Point
Fetch
WXBase

7.0 PROCEDURE

7.1 Pollution Section

7.1.1 Access the Overall Sampling Station Summary at http://163.234.160.101/ (see Appendix A, Figure 1) using Netscape.

7.1.1.1 Check if data has been collected.

7.1.1.2 View status of individual Sampling Station selected from the pull down.

7.1.1.3 Check if data has been collected for the expected time period. If not contact MeteoStar administrator for possible data recovery.

7.1.1.4 Check for any problems noted. If span or cal is overdue, investigate the reason. It may have been collected and not processed.

7.1.1.5 Check if there are any high values.

7.1.1.6 Check if there has been a span or cal and select the test and parameter from the menu (see Appendix A, Figure 3).

7.1.1.7 If there is any unexplained data loss go to the data loss report and check how the data is flagged.

7.1.2 Go to Operator Log -- Use Labview (refer to Continuous Ambient Monitoring Station Operator Interface User Guide)

7.1.2.1 Check if PMIs are up to date.

7.1.2.1 Check for any unusual events.

7.1.3 Go to Manual Validation by logging onto an Hp server through an x-terminal emulation package. Use Exceed on PCs.

7.1.3.1 Open MeteoStar Pollution Interface.

7.1.3.2 Select area of interest.

7.1.3.3 Highlight area of Sampling Station sites to be validated.

7.1.3.4 Under FUNCTIONS pull down menu, select MANUAL VALIDATION.

7.1.3.5 In the Manual Validation Retrieve window, select (see Appendix A, Figure 4).

7.1.3.5.1 CAM site to be validated

7.1.3.5.2 Parameter

7.1.3.5.3 Data Base - "5 minute"

7.1.3.5.4 Start Time - Select time of interest

7.3.7.5.5 End Time - Select time of interest

7.1.3.6 Manual Validation window will display the values which were selected (see Appendix A, Figure 5).

7.1.3.6.1 Check that the information agrees with Daily Status Report and op log. If not, investigate.

7.1.3.6.2 Check to see if there are any negative values. If the hourly average is more negative than -10 ppb (1 ppm for CO), then flag the data invalid.

7.1.3.6.3 Look for any irregular patterns. If there are any, investigate the conditions.

7.1.3.6.4 Check if the data compares with related stations and pollutants.

7.1.3.6.5 Check that data is flagged correctly.

7.1.3.6.6 Check that the correct cal was used to calculate the data.

7.1.3.6.7 Edit any incorrect data.

7.1.3.6.7.1 To invalidate data, pull a box around values that are bad, pull down the EDIT menu and select FLAGS - AQI. This will invalidate that data.

7.1.3.6.7.2 If a value is valid, but has been flagged, pull a box around the values, pull down the EDIT menu and select FLAGS - VALID. This will make the data valid.

7.1.3.6.7.3 If a value needs to be recalculated, pull a box around the values, pull down the FILE menu and select OPEN CALIBRATION CURVES and Highlight the appropriate one, then pull down the EDIT menu and select APPLY SLOPE/INT.

7.1.3.6.7.4 To save the validation, pull down FILE SAVE and fill in the blocks.

7.1.4 Go to hourly spreadsheet (see Appendix A, Figures 6-8).

7.1.4.1 Check that it agrees with Daily Status Report and Manual Validation and that it reflects what you intend to send to EPA.

7.1.5 Run AQS report.

7.2 Meteorological Section

7.2.1 Data must be in an AQS format to plot data using AQPlot software.

7.2.2 Retrieving AQS data files from MeteoStar.

7.2.2.1 Open MeteoStar User Interface.

7.2.2.2 Click on the POLLUTION button.

7.2.2.3 Under the pull down menus, select FILE, then select RETRIEVE.

7.2.2.4 The Pollution Data Retrieval window will then display. Select the following:

7.2.2.4.1 Site - Choose Sampling Station site of interest

7.2.2.4.2 Data Base - "Average"

7.2.2.4.3 Source - "Logger"

7.2.2.4.4 Interval - "1 hour"

7.2.2.4.5 Start Time - Select time of interest

7.2.2.4.6 End Time - Select time of interest

7.2.2.4.7 Average - "No"

7.2.2.4.8 Interval - "1 hour"

7.2.2.5 Select FILE under the pull down menus, then select EXPORT.

7.2.2.5.1 Designate file name and directory using the following convention: "/users/rwells/file name plus the .air extension so AQPlot will read the file.

7.2.2.5.2 The files will then be ready to be exported out of MeteoStar.

7.2.3 Retrieving weather observations from WXBase.

Weather observation are retrieved once daily to plot a noon chart. These files are saved in the MET QA folder on the Macintosh.

7.2.4 Make pict files using AQPlot and WXPlot software.

7.2.4.1 Combine the different AQS files into one document so the data can be plotted on one chart.

7.2.4.2 Make pict files for the following locations with the following maps and site location files.

Austin	AUSAQ.MAP	AUSAQ.SIL
Brownsville	BROAQ.MAP	BROAQ.SIL
Corpus Christi	CRPAQ.MAP	CRPAQ.SIL
DFW area	DFWAQ.MAP	DFWAQ.SIL
El Paso	ELPAQ.MAP	ELPAQ.SIL
Tyler area	GGGAQ.MAP	GGGAQ.SIL
San Antonio	SATAQ.MAP	SATAQ.SIL
Victoria	VCTAQ.MAP	VCTAQ.SIL

7.2.5 Make a slide show using Power Point software by overlaying pict files from WXPlot and pict files from AQPlot.

7.2.6 Validate Wind Speed Resultant, Wind Direction Resultant, and Temperature.

7.2.6.1 Synoptic Plot: Evaluate whether the Sampling Station weather plot logically fits with the other meteorological sites in the area.

7.2.6.2 Wind Direction: Look for a general alignment of wind directions between sites, except in mountainous areas such as El Paso. When winds are light and variable, the direction is meaningless. Be suspicious of wind directions that do not vary. Wind directions often become stuck during ice storms.

7.2.6.3 Wind Speed: Look for wind speeds, which are consistent with other sites in the area. The wind speeds at Sampling Station sites are usually lighter that the wind speeds at an airport. Wind speed should vary. During ice storms, wind speeds indicate zero when the anemometer is frozen.

7.2.6.4 Temperature: Look for large differences in temperature between stations. Differences of 10 degrees or greater should be highly suspect, unless there is a cold front moving through the area or a thunderstorm is in progress at one of the sites.

7.2.7 Check hourly averages using Excel files of Sampling Station data on MO.EXPORT.

Look for extreme values, prolonged periods of calm winds, or any parameter that appears stuck on a certain value.

7.2.8 Manual Validation on MeteoStar

7.2.8.1 Open MeteoStar Pollution Interface.

7.2.8.2 Select area of interest.

7.2.8.3 Highlight area of Sampling Station sites to be validated.

7.2.8.4 Under FUNCTIONS pulldown menu, select MANUAL VALIDATION.

7.2.8.5 In the Manual Validation Retrieve window, select:

7.2.7.5.1 CAM site to be validated

7.2.7.5.2 Parameter - either Temperature, Resultant Wind Speed or Resultant Wind Direction.

7.3.7.5.3 Data Base - "5 minute"

7.3.7.5.4 Start Time - Select time of interest

7.3.7.5.5 End Time - Select time of interest

7.2.8.6 Manual Validation window will display the values which were selected.

7.2.8.6.1 To invalidate data, pull a box around values that are bad, pull down the EDIT menu and select FLAGS - AQI. This will invalidate that data.

7.2.8.6.2 If a value is valid and has been flagged, pull a box around the values, pull down the EDIT menu and select FLAGS - VALID. This will make the data valid.

7.2.8.6.3 To save the validation, pull down FILE SAVE and fill in the blocks.

7.2.9 When a problem has been discovered with the Sampling Station data, send an E-Mail to the Sampling Station operators responsible describing the problems noted.

8.0 CALCULATIONS

8.1 The calculations used within MeteoStar to automatically validate pollution data are detailed in "Appendix D, MeteoStar Processing of Sampling Station Quality Control Data, September 9, 1994."

8.2 The criteria used within MeteoStar to automatically validate meteorological data are detailed in Table 8-1 of the EPA document "On-Site Meteorological Program Guidance for Regulatory Modeling Applications."

9.0 QUALITY CONTROL

9.1 Pollution Section

9.1.1 Each experienced data validator has the responsibility for the review, validation, and verification of the measurements from their assigned stations. The senior validator will oversee the validation procedures and monitor data completeness reports. Senior technical staff will review data summaries and investigate data outliers and unusual data.

9.1.2 Maintain a record of all activities, facts, and follow-up actions relating to invalidation of ambient data. The detail of record keeping should be sufficient to reconstruct the data validation event at a later time without having to rely on memory or other paperwork that may not be readily available. The MeteoStar manual validation has an automatic audit trail to record who changed what and why.

9.1.3 The data validators will review and question any part of the measurement process and initiate data reviews and corrective actions to bring the process back into compliance.

9.2 Meteorological Section

The quality control of meteorological data involves the peer review process. Both meteorologists check the same data at the same time and actively discuss the data's validity. Meteorological data is never declared invalid until agreement is reached.

10.0 DEFINITIONS

Sampling Station Site on State Highway 71
AQS Air Quality System (EPA database)
Meteostar Lockheed Environmental Analysis and Display System.
PMI Preventive Maintenance Instruction

11.0 REFERENCES

11.1 Appendix D, MeteoStar Processing of SAMPLING STATION Quality Control Data, September 9, 1994.

11.2 Table 8-1 of the EPA document "On-Site Meteorological Program Guidance for Regulatory Modeling Applications."

11.3 MeteoStar Operators Manual

12.0 SHORTHAND PROCEDURE

12.1 Pollution Section

- Daily Status Report
  Check if data collected
  Contact MeteoStar administrator for possible data recovery
  Check for any problems noted

- Operator Log
  - Look for any unusual events
- Manual Validation
  - Check agreement with Daily Status Report and Operator Log
  - Look for negative values
  - Look for any irregular patterns
  - Compare related stations and pollutants
  - Check Flagged data
  - Check cals
  - Edit any incorrect data
- Hourly Spreadsheet
  - Check agreement with Daily Status Report and Manual Validation
- Run AQS report--refer to quarterly AQS Report SOP

12.2 Meteorological Section

- Retrieve AQS data files from MeteoStar
- Export AQS files
- Import AQS files on Macintosh using Fetch
- Retrieving weather observations from WXBase
- Make pict files using AQPlot and WXPlot software
- Combine the different AQS files into one document
- Make pict files
- Make a slide show using Power Point software
- Evaluate Sampling Station meteorological data
- Check Excel files of SAMPLING STATION data on MO.EXPORT

REFERENCES

1. *Guidance for Planning the Data Quality Objectives Process.* U.S. Environmental Protection Agency QA/G-4, Final, September 1994.
2. *Quality Assurance Handbook for Air Pollution Measurement Systems, Volume II: Ambient Air Specific Methods.* U.S. Environmental Protection Agency, April 1994.
3. *Ambient Air Quality Network Field Quality Control Manual*. Texas Commission on Environmental Quality, January 2001.
4. *Noncontinuous Ambient Monitoring Station (NCAMS) Operations Manual*. Texas Commission on Environmental Quality, February 1998.
5. *Ambient Monitoring Guidelines for the Prevention of Significant Deterioration.* U.S. Environmental Protection Agency.
6. *Preventive Maintenance Instructions Manual*. Texas Commission on Environmental Quality, revised December 1, 2001.
7. *Quality Assurance Handbook for Air Pollution Measurement Systems, Volume IV: Meteorological Measurements.* U.S. Environmental Protection Agency, revised March 1995.
8. *Quality Assurance Handbook for Air Pollution Measurement Systems, Volume I: A Field Guide to Environmental Quality Assurance.* U.S. Environmental Protection Agency, April 1994.
9. "Ambient Air Quality Surveillance." Title 40 *Code of Federal Regulations* Part 58.
10. "Ambient Air Monitoring Reference and Equivalent Methods." Title 40 *Code of Federal Regulations* Part 53.
11. "National Primary and Secondary Ambient Air Quality Standards." Title 40 *Code of Federal Regulations* Part 50.
12. "Guidelines Establishing Test Procedures for the Analysis of Pollutants." Title 40 *Code of Federal Regulations* Part 136.
13. *Quality Management Plan*. Texas Commission on Environmental Quality, December 2000.
14. *MeteoStar/LEADS Processing of CAMS Quality Control Data, Appendix D*. Texas Commission on Environmental Quality, September 9, 1994.
15. *On-Site Meteorological Program Guidance for Regulatory Modeling Applications, Table 8-1*. U.S. Environmental Protection Agency.
16. *Site Selection and Documentation Procedures Manual.* Texas Commission on Environmental Quality, July 1996.
17. *"Quality Assurance Requirements for State and Local Air Monitoring Stations (SLAMS),"* Title 40 Code of Federal Regultions, Part 58, Appendix A.
18. *"Reference Method for the Determination of Particulate Matter Collected from Ambient Air,"* Title 40 Code of Federal Regulations, Part 50, Appendix J.

19. *"Reference Method of the Determination of Suspended Particulate Matter Collected in the Atmosphere (High-Volume Method),"* Title 40 Code of Federal Regulations, Part 50, Appendix B.
20. *"Reference Method for the Determinations of Lead in Suspended Particulate Matter Collected from Ambient Air,"* Title 40 Code of Federal Regulations, Part 50, Appendix G.
21. *"Measurement Principle and Calibration Procedure for Measurement of Ozone in the Atmosphere,"* Title 40, Code of Federal Regulations, Part 50, Appendix D.
22. Standard Operating Procedures, Texas Commission on Environmental Quality:

HLAB-216:	Air Filters Digestion
HLAB-230:	Operation of the ICP-AES.
DMPOLLDV	Description of procedures for validating pollutant data from TCEQ CAMS operated under the MeteoStar/LEADS system.
DMDATART	Procedures to submit quarterly and annual data return of the criteria pollutant SO_2, NO_2, CO and O_3.
METDV	Procedures for validating pollutant and meteorological data collected from the MeteoStar LEADS system.
DMNCAMS1	Validation Procedures of NCAMS data relating to PM_{10}, lead and other manual.
AMOR-003:	Preparation of Polyurethane Foam (PUF) Plug Cartridges for Method TO-13 Sampling
AMOR-004:	Procedure for Cleaning Summa® Polished Stainless Steel Canisters Using Texas Commission on Environmental Quality Cleaning Manifold
AMOR-006	Determination of Volatile Organic Compounds (VOCs) Canisters by Gas Chromatography/Mass Spectroscopy (GC/MS) Using Modified Method TO-15
AMOR-014	Polycycle Aromatic Hydrocarbon (PAH) Anlysis of Polyurethane Foam (PUF) using Modified Method TO-13
AMOR-010:	Extraction of Polynuclear Aromatic Hydrocarbons (PAHs) from Polyurethane Foam (PUF) Plugs using Modified Method TO-13
AMPM-004:	Weighing of Quartz Filters in the Gravimetric Determination of Ambient Particulate Matter Less than 10 Micrometers (PM_{10})
AMPM-005:	Weighing of Quartz or Glass High-Volume (Hi-Vol) Filters in the Gravimetric Determination of Particulate Matter Less Than 10 Micrometers (PM_{10}) (μm) or Total Suspended Particulate (TSP) Matter
MeteoStar/LEADS-002:	Calibrator (Dasibi 5008), Operation and Troubleshooting
MeteoStar/LEADS-006:	Standardization of CAMS Span Sources (DASIBI 5008)
MeteoStar/LEADS-007:	Span Source Audit of Calibrations Systems (Dasibi 5008)
Meteostar/LEADS-009:	Performance Audit of Weather Measurement Gear

MeteoStar/LEADS-010:	Validation of Five-Minute and Hourly Data
SAMP-002:	Particulate Matter Less Than 10 Micrometers (µm) (PM_{10}) Sampling
SAMP-003:	Total Suspended Particulate (TSP) Sampling
SAMP-005:	High Volume Polyurethane Foam (PUF) Sampling
CALP-005:	Procedure for the use of the Molbloc/ Molbox Mass Flow Calibration System to Calibrate the Mass Flow Controllers (MFCs) in a Dasibi, Programmable Multi-Gas Calibrator, Series 5008 (Dasibi 5008)and for the Manual Calibration of the Ozone Generator in a Dasibi 5008
CALP-009:	Procedure for Calibrating Particulate Matter of 10 Microns or Less (PM_{10}) and Lead Orifices and Variable Restriction Orifices

B1 SAMPLING PROCESS DESIGN (EXPERIMENTAL DESIGN)

B1.1 Site Design

The site consists of an 800 ft long section of Texas tollway 45 located in northwest Austin. The site will be outfitted with four rows of traffic barriers. A 400 ft section of all four rows of barriers will be coated with a photocatalytic plaster. See Appendix A for air monitoring details. All measurements taken are classified as critical to meet project objectives.

B1.2 Measurement Validation

Standard methodology will be followed whenever possible. Sampling and validation efforts are described in Sections A6, B2, and D1. The quality assurance officer will review all data for acceptability. The meteorological data will be compared to those obtainable from nearby sites.

B3 SAMPLE HANDLING AND CUSTODY

All measurement data for this project is collected electronically, each sampling method has procedures that allow for clear custody record keeping for each transfer of information from the collection point to the final data holding mechanism.

B3.1 Documentation and Custody Requirements

B3.1.1 Nitric Oxide (NO)

There are no discrete samples handled by individuals for this method. The identity and disposition of samples are documented electronically by the run log associated with the instrument support computer and processing software. Instrument calibration information is recorded on standard data forms and maintained in the permanent record. Information regarding instrument maintenance is maintained in the Daily Activities Logbook.

B3.1.2 Nitrogen Dioxide (NO_2)

There are no discrete samples handled by individuals for this method. The identity and disposition of samples are documented electronically by the run log associated with the instrument support computer and processing software. Instrument calibration information is recorded on standard data forms and maintained in the permanent record. Information regarding instrument maintenance is maintained in the Daily Activities Logbook.

B3.1.3 Ozone (O_3)

There are no discrete samples handled by individuals for this method. The identity and disposition of samples are documented electronically by the run log associated with the instrument support computer and processing software. Instrument calibration information is recorded on standard data forms and maintained in the permanent record. Information regarding instrument maintenance is maintained in the Daily Activities Logbook.

B3.1.4 Meteorological Measurement Systems

There are no discrete samples handled by individuals for this method. The identity and disposition of samples are documented electronically by the run log associated with the instrument support computer and processing software. Information regarding instrument maintenance and calibration activities is maintained in the Daily Activities Logbook.

B3.2 Sample Handling Procedures

B3.2.1 NO

There are no discrete samples handled by individuals for these methods.

B3.2.2 NO_2

There are no discrete samples handled by individuals for these methods.

B3.2.3 O_3

There are no discrete samples handled by individuals for this method.

B3.2.4 Meteorological Measurement Systems

There are no discrete samples handled by individuals for this method.

B4 ANALYTICAL METHODS

B4.1 Analytical Procedures

This section presents information regarding the analytical methods used to develop ambient air measurements for this project. Where published methods exist, the method reference has been specified and exceptions to the published method are discussed in the TCEQ current version Standard Operating Procedures(SOP) AMOR-002 and AMOR-006. Current versions of the TECQ SOPs mentioned in the document are listed in Appendix E.

B4.1.1 Nitric Oxide (NO)

There are no exceptions to established guidance (see Section B2).

B4.1.2 Nitrogen Dioxide (NO_2)

There are no exceptions to established guidance (see Section B2).

B4.1.2 Ozone (O_3)

There are no exceptions to established guidance (see Section B2).

B4.1.4 Meteorological Measurement Systems

Metrological Data for this project was collected using an Met One Instruments Wind Sensor model 034B.

Wind Direction

Accuracy (absolute difference): ±4 degrees alignment, ±5 degrees overall. (The 1995 guidance for wind direction is agreement within ±5 degrees azimuth.)

Wind Speed

Accuracy (absolute difference): ±0.25 miles per hour (mph) at winds <22.7 mph, ±1.1 percent of true at winds >22.7 mph. (The 1995 guidance specifies a wind speed accuracy of ±0.2 ms^{-1} +5 percent of observed speed from 0.5 to 50 ms^{-1}. This corresponds to ±0.447 mph +5 percent of the observed speed from 1.12 mph to 112 mph. The current acceptable range for wind speed accuracy response using a direct reading sensor is within 0.56 mph at speeds below 11.2 mph and within ±5 percent at speeds above 11.2 mph; and ±5 mph using collocated wind speed measurement equipment.)

B4.2 Corrective Actions

It is expected that the individual discovering a problem will initiate corrective action appropriate to the situation. Documentation of the problem using site activity logs should be used.

At the UT Austin CEER laboratory, trained instrument operators and chemists are responsible for maintaining the equipment. Instrument manuals are available for troubleshooting, and if the problem is beyond the resources of the laboratory, service contracts are used to obtain assistance.

B6 INSTRUMENT/EQUIPMENT TESTING, INSPECTION, AND MAINTENANCE REQUIREMENTS

This section describes the procedures employed to ensure and maintain the readiness of the field equipment throughout all phases of the project. Corrective procedures and responsible staff members for corrective actions on analytical instruments are discussed in Section B4.2 of this plan.

B6.1 Instrument Testing/Inspection

Prior to collection of data, the sampling station is acceptance tested for one week, minimum, in the same configuration and location in the field where it will be operated. The purpose is to run operational checks to catch problems prior to collection of data; repair all malfunctioning equipment; and familiarize and train new operators, technicians, and field auditors. The basis for final acceptance testing is 80 percent valid data capture for all parameters.

B6.2 Preventive Maintenance Procedures

This section describes the routine preventive maintenance procedures performed on field ambient air monitoring/sampling systems. Generally, field technicians are responsible for all minor maintenance of monitoring systems. The field technicians are also responsible for making arrangements for all major maintenance per the contract. A backup technician may be called if the primary technician is not available.

B6.2.1 Nitric Oxide (NO)

Routine preventive maintenance procedures consisted of replacement of the sample line filter every two weeks.

B6.2.2 Nitrogen Dioxide (NO_2)

2.1 Nitric Oxide (NO)

Routine preventive maintenance procedures consisted of replacement of the sample line filter every two weeks.

B6.2.3 Ozone (O_3)

2.1 Nitric Oxide (NO)

Routine preventive maintenance procedures consisted of replacement of the sample line filter every two weeks.

B6.2.4 Meteorological Measurement Systems

Weekly visual inspections of the metrological system.

B6.3 Corrective Maintenance Procedures

This section describes the routine corrective maintenance procedures performed on ambient air monitoring/sampling systems.

B6.3.1 Nitric Oxide (NO)

Corrective maintenance procedures for the continuous NO monitors follow the manufacturer's recommendations in the instrument service manuals.

B6.3.2 Nitrogen Dioxide (NO_2)

Corrective maintenance procedures for the continuous NO_2 monitors follow the manufacturer's recommendations in the instrument service manuals.

B6.3.3 Ozone (O_3)

Corrective maintenance procedures for the continuous O_3 monitoring equipment follow the manufacturer's recommendations in the video service manuals.

B6.3.4 Meteorological Measurement Systems

Corrective maintenance procedures for the meteorological equipment follow the manufacturer's recommendations in the instrument service manuals.

B6.4 Availability of Spare Parts

A minimum stock level shall be maintained and stored in the designated location for all critical parts as determined by either the manufacturer's recommendation, experience or the UT Austin Project Manager.

B8 INSPECTION/ACCEPTANCE REQUIREMENTS FOR SUPPLIES AND CONSUMABLES

This section identifies the quality objectives for supplies and consumables to ensure high, valid data return.

B8.1 Sampling Supplies

The Project Manager from UT Austin is responsible for ordering and inspecting analytical materials and supplies used in the analysis of samples. These include reagents and solvents.

B8.2 Standards

The Project Manager shall order standards for the analytical calibrations on an as needed basis either from EPA or from commercial suppliers who provide standards meeting applicable EPA requirements. Standards are either traceable to National Institute of Standards and Technology (NIST) or are certified by the vendor and certification of traceability is kept on file by each laboratory.

B8.3 Spare Parts

The UT Austin Project Manager shall procure, store, and maintain an inventory of spare parts for all field equipment based on equipment manufacturer's recommendations, experience, and project history. Spare parts are tracked on a PC-based inventory system by UT Austin. These items are normally not expected to be tested upon receipt. However, if problems are observed when they are used in the field, the manufacturer shall be contacted by the subcontractor and tests are to be performed to identify and solve the problem.

B9 DATA ACQUISITION REQUIREMENTS (NON-DIRECT MEASUREMENTS)

All data for this project is expected to be direct measurements.

B2 SAMPLING METHODS REQUIREMENTS

This section addresses the approved sampling methods; the specific collection, preparation, and decontamination procedures of the equipment; the sample requirements, specifically the sampling media, sample preservation methods, holding times, field sample handling procedures; and the procedures to follow in case of a failure in the sampling system. The equipment and operating procedures are specified where the sampling method is automated. Every attempt has been made to be as complete as possible. It should be recognized that some of the procedures might change over the course of the program if logistical or quality related difficulties are encountered.

B2.1 Ozone (O_3), and Oxides of Nitrogen (NO, NO_X, NO_2)

Criteria pollutant (O_3, nitrogen dioxide [NO_2]) sampling procedures used in this monitoring program are consistent with U.S. Environmental Protection Agency (EPA) 40 *CFR* Part 58, Appendices A through G, the *Quality Assurance Handbooks for Air Pollution Measurement Systems, Volumes I and II,* and the reference and equivalent methods designation criteria outlined in 40 *CFR* Part 53. All materials are constructed of either borosilicate glass or Teflon®. The sampling station may use a sampling manifold that is heated by means of heat tape or light bulbs to a maximum of 30 °C in order to prevent water condensation inside the manifold. Also, a water trap may be located below the manifold to collect any water that condenses inside the manifold.

Ambient air is supplied to the continuous analyzers from the manifold through 1/4-inch diameter Teflon® tubing equipped with in-line particulate filters. All tubing is attached to the manifold sampling ports with screw-on connectors and connected to the analyzers with compression fittings. Excess airflow through the sample manifold and blower is vented away from the sample probe inlet.

The pollutant concentrations are automatically sampled and analyzed by the monitor. The output of the monitor is a voltage proportional to the concentration of the pollutant. The voltage outputs from the instruments are connected and sampled by a data logger once per second to form five-minute averages. These continuous monitors are normally connected to the data logger to preassigned channel numbers. Data are transferred to the Texas Commission on Environmental Quality (TCEQ) central office by a modem through a regional hub computer connection.

The continuous monitors for criteria pollutants are EPA approved equivalent or reference methods. Some of the measurement parameters, instrument model numbers, EPA method codes, and the approved full-scale range(s) of the monitors are identified in Table B2.1.A. Additional information may be obtained from the Geographical Common Table, found in the EPA Air Quality System (AQS) Database.

Table B2.1.A Criteria Pollutants

Criteria Pollutant Parameter	Instrument and Model Number	Designation/ Method Code	Method	Operating Range
O3	Dasibi Model 1008	EQOA0577019/019	Photometry	0.5 parts per million (ppm)

O3	Horriba		Photometry	0.5 parts per
NO_2	Teledyne API 200A TECO 42	RFNA1292090/090 RFNA1289074/074	Chemiluminescence	million (ppm)

B2.2 Meteorological Measurement Systems

Meteorological sampling procedures used in this monitoring program are collected using a c

Parameter	Range
Wind Speed	0 to 125 miles per hour
Wind Direction	0 to 359degrees (°)

Specific performance requirements for the meteorological systems include:

- The meteorological system is oriented to magnetic north with a compass.
- The wind direction for the meteorological system is corrected to true north by adding a magnetic declination value to the wind channel intercept in the monitoring station data logger. The magnetic declination is entered into the data logger when it is initialized at the time of installation. This task is performed by the Ambient Monitoring personnel who configure data loggers. Magnetic declinations for all sites are obtained from the United States Geological Service via internet at the following address: Telnet://neis.cr.usgs.gov.

B2.7 Corrective Actions

The field technician or project manager is responsible for operating samplers and initiating minor corrective actions on equipment when required. Equipment problems are generally detected through a failed sample run or through performing routine quality control (QC) checks on a regular basis. The QC checks that are performed on the sampling equipment are identified in Section B5 and detailed in Table B5 in Appendix F of this plan.

When a major equipment problem is involved, the technician refers it to the Project Manager, who has the responsibility to follow up on restoring the equipment to its proper operating status. This may be accomplished through telephone consultation with the field technician, followed up by a shipment of parts or by sending a technician from UT.

Any equipment problems that can result in the loss of data are addressed with a high priority. All situations requiring corrective action will be documented in site activity logs. Section B4.2 contains additional information on documentation of corrective action.

B5 QUALITY CONTROL (QC) REQUIREMENTS

The QC protocol for the sampling station is discussed in this section. An attempt is made to provide adequate information from which to estimate and control the uncertainty and potential limitations of measurements generated by the monitoring. QC activities are generally applied to portions of a measurement process that are both critical to measurement quality and practically subject to evaluation and control. The portions of any given measurement process that are both critical and subject to evaluation and control vary with the measurement being made and the method used. The QC protocol used for any given measurement process may include some or all of the following:

- Sampling system contribution to the measurements
- Measurement system contribution to the measurements
- Qualitative performance of the method
- Quantitative performance of the method
- Precision of the measurements
- Accuracy (bias) of the measurements

B5.1 Ozone (O_3) and Oxides of Nitrogen (NO, NO_X, NO_2)

The Sutron/MeteoStar software performs automated QC checks on three-point span check and five-point calibration data for O_3, and oxides of nitrogen. QC procedures, control limits, and formulas to calculate QC statistics are given in standard operating procedures specific to the monitoring that is part of the MeteoStar System. The primary purpose of the five-point calibration is to establish the calibration curve for a monitor and to evaluate the performance of the monitor at the time of the calibration. The purpose of the three-point span check is to evaluate drift in the calibration curve of a monitor between calibrations, evaluate monitor performance, and assess measurement precision.

In general, a warning and a failure control limit has been established for each of these QC checks for each type of monitor. Warning limits are statistically determined and set at three standard deviations. This means that there should be only a .27 percent probability that any given test will exceed the warning limit if the system being tested is in control. Failure limits are based on data validation criteria used currently such as DQO limits. An exceedance of a failure limit indicates that the system being tested is performing below minimum acceptable requirements and as a result the data should be evaluated for usefulness and that there is a need for corrective action.

The computer system performs a preliminary validation of the ambient data based on the results of these checks. Data validity decisions are based only on whether a QC test exceeds the failure limit. Appendix J describes these automated QC checks and validation rules in detail. Appendix F gives the QC limits for each check used by the computer system at the time of this plan revision.

The following QC checks are performed on all of the above-mentioned monitors:

- Media contribution - Zero Drift Test - Applies to both calibrations, span checks, and span zeros. Checks drift in the "zero" voltage since the last valid calibration. The zero

voltage is the monitor's response to clean air used in the calibration or span check. This is a monitor check that evaluates the drift of the instrument and is primarily a measure of intercept stability.

- Sampling system contribution - Intercept Test - Applies to calibrations only. Checks the intercept of the calibration curve against the expected value. This is a monitor check.
- Measurement system contribution/Precision - Precision/Linearity Test - Applies to calibrations only. Checks the closeness of measured calibration data points to the calibration curve defined by the calculated slope and intercept. This is a monitor check that looks for linearity or erratic response problems. Some calibration system problems will show up in this test also.
- Qualitative performance of the method - Slope Test - Applies to calibrations only. Checks the slope of the calibration curve against the expected value. This is a monitor check.
- Quantitative performance of the method - Span Drift Test - Applies to both calibrations and span checks. Checks drift in the "span" voltage since the last valid calibration. The span voltage is the monitor's response to the highest concentration used in the calibration or span check. This is a monitor check that evaluates the stability of the current calibration curve and is primarily a measure of slope stability.

Additional checks include:

- Completeness Test - Applies to both calibrations and span checks. Checks that the calibration or span check data set is complete before the data are processed.
- Concentration Outlier Test - Applies to each concentration level of both calibrations and span checks. Checks the stability of the reported concentration for each concentration level. This is a calibration system check.
- Monitor Outlier Test - Applies to each concentration level of both calibrations and span checks. Checks the stability of the monitor voltage for each concentration level. This is a monitor check.
- Concentration Spacing Test - Applies to each concentration level of both calibrations and span checks. Checks the reported concentration for each level against the expected concentrations. This is a calibration system check.
- Laboratory Control Checks – Checks the accuracy of the calibration using a second source. This is a calibration and analytical system check.
- Linearity Test - Applies to span checks only. Checks the linearity of the monitor. Some calibration system problems will show up in this test also.
- Converter Efficiency Test for Converting nitrogen dioxide to nitric oxide - Applies to both calibrations and span checks of oxides of nitrogen monitors. This is a monitor check.

B5.2 Meteorological Measurement Systems

Table B5 in Appendix F contains a detailed listing of the QC checks for the meteorological equipment. These QC activities include visual inspection of instrumentation integrity, measurement consistency with current conditions, and corrective actions. There is no collocated meteorological equipment.

- Sampling system contribution to the measurements is determined by the resolution and start threshold for the measurements.
- Measurement system contribution is controlled by the calibration of the sensors and is performed by the vendor. A functional check of the equipment is made before deployment of the equipment.
- Qualitative performance of the method is determined by visual inspection of the sensors and comparison of the data display to ambient conditions.
- Precision of the measurements do not apply to the meteorological parameters.
- Accuracy (bias) of the measurements is determined by comparison of instrument measurements with local conditions.

B7 INSTRUMENT CALIBRATION AND FREQUENCY

This section identifies the instruments, tools, and standards whose quality must be controlled; the methods and frequency of calibration; the calibration and performance standards; and the traceability of the standards. Table B5 in Appendix F contains summaries of the calibration requirements. It is the responsibility of each participant to maintain documentation regarding the traceability of the standard materials used as references for calibration purposes via logbooks or electronic logs.

B7.1 Field Equipment Requiring Calibration

B7.1.1 Ozone (O_3), and Oxides of Nitrogen (NO, NO_X, NO_2)

B7.1.1.1 O_3 Analyzer

Calibrations are performed at the beginning of sampling and monthly thereafter. Additionally, calibrations are performed following any instrument repair, replacement or adjustment. Five levels of O_3 calibration gas are introduced automatically at a programmed time into the inlet of the O_3 analyzer by a Teledyne Automatic Gas Standard Calibrator model number 700E in the monitoring station. The levels correspond to 80 percent, 60 percent, 40 percent, 18 percent, and 0 percent of the analyzer operating range. The O_3 calibration gas is derived from an O_3 generator that has been standardized with an O_3 transfer standard.

B7.1.1.2 Oxides of Nitrogen (NO, NO_X, NO_2) Analyzer

Nitric oxide (NO) calibration gases will be derived from secondary standard span gas bottles that have been certified using the EPA protocol. Procedures for NO gas cylinders are given in Technical Support Laboratory SOPs. Calibrations in the field are performed at the beginning of sampling and monthly thereafter. Five levels of calibration standard gases are introduced automatically at a programmed time into the inlet of the analyzers by a Teledyne Automatic Gas Standard Calibrator model number 700E in the monitoring station. The levels correspond to 80 percent, 60 percent, 40 percent, 18 percent, and 0 percent of the analyzer operating span range.

B7.1.1.3 Calibrator Zero/Span Systems

The Teledyne 700E Calibrator system for O_3 and oxides of nitrogen relies on the operation of flow controllers to maintain a span gas flow and a dilution ambient flow at each of four preset levels. For each concentration level during a calibration or span check, the calibrator reports the calculated concentration to the datalogger based on the measured flows and other calibration information entered into the calibrator.

The procedures for Teledyne 700E Calibrator system (for O_3 and NO_2) for standardizing (and auditing) the span gases are given in SOP MeteoStar/LEADS-006 and MeteoStar/LEADS-007. The standardization involves measuring the system parameters needed to calculate the pollutant concentrations that are generated during a multipoint calibration or span check. The UT CEER Laboratory maintains SOPs that detail the calibration of the flow controllers and ozone generator in the Teledyne 700E. The slopes and intercepts of the curves are entered into the Teledyne 700E.

The NO_2 calibration gas is derived from reaction of NO with O_3 generated by the station calibrator. The NO calibration gas is derived from a secondary standard span gas bottle. A linear regression is used to generate a slope and intercept. The measured zero from the calibration or span are used to adjust the intercept to the measured zero.

B7.1.2 Meteorological Measurement Systems

A functional check of the equipment prior to the start of sampling and following any sensor or system change or adjustment is performed. Table B5 in Appendix F contains further details regarding the calibration of the wind direction, wind speed, and temperature sensors.

B7.2 Laboratory Equipment Calibration Requirements

The UT CEER Laboratory maintains the equipment necessary for calibration of the meteorological equipment measuring wind direction, wind speed, as well as ozone calibration and volumetric flowr ate validation.

B7.2.1 O_3 and Oxides of Nitrogen (NO, NO_X, NO_2)

The gaseous standards are used for verifying transfer standards that in turn are used to calibrate or verify ambient pollution instrumentation in the field. Volumetric primary flow standards and transfer (mass) flow standards are maintained in the laboratory. The transfer flow standards are used in the field for determining flows in samplers and multiple span dilution calibration systems. The Technical Support Laboratory also maintains instruments for measuring O_3 and $NO/NO_2/NO_x$ in order to compare gaseous standards against primary standards. Records of certification and certificates of traceability are kept on file for all standards.

B7.2.1.1 O_3

<u>O_3 Primary Photometer</u>

UT CEER lab maintains a 2B Technology ozonre calibration system. The calibrator is returned to 2B annually for re-calibration using a NIST-traceable ozone standard.

<u>O_3 Transfer Standard</u>

UT CEER will certify the instrument annually.

B7.2.1.2 Oxides of Nitrogen (NO, NOX, NO2)

Cylinder gas standards for NO are maintained in the UT CEER Laboratory. The NO standards are EPA protocol. Standards are certified for stability for two years. Tags on the cylinder and records on file indicate the expiration dates.

<u>Field Standard Blends for NO and NO_2</u>

A Teledyne 700E Calibrator dynamic gas dilution system is used to blend standardized NO cylinder gases with zero air to generate precisely known concentrations of calibration and audit gases.

B7.2.5 Meteorological Measurement Systems

The UT CEER Laboratory maintains the equipment necessary for calibration of the meteorological equipment.

B7.3 Traceability

Continuous Ambient Monitoring Station (CAMS) calibration system flow rates produced by mass flow controllers are calibrated with a primary flow standard. The primary flow standards used for this purpose are listed below.

Standardization of NO Cylinder Gases

.All gases are certified EPA protocol NIST traceable by the Technical Support Laboratory or vendor.

Mass Flow meter Traceability

Flow rates produced in the field by the flow controllers used in transfer standards are directly measured using a Gilibrator Flow meter. Annually, the Gilibrator is returned to the manufacturer for certification traceable to NIST.

Calibration of Teledyne 700E Calibrator

The mass flow controllers in these calibrators are validated using a Gilibrator flow meter.

Meteorological Sensors

Reference equipment used for the calibration and auditing of meteorological parameters is certified as accurate by the vendors.

B7.4 Documentation

It is the responsibility of each participant to maintain documentation regarding the traceability of the standard materials used as references for calibration purposes.

Site logbooks, electronic logs, and data are maintained by the site operator and UT personnel.

B10 DATA MANAGEMENT

Data originates with the activities and individuals associated with implementation of each monitoring event. The final result for each event will be forwarded to the Monitoring Data Management and Analysis (MDMA) task leaders who will then compile the measurement results into an Air Quality System (AQS) compatible data set. Figure B10 summarizes the flow of data throughout the project.

B10.1 Ozone (O_3) and Oxides of Nitrogen (NO, NO_X, NO_2)

Data collected for the criteria pollutants, O_3 and oxides of nitrogen, and by the meteorological data monitors are transferred to the Sutro/MeteoStar. Sutron/Meteo Star automatically downloads data every fifteen minutes by modem over standard telephone lines. Operator messages and the calibration system parameters are also retrieved.

The continuous monitors at the sampling site are connected to Zeno data loggers. The data logger systems sample the analog output voltage of each instrument once a second, digitizes it, and stores the data sequentially as five-minute averages into a record. A record consists of sequential fields of data for as many channels as are activated for sampling.

Every 15 minutes, the Sutron/MeteoStar's computer collects the previous data from the monitoring station's data logger by modem. The data are secured from tampering or corruption over the carrier line through an unlisted telephone number, pass code protection, and error checking protocol.

The MeteoStar processing program checks for correct date, time, sampling site number, and proper formatting of raw data fields. It then performs quality control checks on the calibration and span data, and calculates five-minute and hourly averages, converting voltages to engineering units, as outlined in Appendix J of this document. At this stage, the data are considered "preliminary validated" data and are stored in a temporary disk file. The data validators work from this file through their terminals on a graphical interface. The data validators infrequently edit this file other than to change an incorrect status code that was entered by the field technician. An audit trail is kept of any changes to the data by the entry of the name of the data validator, the date, time, and comments related to any changes made. In addition, the data validators keep individual notebooks of corrections to data files.

After the project validators validate the data, the data are coded in the file. The coded data in this file are considered "validated data" and are archived on optical disk indefinitely. Data maintained on the CFEP are accessible through Internet web page reports.

After the validated data have been archived, data analysts continue to review the data for higher levels of data validation. These analysis reviews include performing comparisons over time between sites that are closely located or in very similar geographic locations and performing comparisons over time between parameters measured at the same site. If there is clear evidence that a problem exists that was not detected by earlier stages of data validation, then the project manager may choose to invalidate the data.

B10.2 Meteorological Measurement Systems

The meteorological equipment consists of the Met One Instruments Wind Sensor model 034B mounted on a cross arm atop a 10 foot mast. The parameters measured are wind speed and wind direction. The UT CEER Laboratory validates the data.

B10.3 Acceptability of the Hardware/Software Configuration

Sutron/MeteoStar's server periodically calls each Zeno data logger, collects the data measurements and operator log entries, makes local backup copies of the measurements and operator logs. Sutron/MeteoStar's server handles the data processing needs, the quality control processing of the O_3, and oxides of nitrogen pollutant data, and the long-term storage of validated continuous data. It provides data access and data editing capability to data validators through remote PC ports. The system is considered adequate to meet the current needs of the data users.

The Sutron/MeteoStar team maintains the computer system for the division.

Downloading and editing of data from Sutron/MeteoStar's server are restricted to data validators by password protection and restricted addresses. Data editing is done on-line on a PC with terminal emulation software. Data entry errors are minimized by the use of customized editing screens and data fields that perform legal character checking and provide an opportunity for the validator to check the data before it is uploaded to the permanent file.

Data validators make corrections to data using a graphical interface. A change in the database creates an automatic entry with an audit trail containing the name of the validator, the date of the change, and dates of the data changes, and a comment field to document why the data were edited. Original raw voltages are stored in the archive.

B10.4 Data to Users

Data that is stored in the MeteoStar system may be provided to internal users by e-mail, on floppy disk, and on printouts.

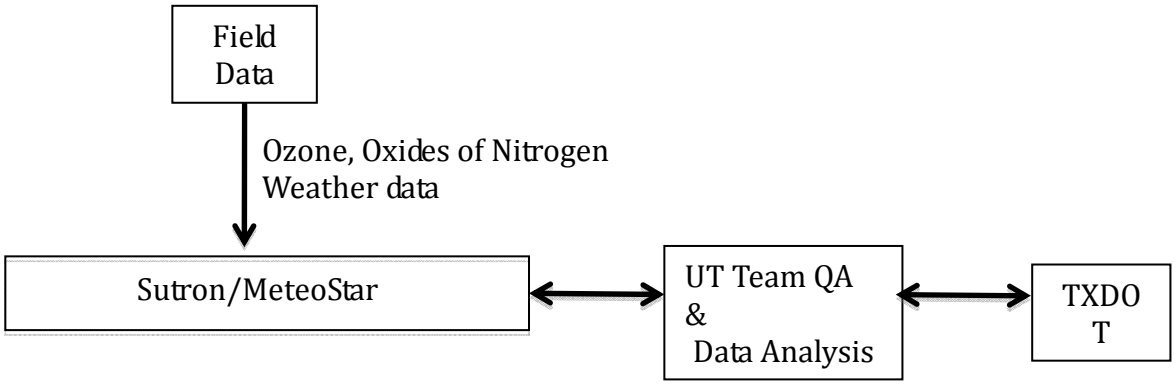

Figure B10 Data Flow and Storage

C1 ASSESSMENTS AND RESPONSE ACTIONS

The management of UT advocates and encourages a "continuous improvement" philosophy in personnel development and work processes. Each employee is responsible for implementing and evaluating the effectiveness of quality improvement activities with which he/she is involved. Fostering a "no-fault" attitude to encourage the identification of opportunities for improvement so they can be brought to the forefront and addressed accordingly is recognized to be a critical factor in a continuous improvement environment. Review of process performance is done on a continuous basis. This section addresses the assessment and response actions for this project.

C1.1 Performance Evaluations

Performance evaluations include response accuracy assessment of the continuous criteria pollutant analyzer for $O_{3V}$and oxides of nitrogen. Performance evaluation methods for the O_3, oxides of nitrogen should conform to EPA guidelines published in the EPA *Quality Assurance Handbook for Air Pollution Measurement Systems*.

All findings from a performance evaluation audit will be shared with the site operator or laboratory chemist.

The following performance evaluations of field systems are performed on the measurement system. They are normally conducted to assess the accuracy of the measurement data.

C1.1.1 Field Assessment

C1.1.1.1 O_3 and Oxides of Nitrogen (NO, NO_X, NO_2),

Assessment of the continuous monitors for gaseous O_3, NO, NO_X, and NO_2 pollutants are performed by QA personnel once per calendar year. Transfer standards used are different from those used in the previous standardization of the calibration systems in the monitoring station. The instruments are evaluated at the following concentration levels:

Level	O_3, NO
1	0.03 - 0.08 ppm*
2	0.15 - 0.20 ppm
3	0.35 - 0.45 ppm
4	0.80 - 0.90 ppm

*Parts per million (ppm)

If the full-scale range of a monitor is 1.0 or 1000 parts per billion (ppb), then level four is audited in addition to levels one through three.

These levels are used to assess the accuracy of each analyzer as required by *40 Code of Federal Regulations (CFR)* 58, Appendix A.

If the percent difference between the known concentration and the measured concentration for any level is more than ±20 percent, then the assessment is failed. A failed assessment

requires investigation of the cause by the monitoring station technician. The instrument is then repaired, if necessary, and recalibrated.

C1.1.1.2 Meteorological Measurement Systems

Once per year, the meteorological instruments are audited by the QA personnel using transfer standards of known, traceable accuracy, or by collocating a second set of transfer standard meteorological instruments.

C1.2 Data Quality Assessment

Data quality assessment activities consist of:

- Repeatability checks and collocated samplers to establish data precision
- Performance evaluations to establish data accuracy
- Valid data return calculations to determine data completeness

C1.2.1 Specific Procedures to Assess Data Quality

C1.2.1.1 Data Precision Assessment

Data precision is expressed in terms of upper and lower 95 percent probability limits. These limits give a quantitative measure of the precision or repeatability of the ambient data that are reported. For a given measured concentration, there is a 95 percent probability that a second measurement will fall within a range bounded by the first measured concentration, plus the upper limit percentage of the value and the measured concentration, minus the lower limit percentage of the value.

The assessment of data precision is based on the results of precision checks as described in 40 *CFR* 58, Appendix A.

In the case of the continuous monitors, the precision check consists of challenging each instrument with a concentration of 0.08 to 0.10 ppm for O_3 and nitric oxide (NO)/NO_2 monitors. The data logger in the air monitoring station performs this precision check as part of each monitor span check.

C1.2.1.2 Data Accuracy Assessment

Continuous monitor network accuracy for O_3, NO, NO_2, and NO_X is expressed in terms of upper and lower 95 percent probability limits. These limits give a quantitative measure of the accuracy of the ambient data that are reported. The true concentration of the data will have a 95 percent probability of falling within a range bounded by the reported value, plus the upper limit percentage of the value and the reported value, minus the lower limit percentage of the value. The results of the performance audits described in Section C1.2 of this plan are used to calculate accuracy for each instrument. Individual monitor accuracy is expressed in terms of percent difference. The equations used to calculate accuracy are given in 40 *CFR* 58, Appendix A.

Accuracy of the meteorological measurements is expressed as a signed difference relative to the audit standard value.

C1.3.1.3 Data Completeness Assessment

Data completeness is calculated as follows:

$$\% \text{ Completeness} = \frac{\text{Number of valid measurements}}{\text{Total possible measurements}} \times 100$$

C1.3 Corrective Actions

Corrective action is an essential part of any quality system and involves those procedures and actions taken to correct situations causing data quality to fall below established expectations. The need for corrective actions will be minimized by the implementation of applicable quality management plans, quality assurance project plans, and the application of statistical quality control to establish appropriate data quality limits for measurement activities. In the Monitoring Operations Division, the person discovering the problem generally initiates corrective action as soon as possible, whether it is by the field operator, an auditor or a data validator. Once a quality concern is identified, verbal and written communication between the affected parties is started and continues until the issue is resolved.

C2 REPORTS TO MANAGEMENT

The following discussion pertains to Project NO. 0-6636 "Photocatalytic NOx/HRVOC/O3 Removal in Transportation Applications" requirements.

C2.1 Annual Project QA Report

The project manager prepares a summary of the sampling station's data precision, accuracy, and completeness for the preceding year.

C2 REPORTS TO MANAGEMENT

The following discussion pertains to Project NO. 0-6636 "Photocatalytic NOx/HRVOC/O3 Removal in Transportation Applications" requirements.

C2.1 Annual Project QA Report

The project manager prepares a summary of the sampling station's data precision, accuracy, calibration activities, maintenance, measurements adjustments and completeness for the preceding year.

At least annually, the project QA officer reviews quality-related deficiencies, nonconformances, and programmatic improvements and prepares a summary report for the principal investigator and any interested parties.

D1 DATA REVIEW, VALIDATION, AND VERIFICATION REQUIREMENTS

D1.1 Data Validation

Data validation is an integral part of quality management. Project staff closely examines all air pollutant data and the conditions under which they were recorded to determine the validity of the data and whether individual measurements can be included for statistical analysis.

The UT project staff is responsible for data validation for ozone (O_3), oxides of nitrogen, wind speed, wind direction, ambient temperature and relative humidity.

TCEQ has individual Standard Operating Procedures (SOP) for the above activities. See Appendix M, References.

D1.1.1 O_3 and Oxides of Nitrogen (NO, NO_X, NO_2)

Initial data review and validation is performed by the software support system as described in B10.1 of this plan. The validation during processing consists of quality control (QC) checks on the five-minute raw data averages. These data processing checks are described in Section B5.1 of this plan.

The computer sets validation flags after the calibrations and span checks are processed. (See Appendix M for flag definitions.)

One of the following corrective actions is taken automatically depending on the type of flag:

- Reject ambient data back to the last good calibration or span check.
- Accept ambient data back to the last span or calibration.
- Reject ambient data forward to the next good calibration.
- Accept ambient data forward to the next good span or calibration.
- Use the old (or current) calibration curve.
- Use the new calibration curve to compute ambient data.

D1.1.2 Meteorological Measurement Systems

Meteorological special purpose monitoring is validated by comparison with meteorological data obtained from the National Weather Service.

D1.2 Data Custody

Custody of data is maintained by Sutron/MeteoStar.

D1.2.1 O_3 and Nitrogen (NO, NO_X, NO_2)

Custody of O_3 and oxides of nitrogen is maintained by by Sutron/MeteoStar. Only authorized personnel have access to the computer records, and only validators have passwords to log-on to the editing screens.

D1.2.2 Meteorological Measurement Systems

Data custody of meteorological data is maintained and managed by Sutron/MeteoStar.

D2 VALIDATION AND VERIFICATION METHODS

The objective of the data processing and validation effort is to obtain quality assured databases containing the monitoring data in a consistent format. As data are loaded into the databases, they will go through a screening process that will flag certain anomalies. The screening routines check all data for outliers, instrument problems, and data system problems. Documentation of changes resulting from review is described in the Data Management Technology Team individual Standard Operation Procedures (SOPs). Comments are added as necessary to explain the basis for the changes.

D2.1 Ozone (O_3) and Oxides of Nitrogen (NO, NO_X, NO_2)

The analysis and flow of the Sampling Station data from the point of collection to storage of validated concentrations is shown in Section B10, Figure B10.

Continuous monitoring data for nitric oxide (NO), nitrogen oxides (NO_x), and nitrogen dioxide (NO_2) are reported in parts per billion (ppb). The equations used by the Sutron/MeteoStar System to convert the monitor voltage outputs to ppm are given in Appendix J.

The data are validated based on the following principal criteria:

D2.1.1 Quality Control Test Results Performed by the MeteoStar Computer

These tests, described in standard operating procedure (SOP) Sutron/MeteoStar/LEADS-010 (Appendix N), check for span drift, zero drift, linearity, data outliers, and proper operation of the calibration system.

D2.1.2 Data Review

If an operator notes any unusual or nonstandard conditions, the operator enters the information in the electronic log, which is reviewed by the data validators. The data validators then determine how these conditions impact the data. Data validators may reject the data based on entries in the operator logs on a case-by-case basis. If, during a review of the ambient data, the data validator discovers abnormal concentrations as compared to expected values based on knowledge of past data, meteorology, and other conditions, the data validator checks electronic logs, span checks, calibrations, and quality control records to determine if there is a reason to invalidate the data in question.

D2.2 Meteorological Measurement Systems

Data obtained through the Sutron/MeteoStar computer are compared to data received from the National Weather Service and nearby stations.

D3 RECONCILIATION WITH USER REQUIREMENTS

Problems with potential limitations of the data are handled at three different levels: (1) at the time of audit of the field samplers by the field technician or project manager, who have prime responsibility for routine field calibrations and sampler repairs; (2) data validators, who monitor the status of the data within a day of the collection and processes of the raw data, or with staff from the Technical Support Team; and (3) by users of data, such project personnel, who may have questions or want to verify the data quality objectives with a data validator or staff at a later date after data is processed. Issues are reconciled at the lowest level and earliest time possible. Data Management Individual Standard Operating Procedures (SOPs) are maintained describing the detail processes (See Appendix O)**.** The mechanisms for communication between the producers and users of data are the telephone, the operator's log in the monitoring station data logger, and the field information data sheets accompanying the field samples.

The auditors, validators, analysts, and data managers are empowered to review and question any part of the measurement process and may initiate data reviews and corrective actions to bring the process back into compliance.

To assess the quality of the data produced during the monitoring efforts, the precision, accuracy, and completeness will be assessed in comparison to the data quality objectives as discussed in Section A7 and listed in Appendix C.

D3.1 Detection Limits

Analytical detection limits for each method are expected to be established according to procedures in 40 *Code of Federal Regulations (CFR)* 136 Part B.

D3.2 Precision

Precision for each method will be determined using the procedures outlined in 40 *CFR* 58, Appendix A.

D3.2.1 Ozone (O_3) and Oxides of Nitrogen (NO, NO_X, NO_2)

Precision for each pollutant will be determined using the procedures outlined in 40 *CFR* 58, Appendix A. The percent difference between the known input concentration (X_i) and the analyzer response (Y_i) is calculated for each individual calibration check. At the end of the reporting period, the mean (D) and standard deviation(s) of the individual percent differences are computed. Then, the UL and LL 95 percent PL are computed and compared to the project objectives.

UL and LL 95 percent PL for method precision using monitoring data are determined as follows:

$$\text{UL 95\% PL} = D + (1.96s)$$

$$\text{LL 95\% PL} = D - (1.96s)$$

where (D) represents the average of measured percent differences of the measured pollutant level from a known sample level during a sampling period and (s) represents the pooled standard

deviation of those averages, computed according to 40 *CFR* Part 58, Appendix A guidance. Average percent difference of a selected compound, (D), is determined as follows:

$$D = \frac{\sum_{i=1}^{n}\left(\frac{Y_i - X_i}{X_i} x\ 100\right)}{n}$$

where X_i is the known input concentration and Y_i is the analyzer response for the i^{th} sample from n number of samples.

D3.2.2 Meteorological Measurement Systems

Precision measurements are not applicable to the meteorological measurements.

D3.3 Accuracy

D3.3.1 O_3 and Oxides of Nitrogen (NO, NO_X, NO_2)

Accuracy will be determined by challenging the O_3 and oxides of nitrogen monitors with gas standards containing the compounds of interest at concentrations representative of the ambient atmospheres typically being monitored during the study. The gas standard component concentrations are expected to be within five to 10 times the estimated detection limits.

Accuracy for each pollutant will be determined using the procedures outlined in 40 *CFR* 58, Appendix A. The percent difference between the known input concentration (X_i) and the analyzer response (Y_i) is calculated for each audit level. At the end of the reporting period, the mean (D) and standard deviation(s) of the individual percent differences are computed. Then, the UL and LL 95 percent PL are computed and compared to the project objectives.

D3.3.2 Meteorological Measurement Systems

Accuracy of the meteorological equipment (wind direction, wind speed, and temperature monitors) will be assessed by comparison to collocated audit equipment or by the use of direct reading sensors.

The absolute difference between the audit measurement (X_i) and the monitor's response (Y_i) for each parameter is calculated and compared to the project objectives, based on EPA *Quality Assurance Handbook, Volume IV*, March 1995 (modifications noted).

Wind Direction

Accuracy of wind direction has a graphical resolution: 22.5°.

Wind Speed

Vendor provided accuracy is ±10%.

D3.4 Completeness

Data completeness is calculated as follows:

$$\% \text{ Completeness} = \frac{\text{Number of valid measurements}}{\text{Total possible measurements}} \times 100$$

Appendix H

Photocatalytic NOx/HRVOC/O3 Removal in Transportation Applications Project - Early Data Analysis Report

Photocatalytic NOx/HRVOC/O_3 Removal in Transportation Applications Project
Data Analysis Report November 15, 2016

Prepared by:
David W. Sullivan, Ph.D.
The University of Texas at Austin
Center for Energy and Environmental Resources
10100 Burnet Rd, Bldg 133, MC R7100, Austin, TX 78758-4445
512-471-7805 office, 512-914-4710 cell
Email: sullivan231@mail.utexas.edu

Contents

Introduction 1
Meteorological Data 2
Diurnal Patterns of NO_2 by Week, March 23–September 19, 2016 6
Diurnal Patterns of O_3 by Week, March 23–September 19, 2016 17
The Relationship between Deltas and Meteorology 29
Conclusions and Recommendations 32

List of Figures

Figure H.1 Google Earth Pro aerial of the vicinity around Monitoring Sites 2001/2002 (yellow pushpin) 1
Figure H.2 Google Earth Pro aerial of Monitoring Sites 2001/2002 (yellow pushpin) and the City of Austin area 2
Figure H.3 Wind rose from hourly resultant wind speed and direction, Monitoring Sites 2001/2002, 3/23/2016–9/19/2016 3
Figure H.4 Wind rose from hourly resultant wind speed and direction, TCEQ CAMS 38, 3/23/2016–9/19/2016 4
Figure H.5 Wind rose from hourly resultant wind speed and direction, TCEQ CAMS 3, 3/23/2016–9/19/2016 4
Figure H.6 Histogram of wind speed percentage for three sites, data from 3/23/2016–9/19/2016 5
Figure H.7 Google Earth Pro aerial of Monitoring Sites 2001/2002 and nearby North Austin monitoring sites with meteorological measurements 6
Figure H.8 NO_2 diurnal patterns for March 23–29, 2016 (week 1)) 9
Figure H.9 NO_2 diurnal patterns for March 30–April 5, 2016 (week 2) 9
Figure H.10 NO_2 diurnal patterns for April 6–12, 2016 (week 3) 9
Figure H.11 NO_2 diurnal patterns for April 13–19, 2016 (week 4) 10
Figure H.12 NO_2 diurnal patterns for April 20–26, 2016 (week 5) 10
Figure H.13 NO_2 diurnal patterns for April 27–May 3, 2016 (week 6) 10
Figure H.14 NO_2 diurnal patterns for May 4–10, 2016 (week 7) 11
Figure H.15 NO_2 diurnal patterns for May 11–17, 2016 (week 8) 11
Figure H.16 NO_2 diurnal patterns for May 18–24, 2016 (week 9) 11
Figure H.17 NO_2 diurnal patterns for May 25–31, 2016 (week 10) 12
Figure H.18 NO_2 diurnal patterns for June 1–7, 2016 (week 11) 12
Figure H.19NO_2 diurnal patterns for June 8–14, 2016 (week 12) 12
Figure H.20 NO_2 diurnal patterns for June 15–21, 2016 (week 13) 13
Figure H.21 NO_2 diurnal patterns for June 22–28, 2016 (week 14) 13
Figure H.22 NO_2 diurnal patterns for June 29–July 5, 2016 (week 15) 13
Figure H.23 NO_2 diurnal patterns for July 6–12, 2016 (week 16) 14
Figure H.24 NO_2 diurnal patterns for July 20–26, 2016 (week 18) 14
Figure H.25 NO_2 diurnal patterns for July 27–August 2, 2016 (week 19) 14
Figure H.26 NO2 diurnal patterns for August 3–9, 2016 (week 20) 15
Figure H.27 NO2 diurnal patterns for August 10–16, 2016 (week 21) 15

Figure H.28 NO_2 diurnal patterns for August 17–23, 2016 (week 22) 15
Figure H.29 NO_2 diurnal patterns for August 31–September 6, 2016 (week 24) 16
Figure H.30 NO_2 diurnal patterns for September 14–19, 2016 (week 26) 16
Figure H.31 Ozone diurnal patterns for March 23–29, 2016 (week 1) 19
Figure H.32 Ozone diurnal patterns for March 30–April 5, 2016 (week 2) 19
Figure H.33 Ozone diurnal patterns for April 6–12, 2016 (week 3) 19
Figure H.34 Ozone diurnal patterns for April 1319, 2016 (week 4) 20
Figure H.35 Ozone diurnal patterns for April 20–26, 2016 (week 5) 20
Figure H.36 Ozone diurnal patterns for April 27–May 3, 2016 (week 6) 20
Figure H.37 Ozone diurnal patterns for May 4–10, 2016 (week 7) 21
Figure H.38 Ozone diurnal patterns for May 11–17, 2016 (week 8) 21
Figure H.39 Ozone diurnal patterns for May 18–24, 2016 (week 9) 21
Figure H.40 Ozone diurnal patterns for May 25–31, 2016 (week 10) 22
Figure H.41 Ozone diurnal patterns for June 1–7, 2016 (week 11) 22
Figure H.42 Ozone diurnal patterns for June 8–14, 2016 (week 12) 22
Figure H.43 Ozone diurnal patterns for June 15–21, 2016 (week 13) 23
Figure H.44 Ozone diurnal patterns for June 22–28, 2016 (week 14) 23
Figure H.45 Ozone diurnal patterns for June 29–July 5, 2016 (week 15) 23
Figure H.46 Ozone diurnal patterns for July 6–12, 2016 (week 16) 24
Figure H.47 Ozone diurnal patterns for July 20–26, 2016 (week 18) 24
Figure H.48 Ozone diurnal patterns for July 27–August 2, 2016 (week 19) 24
Figure H.49 Ozone diurnal patterns for August 3–9, 2016 (week 20) 25
Figure H.50 Ozone diurnal patterns for August 10–16, 2016 (week 21) 25
Figure H.51 Ozone diurnal patterns for August 17–23, 2016 (week 22) 25
Figure H.52 Ozone diurnal patterns for August 31–September 6, 2016 (week 24) 26
Figure H.53 Ozone diurnal patterns for September 7–13, 2016 (week 25) 26
Figure H.54 Ozone diurnal patterns for September 14–19, 2016 (week 26) 26
Figure H.55 Strung-together diurnal graphs of hourly delta O_3 (Site 2 – Site 1) averaged by week, week numbers on x-axis from Table H.3 27
Figure H.56 Strung-together diurnal graphs of hourly delta O_3 (Site 2 – Site 1) averaged by week, week numbers on x-axis from Table H.3, weeks 1–9 27
Figure H.57 Strung-together diurnal graphs for hourly delta O_3 (Site 2 – Site 1) averaged by week, week numbers on x-axis from Table H.3, weeks 10–16 28

Figure H.58 Strung-together diurnal graphs for hourly delta O_3 (Site 2 – Site 1) averaged by week, week numbers on x-axis from Table H.3, weeks 18–26 28

Figure H.59 June 1 to September 19, 2016 hourly delta O_3 and precipitation averaged from three Central Texas weather stations..... 32

List of Tables

Table H.1 Nearby North Austin monitoring sites with meteorological measurements..... 5

Table H.2 Mean difference Site2 minus Site1 NO_2 by 3-hour period & week during 2016 (green for Site1 > Site2, red for Site2 > Site1) 8

Table H.3 Mean difference Site2 minus Site1 O_3 by 3-hour period & week during 2016 (green for Site1 > Site2, red for Site2 > Site1) 18

Table H.4 Simple Statistics from SAS CORR Procedure, Year = 2016, period = daytime 31

Table H.5 Pearson Correlations from SAS CORR Procedure, Year = 2016, period = daytime..... 31

Introduction

The goal of the project is to determine the extent to which two nearby sites measure the difference in concentrations (often referred to as the delta) between similar air parcels where the difference is assigned to a photocatalytic surface coating that lowers nitrogen dioxide (NO2) and ozone (O3) concentrations.

Figure H.1 shows the location of the Photocatalytic NOx/HRVOC/O3 Removal in Transportation Applications Project (Project) monitoring site on the north side of a Texas State Highway 45 toll station north of Austin, TX. The site has two stations that are installed coded in the Sutron LEADS data system as Monitoring Site 2001 and Monitoring Site 2002. Figure H.2 shows the roadside test site (test site) on an aerial map of the Austin metro region. The test site is 23 km north of the urban center in the prevailing downwind direction. At the test site, wind speed and direction are measured at one location, but O_3, NO_2, total nitrogen oxides (NOx), and nitric oxide (NO) are measured at both sampling stations.

Figure H.1 Google Earth Pro aerial of the vicinity around Monitoring Sites 2001/2002 (yellow pushpin)

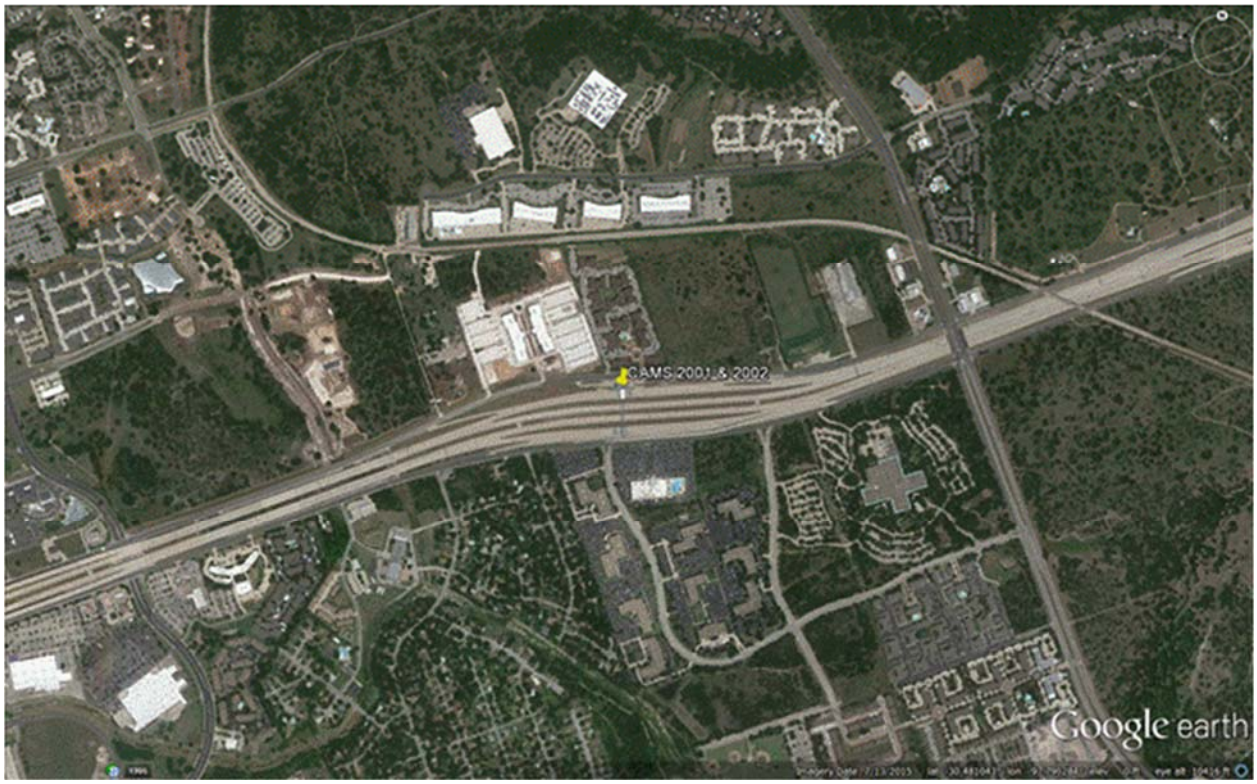

Figure H.2 Google Earth Pro aerial of Monitoring Sites 2001/2002 (yellow pushpin) and the City of Austin area

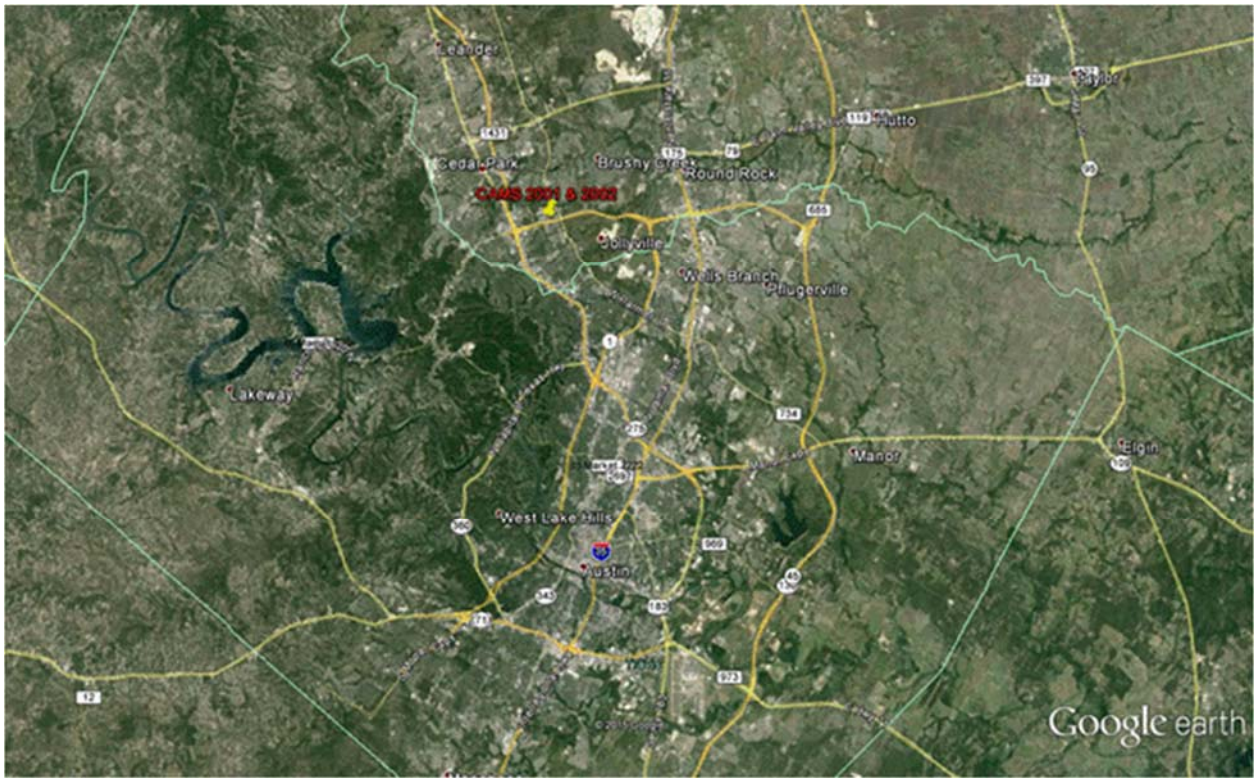

Meteorological Data

As was mentioned above, the test site is in the prevailing downwind direction of Austin TX, (2016 population ~ 926,426) within the Austin-Round Rock MSA (2016 population ~ 2,050,311). As is shown in Figure H.1 the test site is also on the downwind side of a limited access tollway. Figure H.3 is a wind rose created from the hourly wind speed and wind directions resultants measured at the site over the period March 23 to September 19, 2016. Figures H.4 and H.5 are wind roses created from the hourly wind speed and wind directions resultants measured at two nearby TCEQ Continuous Ambient Monitoring Station (CAMS) sites, CAMS 3 and CAMS 38.

The winds used in Figures H.3, H.4, and H.5 were measured over the same time period, but the sites show significant differences. Both CAMS 3 and CAMS 38 have an ensemble of wind directions more tightly clustered from south to southeast compared to Monitoring Sites 2001/2002, for which winds are spread out from southwest through east-southeast. There also appear to be more winds at higher speed at Monitoring Sites 2001/2002. Figure H.6 is a histogram of the wind speeds comparing the three sites. Note that wind speeds have been measured in knots (nautical miles per hour) in Figures H.3 through H.6. Figure H.6 shows the Monitoring Sites 2001/2002 with more observations in the 7 to 11 knot and 11 to 17 knot ranges compared to the other two sites. An assignable cause for the higher wind speeds and wider spread in wind directions observed at Monitoring Sites 2001/2002 could be the small-scale effects that fast moving motor vehicles have on the wind measurements at the test site. The same comparisons were made in the 2015 monitoring report with similar conclusions.

A map of the TCEQ site locations is shown relative to Monitoring Sites 2001/2002 in Figure H.7 and coordinates are listed in Table H.1.

Figure H.3 Wind rose from hourly resultant wind speed and direction, Monitoring Sites 2001/2002, 3/23/2016–9/19/2016

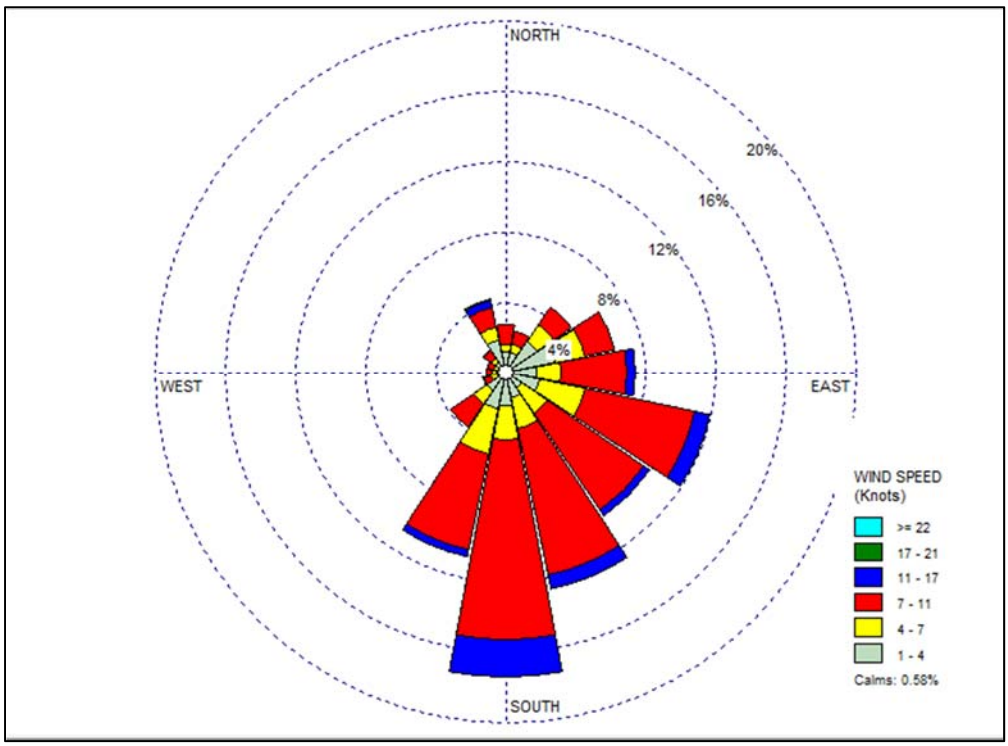

Figure H.4 Wind rose from hourly resultant wind speed and direction, TCEQ CAMS 38, 3/23/2016–9/19/2016

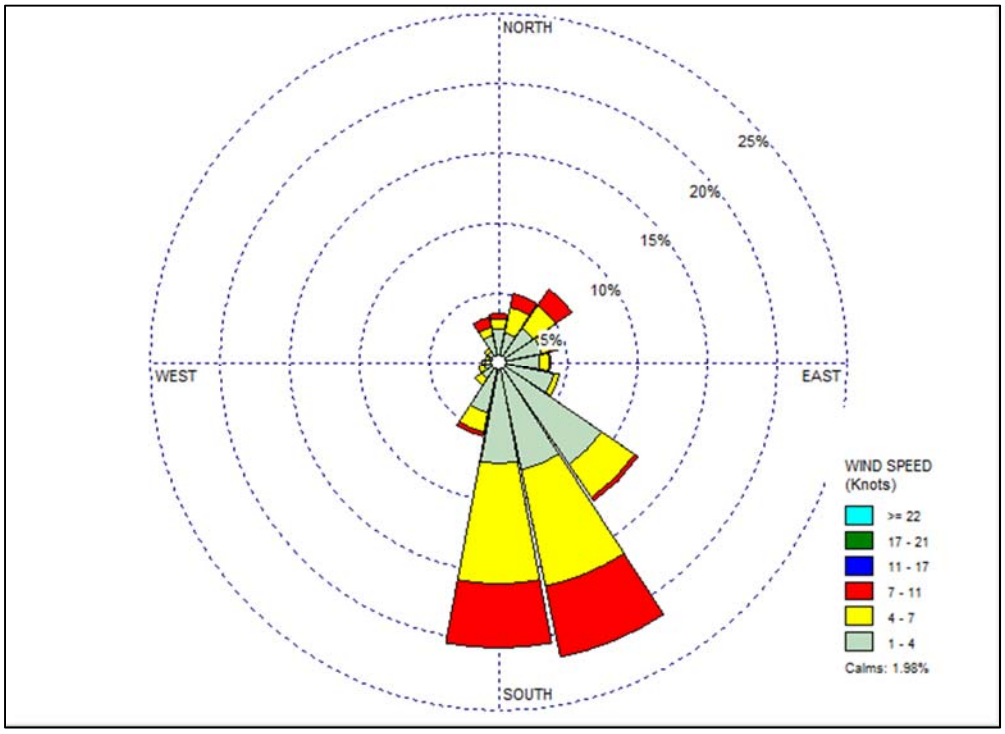

Figure H.5 Wind rose from hourly resultant wind speed and direction, TCEQ CAMS 3, 3/23/2016–9/19/2016

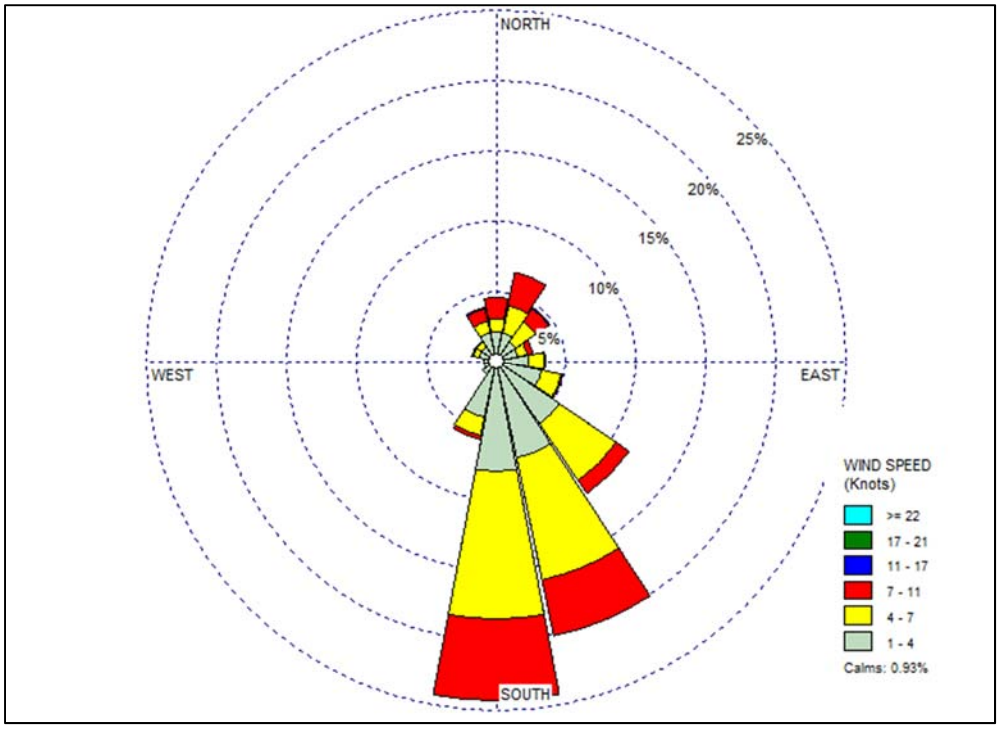

Figure H.6 Histogram of wind speed percentage for three sites, data from 3/23/2016–9/19/2016

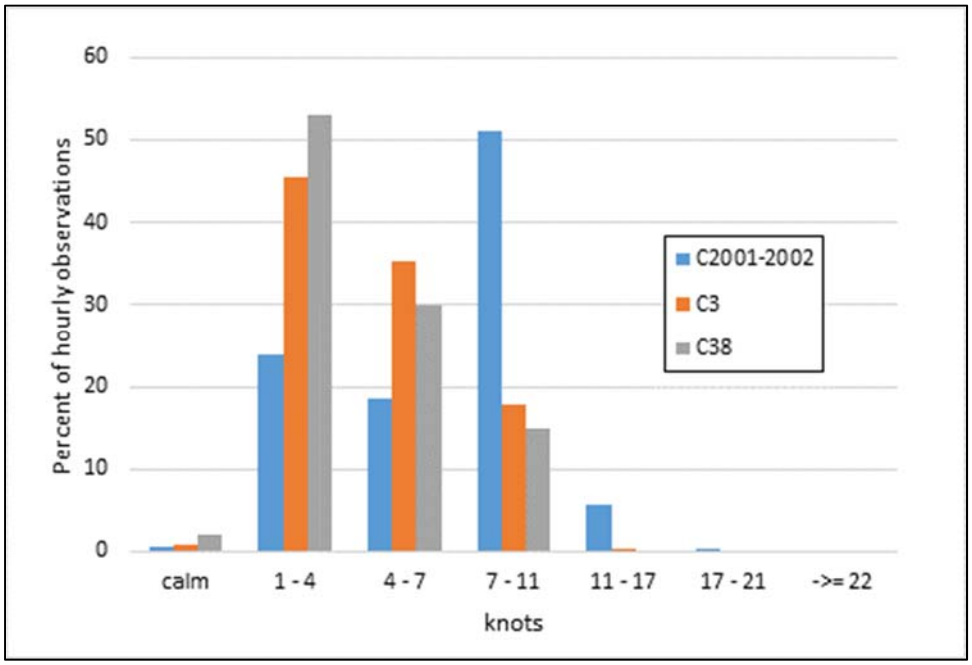

Table H.1 Nearby North Austin monitoring sites with meteorological measurements

Monitoring site	Latitude	Longitude
CAMS 3	30.3544	-97.7603
CAMS 38	30.4832	-97.8723
Monitoring Sites 2001/2002	30.4751	-97.7751

Figure H.7 Google Earth Pro aerial of Monitoring Sites 2001/2002 and nearby North Austin monitoring sites with meteorological measurements

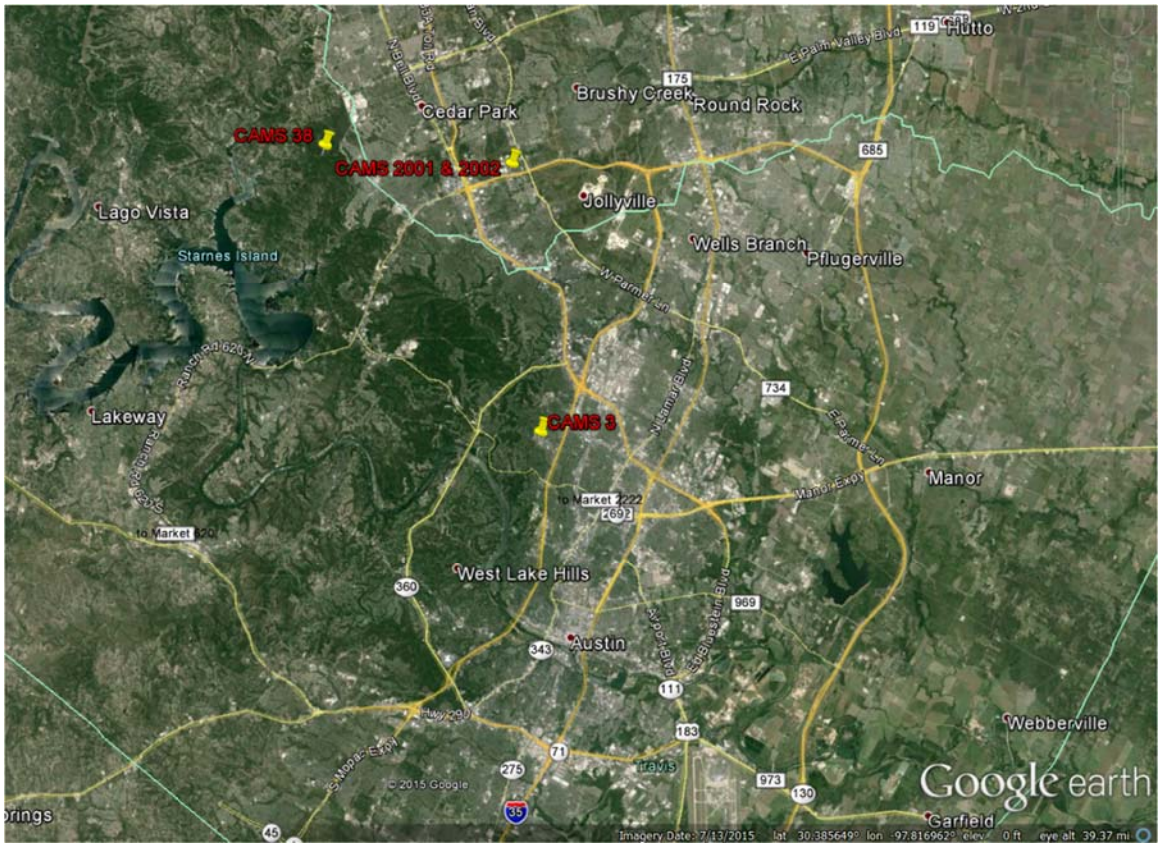

Diurnal Patterns of NO_2 by Week, March 23–September 19, 2016

NOx analyzers measure NO, NO_2, and NOx. One focus of this study is the effect of a particular catalyst treatment on NO_2 concentrations, and so two analyzers were used—one exposed to the treatment, and one not exposed to the treatment. The data analyst assigned to study the measurement data does not know which monitoring station was exposed to the treatment. Table H.2 summarizes the average concentration differences between the two NOx analyzers' NO_2 measurements in 2016. Each instrument is labeled by monitoring site abbreviation of Site 1 and Site 2, for sites 2001 and 2002, respectively. Table H.2 was constructed by first averaging all 5-minute time scale measurements by hour, then averaging the hours across a week (seven day periods), then calculating the difference in average NO_2 from Site 2 minus Site 1 (*Delta* NO_2), then averaging difference by three hour periods. These operations could be carried out in a different order, but were done in this order to facilitate different examinations of the data at intermediate steps.

Within Table H.2, the columns are the eight three-hour periods in a 24-hour day, and the rows are the weeks in 2016 with more than 50 percent data return on coincident sampling at the two analyzers. The last column is the average across all three-hour averages, and the last row is the average across all weeks.

To illustrate the results of Table H.2, Figures H.8 through H.30 show the average concentrations for NO_2 by hour of the day (*diurnal pattern*) for each week for which coincident data were collected from Wednesday March 23, 2016 to Monday September 19, 2016. Each graph caption shows the week numbers (March 23–March 29 = week 1) corresponding to date ranges in Table H.2. These graphs show varying differences between *NO_2 Site 2* and *NO_2 Site 1*. As was the case with the 2015 project report, the differences in many cases persist outside of the periods of sunlight. All graphs have the same y-axis ranging from 14.0 to -10.0 ppb. Three weeks had insufficient data: July 13–July 19, August 24–30, and September 7–September 13. Regarding the comparisons made between monitors in the following notes, it is important to recognize that the measured ambient concentrations taken for this project were relatively low compared to the levels at which the instruments are calibrated and span checked. The observed differences between Site 1 and Site 2 were less than the expected cumulative error tolerance of the NOx analyzers and calibration system.

- From March 23 through the week of April 27 to May 3, *Site 1* average concentrations were higher than *Site 2* average NO_2 concentrations over nearly all 24 hours.
- From May 4 through the week of May 18 to May 24, *Site 2* average concentrations were higher than *Site 1* average NO_2 concentrations from morning until late night, with similar concentrations at other hours.
- From May 25 through the week of July 20–26, *Site 2* average concentrations were higher than *Site 1* average NO_2 concentrations over nearly all 24 hours.
- For the week July 27–August 2, average concentrations are about the same at the two Sites.
- For the week August 3–August 9, *Site 1* average concentrations were higher than *Site 2* average NO_2 concentrations over all 24 hours.
- For the August 10 through the week of September 14 to September 19, *Site 2* average concentrations were higher than *Site 1* average NO_2 concentrations over nearly all 24 hours.

One notices a significant number of hourly averages for NO_2 less than 0.0 ppb in the majority of NO_2 diurnal pattern graphs. In general, compared to other pollutants, NO_2 is relatively difficult to measure. It is not directly measured, but rather is indirectly measured from subtracting an NO measurement from an NO plus reduced NO_2 (to NO, with a catalyst) measurement. With low NOx concentrations, it is often the case that an NO_2 value is quantified as a small negative value.

Table H.2 Mean difference Site2 minus Site1 NO_2 by 3-hour period & week during 2016 (green for Site1 > Site2, red for Site2 > Site1)

Week	Week	00-02	03-05	06-08	09-11	12-14	15-17	18-20	21-23	Grand
1	Mar. 23-Mar.	-1.11	-1	-0.41	-0.92	-0.37	-0.26	-0.61	-0.73	-0.68
2	Mar. 30-Apr. 5	-2.2	-2.02	-2.66	-2.62	-2.57	-1.92	-2.90	-3.27	-2.52
3	Apr. 6-Apr. 12	-2.23	-1.67	-1.94	-1.84	-0.90	-0.96	-1.62	-1.64	-1.60
4	Apr. 13-Apr.	-2.09	-1.72	-1.30	-1.21	-0.91	-0.48	-1.12	-1.59	-1.3
5	Apr. 20-Apr.	-1.89	-1.70	-0.56	-1.00	-1.14	-1.15	-1.73	-1.96	-1.39
6	Apr. 27-May 3	-2.05	-2.29	-1.74	-1.16	-1.05	-1.05	-1.15	-1.62	-1.51
7	May 4-May10	0.05	-0.10	0.46	0.78	0.75	0.55	0.03	0.42	0.37
8	May 11-May	-0.23	-0.24	-0.19	0.36	0.57	0.67	-0.37	-0.22	0.04
9	May 18-May	0.22	0.24	1.04	1.27	1.08	1.60	0.75	0.51	0.84
10	May 25-May	1.78	1.50	1.74	1.47	1.55	1.56	1.30	1.23	1.52
11	Jun. 1-Jun. 7	1.75	2.21	3.68	4.01	3.79	3.86	3.24	2.76	3.16
12	Jun. 8-Jun. 14	3.83	4.14	3.60	3.59	3.52	4.12	3.18	3.46	3.68
13	Jun. 15-Jun.	2.96	3.31	2.74	2.74	2.84	2.97	2.59	2.82	2.87
14	Jun. 22-Jun.	1.49	1.41	1.13	1.69	1.64	1.63	0.88	1.34	1.40
15	Jun. 29-Jul. 5	1.18	1.38	1.90	2.24	2.21	1.80	1.62	1.66	1.75
16	Jul. 6-Jul. 12	2.43	2.33	2.03	2.08	2.13	1.97	1.84	2.07	2.11
18	Jul. 20-Jul. 26	2.53	2.73	2.28	2.65	2.47	2.67	2.59	2.29	2.53
19	Jul. 27-Aug. 2	0.44	0.17	-0.18	-0.21	-0.09	-0.43	-0.33	-0.12	-0.09
20	Aug. 3-Aug. 9	-1.79	-1.66	-1.82	-1.59	-1.55	-1.34	-1.68	-1.77	-1.65
21	Aug. 10-Aug.	0.69	0.66	1.20	1.67	0.91	1.30	1.15	1.02	1.07
22	Aug. 17-Aug.	1.25	1.54	1.78	1.92	2.00	1.74	1.66	1.54	1.68
24	Aug. 31-Sep. 6	0.08	0.28	0.99	0.87	0.99	1.17	0.64	0.19	0.65
26	Sep. 14-Sep.	2.53	2.88	3.19	4.11	4.08	3.15	2.81	2.59	3.17
Grand		0.42	0.54	0.74	0.91	0.96	1.01	0.56	0.48	0.70

Figure H.8 NO_2 diurnal patterns for March 23–29, 2016 (week 1))

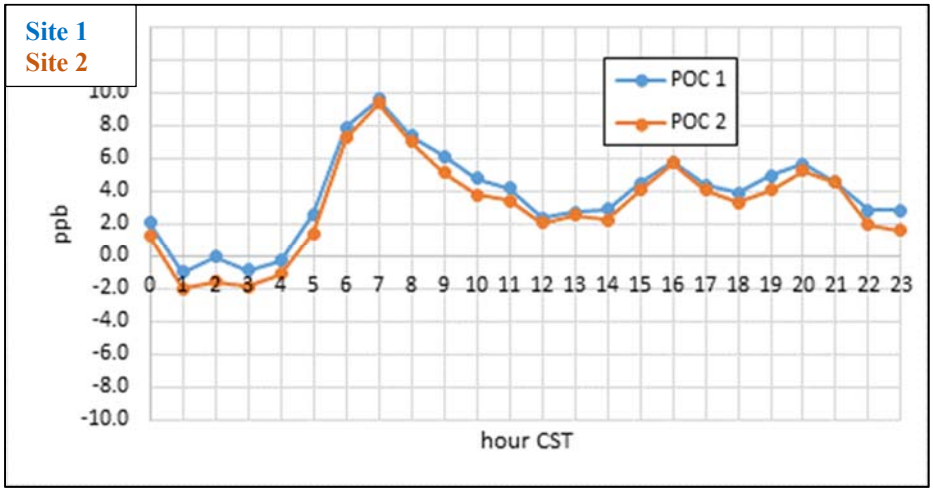

Figure H.9 NO_2 diurnal patterns for March 30–April 5, 2016 (week 2)

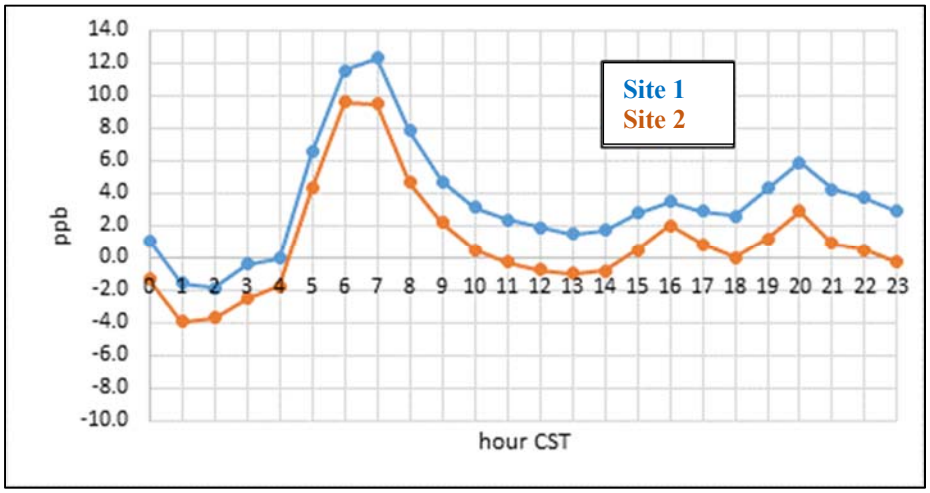

Figure H.10 NO_2 diurnal patterns for April 6–12, 2016 (week 3)

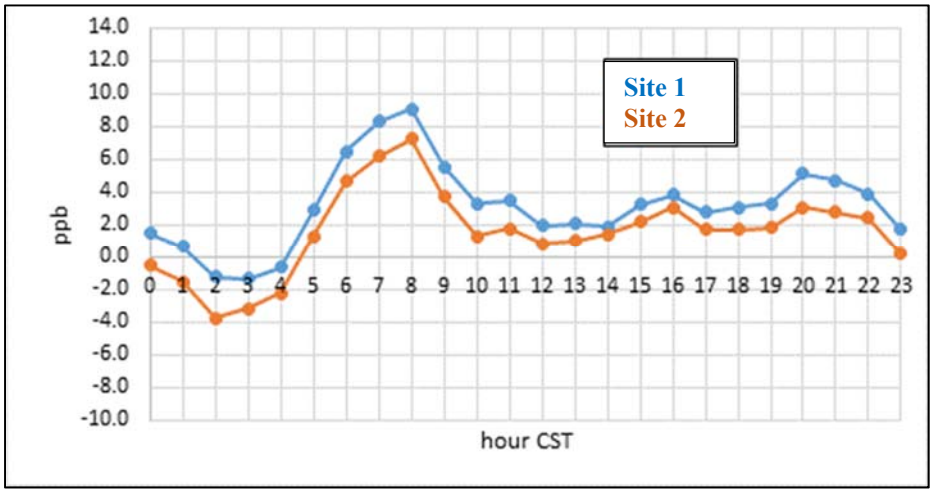

Figure H.11 NO_2 diurnal patterns for April 13–19, 2016 (week 4)

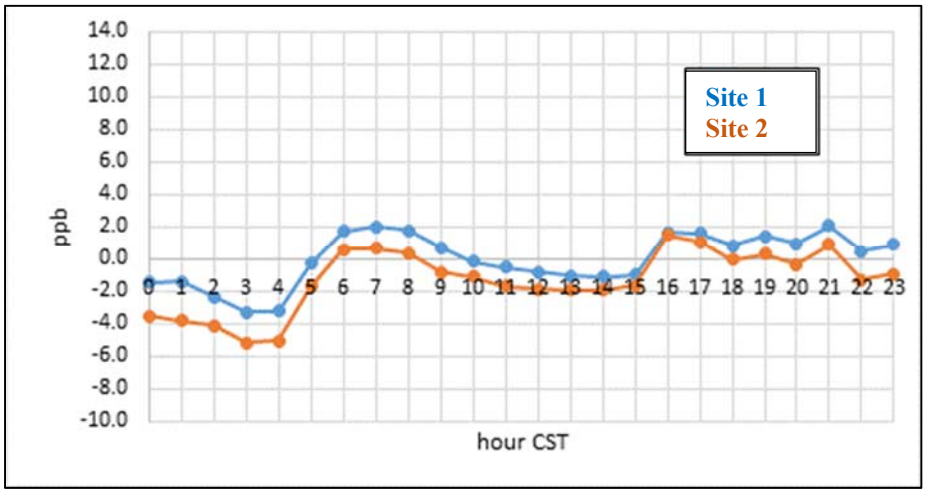

Figure H.12 NO_2 diurnal patterns for April 20–26, 2016 (week 5)

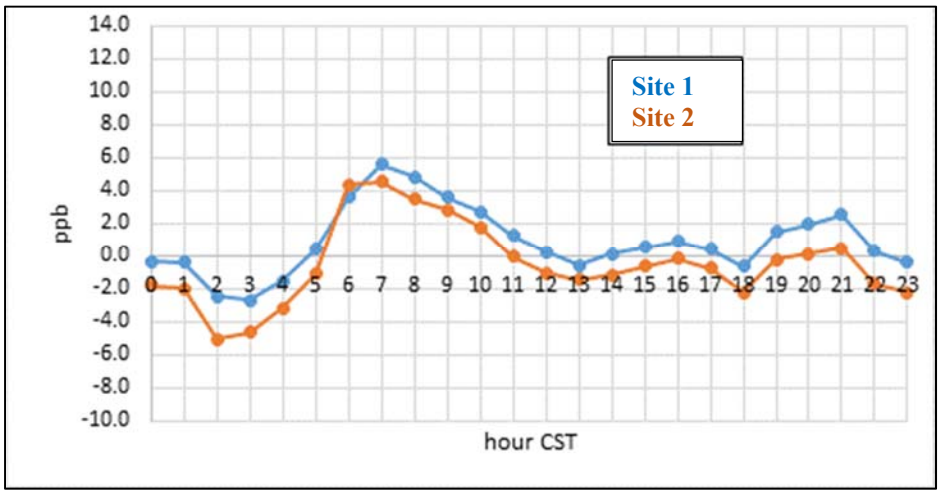

Figure H.13 NO_2 diurnal patterns for April 27–May 3, 2016 (week 6)

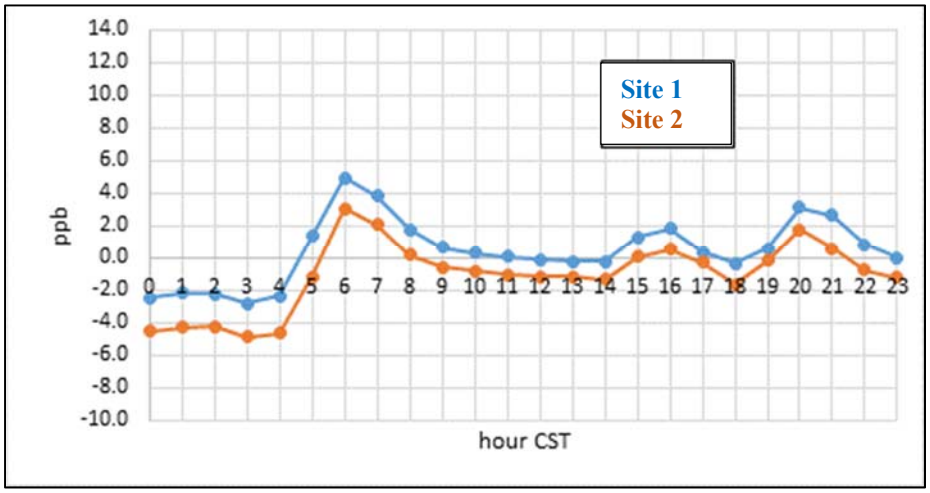

Figure H.14 NO_2 diurnal patterns for May 4–10, 2016 (week 7)

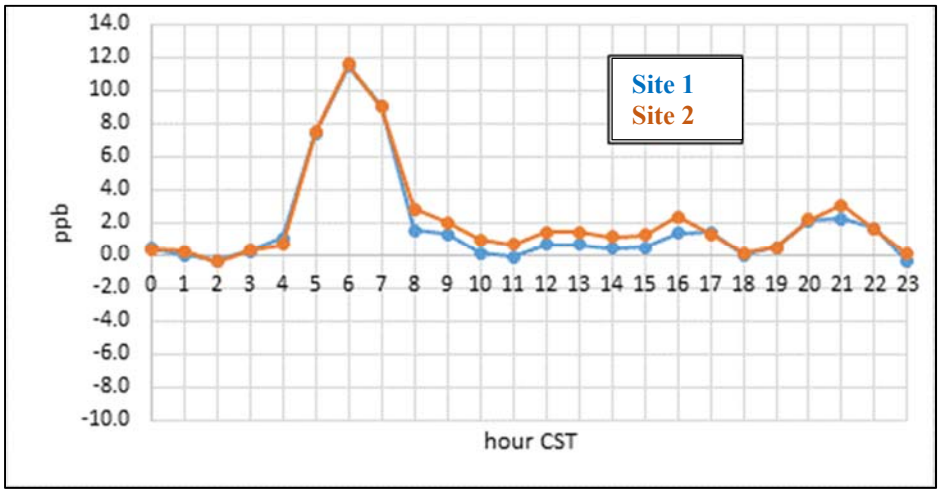

Figure H.15 NO_2 diurnal patterns for May 11–17, 2016 (week 8)

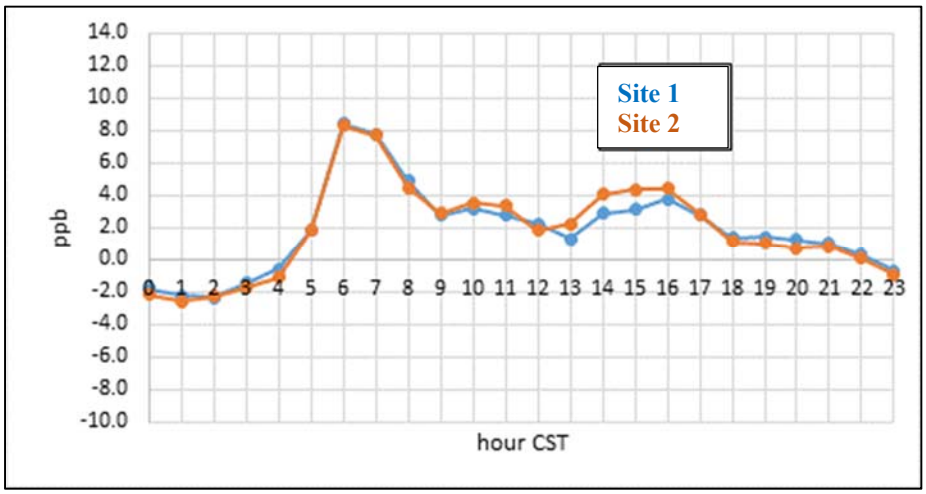

Figure H.16 NO_2 diurnal patterns for May 18–24, 2016 (week 9)

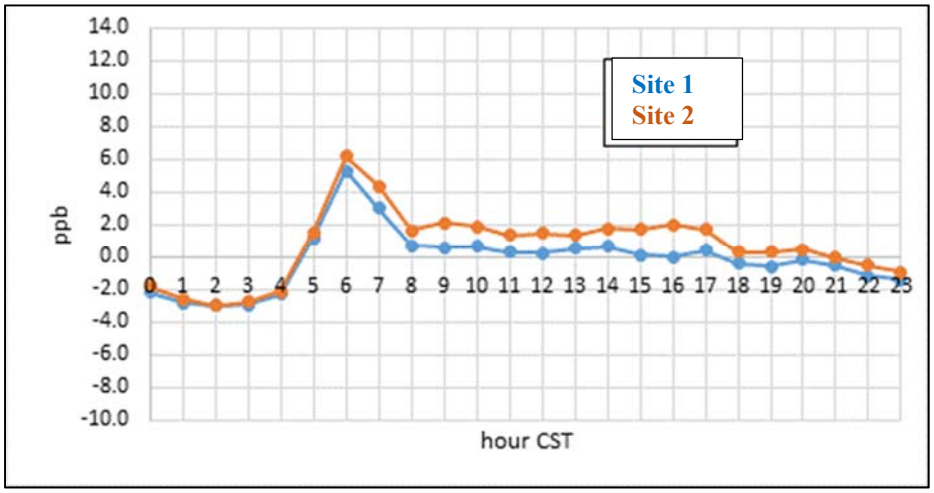

Figure H.17 NO_2 diurnal patterns for May 25–31, 2016 (week 10)

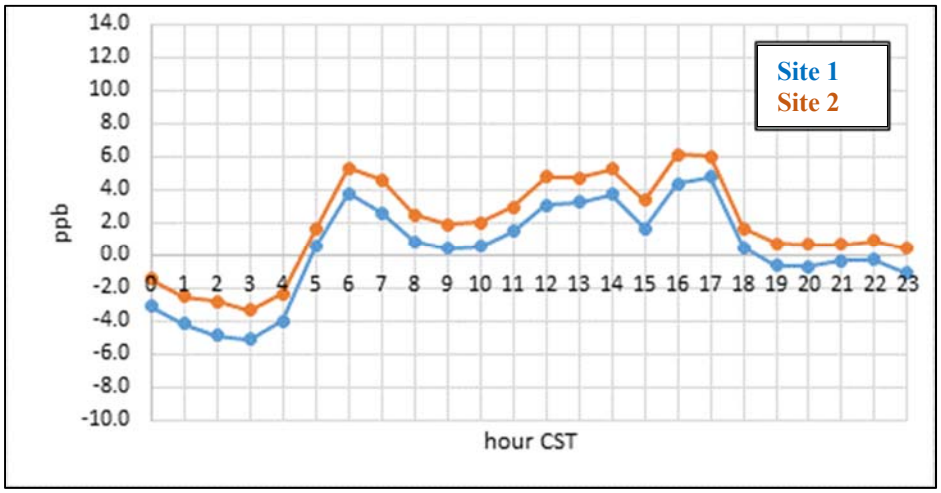

Figure H.18 NO_2 diurnal patterns for June 1–7, 2016 (week 11)

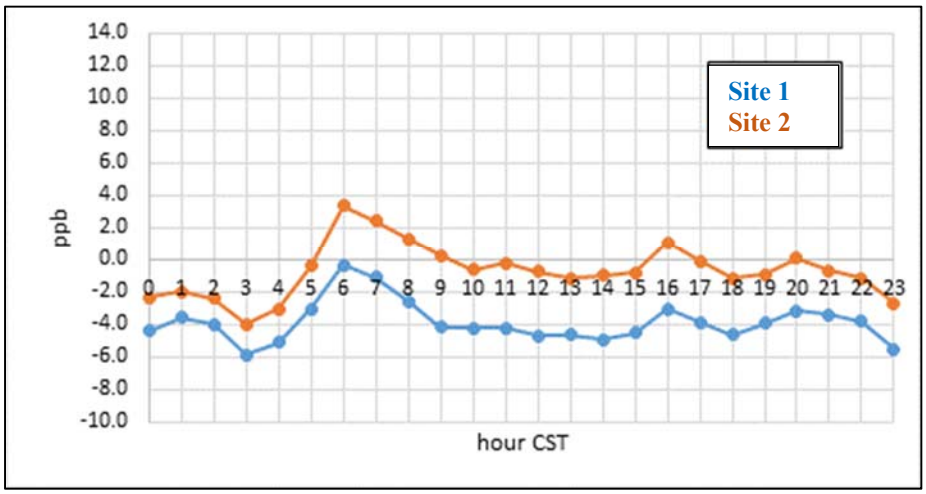

Figure H.19NO_2 diurnal patterns for June 8–14, 2016 (week 12)

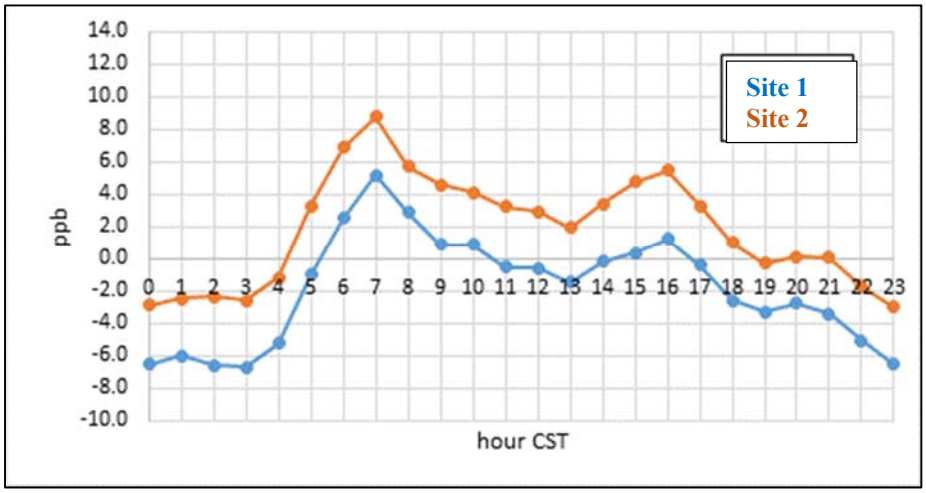

Figure H.20 NO_2 diurnal patterns for June 15–21, 2016 (week 13)

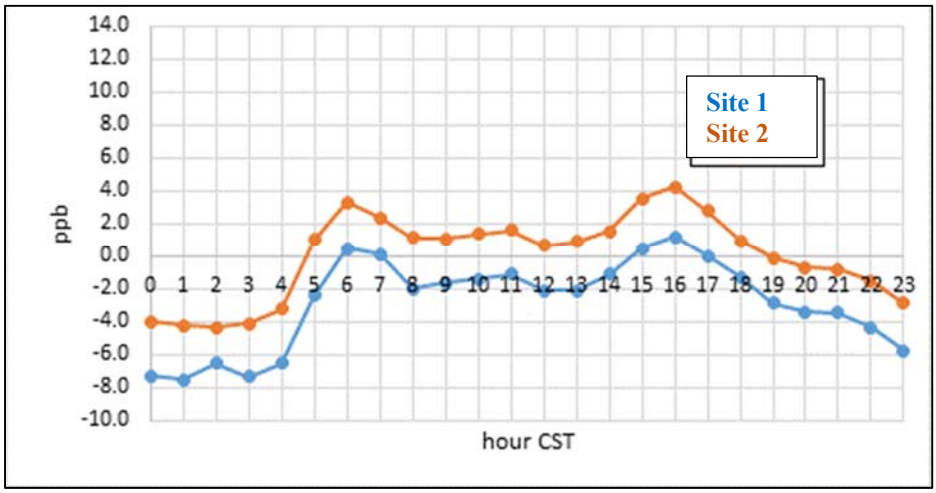

Figure H.21 NO_2 diurnal patterns for June 22–28, 2016 (week 14)

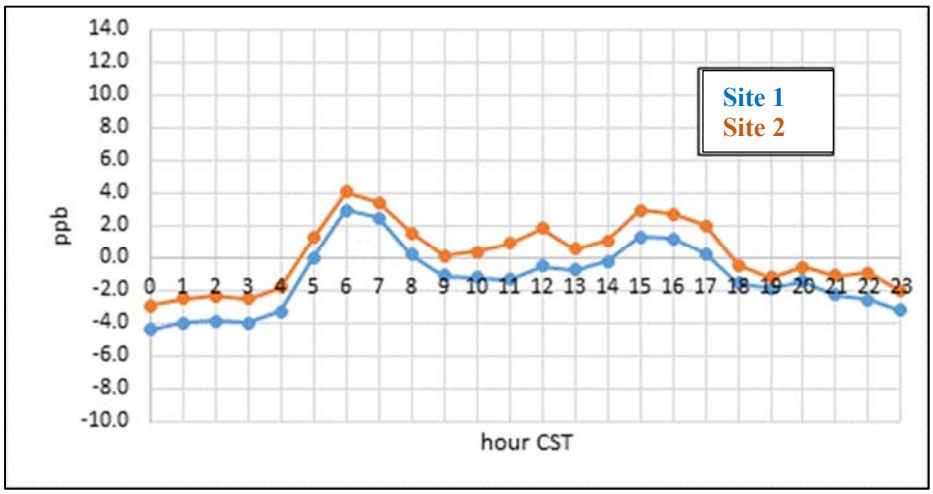

Figure H.22 NO_2 diurnal patterns for June 29–July 5, 2016 (week 15)

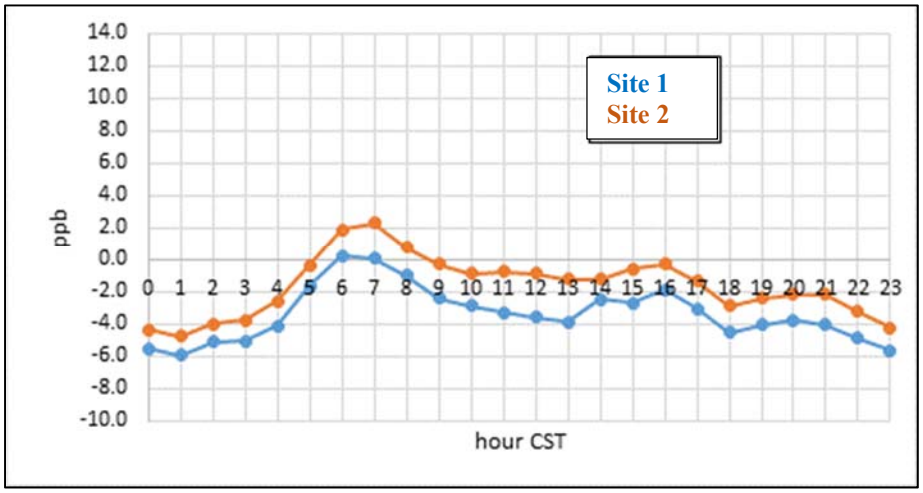

Figure H.23 NO_2 diurnal patterns for July 6–12, 2016 (week 16)

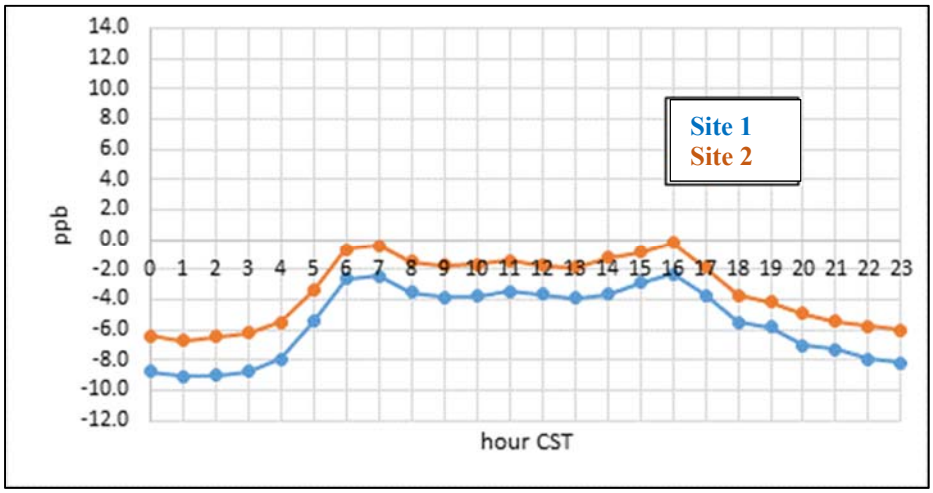

Figure H.24 NO_2 diurnal patterns for July 20–26, 2016 (week 18)

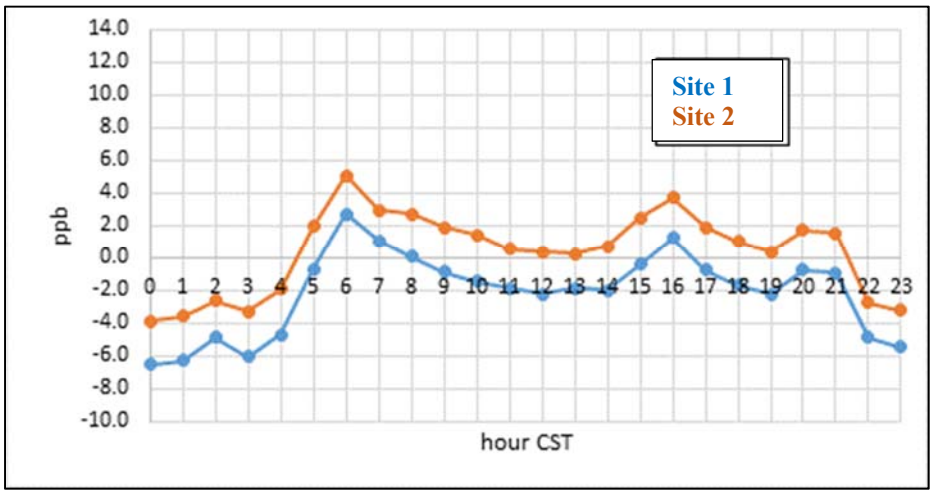

Figure H.25 NO_2 diurnal patterns for July 27–August 2, 2016 (week 19)

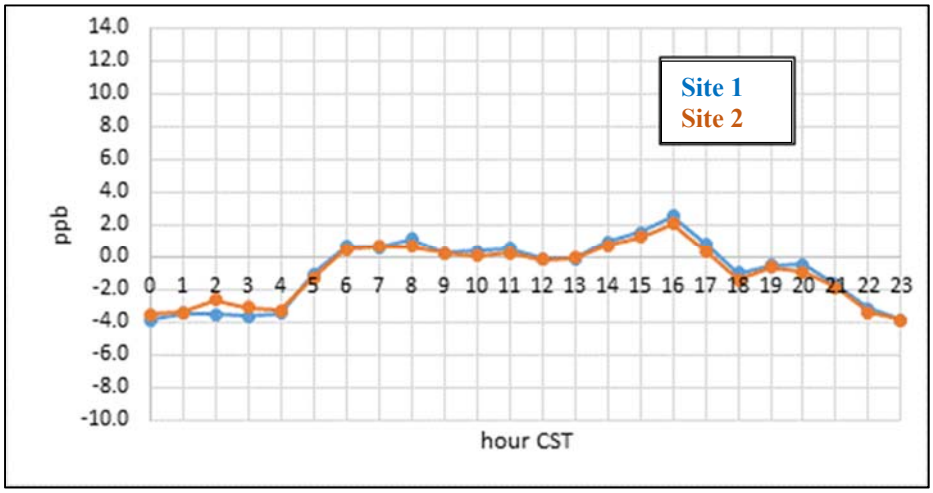

Figure H.26 NO2 diurnal patterns for August 3–9, 2016 (week 20)

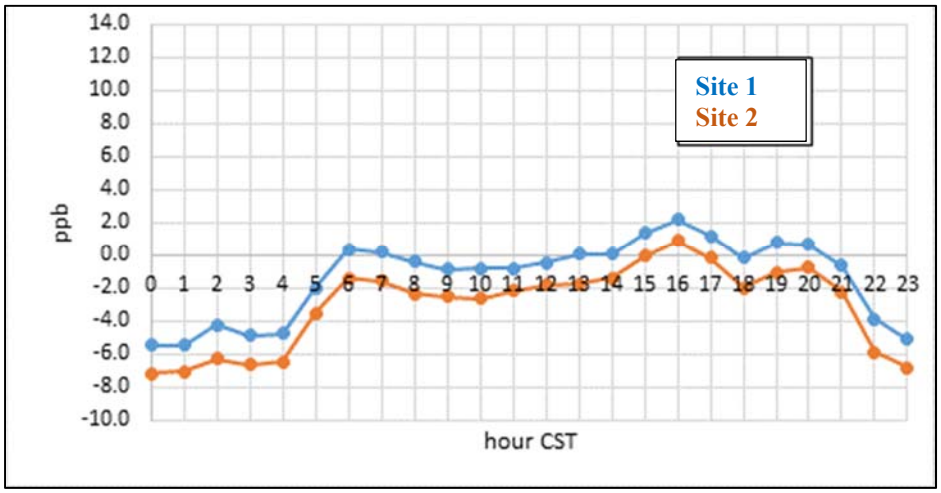

Figure H.27 NO2 diurnal patterns for August 10–16, 2016 (week 21)

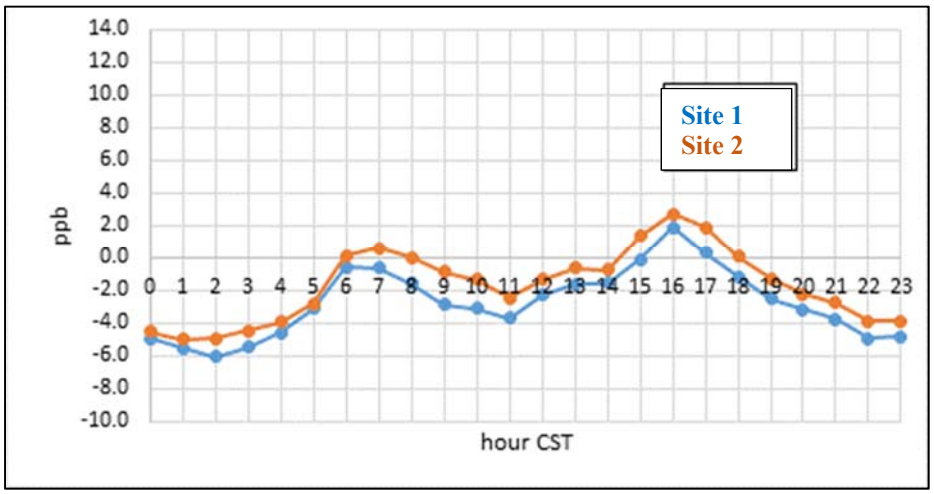

Figure H.28 NO_2 diurnal patterns for August 17–23, 2016 (week 22)

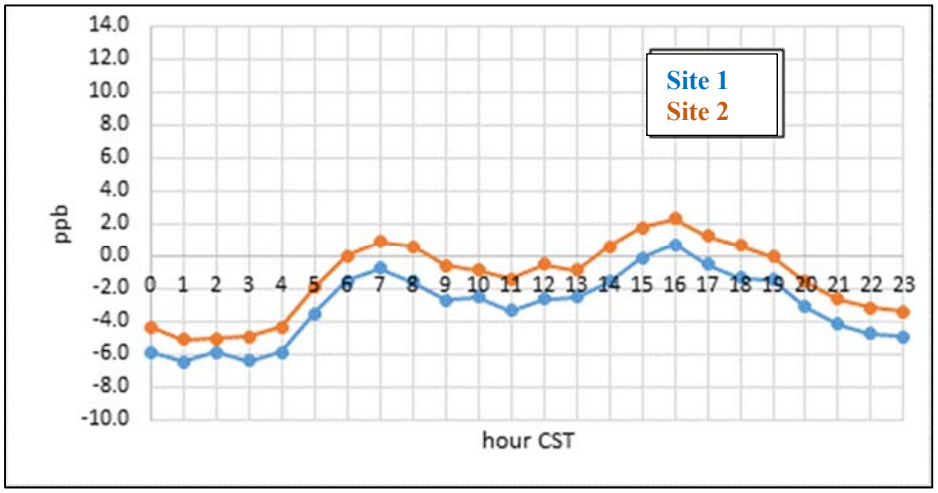

Figure H.29 NO_2 diurnal patterns for August 31–September 6, 2016 (week 24)

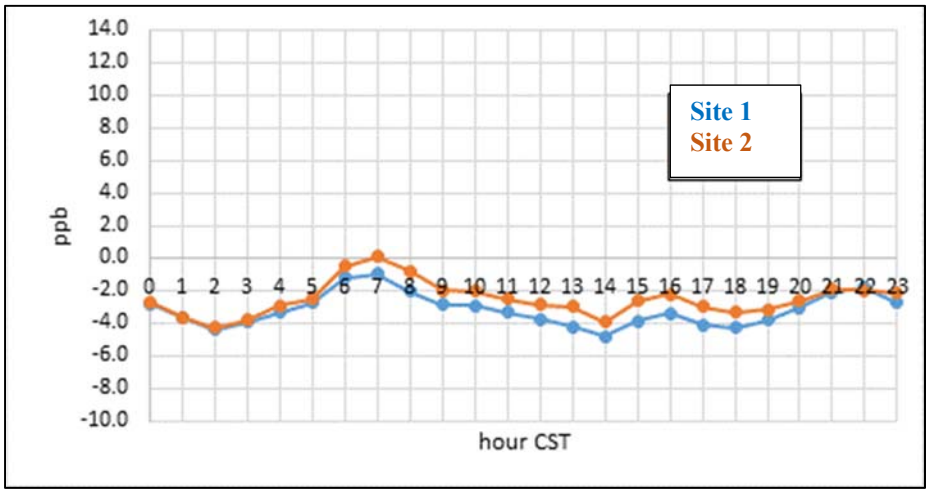

Figure H.30 NO_2 diurnal patterns for September 14–19, 2016 (week 26)

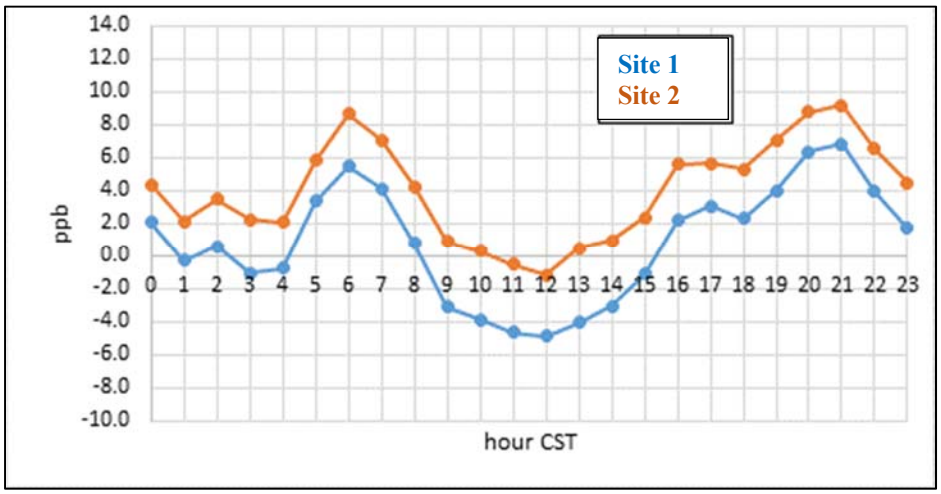

Diurnal Patterns of O_3 by Week, March 23–September 19, 2016

A second focus of this study is on the effect of the catalyst treatment on O_3 concentrations. As with the NO_2 measurements, two analyzers were used, one exposed to the treatment, and one not exposed to the treatment. Table H.3 summarizes the average concentration differences between the two O_3 analyzers' measurements in 2016. Instruments are labeled Site 1 and Site 2. Table H.3 was constructed by first averaging all 5-minute time scale measurements by hour, then averaging the hours across a week (seven day periods), then calculating the difference in average O_3 from Site 2 minus Site 1 (*Delta O_3*), then averaging the difference by three hour periods.

Within Table H.3 the columns are the eight three-hour periods of the day, and the rows are the weeks in 2016 with more than 50 percent data return on coincident sampling at the two analyzers. The last column is the average across all three-hour averages, and the last row is the average across all weeks.

To illustrate the results of Table H.3, Figures H.31 through H.54 show the diurnal patterns for O_3 by hour of the day for each week for which coincident data were collected from Wednesday March 23, 2016 to Monday September 19, 2016. These graphs show a varying difference between *O_3 Site 2* and *O_3 Site 1*. All graphs have the same y-axis ranging from 42.0 to -2.0 ppb. Two weeks had insufficient data: July 13–19 and August 24–30.

- From March 23 through the week of July 27–August 2, *Site 1* and *Site 2* were very close in average O_3 concentrations over nearly all 24 hour hours. For a few weeks from March 23 to the week June 1–7, 2016, *Site 1* averaged 0.38 ppb higher than *Site 2* overall, but the concentration difference was close to 0 ppb overnight and peaked during hour 16 CST at 1.0 ppb.
- From August 3–23, *Site 2* was generally higher than *Site 1*, especially in the afternoons, by up to 3.5 ppb.
- From September 7–19, *Site 1* was generally higher than *Site 2*.

Figures H.55 through H.58 show strung-together differences of *Site 2* minus *Site 1* from the diurnal graphs for hourly O_3 averaged by week, with week numbers on x-axis from Table H.3. In general, there was a small cycling in the differences but these were constrained to within +/- 1.5 ppb, except for much of August weeks 21– 22 (August 10–23).

Table H.3 Mean difference Site2 minus Site1 O_3 by 3-hour period & week during 2016 (green for Site1 > Site2, red for Site2 > Site1)

Week Index	Week	00-02 CST	03-05 CST	06-08 CST	09-11 CST	12-14 CST	15-17 CST	18-20 CST	21-23 CST	Grand Total
1	Mar. 23-Mar. 29	-0.98	-1.01	-0.95	-0.63	-1.10	-0.86	-0.47	-0.41	-0.80
2	Mar. 30-Apr. 5	0.18	0.28	0.54	-0.23	-0.43	-0.79	-0.02	0.26	-0.03
3	Apr. 6-Apr. 12	0.45	0.28	0.22	0.18	-0.24	-0.14	0.55	0.56	0.23
4	Apr. 13-Apr. 19	0.25	0.26	-0.37	-0.69	-1.06	-1.21	-0.40	0.08	-0.39
5	Apr. 20-Apr. 26	0.48	0.59	-0.78	-0.16	-0.76	-0.74	0.24	0.38	-0.10
6	Apr. 27-May 3	-0.32	-0.38	-1.06	-1.71	-1.53	-1.28	-0.64	-0.04	-0.87
7	May 4-May10	-0.09	0.58	-0.10	-0.13	-0.94	-0.98	-0.43	-0.33	-0.30
8	May 11-May 17	-1.04	-0.97	-0.93	-1.21	-1.42	-1.78	-0.52	-0.98	-1.11
9	May 18-May 24	-0.49	-0.61	-0.74	-0.59	-0.65	-1.01	-0.44	0.04	-0.56
10	May 25-May 31	0.00	-0.09	-0.22	0.09	0.24	-0.21	0.02	0.02	-0.02
11	Jun. 1-Jun. 7	-0.34	-0.20	-0.46	0.03	-0.05	-0.64	-0.02	0.10	-0.20
12	Jun. 8-Jun. 14	0.85	0.58	0.39	0.46	0.31	-0.32	0.70	0.73	0.46
13	Jun. 15-Jun. 21	0.64	0.60	0.83	0.72	0.05	0.32	0.82	0.68	0.58
14	Jun. 22-Jun. 28	1.16	0.97	1.07	0.33	0.61	0.47	1.25	1.24	0.89
15	Jun. 29-Jul. 5	0.84	0.86	0.34	0.99	-0.01	0.15	0.86	0.79	0.60
16	Jul. 6-Jul. 12	0.73	0.79	0.71	0.63	0.54	1.24	1.26	0.79	0.84
18	Jul. 20-Jul. 26	0.57	0.56	0.79	0.47	0.03	0.11	0.25	0.41	0.40
19	Jul. 27-Aug. 2	0.11	0.11	0.43	0.70	0.10	0.65	0.58	0.36	0.38
20	Aug. 3-Aug. 9	0.52	0.47	0.95	0.98	1.03	1.19	1.01	1.25	0.92
21	Aug. 10-Aug. 16	2.47	2.35	2.03	1.46	1.96	1.95	2.02	2.27	2.07
22	Aug. 17-Aug. 23	2.87	2.78	3.21	3.53	2.66	2.80	2.81	2.78	2.93
24	Aug. 31-Sep. 6	0.50	0.81	0.55	-0.61	-0.98	-0.64	-0.50	-0.76	-0.20
25	Sep. 7-Sep. 13	-0.99	-0.79	-1.42	-2.05	-1.45	-1.02	-0.62	-0.68	-1.13
26	Sep. 14-Sep. 19	-0.48	-0.22	-0.96	-1.93	-1.93	-1.01	-0.65	-0.50	-0.96
Grand Total		0.33	0.36	0.17	0.03	-0.21	-0.16	0.32	0.38	0.15

Figure H.31 Ozone diurnal patterns for March 23–29, 2016 (week 1)

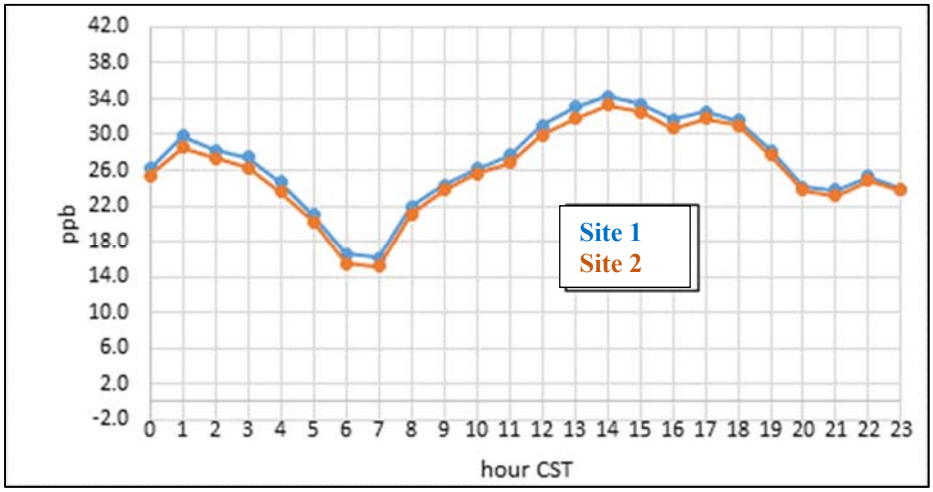

Figure H.32 Ozone diurnal patterns for March 30–April 5, 2016 (week 2)

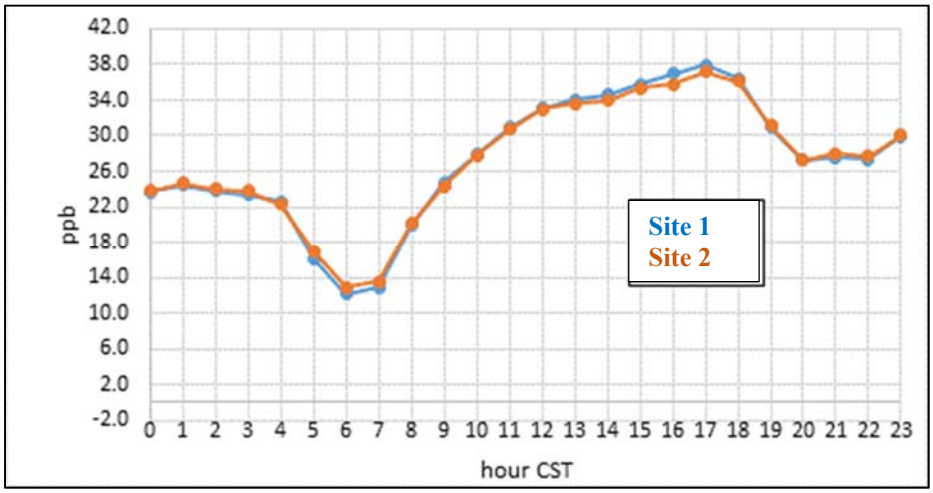

Figure H.33 Ozone diurnal patterns for April 6–12, 2016 (week 3)

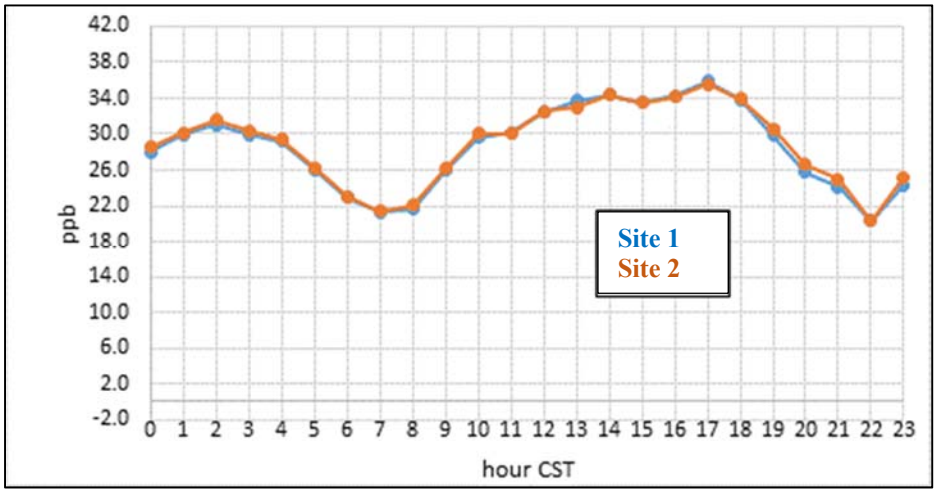

Figure H.34 Ozone diurnal patterns for April 1319, 2016 (week 4)

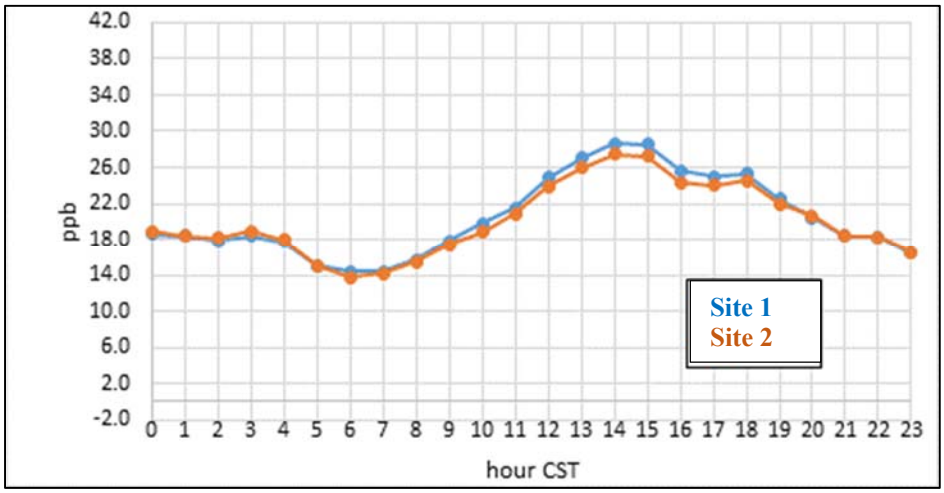

Figure H.35 Ozone diurnal patterns for April 20–26, 2016 (week 5)

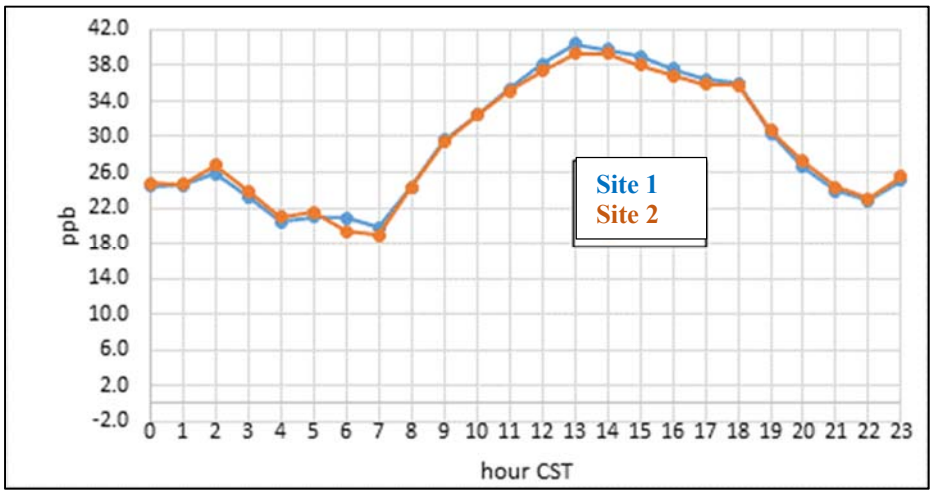

Figure H.36 Ozone diurnal patterns for April 27–May 3, 2016 (week 6)

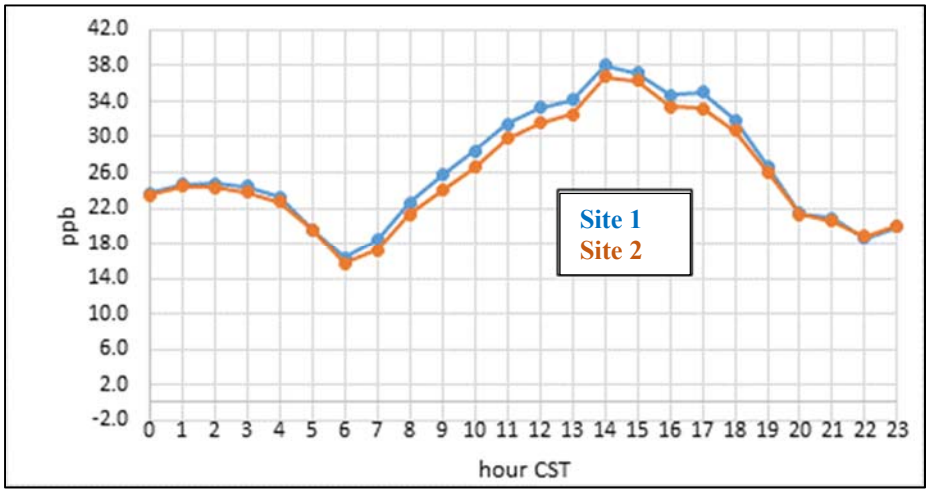

Figure H.37 Ozone diurnal patterns for May 4–10, 2016 (week 7)

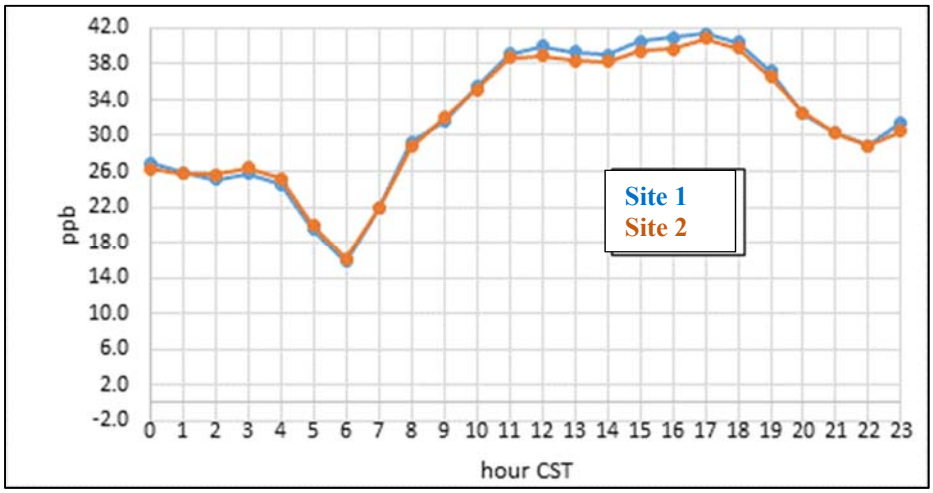

Figure H.38 Ozone diurnal patterns for May 11–17, 2016 (week 8)

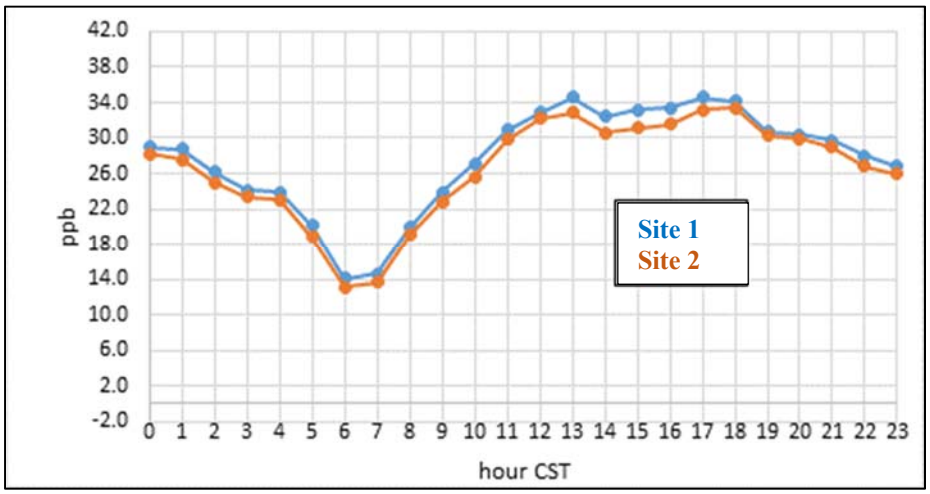

Figure H.39 Ozone diurnal patterns for May 18–24, 2016 (week 9)

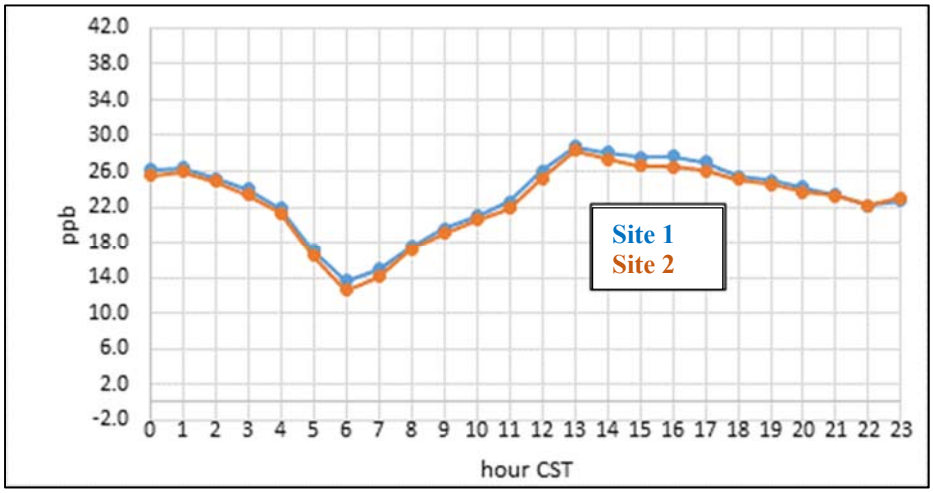

Figure H.40 Ozone diurnal patterns for May 25–31, 2016 (week 10)

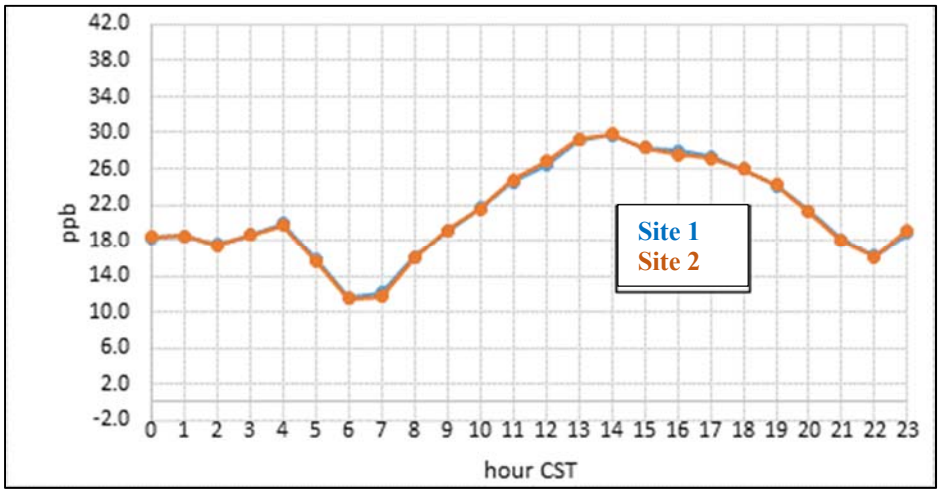

Figure H.41 Ozone diurnal patterns for June 1–7, 2016 (week 11)

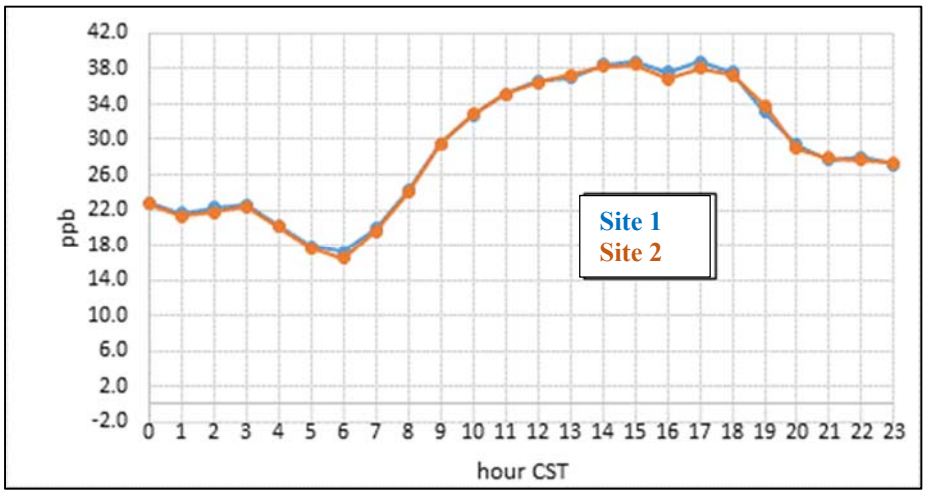

Figure H.42 Ozone diurnal patterns for June 8–14, 2016 (week 12)

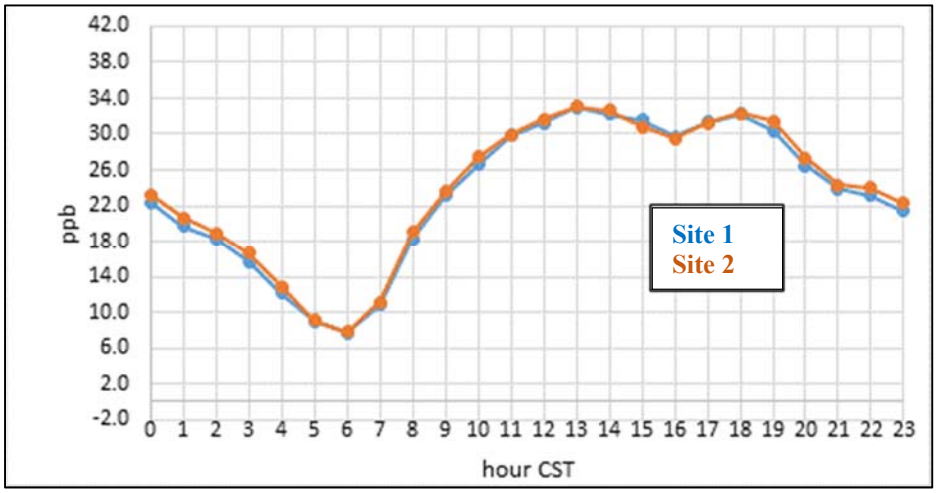

Figure H.43 Ozone diurnal patterns for June 15–21, 2016 (week 13)

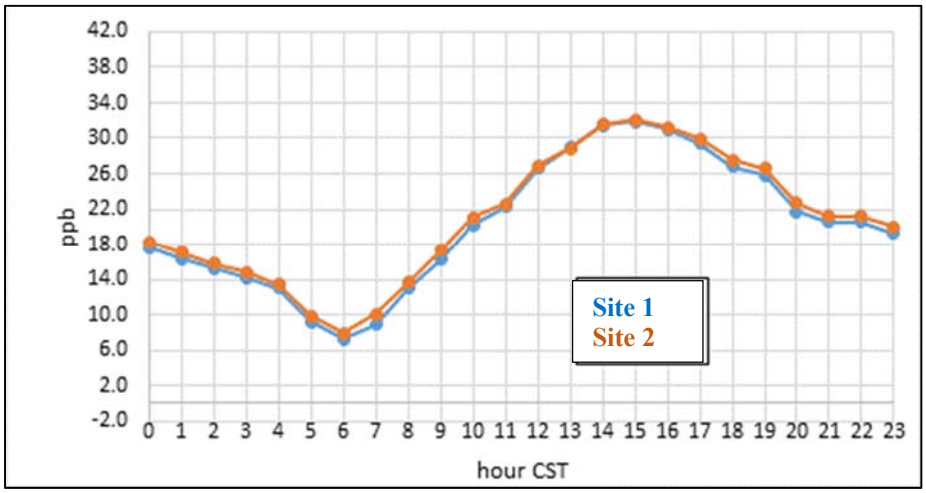

Figure H.44 Ozone diurnal patterns for June 22–28, 2016 (week 14)

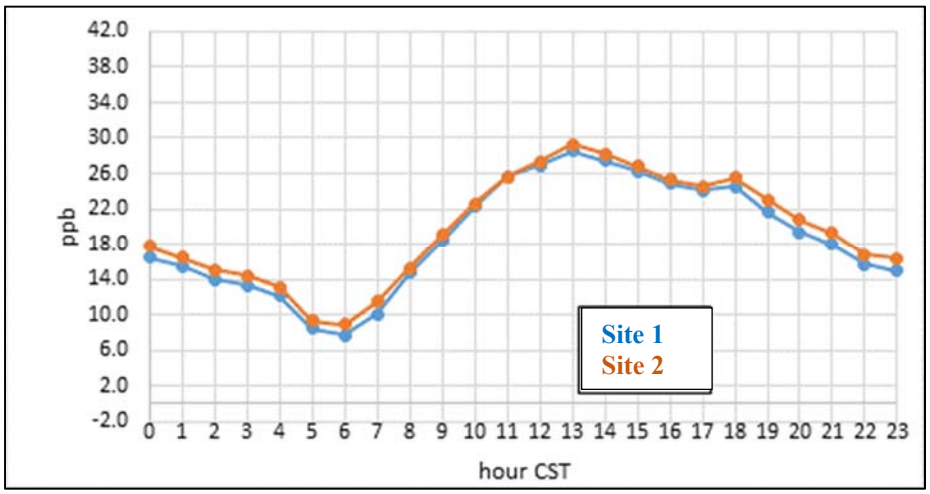

Figure H.45 Ozone diurnal patterns for June 29–July 5, 2016 (week 15)

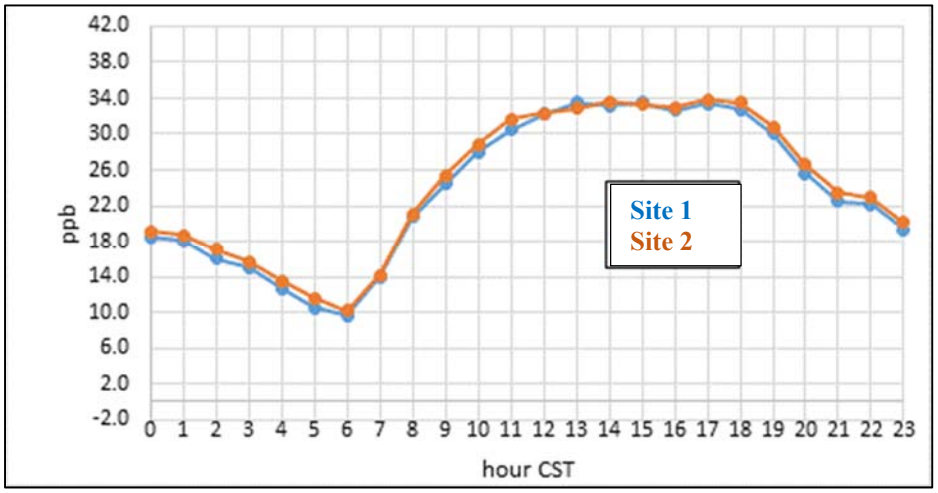

Figure H.46 Ozone diurnal patterns for July 6–12, 2016 (week 16)

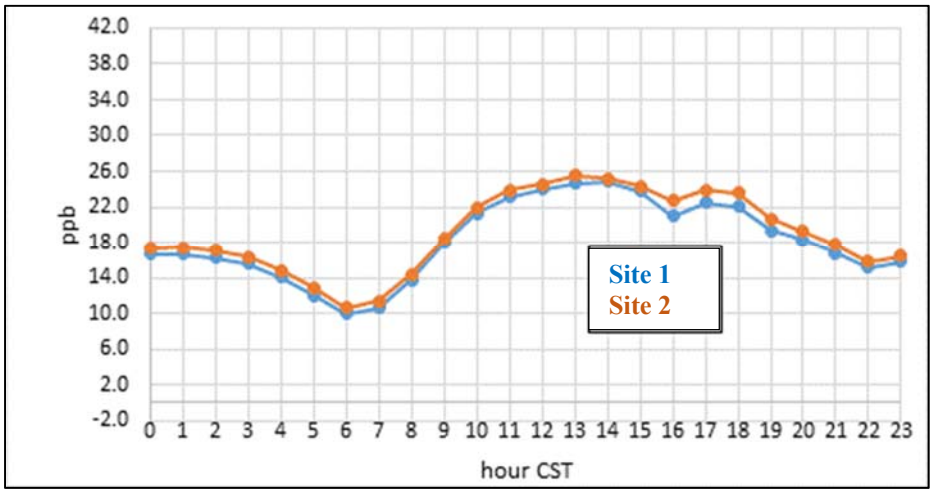

Figure H.47 Ozone diurnal patterns for July 20–26, 2016 (week 18)

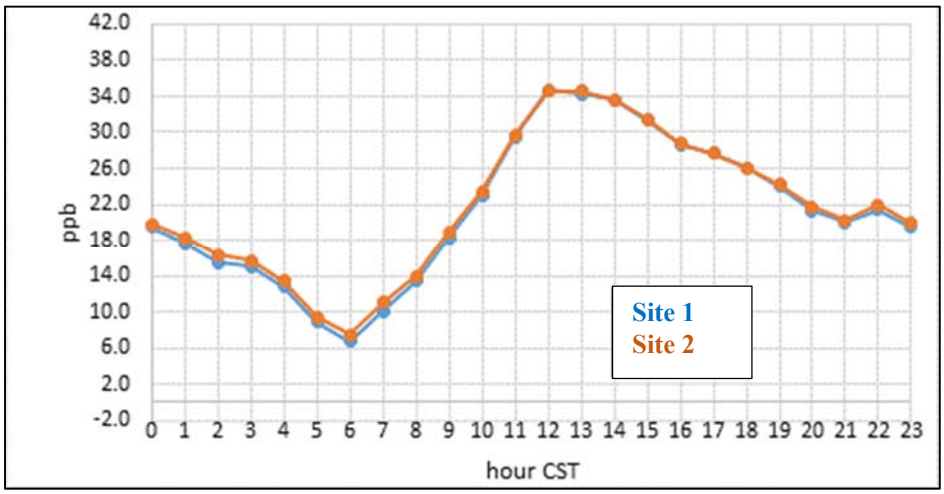

Figure H.48 Ozone diurnal patterns for July 27–August 2, 2016 (week 19)

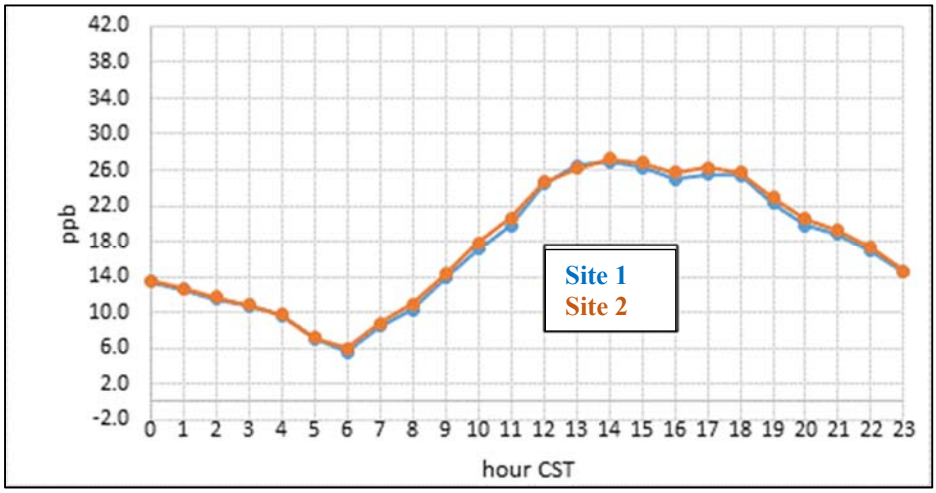

Figure H.49 Ozone diurnal patterns for August 3–9, 2016 (week 20)

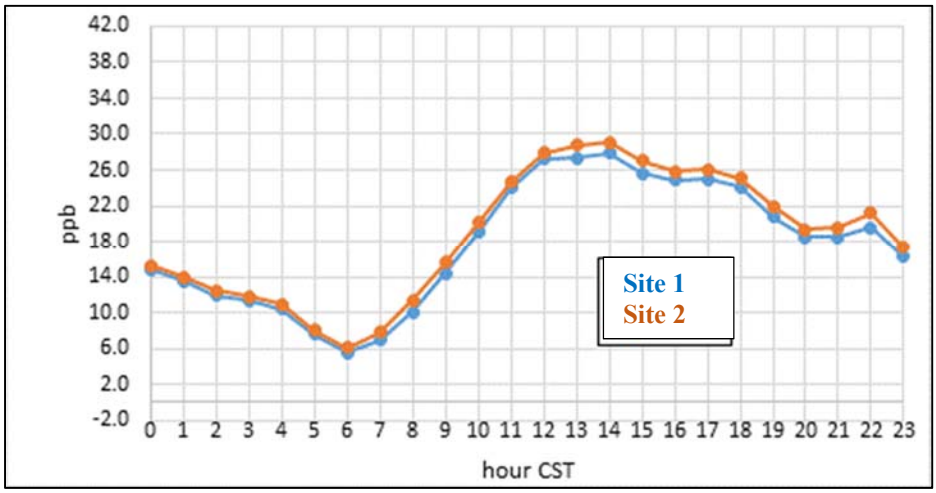

Figure H.50 Ozone diurnal patterns for August 10–16, 2016 (week 21)

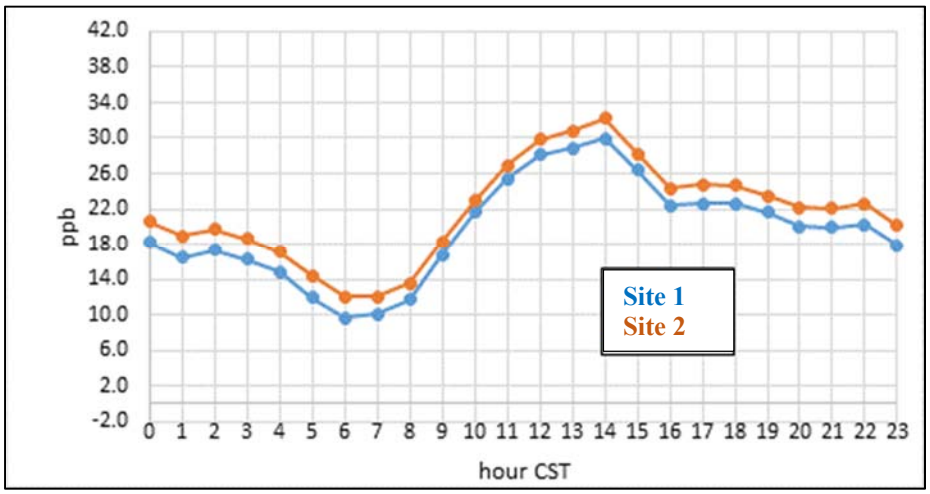

Figure H.51 Ozone diurnal patterns for August 17–23, 2016 (week 22)

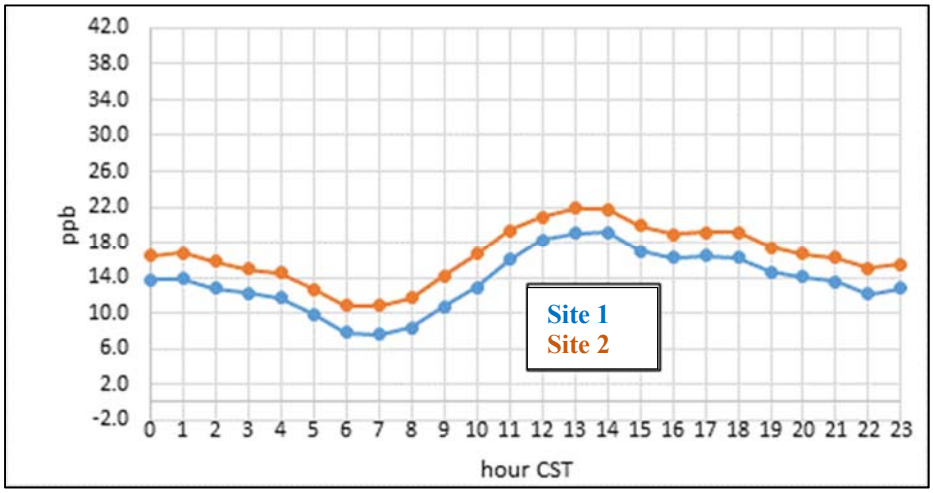

Figure H.52 Ozone diurnal patterns for August 31–September 6, 2016 (week 24)

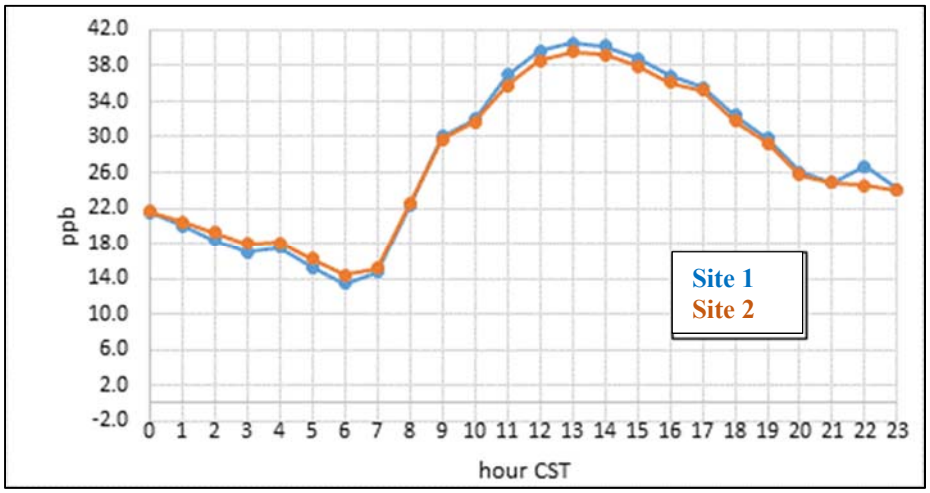

Figure H.53 Ozone diurnal patterns for September 7–13, 2016 (week 25)

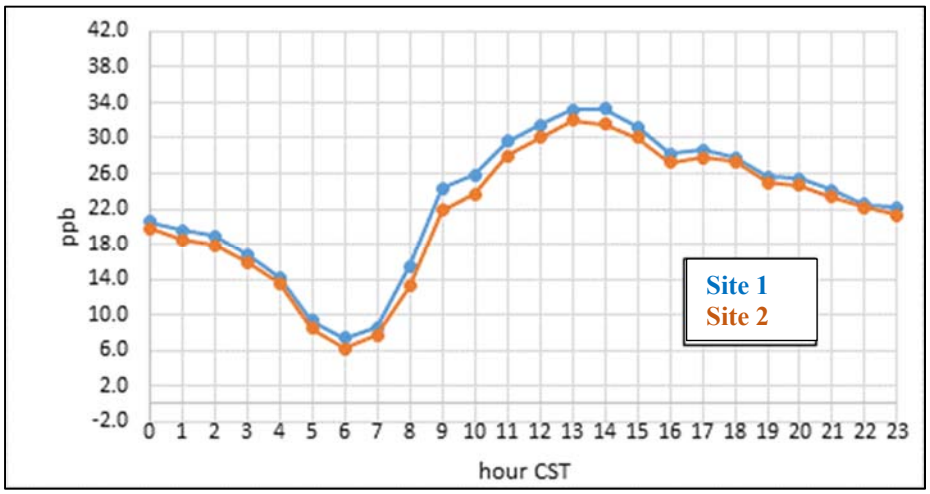

Figure H.54 Ozone diurnal patterns for September 14–19, 2016 (week 26)

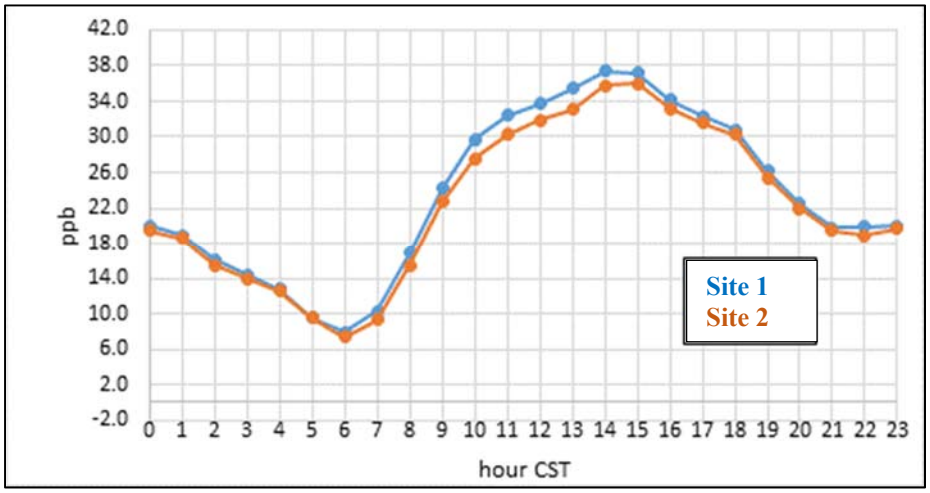

Figure H.55 Strung-together diurnal graphs of hourly delta O_3 (Site 2 – Site 1) averaged by week, week numbers on x-axis from Table H.3

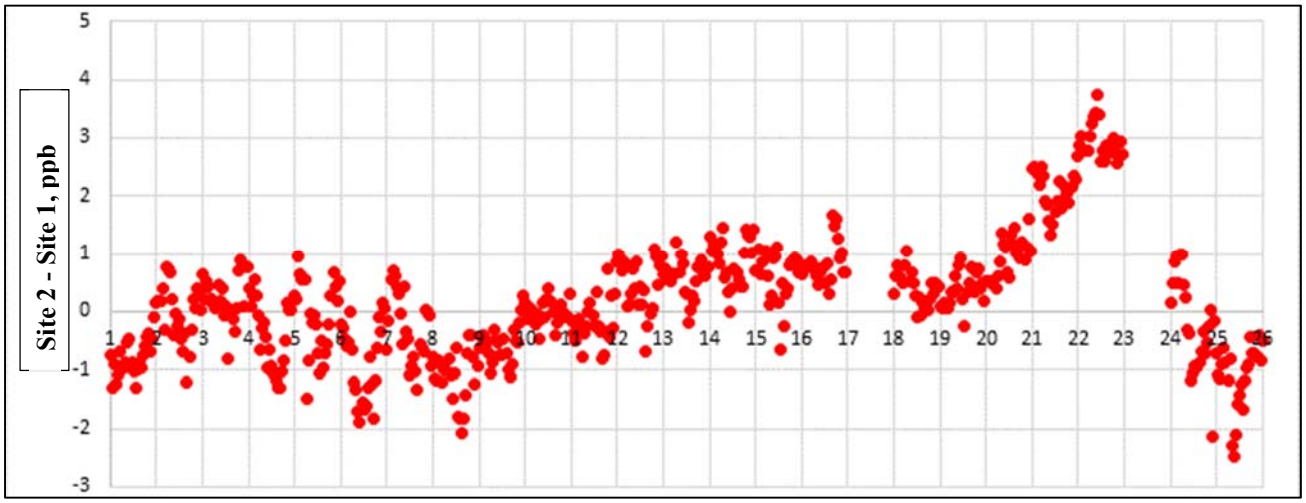

Figure H.56 Strung-together diurnal graphs of hourly delta O_3 (Site 2 – Site 1) averaged by week, week numbers on x-axis from Table H.3, weeks 1–9

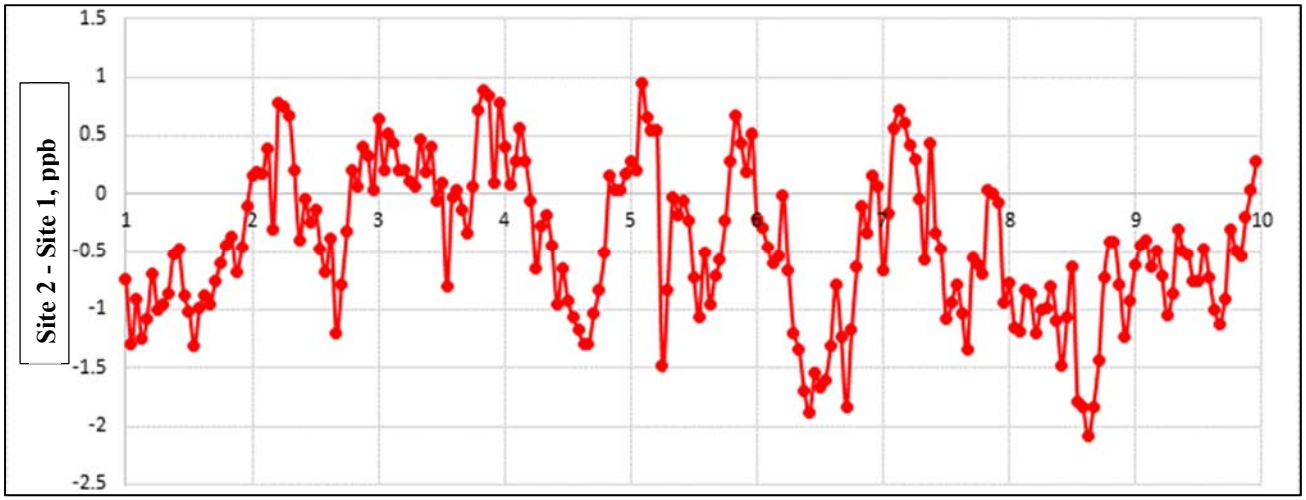

Figure H.57 Strung-together diurnal graphs for hourly delta O_3 (Site 2 – Site 1) averaged by week, week numbers on x-axis from Table H.3, weeks 10–16

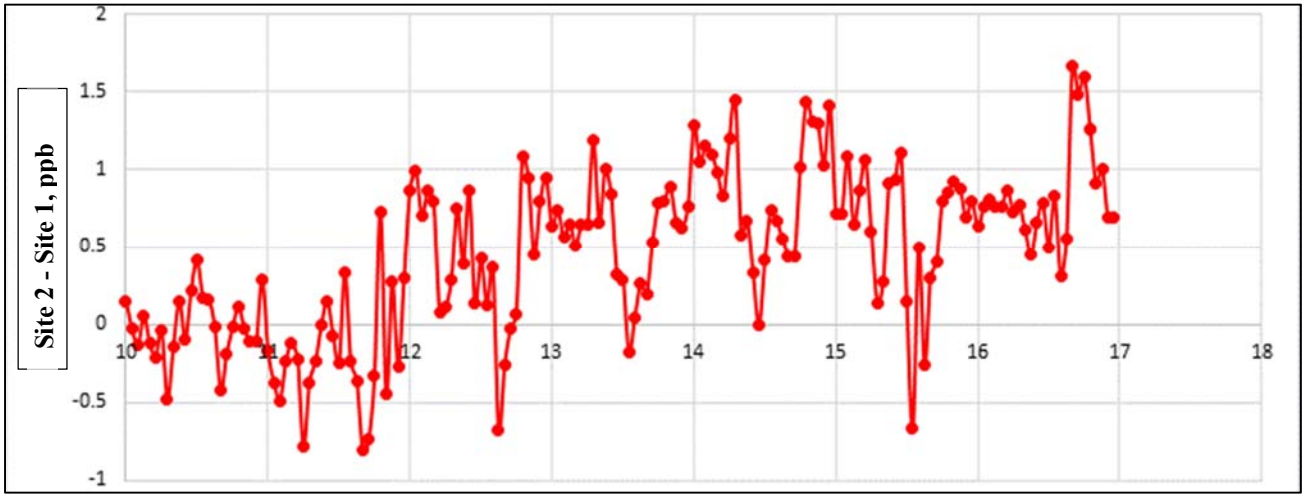

Figure H.58 Strung-together diurnal graphs for hourly delta O_3 (Site 2 – Site 1) averaged by week, week numbers on x-axis from Table H.3, weeks 18–26

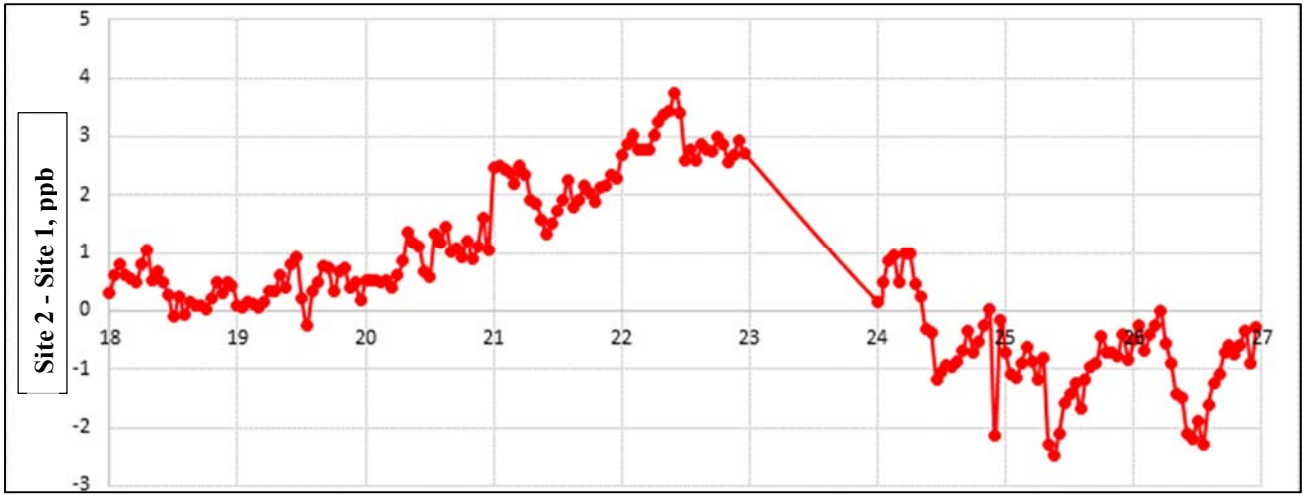

The Relationship between Deltas and Meteorology

It is well known that meteorology has a very significant effect on ozone concentrations and the concentrations of several other pollutants. For a secondary pollutant, such as ozone, that forms in the air under bright sunlight and then accumulates under light winds, summer daytime is the most intense period. For many primary pollutants that are directly emitted by sources, such as NOx, concentrations are generally highest overnight under the nocturnal boundary layer that prevents vertical mixing. Given the conditions of this study, it is important to examine the possible influence of weather on the behaviors of the deltas between the two instruments.

To test the effects of weather, the following procedure was followed:

1. The 5-minute wind data reported in degrees for direction and miles per hour for speed were converted into north/south and east/west components. This allows the computation of hourly averages for wind direction and speed.
2. Time periods were censured to only include 5-minute values for which both NO_2 and O_3 measurements were available.
3. The 5-minute data for north/south and east/west wind components, O_3, and NO_2, were averaged by hour.
4. Hourly outdoor temperature, solar radiation, and rainfall data from other monitoring sites in the area for the 2015–2016 time period covered by the TxDOT monitoring for this project were downloaded from the TCEQ Website.
5. The hourly average TxDOT data were merged with the TCEQ data.
6. The hourly data were classified into two categories: hours 9 CST through 20 CST as "daytime," and hours 0 through 8 CST and 21, 22, 23 CST as "nighttime." This placed 12 hours of the day in each category. Granted, 8 a.m. CST is not "nighttime" but it is a period of relatively low solar radiation before ozone begins to form in large amounts.
7. For each day, the merged hourly data were averaged by daytime and nighttime, giving two composite observations for each date for pollutants and meteorological data.
8. A correlation analysis was run to calculate the Pearson correlations and statistical significance of the correlations for the variables Delta_O3, Delta_NO2, east/west wind, north/south wind, outdoor temperature, and solar radiation (Solar).
9. In addition, multivariate regressions and simple linear regressions were run to look at the relationships among variables.
10. In several cases, data were examined graphically to consider possible associations. This was particularly important for rainfall, since rain is an intermittent event (most days have zero precipitation), and is not as well-suited for statistical analysis compared to other variables.

Table H.4 shows the statistical summary for six variables using the daytime calculated variables for O_3 and NO_2 deltas, winds, temperature, and solar radiation. Data from June 1 to September 19, 2016, 83 valid days, were used. Table H.5 shows the correlation among the variables for this data set. Within each numeric cell in Table H.5, there are two numbers. The top number is the

correlation between the two variables for which the cell is the intersection of a row and column. Correlations can range from +1.0 to -1.0. Every variable is correlated with itself with a value of 1.0, so these cells along the diagonal are omitted. The bottom number in each numeric cell relates the statistical significance, or *p-value*, of the correlation value. The p-value ranges between 0.0 and 1.0. The p-value is the probability that a correlation coefficient as far from 0.0 as the realized value derived from the sample of data would be calculated from a pair of variables for which the true correlation was actually 0.0. If the p-value is 0.05 or lower, one would say it is unlikely that the true correlation is 0.0, and thus is statistically significantly greater than (or less than) 0.0. For example, in the cells for the correlation between solar radiation (Solar) and outdoor temperature (TempF), the correlation is 0.756 with a p-value less than 0.0001. This makes sense, as one would expect the higher the incidence of solar radiation, the higher the temperature, in general. Similarly, the correlation of outdoor temperature with the north/south wind component is -0.598, with a p-value less than 0.0001. This makes sense, as one would expect, in general in Austin, TX, that a southerly wind would be associated with higher temperatures and a northerly wind would be associated with lower temperatures. In contrast, the correlation of outdoor temperature with east/west wind component is 0.046 with a p-value of 0.678, indicating there are no significant relations between east-west wind component and temperature in Austin, TX for the data set. In examining the way the deltas for O_3 and NO_2 are related to other variables, one observes that delta NO_2 and delta O_3 are statistically significantly negatively correlated. Both delta NO_2 and delta O_3 appear to be affected by the north/south wind direction, with delta NO_2 higher under northerly winds, and delta O_3 higher under southerly winds.

Figure H.59 shows the time series for hourly delta O_3 and for the rainfall averaged from three Central Texas weather stations from June 1 to September 19, 2016. One can note that the higher delta O_3 measured in mid-August 2016 was coincident with a rainy period.

At this point we posit no assignable cause for the wind direction or rainfall associations with delta O_3 or the wind direction association with delta NO_2.

Table H.4 Simple Statistics from SAS CORR Procedure, Year = 2016, period = daytime

Variable	Units	Number of Days	Mean	Std Dev	Minimum	Maximum
delta_o3	ppb	83	0.60649	1.04449	-1.78344	3.23234
delta_no2	ppb	83	1.75713	1.74276	-2.92977	5.61632
East/west wind	mph	83	3.82693	2.87926	-4.52376	11.20578
North/south wind	mph	83	-4.74038	4.71978	-13.73165	7.85428
TempF	degrees F.	83	86.77218	5.24354	71.95833	95.10625
Solar	langleys/minute	83	0.65119	0.18451	0.08400	0.88750

Table H.5 Pearson Correlations from SAS CORR Procedure, Year = 2016, period = daytime

Pearson Correlation Coefficients, N = 83 , Prob > |r| Under H0: Rho=0						
	delta_O3	**delta_NO2**	**East/west wind**	**North/south wind**	**TempF**	**Solar**
delta_O3		-0.28142 0.0100	-0.11465 0.3020	-0.29680 0.0064	-0.03325 0.7654	-0.14405 0.1938
delta_NO2	-0.28142 0.0100		0.12423 0.2632	0.22023 0.0454	-0.24468 0.0258	-0.08741 0.4320
East/west wind	-0.11465 0.3020	0.12423 0.2632		0.10803 0.3310	0.04630 0.6777	0.01223 0.9126
North/south wind	-0.29680 0.0064	0.22023 0.0454	0.10803 0.3310		-0.59811 <.0001	-0.51603 <.0001
TempF	-0.03325 0.7654	-0.24468 0.0258	0.04630 0.6777	-0.59811 <.0001		0.75633 <.0001
Solar	-0.14405 0.1938	-0.08741 0.4320	0.01223 0.9126	-0.51603 <.0001	0.75633 <.0001	

Figure H.59 June 1 to September 19, 2016 hourly delta O_3 and precipitation averaged from three Central Texas weather stations

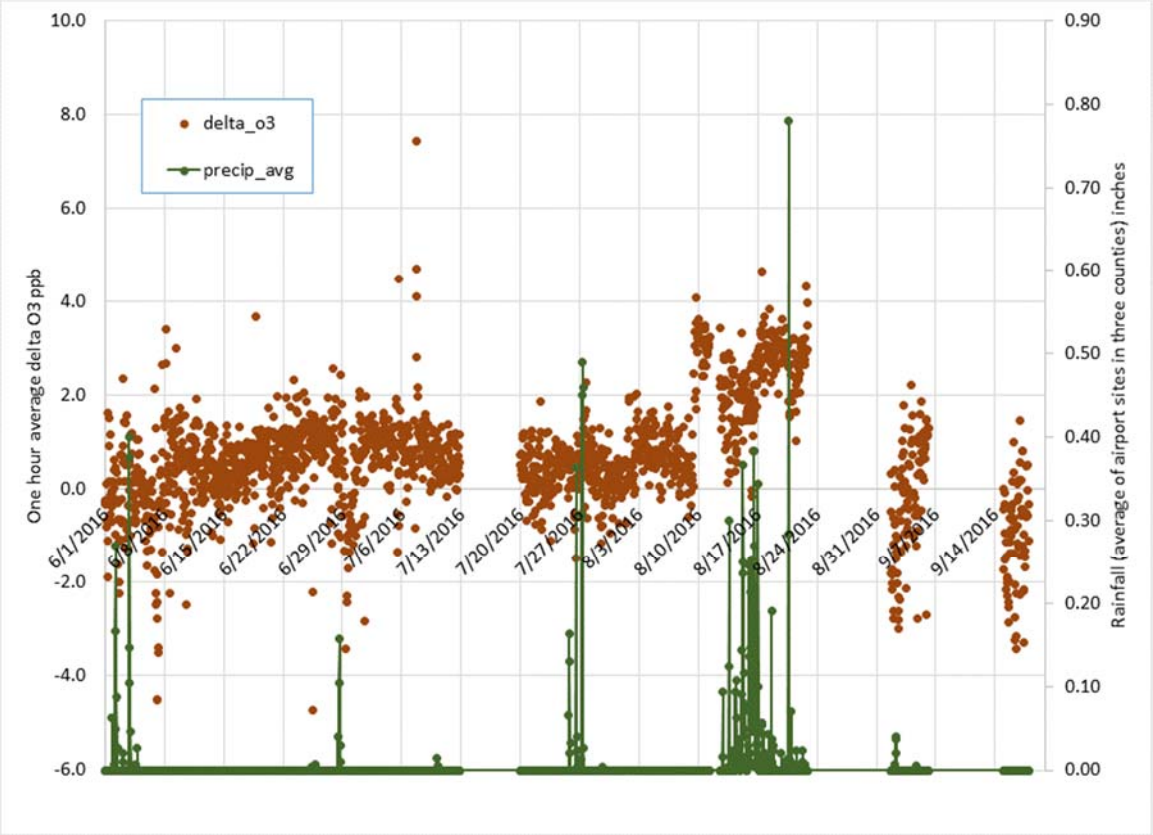

Conclusions and Recommendations

Overall, after monitoring over parts of two calendar years, there does not appear to be any consistent evidence of the effectiveness of the photo-catalyst treatment. Specific observations include:

- In 2015, the diurnal patterns for O_3 by months August through November 2015 showed a consistent bias for *O_3_Site 1 > O_3_Site 2* for all hours in each month. Differences should not have been observed outside of daylight hours, and the fact that a differences were observed over all hours suggests the differences were not related to a day-time effect, such as incident ultraviolet light.
- In 2015, the diurnal patterns for NO_2 for four weeks in August plus a fifth week for late August and early September were studied, and a consistent bias was measured for *NO_2_Site 2 > NO_2_Site 1* for the large majority of hours in each week. As with O_3 in 2015, this difference generally persisted outside of the periods of sunlight.
- In 2015, the bias for O_3 was for Site 1 to be higher than Site 2; the bias for NO_2 was for Site 2 to be higher than Site 1. Thus, the 2015 data did not suggest the same external effect in the different instruments on O_3 and NO_2.

- In 2016, with a longer period of study from March to September, there were trade-offs between Site 1 > Site 2 and Site 2 > Site 1 that suggested that the observed differences in concentrations were associated with instrument drift as opposed to the effect of an external treatment on one instrument and not the other.

As was noted earlier in the report, the analysis of the data was single blinded in that information as to which instrument was exposed to the treatment was withheld.

Over the course of the analysis of this data, some recommendations were developed for similar future projects. These recommendations include:

- While there was no statistically significant reduction in NOx or O_3 concentrations associated with the photocatalytic treatment investigated in this study it is possible that the Texas Commission on Environmental quality (TCEQ) and or TxDOT will investigate other roadside pollution control techniques to mitigate vehicular pollution. Beginning in 2014, the TCEQ initiated a near roadway-monitoring program in Houston, Dallas, and San Antonio. The traffic patterns in these so-called “hot spots” generate significant concentrations of NOx, up to 20 times greater than observed in this study. It is understood that the logistics of using these high volume traffic areas as test sites are complicated, however, the elevated pollutant levels would increase confidence in the measured concentrations improving the chances of generating statistically significant results.
- The calibration routines employed in the LEADS data collection and monitoring systems were developed when the ambient concentration of NOx and O_3 were higher than they are today. Projects evaluating pollution control technologies should consider updating the calibration procedures to reflect current ambient pollution levels when appropriate.

Appendix I

Photocatalytic NOx/HRVOC/O3 Removal in Transportation Applications Project
Data Analysis Report November 15, 2016

Photocatalytic NOx/HRVOC/O_3 Removal in Transportation Applications Project
Early Data Analysis Report

Prepared by:
David W. Sullivan, Ph.D.
The University of Texas at Austin
Center for Energy and Environmental Resources
10100 Burnet Rd, Bldg 133, MC R7100, Austin, TX 78758-4445
512-471-7805 office, 512-914-4710 cell
Email: sullivan231@mail.utexas.edu

Contents

Introduction 1
Meteorological Data 3
Gas Species Data 7
Time series 7
Distributions of data 8
Linear regressions 15
NO_2 Diurnal Patterns 17
NO_2 Diurnal Patterns in Other Texas Urban Areas 22
NO_2 Concentrations by Wind Direction 25
Ozone (O_3) Diurnal Patterns 26

Introduction

The goal of the project is to determine the extent to which two nearby sites measure the difference in concentrations between similar air parcels where the difference is assigned to a photocatalytic surface coating that lowers NO2, O3 and some highly reactive volatile organic compound (HRVOC) concentrations.

Figure I.1 shows the location of the *Photocatalytic NOx/HRVOC/O3 Removal in Transportation Applications Project* (Project) monitoring site on the north side of a Texas State Highway 45 toll station north of Austin, TX. The site has two stations installed coded in the Texas Commission on Environmental Quality (TCEQ) data system as Continuous Ambient Monitoring Station (CAMS) 2001 and CAMS 2002. Figure I.2 shows the site on an aerial map of the Austin metro region. The site is 23 km north of the urban center in the prevailing downwind direction. At the site, wind speed and direction are measured at one location, but ozone (O_3), total nitrogen oxides (NOx), nitrogen dioxide (NO_2), and nitic oxide (NO) are measured at both stations.

Figure I.1 Google Earth Pro aerial of the vicinity around CAMS 2001/2002 (yellow pushpin)

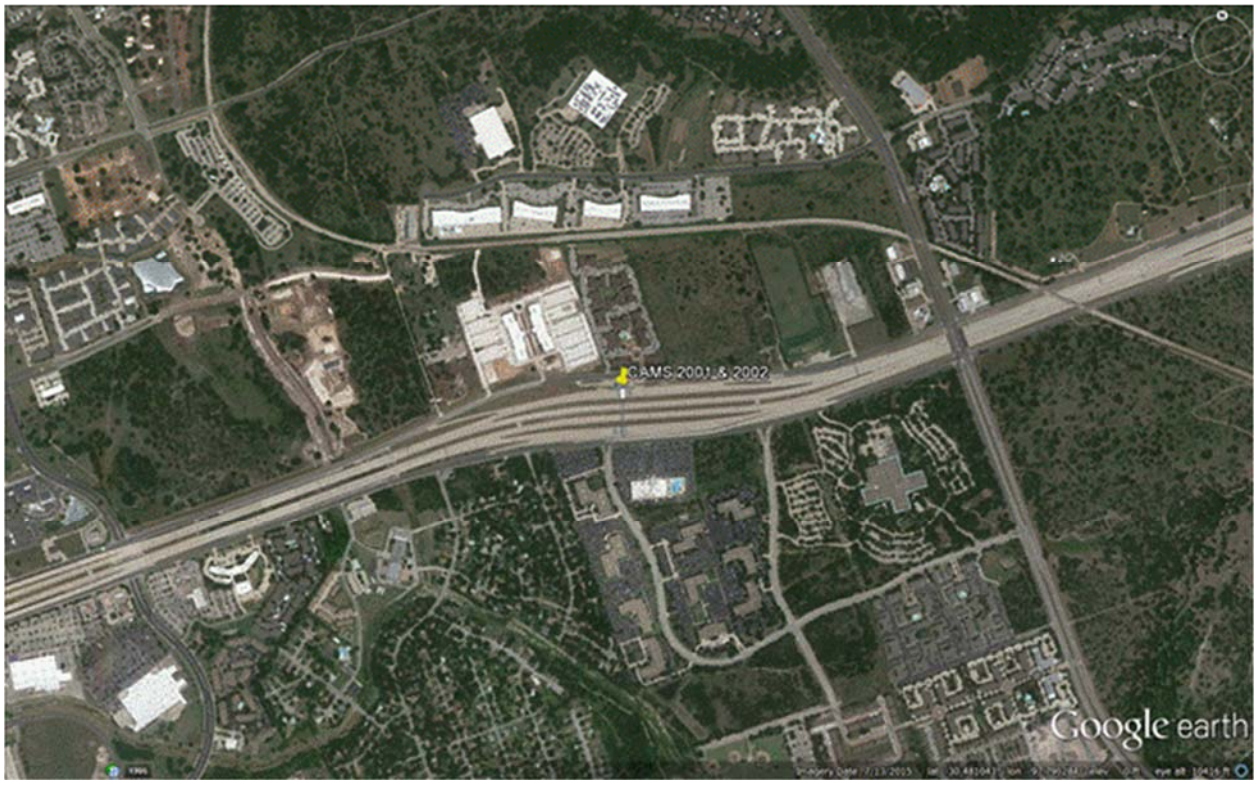

Figure I.2 Google Earth Pro aerial of CAMS 2001/2002 (yellow pushpin) and the City of Austin area

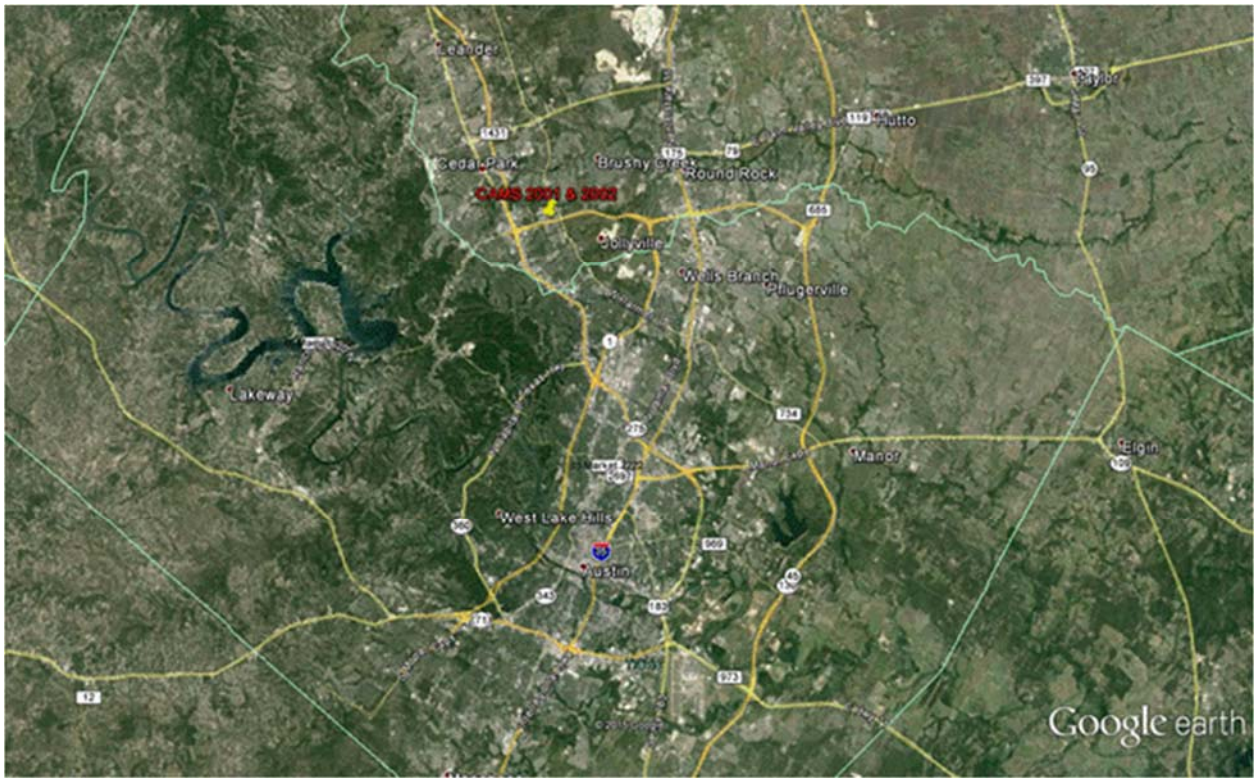

Meteorological Data

Figure I.3 is a wind rose created from the hourly wind speed and wind directions resultants measured at the site. As was mentioned above, the site is in the prevailing downwind direction of Austin TX (2015 population ~ 900,000). As is shown in Figure I.1, the site is also on the downwind side of a limited access tollway. Figures I.4 and I.5 are wind roses created from the hourly wind speed and wind directions resultants measured at two nearby sites, whose locations are shown relative to CAMS 2001/2002 in Figure I.6 and listed in Table I.1. The winds used in Figures I.3, I.4, and I.5 were measured over the same time period, but the site's show significant differences. Both CAMS 3 and CAMS 38 have an ensemble of wind directions more tightly clustered from south-southwest to southeast compared to CAMS 2001/2002, for which winds are spread out from southwest through east-southeast. There also appear to be more winds at higher speed at CAMS 2001/2002. An assignable cause for the observed differences could be the small-scale effects that fast moving motor vehicles have on the wind measurements at the Project site.

Figure I.3 Wind rose for Project CAMS 2001/2002 site, 5/27/2015–11/10/2015

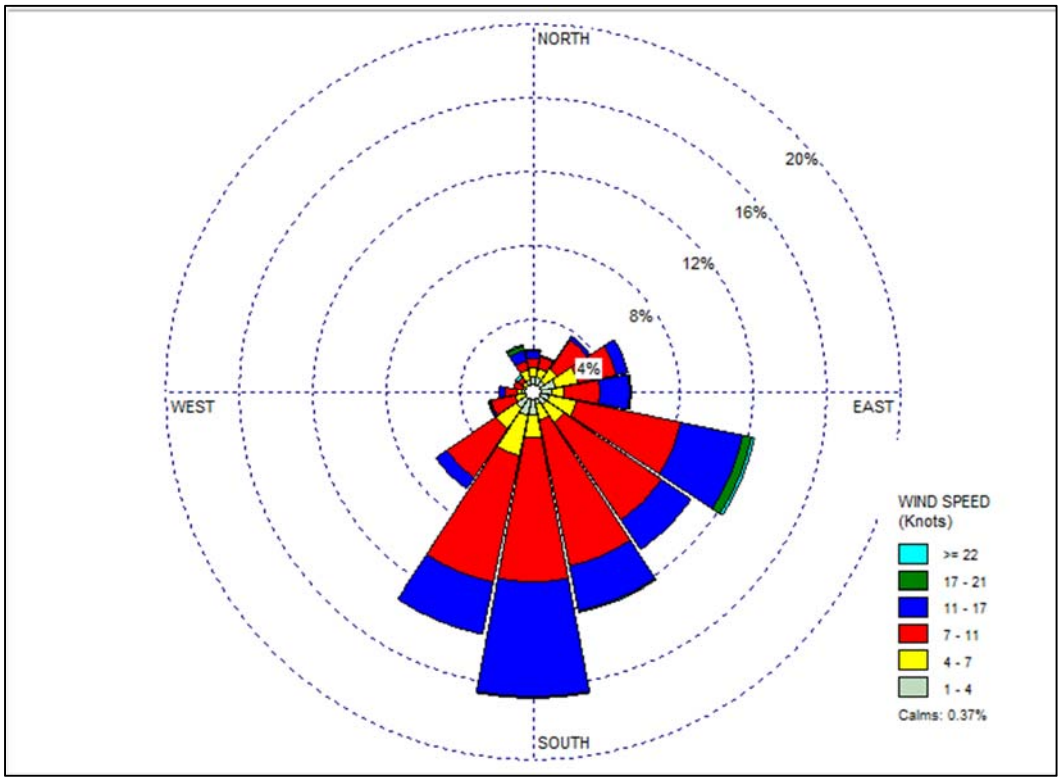

Figure I.4 Wind rose for TCEQ's CAMS 3 Austin NW site, 5/27/2015–11/10/2015

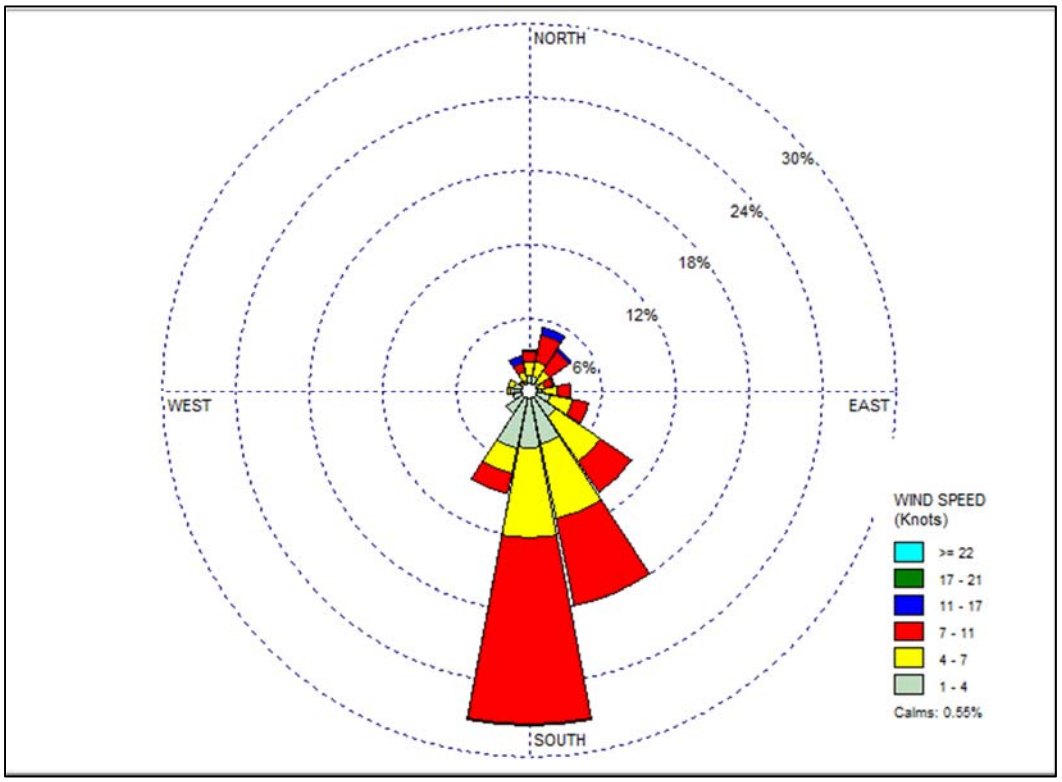

Figure I.5 Wind rose for TCEQ's CAMS 38 Audubon site, 5/27/2015–11/10/2015

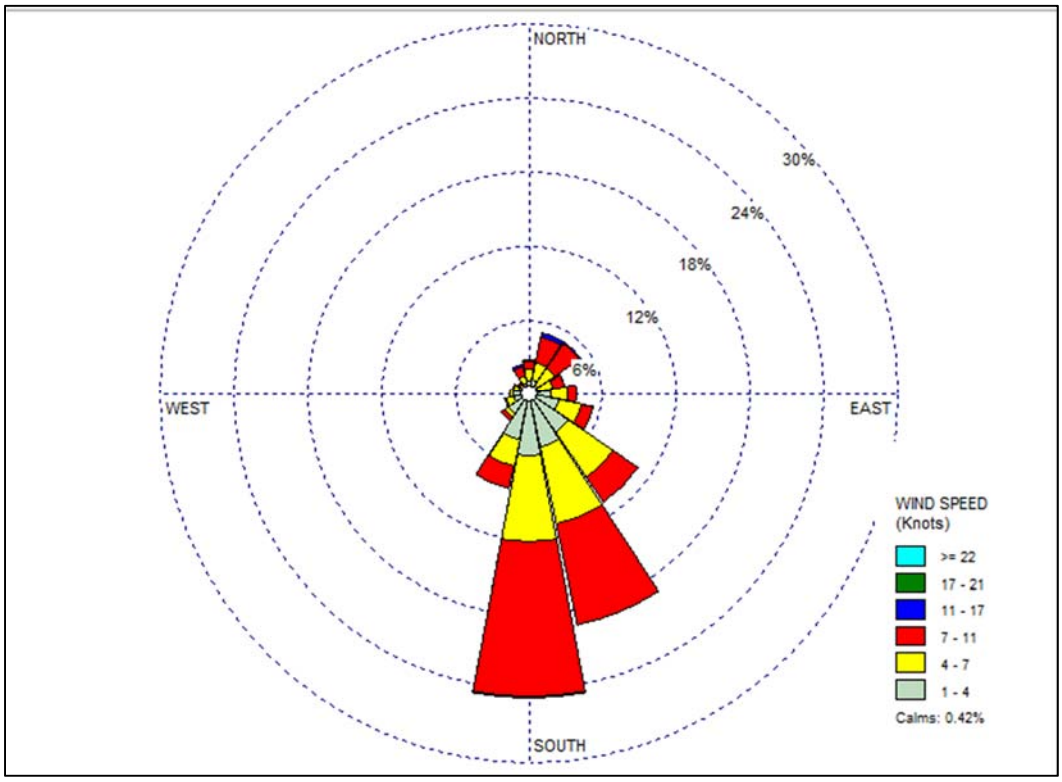

Table I.1 Nearby North Austin monitoring sites with meteorological measurements

Monitoring site	Latitude	Longitude
CAMS 3	30.3544	-97.7603
CAMS 38	30.4832	-97.8723
CAMS 2001/2002	30.4751	-97.7751

Figure I.6 Google Earth Pro aerial of CAMS 2001/2002 and nearby North Austin monitoring sites with meteorological measurements

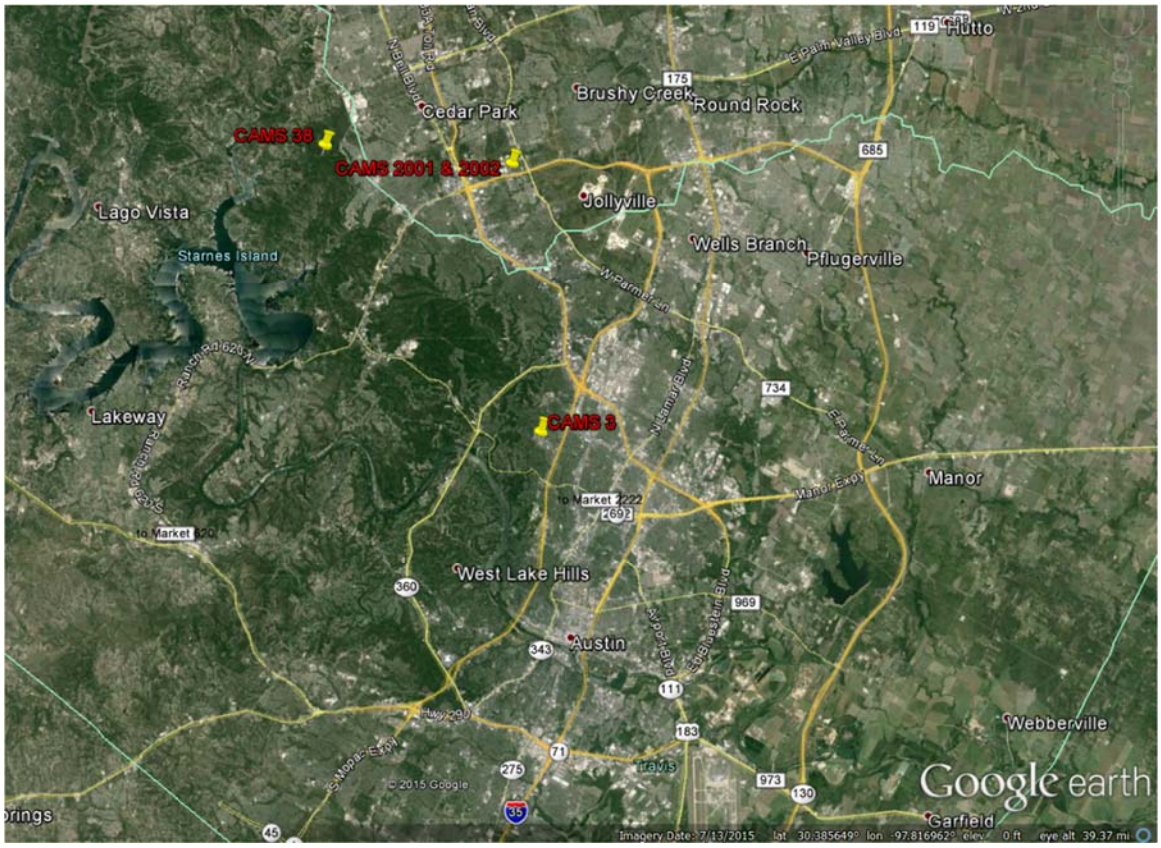

Gas Species Data

Time Series

Figure I.7 shows the time series graphs for:

- NO measured at the two stations (NO_1 and NO_2),
- NO_2 measured at the two sites (NO2_1 and NO2_2),
- NOx measured at the two stations (NOx_1 and NOx_2), and
- O_3 measured at the two stations (O3_1 and O3_2)

The utility of these graphs is that they show the ranges of the data and to some extent allow one to judge variability in the data over time and seasons.

Figure I.7 CAMS 2001/2002 (POC 1 & 2) data late May–late November 2015

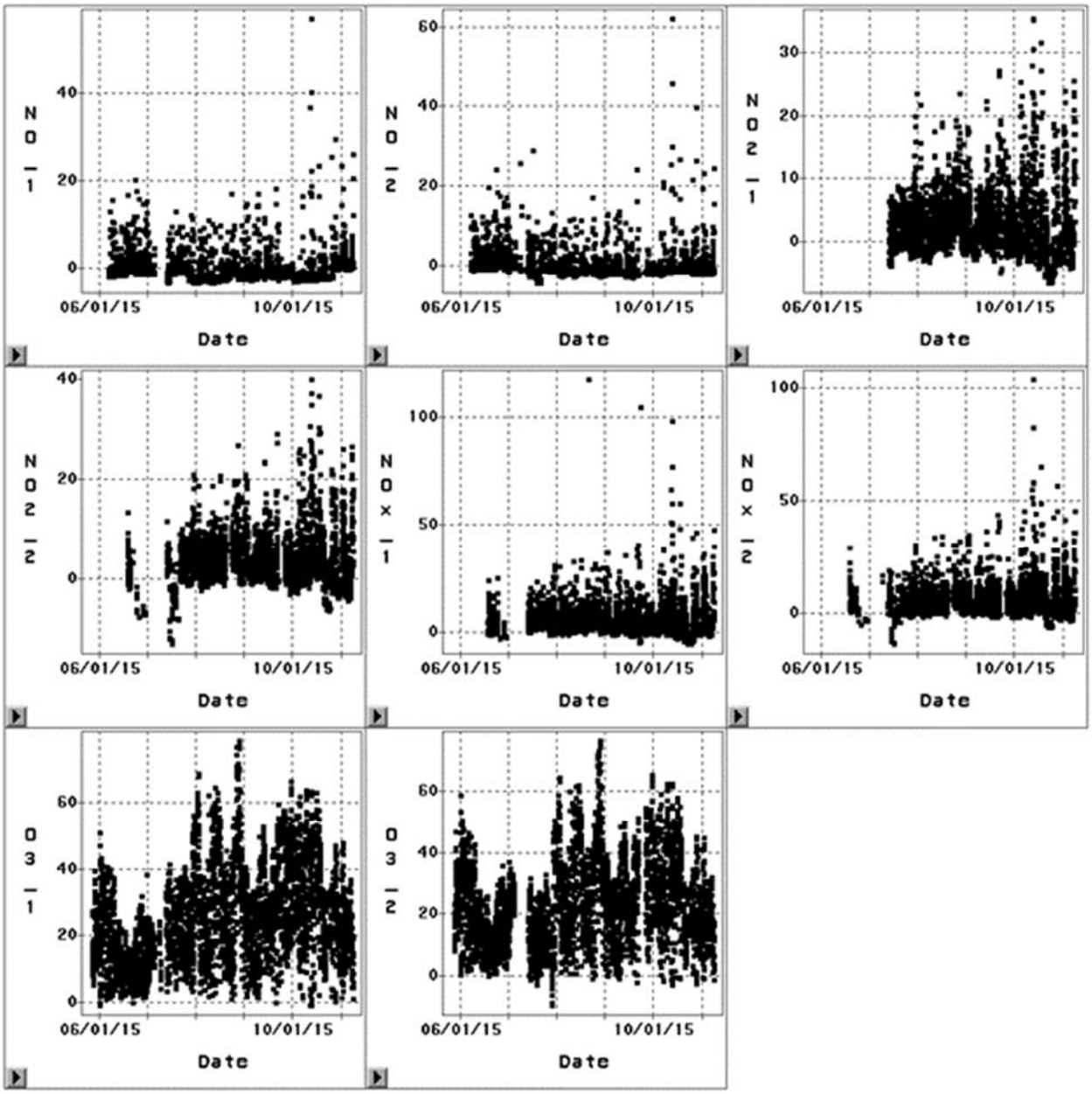

Distributions of Data

Figures I.8 and I.9 show stations 1 and 2 NO_2 daily summary data in the form of the daily hourly maxima, minima, and means. Only data from days with at least 18 hours valid data were considered "complete" and were used. Note that not all days on which one station took complete data did the other station also take complete data. Similarly, Figures I.10 and I.11 show O_3 daily summary hourly data for stations 1 and 2.

Figure I.12 shows four histograms for the distributions of the daily minima and maxima for NO_2 at stations 1 and 2, again using only days with at least 18 hours valid data. Station 1 has 96 complete NO_2 days, and station 2 has 91. The number of dates for which both sites have complete data is

90. Figure I.13 compares the cumulative distributions of the daily maximum one hour measurements at the two sites for the 90 days each were complete from August 1 to November 10. Excluding the 90 day extrema (maxima and minima), the difference between the station 1 and station 2 values at the same percentiles (10 percent to 90 percent) range from -2.1 to –1.1 ppb, averaging -1.8 ppb. In other words, because every point on the station 2 cumulative distribution curve is to the right (greater than) every point on the station 1 cumulative distribution curve, station 2 NO_2 distribution dominates the station 1 distribution for daily one hour maxima.

Figure I.14 shows four histograms for the distributions of the daily minima and maxima for O_3 at stations 1 and 2, again using only complete days. Station 1 has 98 complete O_3 days, and station 2 has 96. The number of dates for which both sites have complete data is 95. Figure I.15 compares the cumulative distributions of the daily maximum one hour O_3 measurements at both sites for the complete days. Excluding the 95 day extrema (maxima and minima), the difference between the station 1 and station 2 values at the same percentiles (10 percent to 90 percent) differ from 2.2 to 3.6 ppb, averaging 2.9 ppb. Thus, because every point on the station 1 cumulative distribution curve is to the right (greater than) every point on the station 2 cumulative distribution curve, the station 1 O_3 distribution dominates the station 2 distribution for daily one hour maxima.

Figure I.8 The distribution for NO_2 station 1 measurements within each 24-hour date (minimum 18 hours of data)—bars show daily minima, mean, and maxima

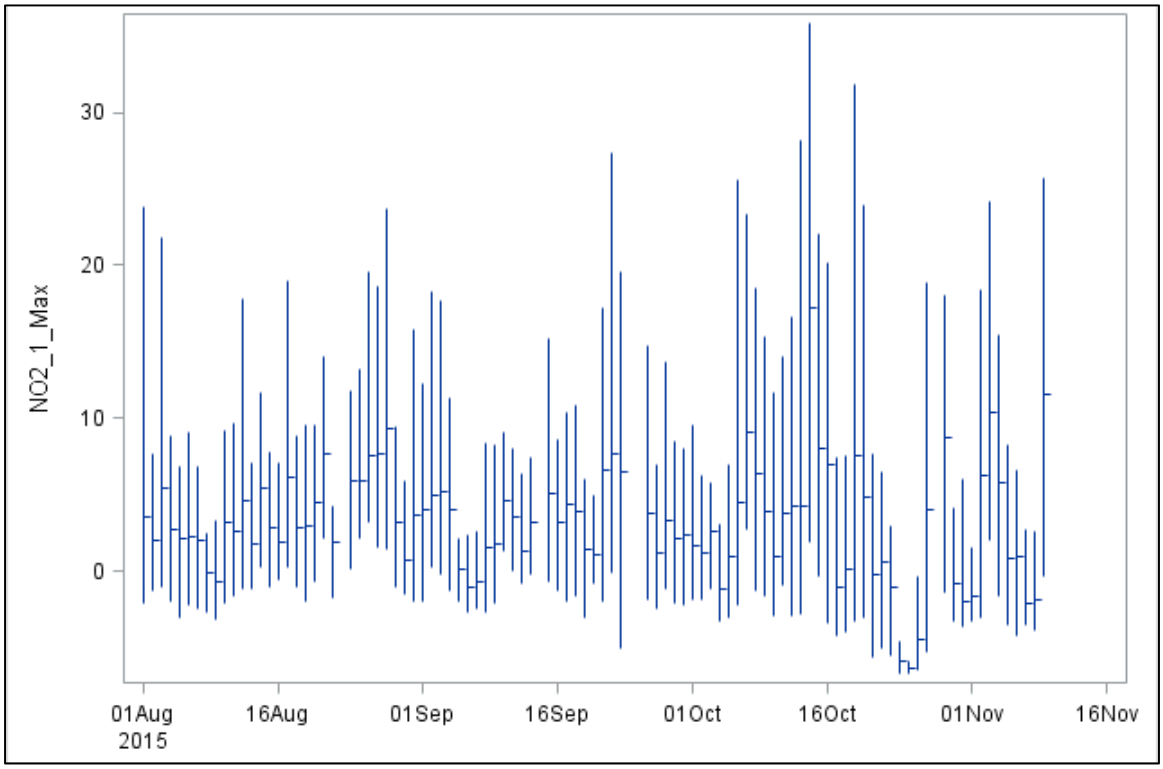

Figure I.9 The distribution for NO_2 station 2 measurements within each 24-hour date (minimum 18 hours of data)—bars show daily minima, mean, and maxima

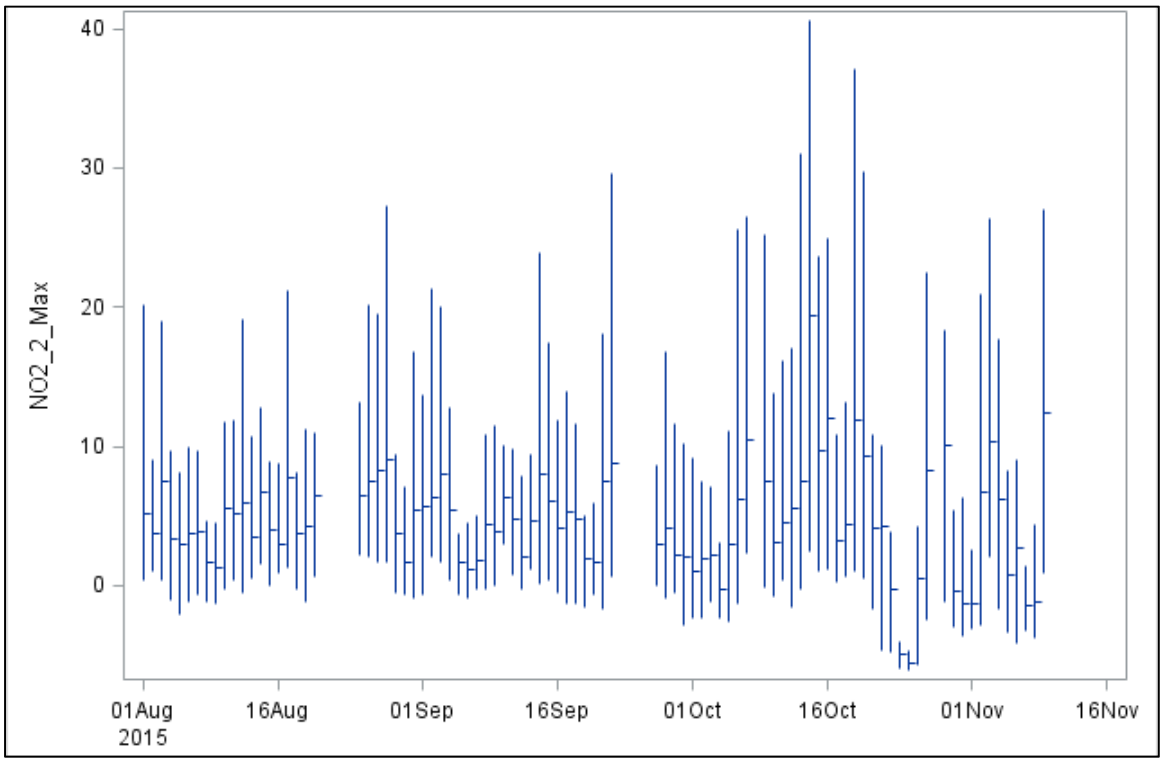

Figure I.10 The distribution for O_3 station 1 measurements within each 24-hour date (minimum 18 hours of data)—bars show daily minima, mean, and maxima

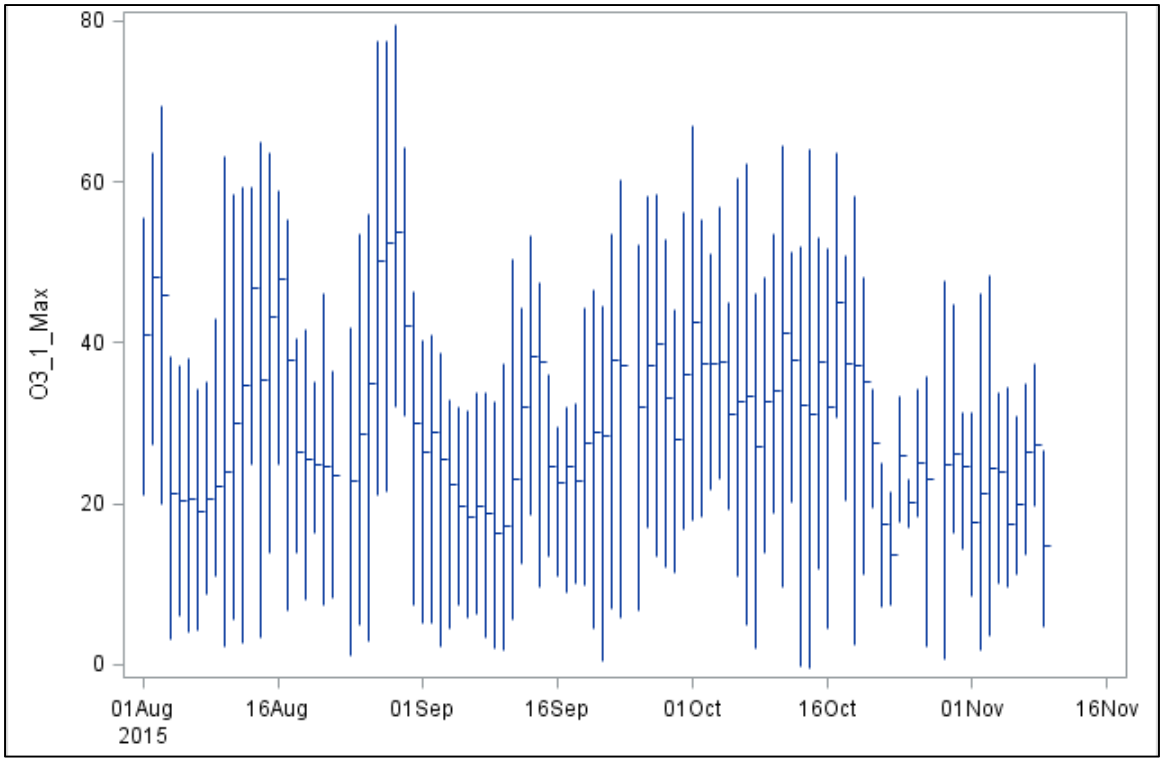

Figure I.11 The distribution for O_3 station 2 measurements within each 24-hour date (minimum 18 hours of data)—bars show daily minima, mean, and maxima

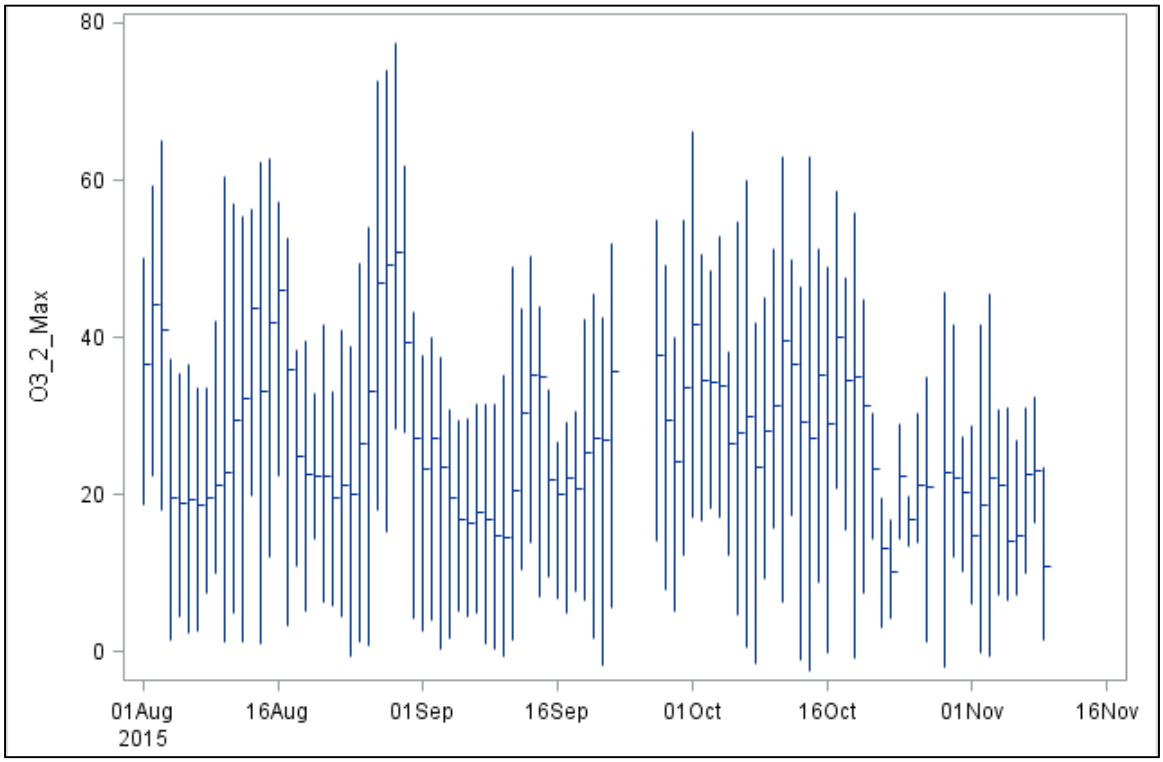

Figure I.12 Histograms on data for all daily NO_2 stations 1 & 2 minima & maxima, Aug. 1–Nov. 10

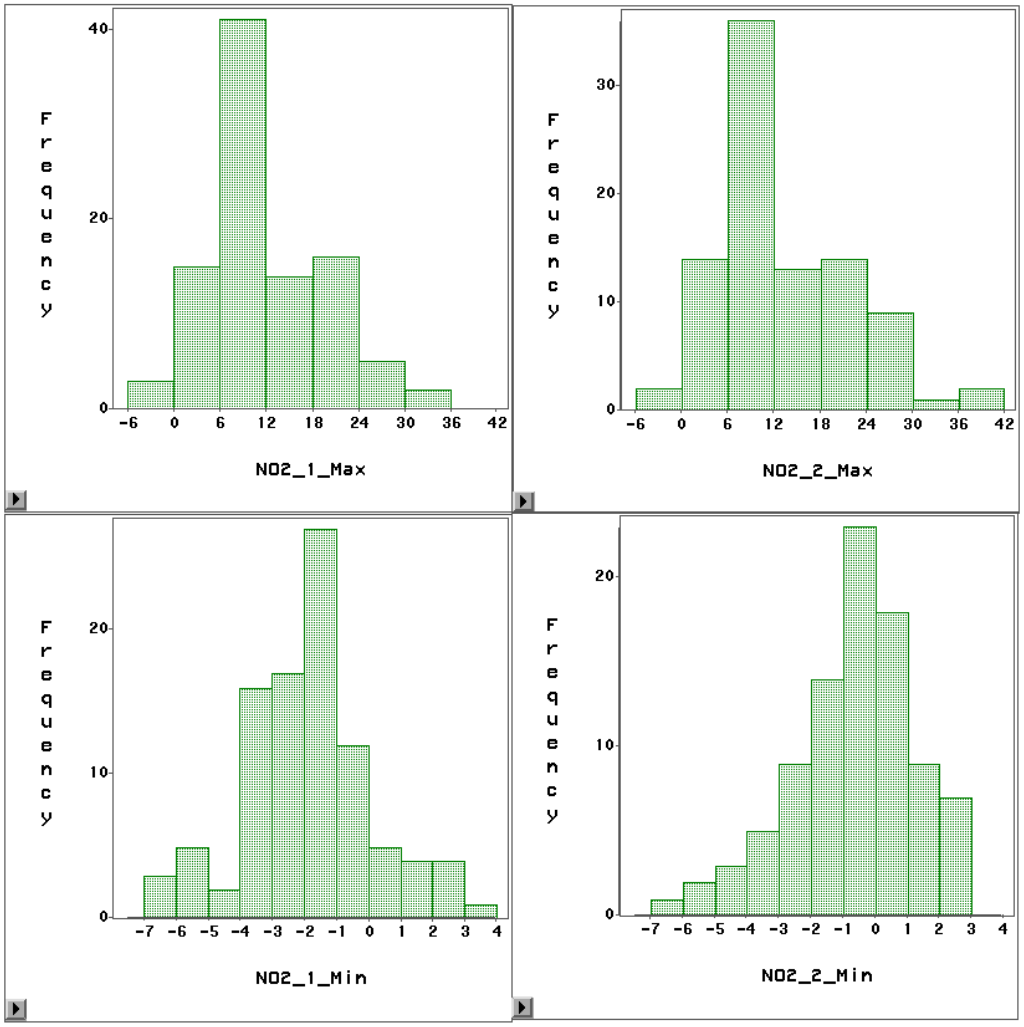

Figure I.13 Cumulative distributions of the daily maximum one-hour NO_2 values at the two stations for the 90 days both stations had complete data

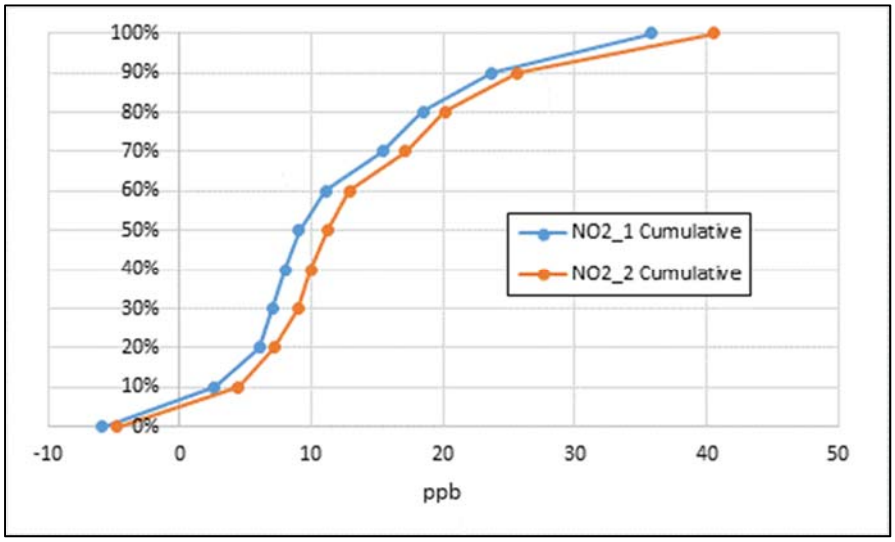

Figure I.14 Histograms on data for all daily O_3 stations 1 & 2 minima & maxima, Aug. 1–Nov. 10

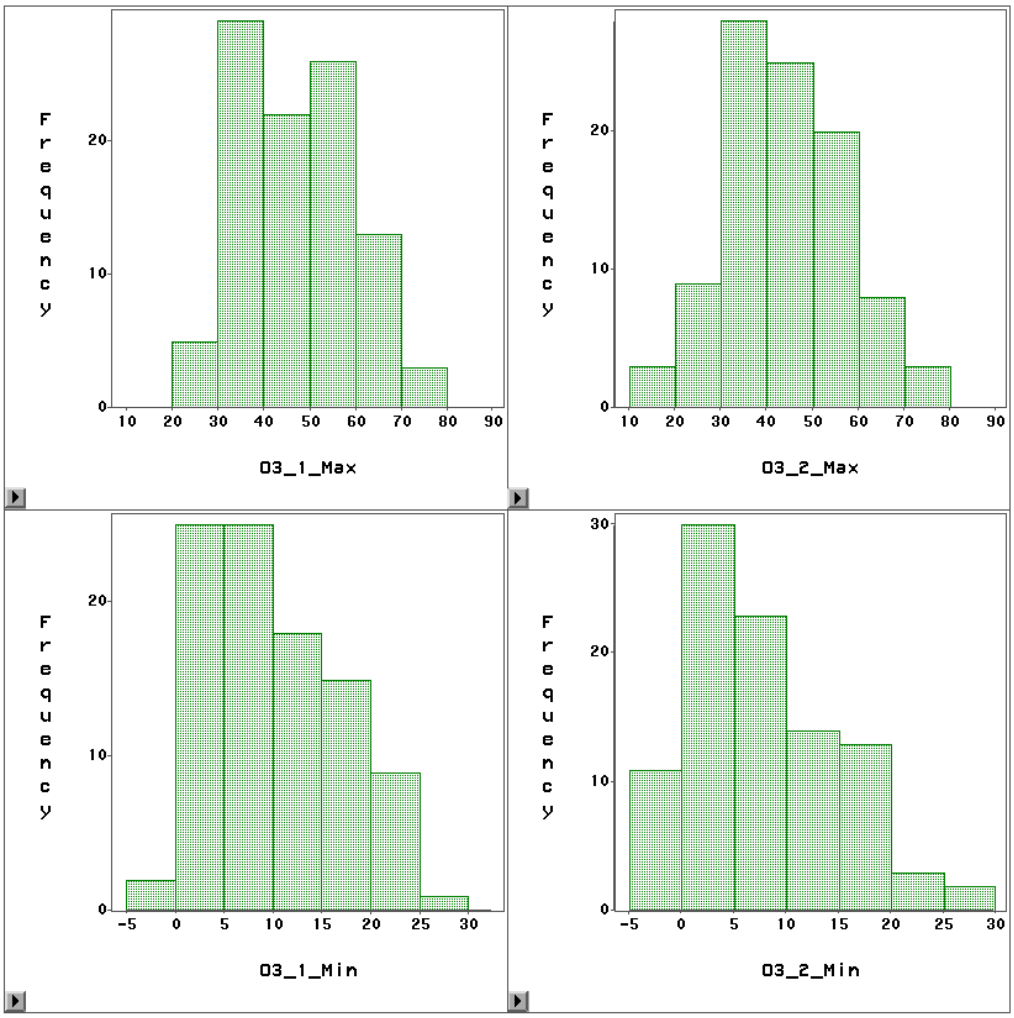

Figure I.15 Cumulative distributions of the daily maximum one-hour O_3 values at the two stations for the 95 days both stations had complete data

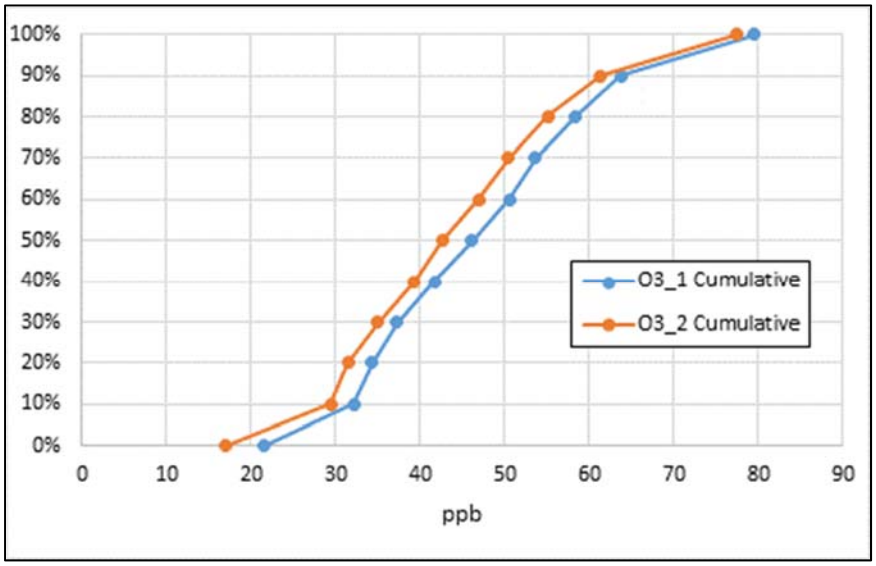

Linear Regressions

A better means of comparison is the series of linear regressions for NO_2 vs NO_1 in Figure I.16, NO2_2 vs NO2_1 in Figure I.17, NOx_2 vs NOx_1 in Figure I.18, and O3_2 vs O3_1 in Figure I.19. Each regression is statistically significant at $p < 0.0001$. For both O3 and NO2, the slopes are practically equal to 1.0 and the y-intercepts are statistically significant: -2.43±0.13 ppb for O3 and +1.50±0.01 ppb for NO2. This suggests a consistent 2.4 ppb bias for O3_1 > O3_2 and a consistent 1.5 ppb bias for NO2_2 > NO2_1. If concentrations of O3_1 below 40 ppb are excluded, the O3_1 > O3_2 bias is still approximately the same at -2.62±0.80. If concentrations of NO2_1 below 5 ppb are excluded the y-intercept shrinks to 1.10±0.31 ppb and the slope increases to 1.04±0.03, which help sustain the NO2_2 > NO2_1 relationship.

Figure I.16 Linear regressions for *NO_2* vs *NO_1*

Model Equation
NO_2 = - 0.0803 + 0.9428 NO_1

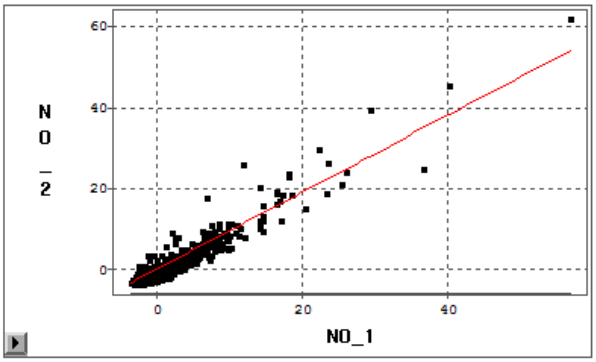

Parametric Regression Fit								
		Model		Error				
Curve	Degree(Polynomial)	DF	Mean Square	DF	Mean Square	R-Square	F Stat	Pr > F
	1	1	24774.0973	2100	1.7778	0.8690	13935.21	<.0001

Parameter Estimates							
Variable	DF	Estimate	Std Error	t Stat	Pr >|t|	Tolerance	Var Inflation
Intercept	1	-0.0803	0.0294	-2.73	0.0064	.	0
NO_1	1	0.9428	0.0080	118.05	<.0001	1.0000	1.0000

Figure I.17 Linear regressions for *NO2_2* vs *NO2_1*

Model Equation
NO2_2 = 1.4985 + 1.0009 NO2_1

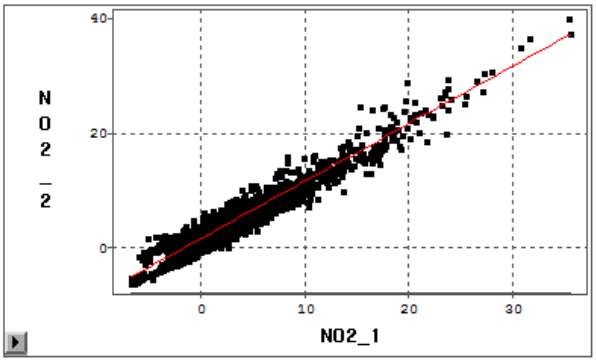

Parametric Regression Fit								
		Model		Error				
Curve	Degree(Polynomial)	DF	Mean Square	DF	Mean Square	R-Square	F Stat	Pr > F
	1	1	67191.9485	2100	2.3054	0.9328	29145.19	<.0001

Parameter Estimates							
Variable	DF	Estimate	Std Error	t Stat	Pr >|t|	Tolerance	Var Inflation
Intercept	1	1.4985	0.0382	39.26	<.0001	.	0
NO2_1	1	1.0009	0.0059	170.72	<.0001	1.0000	1.0000

Figure I.18 Linear regressions for *NOx_2* vs *NOx_1*

Model Equation

NOx_2 = 0.1027 + 1.0078 NOx_1

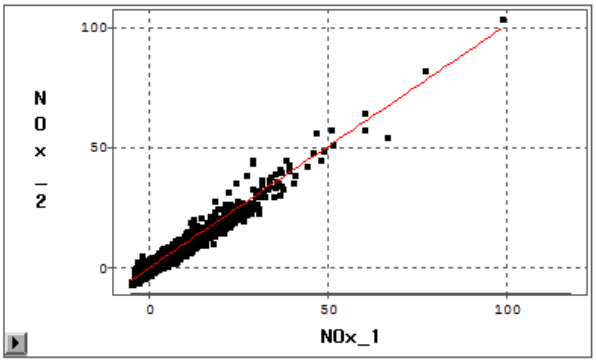

Parametric Regression Fit

Curve	Degree(Polynomial)	Model DF	Model Mean Square	Error DF	Error Mean Square	R-Square	F Stat	Pr > F
	1	1	144446.883	2100	3.9176	0.9461	36871.73	<.0001

Parameter Estimates

Variable	DF	Estimate	Std Error	t Stat	Pr >|t|	Tolerance	Var Inflation
Intercept	1	0.1027	0.0554	1.86	0.0637	.	0
NOx_1	1	1.0078	0.0052	192.02	<.0001	1.0000	1.0000

Figure I.19 Linear regressions for *O3_2* vs *O3_1*

Model Equation

O3_2 = - 2.4254 + 0.9933 O3_1

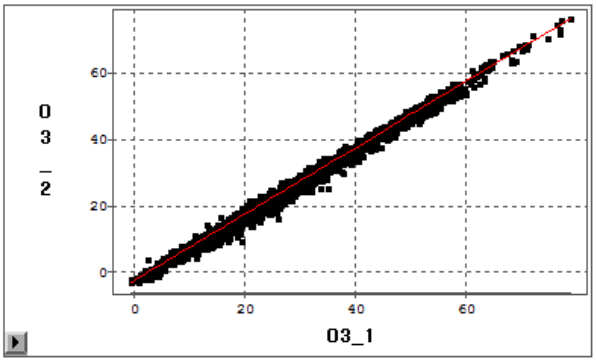

Parametric Regression Fit

Curve	Degree(Polynomial)	Model DF	Model Mean Square	Error DF	Error Mean Square	R-Square	F Stat	Pr > F
	1	1	468056.204	2211	1.8728	0.9912	249929.7	<.0001

Parameter Estimates

Variable	DF	Estimate	Std Error	t Stat	Pr >|t|	Tolerance	Var Inflation
Intercept	1	-2.4254	0.0656	-36.99	<.0001	.	0
O3_1	1	0.9933	0.0020	499.93	<.0001	1.0000	1.0000

NO_2 Diurnal Patterns

Figures I.20–I.24 show the average concentration for NO_2 by hour of the day (*diurnal pattern*) for the four weeks in August 2015 plus a fifth week for late August and early September. These graphs

show a consistent bias for *NO2_2 > NO2_1* for the large majority of hours in each week. This difference generally persists outside of the periods of sunlight.

Figures I.25–I.28 show the diurnal patterns for NO_2 by months August through November 2015, where only Nov. 1–10 have data. These graphs show a consistent bias for *NO2_2 > NO2_1* for the large majority of hours in each month.

Figure I.20 Mean hourly concentration for NO_2 for seven days Aug. 1–7

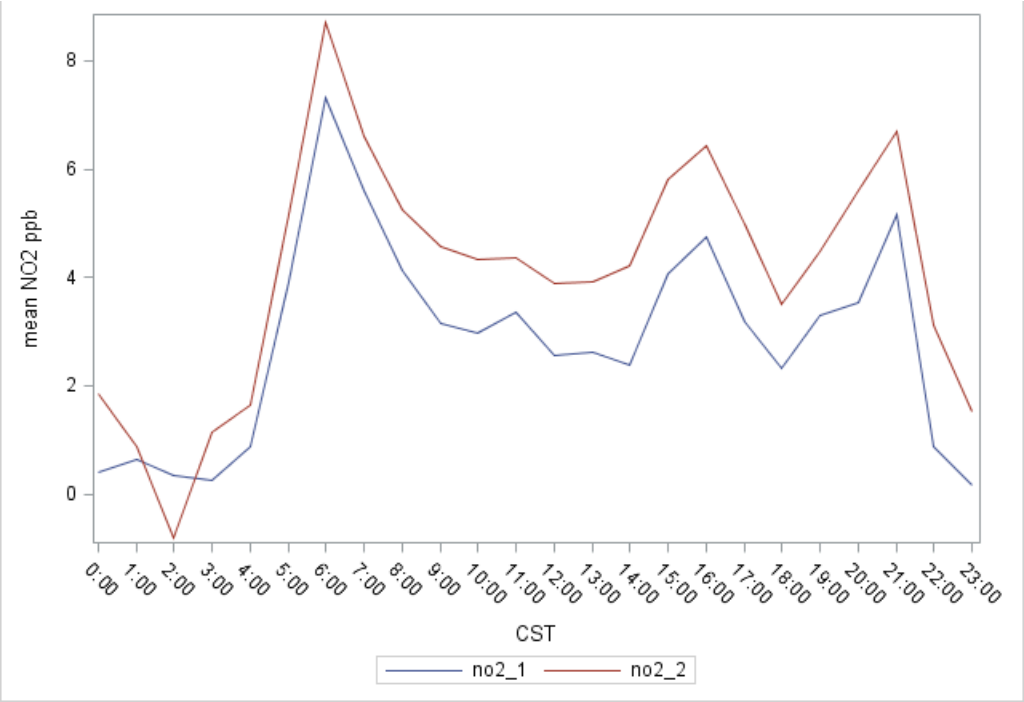

Figure I.21 Mean hourly concentration for NO_2 for seven days Aug. 8–14

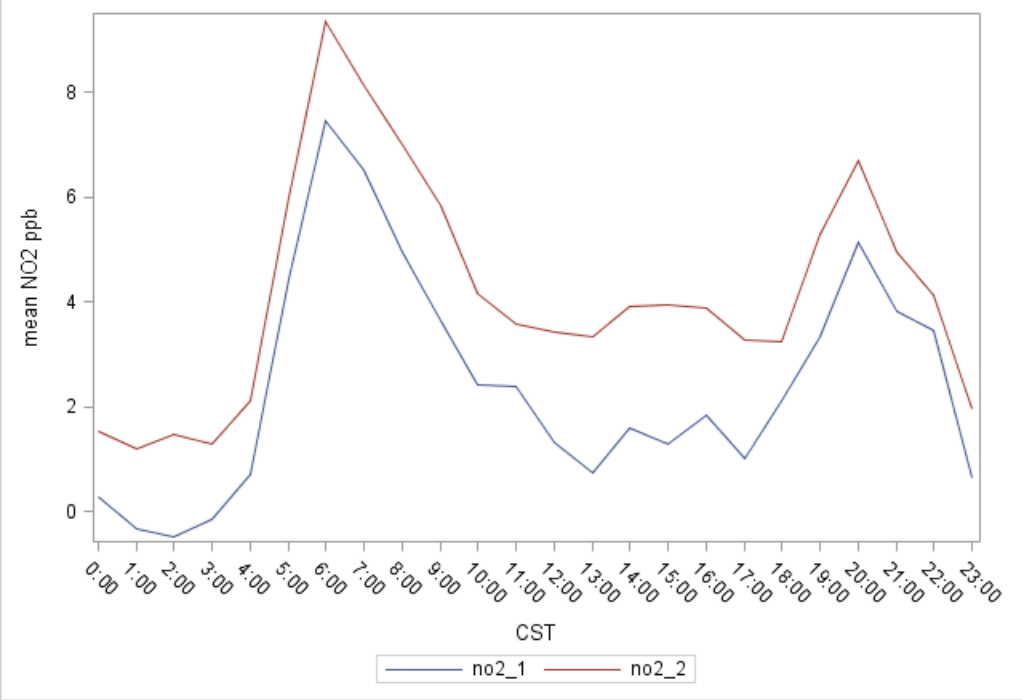

Figure I.22 Mean hourly concentration for NO_2 for seven days Aug. 15–21

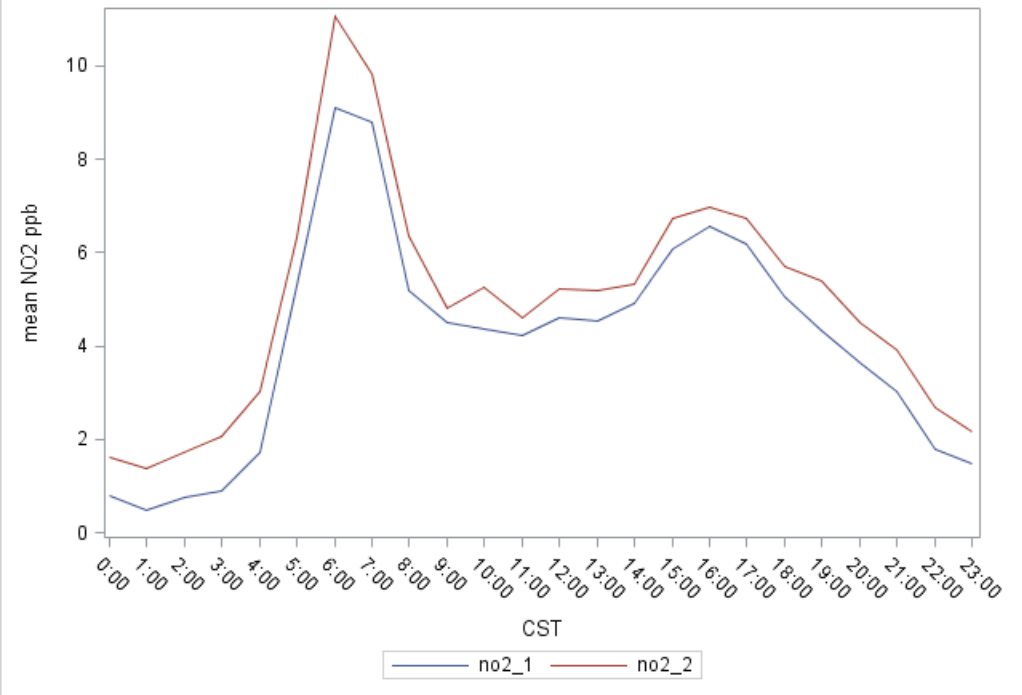

Figure I.23 Mean hourly concentration for NO_2 for seven days Aug. 22–28

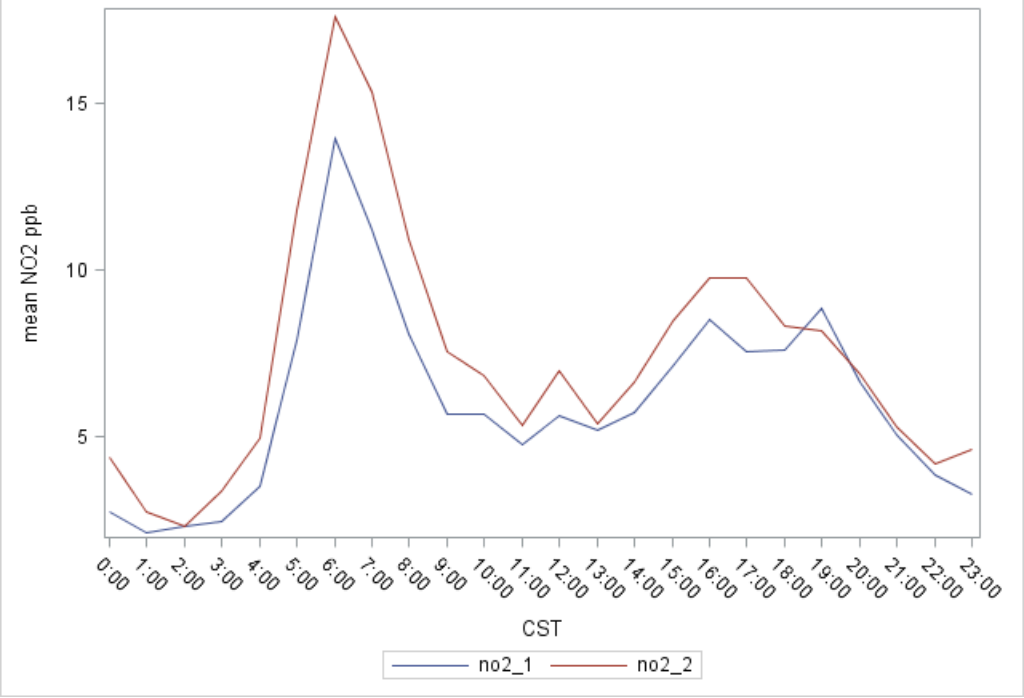

Figure I.24 Mean hourly concentration for NO_2 for seven days Aug. 29–Sep. 4

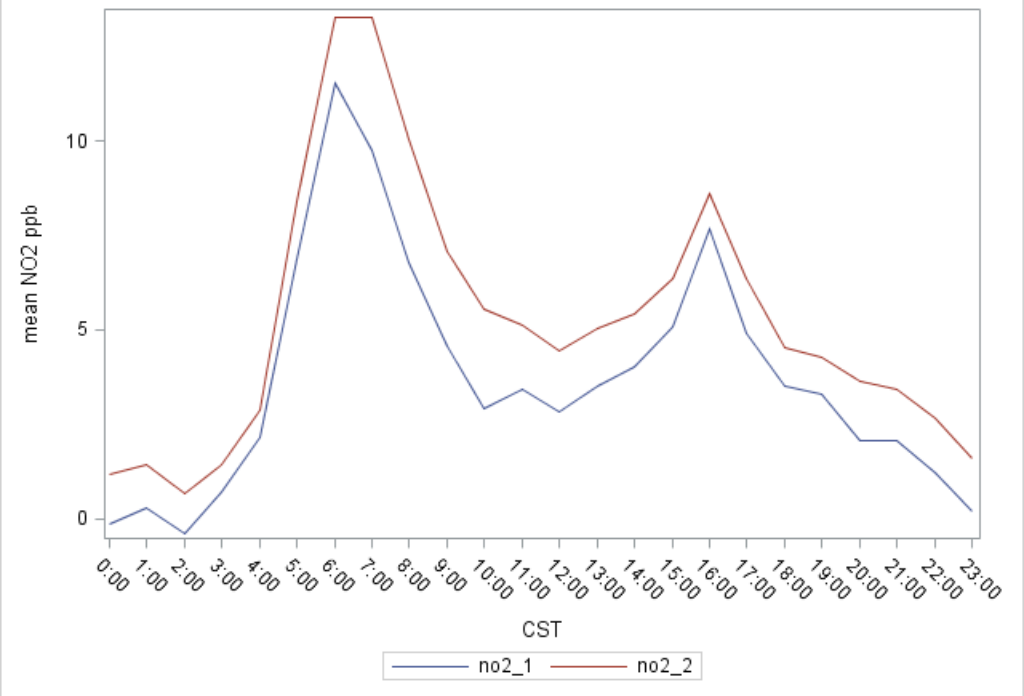

Figure I.25 Mean hourly concentration for NO_2 for August 2015

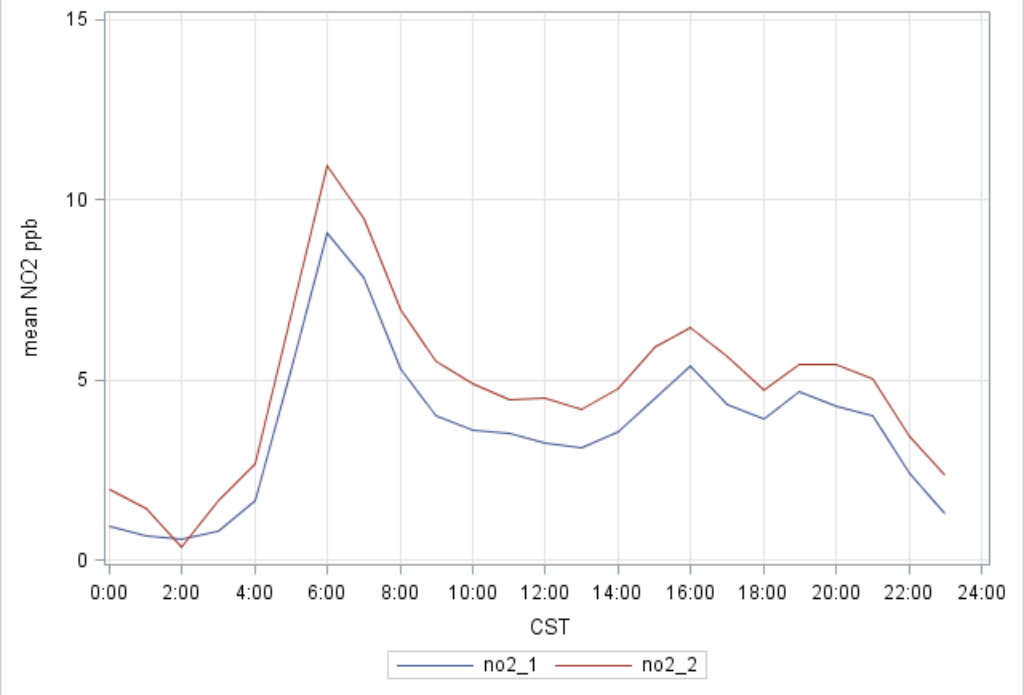

Figure I.26 Mean hourly concentration for NO_2 for September 2015

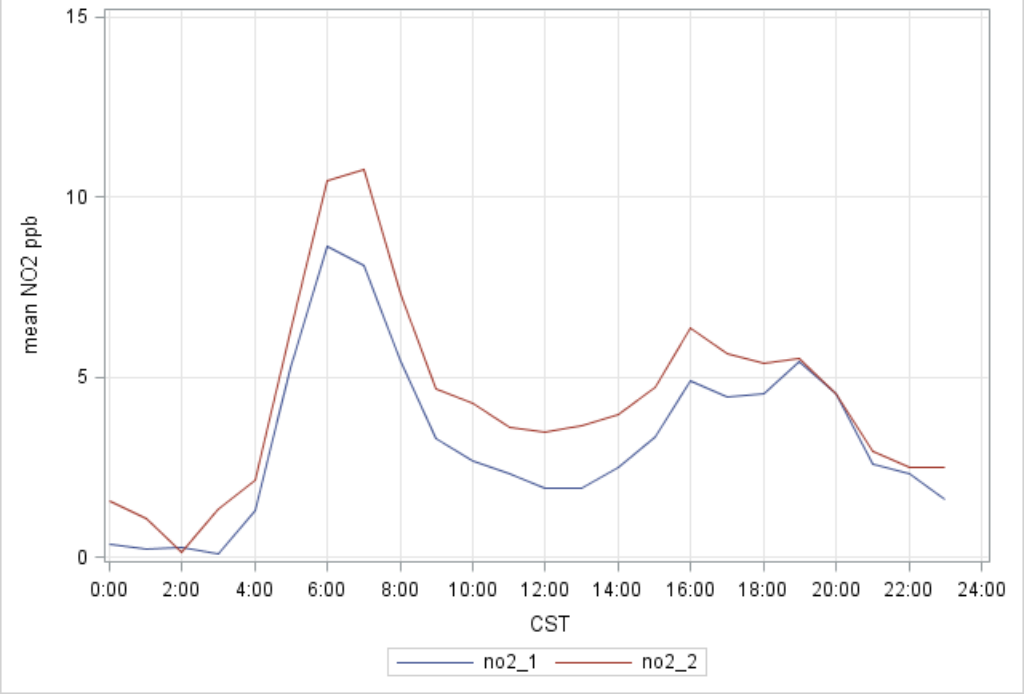

Figure I.27 Mean hourly concentration for NO_2 for October 2015

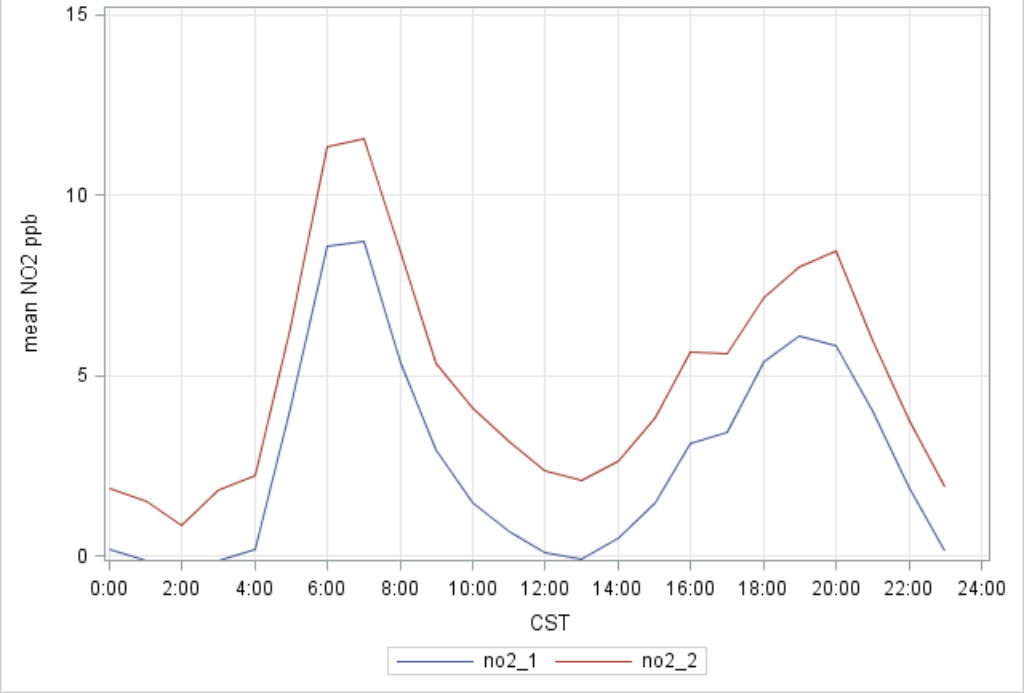

Figure I.28 Mean hourly concentration for NO_2 for November 2015 (Nov. 1–10)

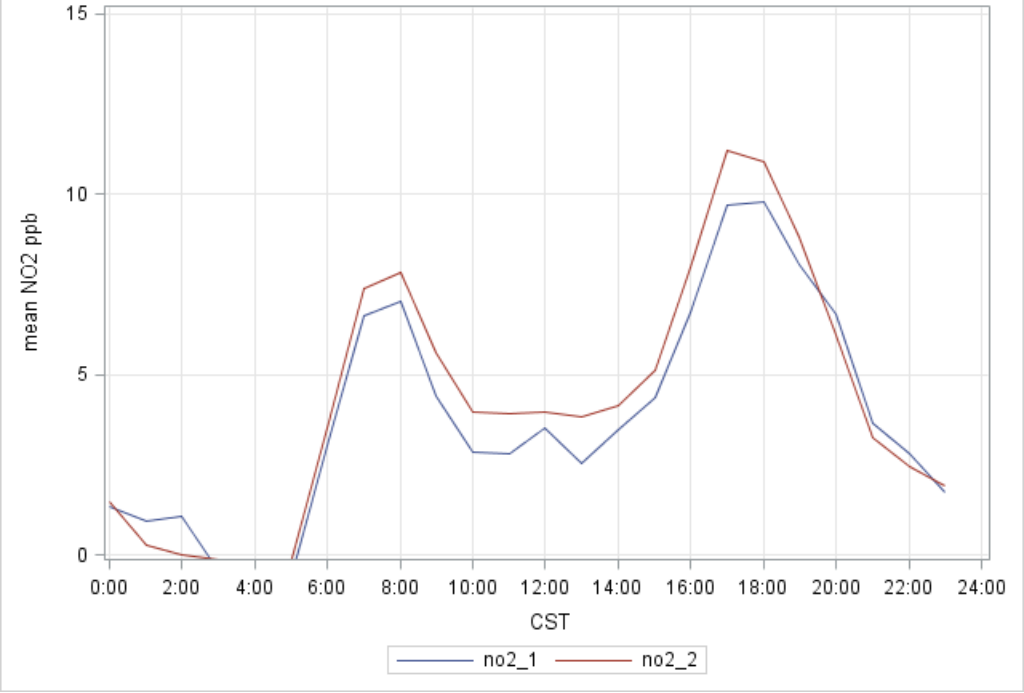

NO_2 Diurnal Patterns in Other Texas Urban Areas

Figures I.29–I.32 are provided for comparisons other NO_2 monitors around the state. These graphs were created by averaging together the hourly measurements across all of the NO_2 monitors in a TCEQ region by hour CST. The key for the graphs is:

- dfw = 16 monitors around the Dallas-Fort Worth area
- tlm = 3 monitors around the Tyler-Longview-Marshall area
- bpa = 9 monitors around the Beaumont/Port Arthur area
- aus = 2 monitors around the Austin area
- hgb = 23 monitors around the Houston-Galveston-Brazoria area
- san = 8 monitors around the San Antonio area

All composite graphs for each of the four months show a morning peak around 6 to 7 CST and an evening peak around 18 to 20 CST. This is very similar to the observed behavior at CAMS 2001/2002.

Figure I.29 Composite TCEQ Region NO_2 diurnal patterns for August 2015

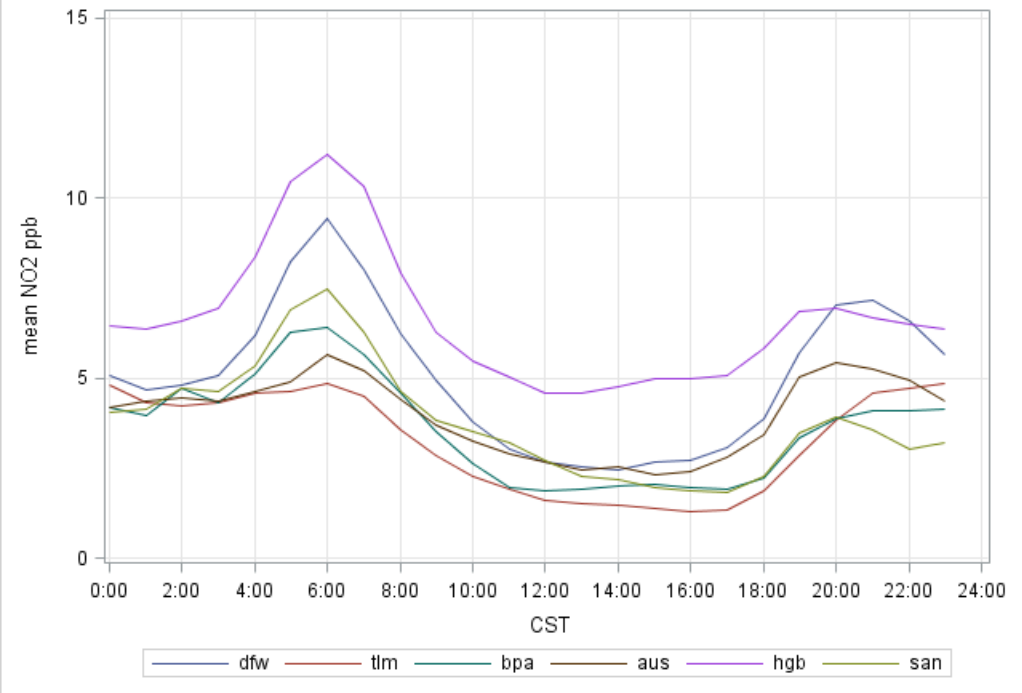

Figure I.30 Composite TCEQ Region NO_2 diurnal patterns for September 2015

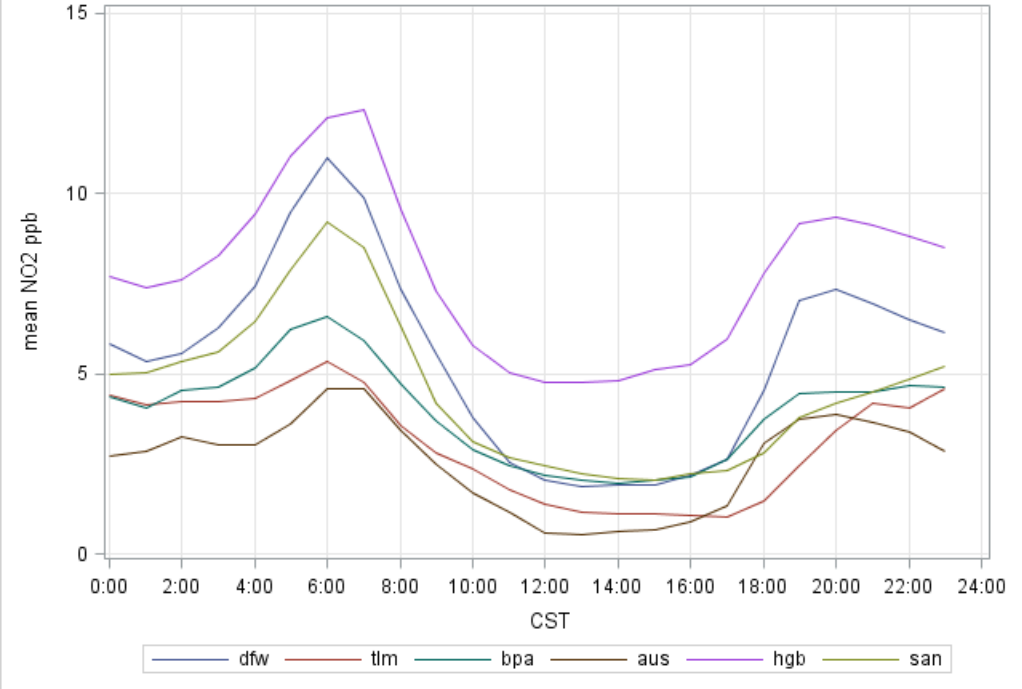

Figure I.31 Composite TCEQ Region NO_2 diurnal patterns for October 2015

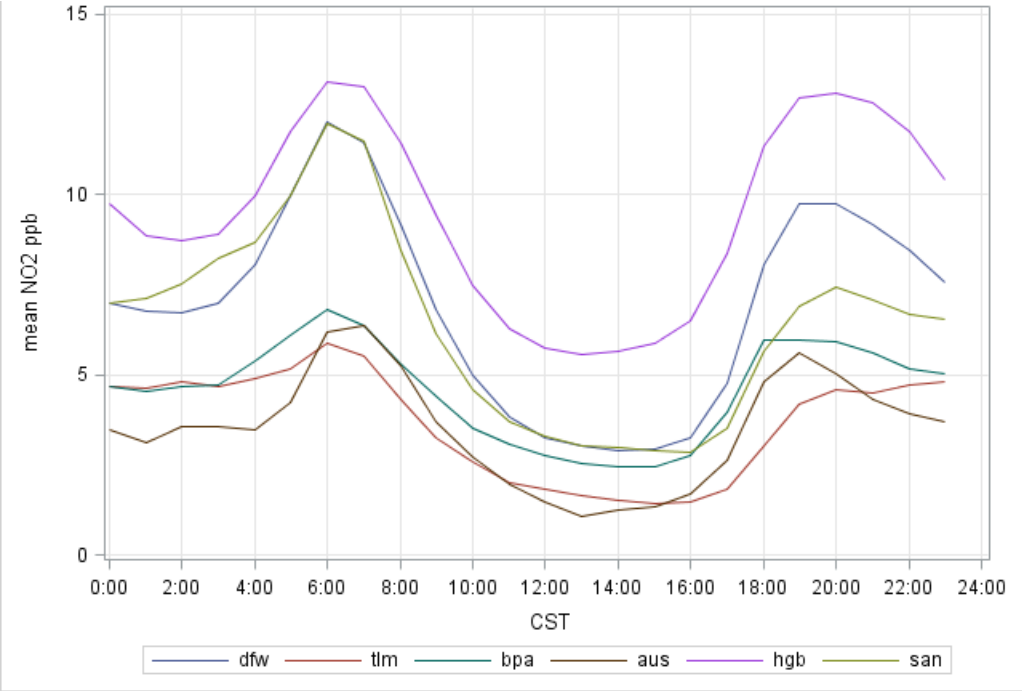

Figure I.32 Composite TCEQ Region NO_2 diurnal patterns for Nov. 1–10, 2015

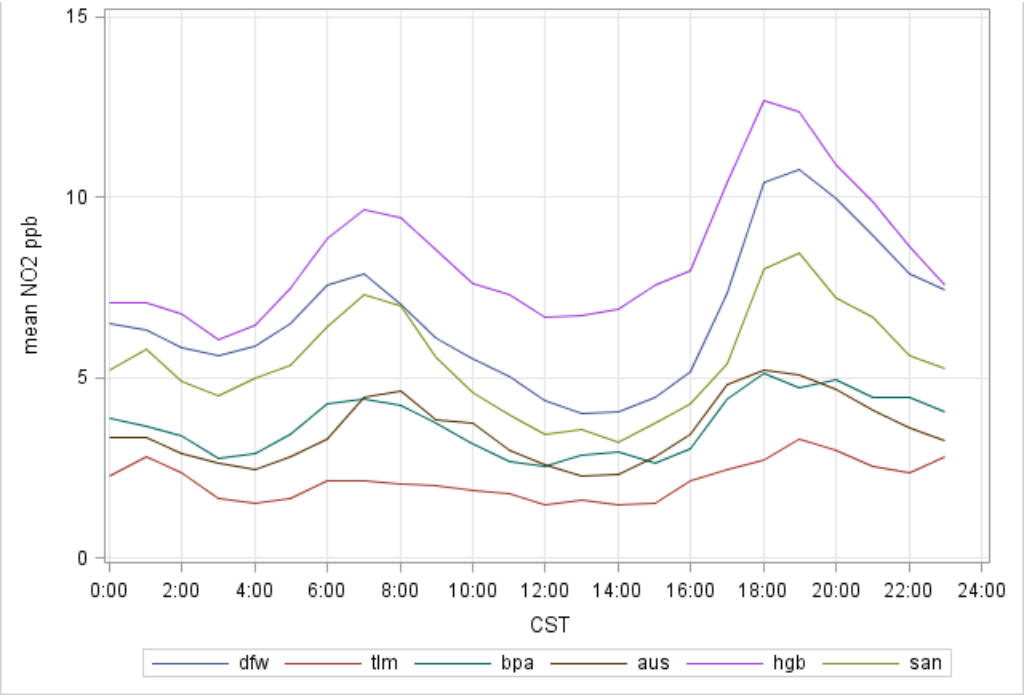

NO_2 Concentrations by Wind Direction

With no consideration of wind speed, season, or time of day, the mean concentrations of NO_2 by 15-degree wind bin are shown in Figure I.33 for the two sites. As was shown in the wind rose image in Figure I.3, there is likely some increased turbulence around CAMS 2001/2002 owning to proximity to the tollway. As a result, the graph in Figure I.33 may be of limited utility in identifying upwind direction to NO2 or NOx sources; however, it is important to note that the bias between *NO2_1* and *NO2_2* is fairly consistent in direction. Figure I.34 shows the difference of *NO2_1 – NO2_2* by wind direction.

Figure I.33 Mean NO_2 by 15-degree wind bin, Aug. 1–Nov. 10, 2015 CAMS 2001/2002

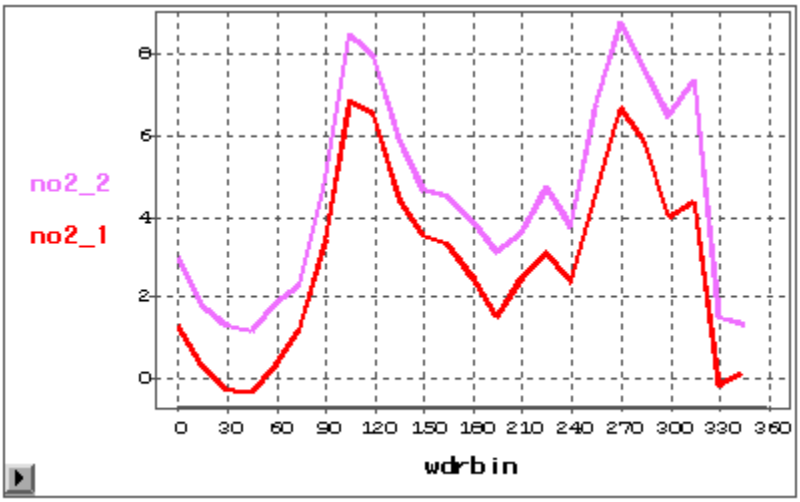

Figure I.34 Mean difference between the two parameters in the preceding figure by 15-degree wind bin, Aug. 1–Nov. 10, 2015 CAMS 2001/2002

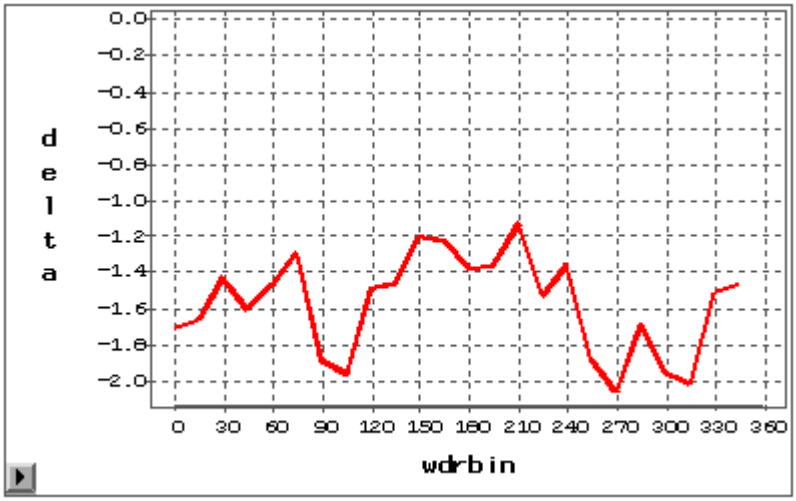

Ozone (O_3) Diurnal Patterns

Figures I.35, I.37, I.39, and I.41 show the diurnal patterns for O_3 by months August through November 2015, where only Nov. 1–10 have data. These graphs show a consistent bias for *O3_1* > *O3_2* for all hours in each month. The graphs of the differences *O3_1* - *O3_2* = *deltaO3* for each hour of each month are shown in Figures I.36, I.38, I.40, and I.42. The *deltaO3* graphs show that the mean difference in O_3 measurements is minimized from 20 to 22 CST.

Figure I.35 Diurnal patterns for O_3 for August 2015

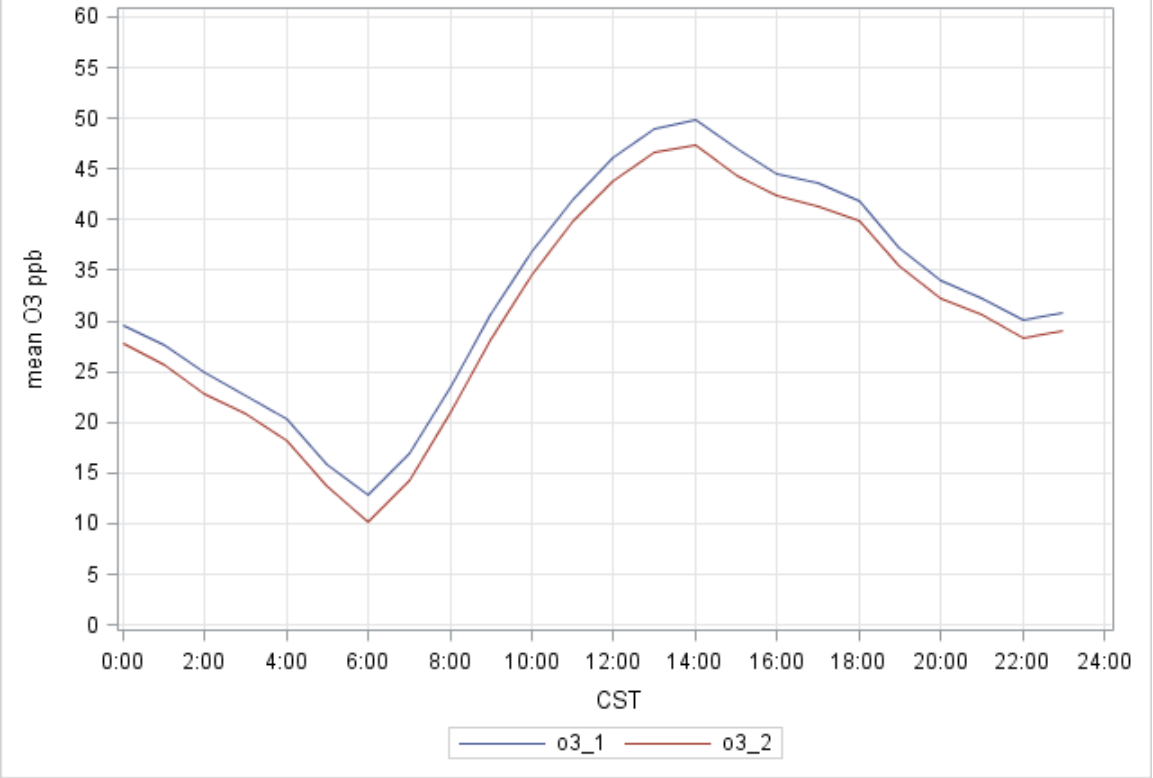

Figure I.36 Mean difference between the two parameters in the preceding figure August 2015

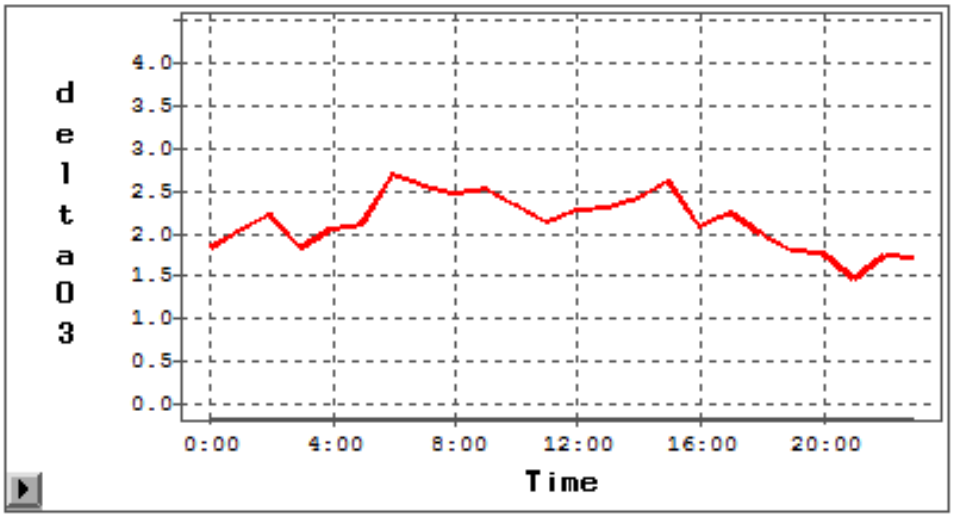

Figure I.37 Diurnal patterns for O_3 for September 2015

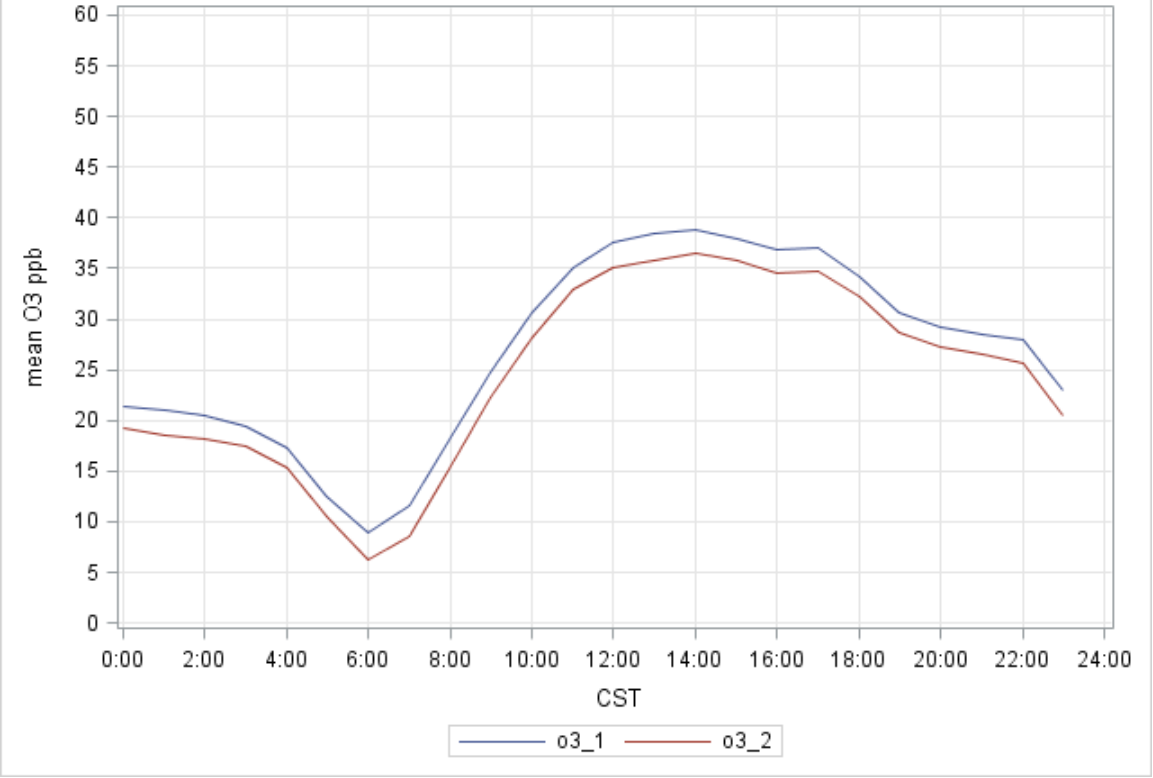

Figure I.38 Mean difference between the two parameters in the preceding figure September 2015

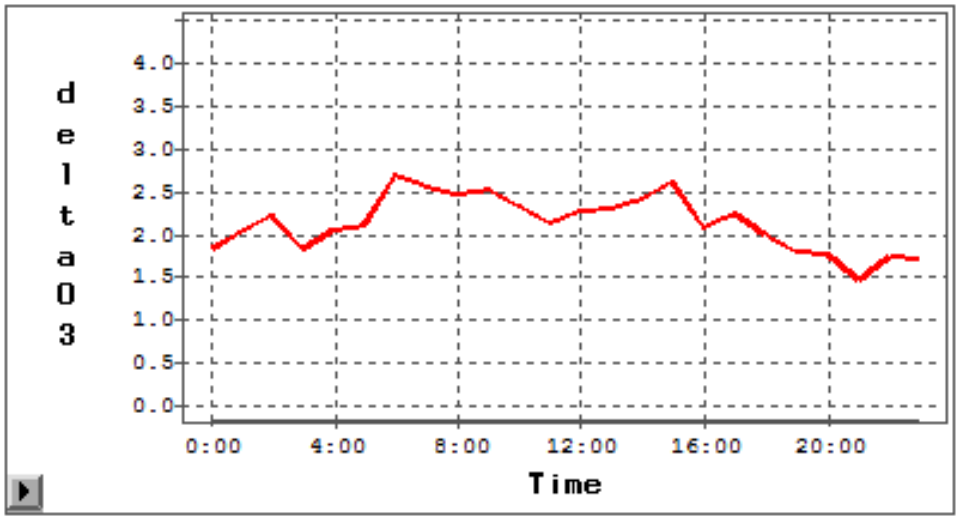

Figure I.39 Diurnal patterns for O_3 for October 2015

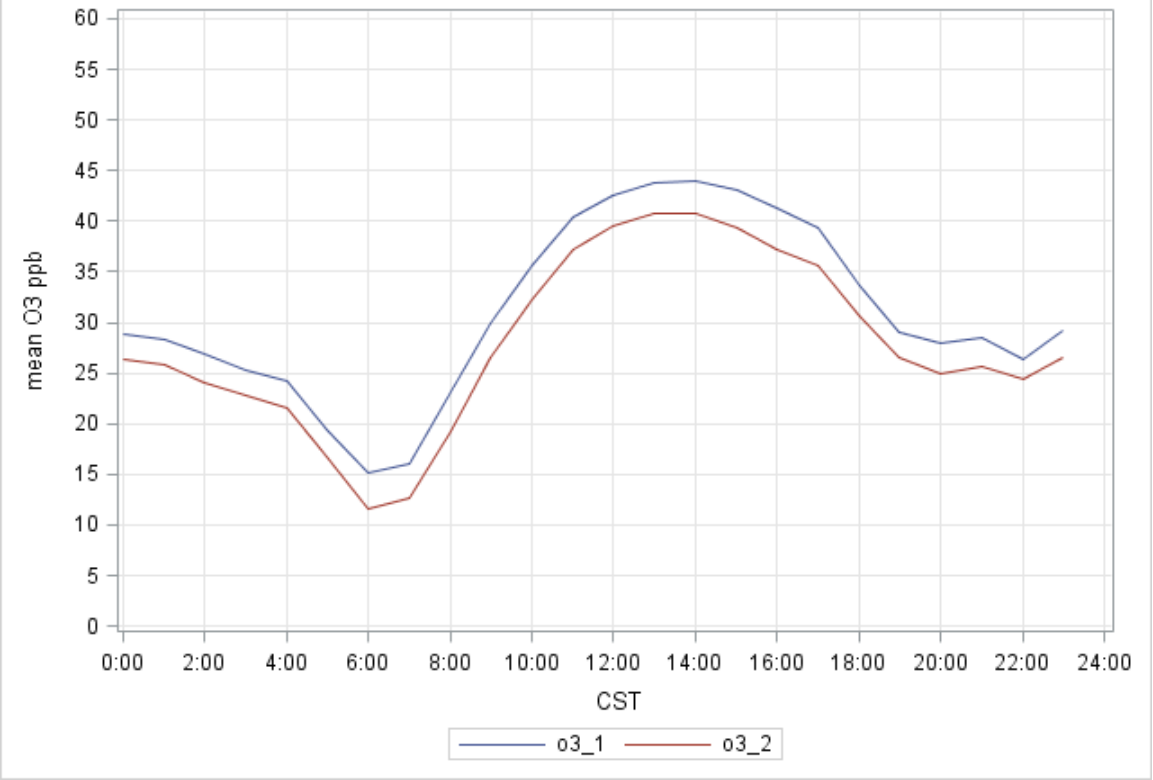

Figure I.40 Mean difference between the two parameters in the preceding figure October 2015

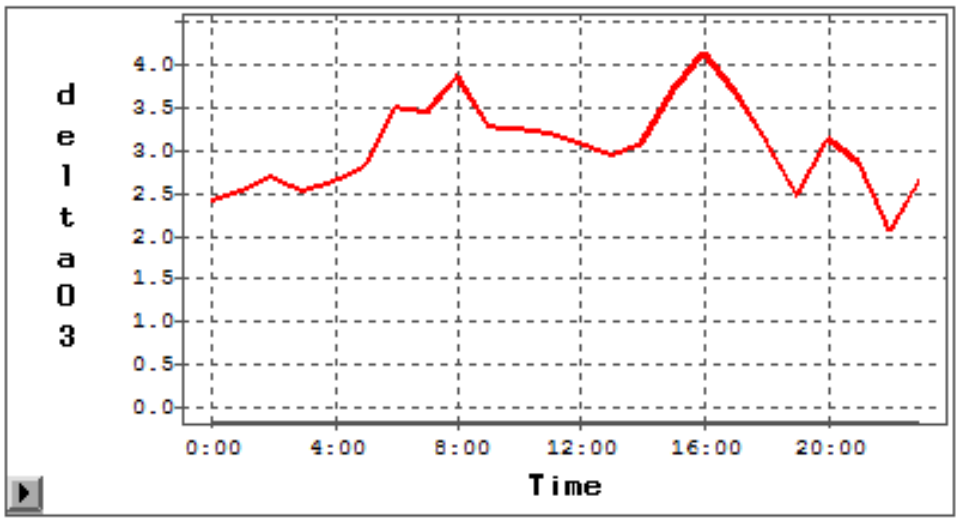

Figure I.41 Diurnal patterns for O_3 for November 1–10, 2015

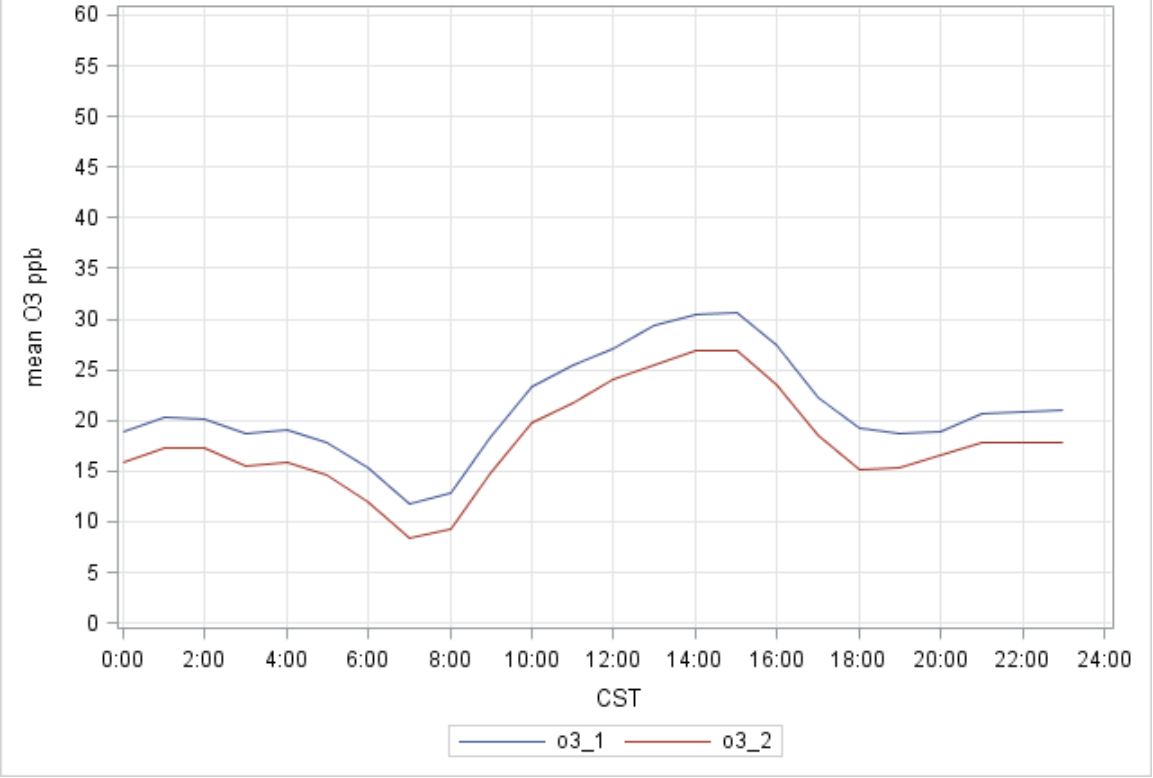

Figure I.42 Mean difference between the two parameters in the preceding figure Nov. 1–10, 2015